School of Civil and Mechanical Engineering

Motion Control for Nonholonomic Wheeled Mobile Robots with Obstacle Avoidance

Luc Quan Tran

This thesis is presented for the Degree of
Doctor of Philosophy
of
Curtin University

September 2019

Declaration

I hereby declare that I am the sole author of this thesis. The contents of this thesis are original work except where specific reference is made to the work of others.
This thesis contains no material which has been accepted for the award for any other degree or diploma in any university.

Luc Quan Tran
6th September, 2019

Abstract

In the last few decades, an autonomous wheeled mobile robot (WMR) system has gained a great deal of attention from the control and robotics communities. This system finds various applications in civilian and military areas because they can perform tasks autonomously in hostile or dangerous environments without human intervention. Also, rapid advances in sensing and computing technologies have contributed to considerable growth in research activities in the WMR system.

A unicycle-type WMR is described as an under-actuated mechanical system because it has more degrees of freedom to be controlled (three variables, i.e., position in x-axis and y-axis, and heading angle) than the number of independent control inputs (two commands). The control of an under-actuated WMR system has become an active research field recently because of both challenges in applied nonlinear control theory and its practical importance. While the WMR works autonomously and safely in a clustered environment, it should have a capability to follow/track predefined paths and to avoid colliding obstacles.

The main aims of this research are to deploy the smooth time-varying feedback control strategies to solve these two motion control problems, namely, path-following/ tracking and obstacle avoidance. Recently, some techniques have been developed to deal with these problems. These include a new level curve approach [1], the novel local potential functions [2, 3], bounded control for second-order systems [4], and the practical control algorithm [5]. The first work attempts to build global state-feedback controllers for the WMR following the reference path in the obstacle-free environment. Globally asymptotic convergence to zero of variables' errors and boundedness of control inputs are considered. In the next three parts, the research attempts to extend the above works to the scenario where collision avoidance between the WMR and obstacles, and constraints in the control inputs (saturation control) are considered. The feasibility and efficiency of the designed control laws are verified throughout the thesis with simulations.

Acknowledgments

Firstly, I would like to express my sincere gratitude and admiration to my supervisor, Professor Khac Duc Do. Without your consistent support and patience, I would have never completed this work. As an academic advisor, your informative lectures and guidance have always been invaluable to my research and future work.

Additionally, I wish to acknowledge several sources of support. I thank administrative staff for providing their support during all the time I do research in the School of Civil and Mechanical Civil Engineering. I also thank Ms Raquel Tsuji Iliano, the Sponsored Students Coordinator, Curtin International Student Office, for her great assistance during the difficult time of studying I have struggled. Besides, my Ph.D. research course at Curtin University has been sponsored by the joint scholarship between the Ministry of Education and Training of Vietnam (MOET) and the Curtin International Postgraduate Research Scholarship (CIPRS). The financial support from this scholarship is greatly appreciated.

I would also like to thank friends who I have chances to meet during the time of studying at the Curtin University, Perth, Western Australia. Sharing enjoyable moments and helping each other in life are always great memories.

Most importantly, I truly appreciate my family. Their constant understanding and encouragement is the huge source of my strength and confidence. My deepest appreciation sends to my dear mother who has sacrificed her personal life to nurture me and my sister. Especially, I profoundly thank my beloved wife, Nguyen Thuy Duong and my children, Tran Luc Minh Quang and Tran Luc Minh Hieu who always provide me endless love, inspiration, and motivation.

Dedication

This dissertation is dedicated to my dear mother Dao Thi Mai and my beloved wife Nguyen Thuy Duong.

Contents

List of plots

Tables

Abbreviations

Table 1: List of abbreviations

Abbreviations	Meaning
UAV	Unmanned Aerial Vehicle
AGV	Autonomous Ground Vehicle
USV	Unmanned Surface Vehicle
UUV	Unmanned Underwater Vehicle
WMRs	Wheeled Mobile Robots
PE	Persistent Excitation
GNRON	Goals Non Reachable with Obstacles Nearby
DVZ	Deformable Virtual Zone
ODIN	Omni-directional Intelligent Navigator
ODEs	Ordinary Differential Equations
CoM	Center of Mass
PE	Persistent Excitation
GAS	Globally Asymptotically Stable

List of symbols

Table 2: List of symbols

Symbols	Description
$\mathbb{R}$	Field of real numbers
x	$x-$coordinate of the actual WMR
y	$y-$coordinate of the actual WMR
ϕ	heading angle of the actual WMR
v	linear velocity of the actual WMR
ω	angular velocity of the actual WMR
x_d	$x-$coordinate of the virtual reference vehicle
y_d	$y-$coordinate of the virtual reference vehicle
ϕ_d	heading angle of the virtual reference vehicle
v_d	linear velocity of the virtual reference vehicle
ω_d	angular velocity of the virtual reference vehicle
$\boldsymbol{\tau}$	torque control vector
r	radius of the wheel
b	half width of the WMR
a	distance between the CoM, P_C, and the middle point, P_0
m	total mass
m_w	mass of the wheel with a motor
m_c	mass of robot body
I_c	moment of inertia of the body about the vertical axis through CoM
I_w	moment of inertia of the wheel with a motor about the wheel axis
I_m	moment of inertia of the wheel with a motor about the wheel diameter
R_{safe}	radius of the physical safety of robot
R_{sen}	radius of the active sensing region of robot
R_{obs}	distance of influence of a convex polygon obstacle

Chapter 1

Introduction

1.1 Literature review

In recent years, autonomous vehicle systems have gained a great deal of attention from research and development communities, and it is predicted that their applications will increase significantly from domestic services to industry and military areas in the near future. They include transportation, discovery, surveillance, search and rescue, mapping of unknown or partially known environments and many others. In general, autonomous vehicle systems can be defined as unmanned vehicles which perform a variety of tasks in various environments without any human intervention. Depending on the operating environment, autonomous vehicle systems can roughly be classified by three different groups: UAV systems, AGV systems, and USV or UUV systems [8–10].

As a typical example of the AGV systems, a WMR is described as a nonholonomic system. This means that the WMR system has non-integrable constraints on its velocities [11]. According to the Brockett's necessary condition [12], such a typical system cannot be asymptotically stabilized to a given configuration under any smooth time-invariant feedback control as the mobility is restricted [13–16]. A comprehensive introduction to nonholonomic systems modelling, analysis, and control can be found in [16–18], and controlling of the WMR can be mentioned in [8, 19, 20].

Previous studies in [11, 13, 21, 22] demonstrated that methods of linear control theory are not applicable to this inherent problem of nonholonomic systems since kinematic equations of these physical systems are highly nonlinear. As such, it is

vitally important to develop appropriate nonlinear approaches for these nonlinear control problems. In general, there have been two major research directions to tackle inherent challenges of nonholonomic constraint problems, to which the WMR is subjected, namely non-smooth feedback and smooth time-varying feedback strategies [14, 22, 23]. In [24], the authors presented a pioneering study on the non-smooth feedback control method, and other authors in [25–31] also contributed notably to the method, among others. Generally, this non-smooth feedback control can achieve exponential convergence. The authors in [14, 32] initiated the time-varying continuous feedback control method, and in [33], the authors also provided by several smooth feedback control laws to solve these problems during this time. In [34], the authors have stated that convergence rates of this time-varying feedback control are slow. However, with the attractive feature of explicitly time-depending feedback signals, subsequent studies exploring the potentialities of this direction were introduced, see, e.g., [22, 35–41]. It is of interest to mention that some variant forms combined by both elegant methods, see, e.g., [23, 42–44], were also applicable to faster convergent solutions. There has been a comprehensive introduction towards the control of nonholonomic systems [11], and the development of nonlinear control theory [45], and references therein.

Another attractive feature of nonholonomic mechanical systems is that proposed control methods for such systems are applicable to under-actuated mechanical systems, i.e., systems having fewer independent control inputs than degrees of freedom to be controlled [21]. The WMR and other autonomous vehicle systems, including the UAV, and the USV, present examples involving under-actuation matters. With the richness in both control problems and applications, the class of under-actuated mechanical systems receives significant interest in the nonlinear control-oriented research community recently. Although challenges of controlling the WMR are mentioned in two separate issues, i.e., nonholonomy and under-actuation, recent research normally considers two such issues as one problem and to seek unified methods to solve this fully. There is abundant information of modeling, control, and analysis of these systems in [46–52].

In essence, the development of control strategies is oriented by different types of control objective. Dealing with motion control of the WMR can be generally classified into three categories: trajectory-tracking, path-following and point-to-

point stabilization [13, 20, 39, 47]. There have been extensive works devoted to either the stabilization and tracking/path-following separately or simultaneously of this dynamical system, see, e.g., [41,47,53–56]. Regarding a solution to motion control problems of the WMR system, there has been a great deal of literature on advanced control engineering. Control laws fall into several methods such as Lyapunov's direct method [57] and standard backstepping technique [58], see e.g., [6, 22, 39, 59], feedback linearization [60–62], sliding mode approaches, see e.g., [31, 44, 63–65], receding horizon control [66, 67], inverse optimal control, see e.g., [68–71], and fuzzy/fuzzy neural networks [72–75].

Concerning the tracking problem, the WMR is forced to track and follow the time parameterized reference trajectory. The activity can be considered as a tracking task of an actual vehicle and a virtual moving reference vehicle. Tracking activity should satisfy both the reference path and the reference linear and angular velocities. Various approaches have been proposed to determine control inputs; namely, linear velocity, v, and angular velocity, ω, for the kinematic model of the WMR [40, 76–78], see (2.41) for the details of the model. The system dynamics is not included or is considered in the simplified form [22, 23]. Observer-based control design was proposed in [79, 80] as some of tracking error coordinates were assumed not to be measurable. The ultimate objective has been obtained when tracking errors were globally asymptotically stabilized to the origin over time [20, 22, 41, 54, 55]. This normally resulted in complicated control laws. In [38, 56, 79], some types of persistent excitation (PE) conditions were imposed to the reference linear and/or angular velocities to ensure asymptotic tracking. Consequently, these restrictive assumptions limited the reference trajectories, i.e., straight-line reference was not applicable if the angular velocity had to be non-zero. A significant improvement has been made in [81] for tracking control design of underactuated surface vessels as the authors have removed the restrictive assumptions above to relax conditions on the reference. As a result, globally asymptotically tracking was obtained. Next, in [53], the authors have successfully applied this advantage to the WMR to achieve globally asymptotically tracking and stabilization simultaneously.

Regarding the path-following problem, the task is relaxed to be a variant of standard reference tracking, in which the virtual reference vehicle is not necessarily provided. In this problem, the entire path is considered rather than

a point tracking to the reference path. The primary control objective is that the controller forces the vehicle's heading angle to steer it along to a predefined geometric path at desired forward speed profile without a timing law of motion [1, 20, 55, 82–84]. Moreover, in terms of the convergence to the desired path, the latter performs more smoothly than the former does. There have been some popular path-following techniques developed for the WMR. These can be listed as the Serret-Frenet frame method [14], the polar coordinate-based method [85], the transverse feedback linearization method [86, 87], and the recent level curve method [88] developed for the WMR in [1]. Either local stability, see e.g., [14,85], or global stability results, see e.g., [1, 83, 84, 89] was achieved. In general, both trajectory tracking and path-following approaches are developed to guarantee the autonomous vehicle to track a predetermined path by calculating the desirable control inputs for the vehicle to follow.

By considering the link between trajectory tracking and path-following, a remarkable study of maneuvering problem has been introduced in [90, 91]. The general maneuvering problem is separated into a geometric task and a dynamic task. In the first task, vehicles are forced to converge to the desired path parameterized by a continuous scalar variable. In the second task, a desired dynamic behaviour along the path must be satisfied. The dynamic task can be assigned by a desired time, velocity, or acceleration [92]. Identically, path tracking treats the reference path as two separated components: a geometric function representing a predefined reference curve and a path parameter specifying the reference path function. Hence, it belongs to the class of known reference trajectories [93, 94]. Owing to an additional control input of the path parameter, both maneuvering and path tracking problems offer flexibility for control design. These approaches have been deployed in different applications including Lagrange systems, mobile robots, and marine vessels [6, 95–98].

The last category is the point-to-point stabilization problem which can be addressed in a local or global sense. This stabilization problem can be regarded as the generation of control inputs to force the WMR from an initial point to the target point. Because there are critical challenges of nonholonomic constraints in the WMR systems, classical smooth control approaches are not applicable. Subsequently, different sophisticated control algorithms have been proposed. In [14], the authors proposed the first time-varying smooth feedback control schemes

for the problem of point stabilization. An alternative discontinuous scheme was formulated in [99]. A combined path tracking and practical point stabilization control deploying input-output feedback linearization was proposed in [100]. The local asymptotic stability was achieved.

In practice, applications of the WMR might encounter sensoring uncertainties, unmodeled dynamics or mass variation. Such issues might worsen the system's performance. Additionally, the robustness of the system model might be affected if external disturbances are not confined. Meanwhile, some of the aforementioned control schemes have been restricted to the precise knowledge of the system dynamics and have ignored the presence of system uncertainties or environmental disturbances. Given careful consideration of the aforementioned issues, a remarkable adaptive controller based on both kinematic and dynamic models with unknown parameters has been designed in [41]. The authors in [39,73,75] utilized neural network tools to present a robust adaptive controller which has been able to deal with disturbances in the robot dynamics. In [72,73], the authors employed fuzzy tools to tackle the uncertainties in the robot kinematics. Other recent adaptive controllers developed for the WMR can be found in [54, 59, 101–103], among others.

It is also imperative to mention of the output feedback control for the WMR in the issues of inaccuracy and expensive cost of measurement devices. It should be noted that available solutions developed for Lagrangian systems, see e.g., [104, 105], cannot be applied directly to the WMR because of nonholonomic constraints and the quadratic cross-terms of unmeasured velocities in *Coriolis/Centripetal* term in the dynamic model, see (2.49) for the details. In [1,6], the authors have proposed a novel output-feedback control method using a coordinate transformation to eliminate the aforementioned across-term velocities while all parameters were assumed to be known. Alternatively, the high-gain observer design scheme [106] is applied in [59] to estimate unknown states. The dynamic surface design technique [107] was utilized in the work of the authors in [101]. Both types of research dealt with the problem of adaptive output-feedback control of the WMR.

On the other hand, obstacle avoidance has become a fundamental requirement for the WMR since vehicles are expected to move autonomously and safely

to the goal in a clustered environment. In terms of position and orientation, an obstacle is often classified into two categories: stationary and moving. While designing obstacle avoidance algorithms in this research, we only focus on stationary obstacles existing in the workspace of the WMR. Amongst a wide range of feasible solutions addressing path planning and collision avoidance problems in the literature, the potential field method, originally presented in [108, 109], is most commonly used due to its advantages based on mathematical simplicity, elegant computation, and requirement of local gradient vector fields for real-time avoidance [110–112]. However, it presented some inherent limitations in the performance which were mentioned in [113, 114]. To overcome the particular local minima problem, diverse solutions have been proposed based on the potential field ideas, i.e., GNRON [113], navigation functions [115], and attractive/repulsive potential fields [2, 116]. A comprehensive survey of collision avoidance algorithms for mobile robots can be found in [117].

A WMR equipped with sensors on-board can collect information on-line, e.g., the relative distance is collected by infrared sensors, to generate repulsive force through path planning and collision avoidance algorithms. Advances in high-performance and fast computation of electronics equipment have enabled attractive and repulsive forces to be computed in real-time in the potential field method. This significance is utilized to design obstacle avoidance algorithms in this research later. Details of this approach are described in Chapter 2. Another approach called off-line, global path planning method deals with global mapping covering the entire workspace and plans an ideal path for vehicles to move from the current location to the goal. This method requires considerable computational complexity to provide prior knowledge of a highly dynamic environment. For this reason, this method is not introduced and applied to this research. A detailed explanation of the difference between the two approaches was elaborated by the authors in [118]. Moreover, a comprehensive introduction of robot motion planning algorithms can be found in [109]. Recently, local potential field based navigation functions have widely been developed for various applications such as fully actuated agents [119, 120], mobile robots [121, 122], underwater vehicles [123], and manipulators [96, 124]. An advantage of this approach is that it demands less computational efforts while it suggests solutions to the local minima problem. However, the navigation function has a saddle point near each isolated obstacle which poses a challenge to stability analysis of control design [3, 123].

One has to guarantee that the only designed equilibrium point is asymptotically stable while the other critical point is unstable. Similarly to that of navigation functions, saddle points emerging in the potential function method is a critical issue. To avoid saddle points, controllers designed in [123] were modified to make the system escape from them. In terms of formation control of a group of agents/vehicles, the authors in [2, 3, 125] have represented new local attractive/repulsive potential functions to handle collision avoidance. These functions gave minimum value when the desired formation was achieved and tended to infinity when a collision was about to occur. The authors gave an analytical analysis to prove that only the equilibrium points were locally asymptotically stable while the saddle points were unstable. Thus, the system did not converge to saddle points.

Although extensive research has been carried out on problems of obstacle avoidance, it is often investigated separately from path-following/tracking, see, e.g., [108, 109, 113, 121, 123, 126]. Recently, some combined approaches of obstacle avoidance scheme and path-following/tracking method have been considered. All solutions supported a general idea that an integrated controller forces the vehicle to track a reference path globally while it is capable of avoiding obstacles locally. The authors in [127] proposed the DVZ principle, which was embedded in the path-following method to define a safe zone around the vehicle. The overall controller was synthesized by Lyapunov's direct method [57] and backstepping techniques [58]. However, the stability analysis of the local minimum problem was not given. In [96], navigation functions were integrated into path tracking to produce a feedback control law with bounded control inputs. Static obstacles were assumed not being on the reference paths in this work. Decentralized scheme in navigation functions [119, 128] and optimal control law [129] was utilized to solve the obstacle avoidance problem for reference tracking of nonholonomic mobile robots in [130, 131]. In [132], an integrated control method for obstacle avoidance and level curve based path-following [88] was introduced for mobile robots at the kinematic level only. While the level curve approach has illustrated its effectiveness in applications [1, 133], the obstacle avoidance algorithm applied in this work seemed not to be impressive since it allowed a small deviation from the reference path. Furthermore, the mathematical analysis was not provided to support the avoiding algorithm.

As concerns a unified control scheme, it is difficult to incorporate obstacle avoidance to the reference tracking method of the WMR (e.g. [6, 22, 41]), in which tracking errors were converted into a new form to deal with nonholonomic constraints by using a special coordinate transformation [76]. This led to the alternative representation to surpass this difficulty for collision avoidance between a group of nonholonomic autonomous vehicles [3, 134, 135] working in formation or coordinated manners.

Practically, the magnitude of control signals should always be limited to guarantee the boundedness on controlled torques applied to the driving actuators. To this end, the boundedness of immediate controls is also considered carefully. Literature reveals some works dealing with limited control inputs of mobile robots. In [23], designed linear and angular velocity inputs (at kinematic level), and designed torque inputs, in [54] (at dynamic level), were saturated to gain bounded controllers. Both cases addressed the designing of controllers for the stabilization and tracking simultaneously problem. Another recent work in [95] presented the so-called one-step ahead backstepping method to yield bounded control laws for global path tracking of the WMR. While the standard backstepping technique has effectively provided a constructive design procedure for many nonlinear control problems, the author in [4] has pointed out that it was hard to apply this technique in designing a bounded formation controller for second-order dynamic systems when collision avoidance between agents was considered. Instead of using the standard backstepping technique and local potential functions as in [2], the author proposed a new bounded control design technique with a combination of pairwise collision functions. The pairwise collision functions in [4] are different from the potential functions as in the literature, see e.g., [3, 113]. Both relative positions and relative velocities of agents were utilized in a new technique to form the pairwise collision functions. The functions then facilitated the control design scheme to ensure the boundedness of the control inputs with a predetermined bound and without collision among agents. The effectiveness of the method has been proven on fully actuated second-order dynamic agents and an under-actuated ODIN system. Both applications focused on formation control.

A large number of studies focused on feedback linearization when they dealt with the inherent non-integrable dynamics of the WMR systems. Subsequently, nonholonomic kinematics can be converted to double integrator dynamics. In

[61, 136], a new coordinate frame was created by redefining a new reference point which was L distance from the original point. The system then could be input-output linearized and decoupled. This was called "look-ahead" control. Similarly, a so-called "hand" position coordinate transformation was introduced in [62]. While these methods utilized input-output linearization technique for a simplification, the orientation of the WMR was not controlled. From the practical view, authors in [20, 137] indicated that stabilizing control objectives for such system might be less demanding if the system was asymptotically stable at a small set containing the origin of the system error, instead of achieving asymptotic stabilization at the origin. Then, the transverse function approach introduced in [138] was applied to yield practical stabilization for nonholonomic systems. This practical control method was also developed for nonholonomic mobile manipulators [139]; the WMR with trailers [140]. The authors in [5] took the advantages of this method to represent a new coordinate transformation in which an "additional control input" was generated. As a result, practical formation controllers [5] for a group of the WMRs and practical controllers for underactuated ships [141] were successfully produced.

1.2 Motivation and contributions

1.2.1 Motivation

The initial motivation for the dissertation comes from the need for path planning and motion control for under-actuated vehicle systems. These systems are characterized by the presence of nonholonomic constraints on their generalized velocities. While nonholonomic and under-actuation characteristics of such systems are obstructive for control design, these characteristics attract a large number of studies to tackle these challenges. Another main motivation is raised in practical situations. While moving in their workspace, how autonomous vehicles react to obstacles along their path? How to ask the vehicles to avoid obstacles smoothly? Hence, obstacle avoidance algorithms are needed for autonomous vehicles to work safely and efficiently. Based on the two aforementioned issues, the particular objective of the thesis is motivated by studies on control design for the WMR in [1, 3–6].

Precise path-following/tracking is desirable when the WMR is forced to perform a task in a clustered environment without colliding with obstacles. Accordingly, this dissertation intends to present several motion planning and control algorithms for a WMR platform to work in two different scenarios: obstacle-free and existence of obstacles in the workspace. In other words, the main work will be twofold. First, without any obstacle on the WMR's workspace, a proper solution for the path-following problem is sought. The expected solution should be globally stable at the origin from any initial configuration. Second, when the obstacle problem is included, a combined solution of motion control and obstacle avoidance is investigated. The proposed controllers will be able to force the WMR to track the desired path and to avoid any obstacle along its path. Control signals are also continuous. Thus, control schemes do not need switching mode.

1.2.2 Contributions

The main contributions of this dissertation are briefly stated in the following paragraphs, which are sorted by four different problems to be solved.

1. Based on the level curve method [1], globally state-feedback controllers for path-following of the WMR to a certain class of reference paths are designed by using Lyapunov's direct and standard backstepping methods. Compared to the original method in [88], proposed immediate controls and actual controls in this study are bounded.

2. Path tracking and obstacle avoidance problems are solved constructively in a combined framework. Results show that the closed-loop system is globally asymptotically stable. About obstacle avoidance matter, the local minimum problem, a critical issue in the classical potential function approach, is no longer available since the novel local potential functions in [3] are applied. Moreover, this work provides an analytical analysis to prove that the closed system only converges to the equilibrium point and does not converge to the saddle point.

3. A new bounded position control algorithm for the problem of path tracking and obstacle avoidance is represented. The control scheme adopted the works of pairwise collision avoidance functions introduced in [4] and coordinate transformation in [62]. The boundedness of designed control signals

ensures control efforts not to exceed a certain value in terms of relative distance and speed. The inherent saddle point problem is also carefully analyzed. Hence, only the equilibrium points are locally asymptotically stable while the saddle points are unstable.

4. A new algorithm for the so-called practical control of path tracking and obstacle avoidance is proposed. A special coordinate transformation borrowed from [5] is deployed to handle the orientation of the vehicle. Although tracking errors could not converge to zero, they converged to a ball having center at the origin and small adjustable radius. No collision is guaranteed under suitable initial conditions. Also, instability of the saddle point is justified in the stability analysis section.

1.3 Thesis outline

The organization of this dissertation comprises seven chapters including this first introduction chapter. To investigate motion control for the WMR, useful results on design and analysis of control systems are reviewed firstly in Chapter 2. This chapter gives a brief of relevant mathematical concepts, stability analysis of nonlinear systems, and associated control techniques. The chapter also presents in detail the derivation of mathematical models in terms of kinematics and dynamics of the WMR system. Physically, the kinematic and dynamic models of a WMR system are a set of cascaded equations. This model will be used in subsequent chapters to develop different control schemes. An introduction to motion planning for autonomous vehicles is another part of this chapter. This method is then integrated into proposed control designs as the obstacle avoidance problem is considered.

Chapter 3 focuses only on the path-following problem of the WMR without obstacles in the workspace. Constructive design of state-feedback controllers is described which applies the recently developed Level curve approach for the path-following task. Before control design steps, level curve approach is briefly introduced in this chapter. Proof of results is presented via stability analysis. Finally, numerical simulations and experiments are shown to illustrate the effectiveness of the proposed controllers.

In chapter 4, the issue of stationary obstacles existing in the workspace is considered. This emerging problem suggests the author develop a unified solution for path tracking and obstacle avoidance of the WMR. A local potential function is constructed to handle obstacle avoidance matter. Based on results achieved, stability analysis is carried out. At the end of this chapter, the rightness of proposed controllers is demonstrated by numerical simulations.

Chapter 5 proposes a new bounded position control algorithm for the problem of path tracking and obstacle avoidance of the WMR. Before proceeding to design controllers, a coordinate transformation is used to convert the nonholonomic kinematics to double integrator dynamics. The pairwise collision function developed in [4] is adopted to deal with obstacle avoidance. To achieve the control objective of this chapter, a new approach is deployed instead of the standard backstepping techniques. Next, the findings are supported through Lyapunov-based stability analysis and other relevant lemmas. Numerical simulations are illustrated in the last section for the effectiveness of the proposed control design.

In chapter 6, an alternative practical control algorithm to improve the performance of the WMR system is represented. In this approach, heading angle is controlled by using a special technique of coordinate transformation. The Lyapunov's direct method and the standard backstepping technique are applied to derive controllers. Switching control is not needed between two modes, i.e., without obstacle and with an obstacle, because the smooth step functions are introduced. Similarly, stability analysis is provided as a solid proof for the results. Numerical simulations are implemented in the last section for the illustration of the effectiveness of the proposed control design.

Finally, chapter 7 summarizes the results and contributions of this dissertation. Some possible scopes of future work are also discussed.

Chapter 2

Preliminaries, system modeling and motion planning

In this chapter, essential concepts, mathematical fundamentals, Lyapunov stability, and control techniques that are employed throughout this work are covered. Apart from that, a mathematical model of the WMR system is also derived by using physical laws. This mathematical model is the subject to apply different control schemes developed in the main contents of the research. Motion planning is also briefly introduced as an indispensable part of control design tasks.

2.1 Preliminaries

As mentioned above, it is necessary to re-introduce some of the fundamental concepts on ordinary differential equations, Lyapunov stability, Young's inequality, smooth saturation functions, smooth step functions, differentiable and bounded functions, and control techniques, namely, standard backstepping and bounded control techniques in the form of definitions, theorems, and lemmas. The proofs of most of the following theorems and lemmas are not shown in this thesis but can be found in the associated references. These effective tools contribute directly to control design and stability analysis of this research.

2.1.1 Nonautonomous systems

Consider a general nonautonomous system consisting of n first-order one dimensional ordinary differential equations (ODEs) in the vector form:

$$\dot{x} = f(t, x), \tag{2.1}$$

where $x = [x_1 \cdots x_n]^T$ is the state vector, $f = [f_1 \cdots f_n]^T$ is the vector of nonlinear functions f_i in general, $(i = 1, n)$, and n is the dimension of the system (2.1). Assume that function f_i is piecewise continuous in t and locally Lipschitz in its state variables x_i. The ODEs characterize the evolution of the state variables x_i with respect to t. with $x \in \mathbb{R}^n$ and for all $t \geq 0$. Since f depends on time, the systems (2.1) are called *time-varying systems*.
Local and global existence and uniqueness results of solutions of the system (2.1) are re-introduced through the statements of two theorems below.

Theorem 2.1.1 (Theorem 3.1 - Local existence and uniqueness [57]). *Let $f(t, x)$ be piecewise continuous in t and satisfy the Lipschitz condition*

$$\|f(t, x) - f(t, y)\| \leq L\|x - y\| \tag{2.2}$$

$\forall x, y \in B = \{x \in \mathbb{R}^n | \|x - x_0\| \leq r\}$, $\forall t \in [t_0, t_1]$, and L is a positive constant. Then, there exists some $\delta > 0$ such that the equation (2.1) with $x(t_0) = x_0$ has a unique solution over $[t_0, t_0 + \delta]$.

Proof. See [57]. □

Theorem 2.1.2 (Theorem 3.2 - Global existence and uniqueness [57, 142]). *Suppose that $f(t, x)$ is piecewise continuous in t and satisfies*

$$\|f(t, x) - f(t, y)\| \leq L\|x - y\| \tag{2.3}$$

$\forall x, y \in \mathbb{R}^n$, $\forall t \in [t_0, t_1]$, and L is a positive constant. Then the state equation (2.1), with $x(t_0) = x_0$ has a unique solution over $[t_0, t_1]$.

Proof. See [57, 142]. □

If a solution $x(t, t_0, x_0)$ of the system (2.1) satisfies to be existence and uniqueness for all $t \geq t_0$ for all initial conditions $x(t, t_0, x_0) = x_0$, the system (2.1) is *forward completeness* [143].

A constant vector $\boldsymbol{x}_e \in \mathbb{R}^n$ is said to be an equilibrium point of the system (2.1) if

$$f(t, \boldsymbol{x}_e) = 0, \quad \forall t \geq t_0 \geq 0.$$

where $\boldsymbol{x}_e = (x_{1e}, \cdots, x_{ne})^T$. Generally, it can be assumed that the origin, i.e., $\boldsymbol{x}_e = 0$ is an equilibrium point of the system (2.1). Hence, studying the stability behaviors of the equilibria can be implemented by different methods of stability

analysis for nonlinear systems. However, there has been rarely a general methodology allied to nonlinear systems. It depends on particular classes of systems and problems, then appropriate and efficient analysis methods can be chosen. Several popular stability analysis frameworks for investigation of solutions' behaviors can be named: feedback linearization [142,144–146], Lyapunov stability [57,142], and contraction analysis [147]. The intention of this research is only to employ the Lyapunov stability for analysis. As such, some relevant important definitions and theorems in [57, 58, 148, 149] are represented. For the proofs of these theorems, readers are advised to see those materials for the details.

2.1.2 Lyapunov stability

Some fundamental control theories about the stability of equilibrium points of nonautonomous nonlinear systems are recalled. The definitions, theorems, and lemmas are mainly borrowed from [57]. With respect to the equilibrium point at the origin, important stability concepts are defined below.

Definition 2.1.1 (Definition 4.4 [57])**.** The equilibrium $x = 0$ is the equilibrium point of the system (2.1) is

- stable if, for each $\epsilon > 0$, there is $\delta = \delta(\epsilon, t_0) > 0$ such that

$$\|x(t_0)\| < \delta \Rightarrow \|x(t)\| < \epsilon, \quad \forall t \geq t_0 \geq 0. \tag{2.4}$$

- uniformly stable if, for each $\epsilon > 0$, there is $\delta = \delta(\epsilon) > 0$, independent of t_0, such that (2.4) is satisfied.

- unstable if it is not stable.

- asymptotically stable if it is stable and there is a positive constant $c = c(t_0)$ such that $x(t) \to 0$ as $t \to \infty$, for all $\|x(t_0)\| < c$.

- uniformly asymptotically stable if it is uniformly stable and there is a positive constant c, independent of t_0, such that for al $\|x(t_0)\| < c$, $x(t) \to 0$ as $t \to \infty$, uniformly in t_0; that is, for each $\eta > 0$, then there is $T = T(\eta) > 0$ such that

$$\|x(t)\| < \eta, \quad \forall t \geq t_0 + T(\eta), \quad \forall \|x(t_0)\| \leq c. \tag{2.5}$$

- globally uniformly asymptotically stable if it is uniformly stable, $\delta(\epsilon)$ can be chosen to satisfy $\lim_{\epsilon \to \infty} \delta(\epsilon) = \infty$, and, for each pair of positive numbers η

and c, there is $T = T(\eta, c) > 0$ such that

$$\|x(t)\| < \eta, \quad \forall t \geq t_0 + T(\eta, c), \quad \forall \|x(t_0)\| \leq c. \tag{2.6}$$

Concepts of uniformly stable, uniformly asymptotically stable, and globally uniformly asymptotically stable can be equivalently stated in terms of class $\mathcal{K}$ and class $\mathcal{KL}$ functions described as follows

Lemma 2.1.3 (Lemma 4.5 [57]). *the equilibrium point $x = 0$ of system (2.1) is*

- *uniformly stable if and only if there exist a class $\mathcal{K}$ function α and a positive constant c, independent of t_0, such that*

$$\|x(t)\| \leq \alpha(\|x(t_0)\|), \qquad \forall t \geq t_0 \geq 0, \qquad \forall \|x(t_0)\| < c. \tag{2.7}$$

- *uniformly asymptotically stable if and only if there exist a class $\mathcal{KL}$ function β and a positive constant c, independent of t_0, such that*

$$\|x(t)\| \leq \beta(\|x(t_0), t - t_0\|), \qquad \forall t \geq t_0 \geq 0, \qquad \forall \|x(t_0)\| < c. \tag{2.8}$$

- *globally uniformly asymptotically stable if and only if inequality (2.8) is satisfied for any initial state $x(t_0)$.*

Proof. See [57]. □

Theorem 2.1.4 (Theorem 4.1 [57]). *Let $x = 0$ be an equilibrium point for (2.1) and $D \subseteq \mathbb{R}^n$ be a domain containing $x = 0$. Let $V : D \to \mathbb{R}$ be a continuously differentiable function such that*

$$\begin{aligned} &V(0) = 0 \quad \text{and} \quad V(x) > 0 \quad \text{in} \quad D - \{0\} \\ &\dot{V}(x) \leq 0 \quad \text{in} \quad D \end{aligned} \tag{2.9}$$

Then, $x = 0$ is stable. Moreover, if

$$\dot{V}(x) < 0 \quad \text{in} \quad D - \{0\} \tag{2.10}$$

then $x = 0$ is asymptotically stable.

Proof. See [57]. □

Theorem 2.1.5 (Theorem 4.2 [57]). *Let $x = 0$ be an equilibrium point for (2.1). Let $V : \mathbb{R}^n \to \mathbb{R}$ be a continuously differentiable function such that*

$$\begin{aligned} &V(0) = 0 \quad \text{and} \quad V(x) > 0, \quad \forall x \neq 0 \\ &\|x\| \to \infty \Rightarrow V(x) \to \infty \\ &\dot{V}(x) \leq 0 \quad \forall x \neq 0 \end{aligned} \tag{2.11}$$

then $x = 0$ is globally asymptotically stable.

Proof. See [57]. □

Theorem 2.1.6 (Theorem 4.3 (or Instability Theorem) [57]). *Let $x = 0$ be an equilibrium point for the system $\dot{x} = f(x)$. Let $V : D \to \mathbb{R}$ be a continuously differentiable function such that $V(0) = 0$ and $V(x_0) > 0$ for some x_0 with arbitrarily small $\|x_0\|$. Choose $r > 0$ such that the ball $B_r = \{x \in \mathbb{R}^n | \|x\| \leq r\}$ is contained in D. Define a set $U = \{x \in B_r | V(x) > 0\}$ and suppose that $\dot{V}(x) > 0$ in U. Then, $x = 0$ is unstable.*

Proof. See [57]. □

Theorem 2.1.7 (Lasalle's Invariant Theorem 4.4 [57]). *Let $\Omega \subset D$ be a compact set that is positively invariant with respect to (2.1). Let $V : D \to \mathbb{R}$ be a continuously differentiable function such that $\dot{V}(x) \leq 0$ in Ω. Let E be the set of all points in Ω where $\dot{V}(x) = 0$. Let M be the largest invariant set in E. Then every solution starting in Ω approach M as $t \to \infty$.*

Proof. See [57]. □

Theorem 2.1.8 (Theorem 8.4 [57]). *Let $D \subset \mathbb{R}^n$ be a domain containing $x = 0$ and suppose $f(t, x)$ is piecewise continuous in t and locally Lipschitz in x, uniformly in t, on $[0, \infty) \times D$. Furthermore,suppose $f(t, 0)$ is uniformly bounded for all $t \geq 0$. Let $V : [0, \infty) \times D \to \mathbb{R}$ be a continuously differentiable function such that*

$$\begin{aligned} &W_1(x) \leq V(t, x) \leq W_2(x) \\ &\dot{V}(t, x) = \frac{\partial V}{\partial t} + \frac{\partial V}{\partial x} f(t, x) \leq -W(x) \end{aligned} \tag{2.12}$$

$\forall t \geq 0$, $\forall x \in D$, where $W_1(x)$ and $W_2(x)$ are continuous positive definite functions and $W(x)$ is a continuous positive semidefinite function on D. Choose $r > 0$ such that $B_r \subset D$ and let $\rho < min_{\|x\|=r} W_1(x)$. Then, all solutions of $\dot{x} = f(t, x)$ with $x(t_0) \in x \in B_r | W_2(x) \leq \rho$ are bounded and satisfy

$$W(x(t)) \to 0 \quad \text{as} \quad t \to \infty. \tag{2.13}$$

Moreover, if all the assumptions hold globally and $W_1(x)$ is radially unbounded, the statement is true for al $x(t_0) \in \mathbb{R}^n$.

Proof. See [57]. □

Lemma 2.1.9 (Barbalat's Lemma 8.2 [57]). *Let $\phi : \mathbb{R} \to \mathbb{R}$ be a uniformly continuous function on $[0, \infty)$. Suppose that $\lim_{t\to\infty} \int_0^t \phi(\tau)d\tau$ exists and is finite. Then,*

$$\phi(t) \to 0 \quad \text{as} \quad t \to \infty.$$

Proof. See [57] □

Lemma 2.1.10 (Barbalat-like Lemma [2]). *Assume that a nonnegative scalar differentiable function $f(t)$ enjoys the following conditions*

$$\Big|\frac{d}{dt}f(t)\Big| \leq k_1 f(t) \quad \text{and} \int_0^\infty f(t)dt \leq k_2 \qquad \forall t \geq 0,$$

where k_1 and k_2 are positive constants, then $\lim_{t\to\infty} f(t) = 0$

Remark. Lemma (2.1.10) is different from Lemma (2.1.9). Instead of using the assumption that function $f(t)$ is uniformly continuous, Barbalat-like Lemma (2.1.10) assumes that absolute value of $\frac{d}{dt}f(t)$ is bounded by $k_1 f(t)$.

Proof. See [2] □

Lemma 2.1.11 (Comparison Lemma [150]). *Let $V(t) \in \mathbb{R}$ be a non-negative function of time on $[\,0, \infty)$ which satisfies the differential inequality*

$$\dot{V} \leq -\gamma V + \epsilon, \tag{2.14}$$

where $\gamma \in \mathbb{R}$ and $\epsilon \in \mathbb{R}$ are positive constants. Given (2.14), then

$$V(t) \leq e^{-\gamma t}V(0) + \frac{\epsilon}{\gamma}(1 - e^{-\gamma t}) \qquad \forall t \in [\,0, \infty) \tag{2.15}$$

where e is the base of the natural logarithm.

Proof. See [150] □

Lemma 2.1.12. *Let $\mathbf{A} \in \mathbb{R}^{n\times n}$ be a real, symmetric, positive definite matrix; therefore, all of the eigenvalues of $\mathbf{A}$ are real and positive. Let $\lambda_{min}(\mathbf{A})$ and $\lambda_{max}(\mathbf{A})$ denote the minimum and maximum eigenvalues of $\mathbf{A}$, respectively, then for any $x \in \mathbb{R}^n$*

$$\lambda_{min}(\mathbf{A})\|x\|^2 \leq x^T\mathbf{A}x \leq \lambda_{max}(\mathbf{A})\|x\|^2, \tag{2.16}$$

where $\| \bullet \|$ denotes the standard Euclidean norm.

Young's Inequality

For $x, y \in \mathbb{R}^2$, the following Young inequality holds [58]:

$$xy \leq \frac{\epsilon^p}{p}|x|^p + \frac{1}{q\epsilon^q}|y|^q, \tag{2.17}$$

where ϵ is a positive constant, and the constants $p > 1$ and $q > 1$ satisfy $(p-1)(q-1) = 1$. By selecting $p = q = 2$ and $\epsilon^2 = 2\kappa$, (2.17) becomes

$$xy \leq \kappa x^2 + \frac{1}{4\kappa}y^2, \tag{2.18}$$

2.1.3 Useful functions

A brief introduction of smooth saturation function, smooth step function, and scalar, differentiable and bounded function are represented this section. These functions are utilized as effective mathematical tools to the control design and stability analysis later.

Smooth saturation function

Definition 2.1.2. [95] The function $\sigma(x)$ is said to be a smooth saturation function if it is smooth and processes the properties:

1. $\sigma(x) = 0$ if $x = 0$, $\quad \sigma(x)x > 0$ if $x \neq 0$,
2. $\sigma(-x) = -\sigma(x)$, $\quad (x-y)\left[\sigma(x) - \sigma(y)\right] > 0$,
3. $|\sigma(x)| \leq 1$, $\quad |\frac{\sigma(x)}{x}| \leq 1$, $\quad |\frac{d\sigma(x)}{dx}| \leq 1$,

for all $(x, y) \in \mathbb{R}^2$. For the vector $\boldsymbol{x} = [x_1, \ldots, x_i, \ldots, x_n]^T$, the notation $\sigma(\boldsymbol{x}) = [\sigma(x_1), \ldots, \sigma(x_i), \ldots, \sigma(x_n)]^T$ is used to denote the smooth saturation function vector of the vector $\boldsymbol{x}$.

Some functions satisfying the properties in the definition above include $\sigma(x) = tanh(x)$ and $\sigma(x) = \frac{x}{\sqrt{1+x^2}}$.

Smooth step function

Definition 2.1.3. [125] A scalar function $h(x, a, b, c)$ is said to be a smooth step function if it enjoys the following properties:

1. $h(x, a, b, c) = 0 \quad \forall x \leq a$,
2. $h(x, a, b, c) = 1 \quad \forall x \geq b$,

3. $0 < h(x,a,b,c) < 1 \qquad \forall x \in (a,b)$,

4. $h(x,a,b,c)$ is smooth,

5. $h'(x,a,b,c) > 0 \qquad \forall x \in (a,b)$,

6. $h''(x,a,b,c) = 0$ at $x = x^* \in (a,b)$,

where $x \in \mathbb{R}$, $h'(x,a,b,c) = \frac{\partial h(x,a,b,c)}{\partial x}$, $h''(x,a,b,c) = \frac{\partial h^2(x,a,b,c)}{\partial x^2}$, a and b are constants such that $a < b$, and c is a positive constant.

Lemma 2.1.13. *[125] Let the scalar function $h(x,a,b,c)$ be defined as*

$$h(x,a,b,c) = \frac{f(x)}{f(x) + cf(1-x)}, \qquad \textit{with} \quad \tau = \frac{x-a}{b-a}, \tag{2.19}$$

where $f(\tau)$ is introduced as

$$f(\tau) = \begin{cases} e^{-\frac{1}{\tau}} & \textit{for } \tau > 0, \\ 0 & \textit{for } \tau \leq 0 \end{cases} \tag{2.20}$$

The function $h(x,a,b,c)$ is then called a smooth step function.

Proof. See [125] □

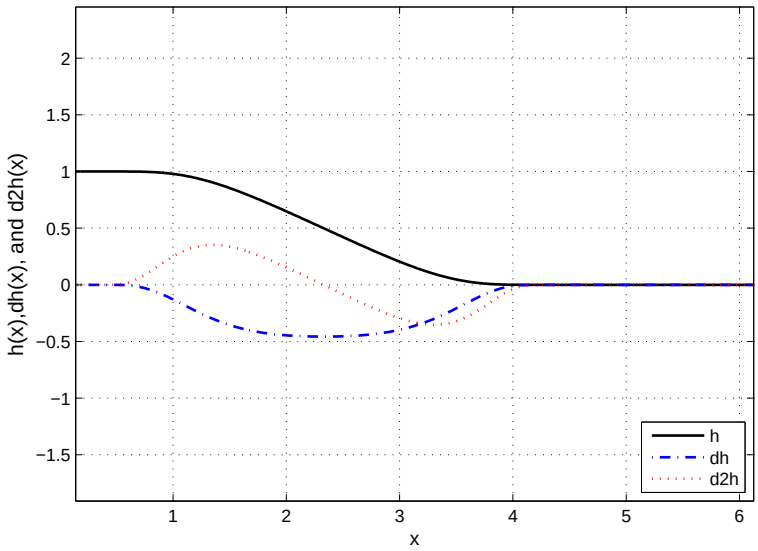

Figure 2.1: Illustration of a smooth step function $h(x, 0.5, 3)$ and its derivatives $dh = \frac{\partial h}{\partial x}$, $d2h = \frac{\partial^2 h}{\partial x^2}$ with $a = 0.5$, $b = 3$, and $c = 1$.

Differentiable and bounded function

The function $\Psi(x)$ is a scalar, differentiable and bounded function if it satisfies below properties [2]:

1. $|\Psi(x)| \leq M_1$
2. $\Psi(x) = 0$, if $x = 0$; $\quad x\Psi(x) > 0$, if $x \neq 0$
3. $\Psi(-x) = -\Psi(x)$; $\quad (x - y)\left[\Psi(x) - \Psi(y)\right] \geq 0$
4. $|\frac{\Psi(x)}{x}| \leq M_2$, $\quad |\frac{\partial \Psi(x)}{\partial x}| \leq M_3$, $\quad \frac{\partial \Psi(x)}{\partial x}\big|_{x=0} = 1$,

for all $(x, y) \in \mathbb{R}^2$, where M_1, M_2, M_3 are strictly positive constants. Some functions satisfying the properties in the definition above include $\Psi(x) = arctan(x)$ and $\Psi(x) = tanh(x)$.

2.1.4 Control techniques

Backstepping is one of the most powerful control design frameworks for nonlinear systems. In this section, some fundamental issues of standard backstepping technique which are applied in this research are introduced. This knowledge is fully represented in [58]. Besides, a useful technique for bounded control design developed in [4] is also revised. These methods are adopted to the main control design tasks.

Integrator Backstepping

Assumption 2.1.14

The assumption 2.7 in [58] is re-stated by considering the system

$$\dot{x} = f(x) + g(x)u, \quad f(0) = 0, \tag{2.21}$$

where $x \in \mathbb{R}^n$ is the state and $u \in \mathbb{R}$ is the control input. There exists a continuously differentiable feedback control law

$$u = \alpha(x), \quad \alpha(0) = 0, \tag{2.22}$$

and a smooth, positive definite, radially unbounded function $V : \mathbb{R}^n \to \mathbb{R}$ such that

$$\frac{\partial V}{\partial x}[f(x) + g(x)\alpha(x)] \leq -W(x) \leq 0, \quad \forall x \in \mathbb{R}^n \tag{2.23}$$

where $W : \mathbb{R}^n \to \mathbb{R}$ is positive semidefinite.

Lemma 2.1.14 (Lemma 2.8, Integrator Backstepping [58]). *Let the system (2.11) be augmented by an integrator:*

$$\dot{x} = f(x) + g(x)\xi \tag{2.24a}$$

$$\dot{\xi} = u \tag{2.24b}$$

and suppose that (2.24a) satisfies assumption 2.7 with $\xi \in \mathbb{R}$ as its control.

- *If $W(x)$ is positive definite then*

$$V_a = V(x) + \frac{1}{2}[\xi - \alpha(x)]^2 \tag{2.25}$$

is a CLF for the system (2.24), that is, there exists a feedback control law $u = \alpha_a(x, \xi)$ which renders $x = 0, \xi = 0$ the GAS equilibrium of (2.12).

$$u = -c(\xi - \alpha(x)) + \frac{\partial \alpha}{\partial x}[f(x) + g(x)\xi] - \frac{\partial V}{\partial x}g(x), \quad c > 0, \tag{2.26}$$

- *if $W(x)$ is only positive semidefinite, then there exists a feedback control which renders $\dot{V}_a \leq -W_a(x, \xi) \leq 0$, such that $W_a(x, \xi) > 0$ whenever $W(x) > 0$ or $\xi \neq \alpha(x)$. This guarantees global boundedness and convergence of $\begin{bmatrix} x(t) \\ \xi(t) \end{bmatrix}$ to the largest invariant set M_a contained in the set $E_a = \left\{ \begin{bmatrix} x \\ \xi \end{bmatrix} \in \mathbb{R}^{n+1} \middle| W(x) = 0, \xi = \alpha(x) \right\}$.*

Proof. See [58]. □

Bounded Control Design for Second-Order Systems

This section adopts the idea of a bounded control design technique initialised in [4] through a simple example. This technique will be applied to design bounded controllers later. As such, the following second-order is considered:

$$\begin{cases} \dot{x}_1 = x_2, \\ \dot{x}_2 = u \end{cases} \tag{2.27}$$

where x_1 and x_2 are the states, and u is the control input. Let us address acontrol problem of designing the control input u to asymptotically stabilize (2.27) at the origin for any initial values $(x_1(t_0), x_2(t_0)) \in \mathbb{R}^2$ at the initial time $t_0 \geq 0$ such that $|u(t)| \leq \varepsilon$ for all $t \geq t_0$, and ε is a positive constant. A solution to the above control problem is given in the following lemma.

Lemma 2.1.15. *[4]: Let the positive constants k and c be chosen such that $0.5k+c \leq \varepsilon$, and let $\sigma(\bullet)$ be a smooth saturation function of $\bullet$ defined in Definition3.1. The bounded control law*

$$u = \frac{1}{1+1.5x_2^2}\big(-kx_2 - c\sigma(kx_1 + (1+0.5x_2^2)x_2)\big), \tag{2.28}$$

globally asymptotically stabilizes the system at the origin.

Proof. See [4] □

Lemma 2.1.16. *[4]: Assume the vector $\boldsymbol{x}(t) \in \mathbb{R}^n$ satisfies the following conditions*

$$\begin{aligned} &\|\boldsymbol{x}(t_0)\| \geq a_0, \\ &\boldsymbol{x}^T(\dot{\boldsymbol{x}} + \mathbf{B}\boldsymbol{x}) \geq a, \forall t \geq t_0 \geq 0, \end{aligned} \tag{2.29}$$

where $t_0 \geq 0$ is the initial time, $\mathbf{B}$ is a symmetric positive definite matrix, and a_0 and a are strictly positive constants. Then

$$\|\boldsymbol{x}(t)\| \geq min\Big(a_0, \sqrt{\frac{a}{\lambda_M(\mathbf{B})}}\Big) \tag{2.30}$$

$\forall t \geq t_0 \geq 0$, where $\lambda_M(\mathbf{B})$ is the maximum eigentvalue of the matrix $\mathbf{B}$.

Proof. See [4] □

2.2 Modelling of the WMR

In studying the control system, one must be able to model physical systems in mathematical terms. Thus, kinematic and dynamic characteristics of physical systems should be investigated and analyzed. The more complete the mathematical model can be built, then the more accurate analysis may be gained. The modelling of the WMR is a crucial step since it provides proper mathematical models transformed from physical systems by applying physical laws governing the system. Besides, a WMR's model has been one of the excellent cases in literature for demonstrating different concepts of design and analysis of advanced control theories because the model possesses inherent high nonlinearities.

2.2.1 Kinematics of the WMR

Kinematics deals with the configuration of the WMR in its workspace, the relations between its geometric parameters, and the constraints imposed in its trajectories. The kinematic equations depend on the geometrical structure of the

vehicle. The study of kinematics is a fundamental prerequisite for the study of dynamics, control methods, and stability features. In this part, some fundamental concepts required for the study of the kinematics are represented. In particular, the kinematic model of a differential-type nonholonomic WMR is considered.

Rotation transformation

Moving on a two dimensional plane, a WMR rotates only with respect to the vertical axis z. Thus, the orthogonal rotation matrix with respect to $z-$axis is expressed [17]

$$\mathbf{R}(\phi) = \begin{bmatrix} \cos(\phi) & -\sin(\phi) & 0 \\ \cos(\phi) & \sin(\phi) & 0 \\ 0 & 0 & 1 \end{bmatrix} \tag{2.31}$$

Kinematics

A WMR is capable of moving autonomously on a horizontal plane. Its configuration can be specified in terms of the two generalized coordinates (x, y) of the WMR's center P_0 in the Cartesian space, the heading angle ϕ (orientation), and the right and left angles of driving wheels, θ_R, θ_L

$$\boldsymbol{q} = [x, y, \phi, \theta_R, \theta_L]^T. \tag{2.32}$$

The posture of the WMR can be directly specified by three variables x, y, ϕ and is described in Fig (2.2). Under the assumption of nonholonomic issues including

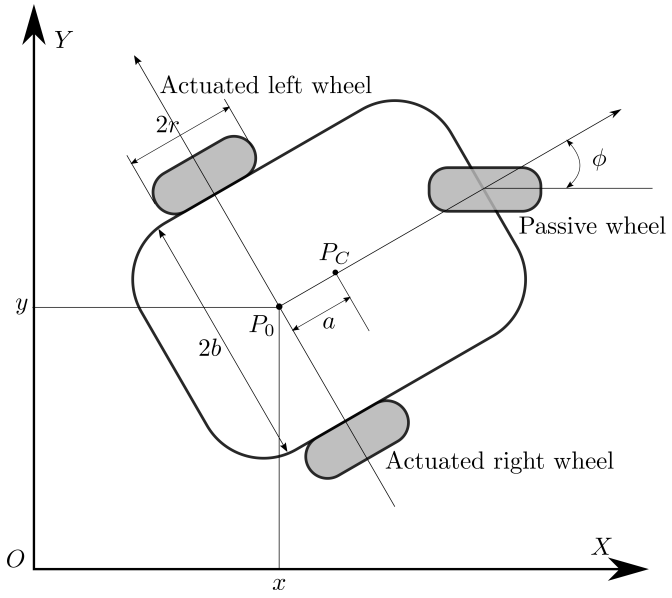

Figure 2.2: Description of a unicycle-type WMR on Cartesian plane [6]

pure rolling and non-slipping, there exist three constraints. The first one is that the WMR must move in the direction of the axis of symmetry. The last two constraints are the rolling constraints. The velocity of P_0 must be in the direction of the axis of symmetry [19, 41, 136, 151]

$$\begin{aligned} -\dot{x}\sin(\phi) + \dot{y}\cos(\phi) - \dot{\phi}a &= 0 \\ \dot{x}\sin(\phi) + \dot{y}\cos(\phi) + b\dot{\phi} &= r\dot{\theta}_R \\ \dot{x}\sin(\phi) + \dot{y}\cos(\phi) - b\dot{\phi} &= r\dot{\theta}_L \end{aligned} \tag{2.33}$$

where r is the radius of the wheel; a is the distance from middle point P_O to the center of mass P_C along the $X-$axis; b is the distance between the driving wheel and the axis of symmetry. Then three nonholonomic constraints can be written in the form

$$\mathbf{A}(\boldsymbol{q})\dot{\boldsymbol{q}} = 0, \tag{2.34}$$

where $\mathbf{A}(\boldsymbol{q})$ is an (3×5) full-rank matrix and

$$\mathbf{A}(\boldsymbol{q}) = \begin{bmatrix} \cos(\phi) & -\sin(\phi) & -a & 0 & 0 \\ \cos(\phi) & \sin(\phi) & b & -r & 0 \\ \cos(\phi) & \sin(\phi) & -b & 0 & -r \end{bmatrix}$$

Let $\mathbf{S}(\boldsymbol{q})$ be a (5×2) full rank matrix formed by a set of smooth and linearly independent vector fields spanning the null space of $\mathbf{A}(\boldsymbol{q})$, we have [39, 152, 153]

$$\mathbf{S}^T(\boldsymbol{q})\mathbf{A}^T(\boldsymbol{q}) = 0. \tag{2.35}$$

It is easy to find a time-dependent velocity vector $\boldsymbol{\omega}(t) \in \mathbb{R}^2$ such that

$$\dot{\boldsymbol{q}} = \mathbf{S}(\boldsymbol{q})\boldsymbol{\omega}(t), \qquad \forall t \geq 0, \tag{2.36}$$

where $\boldsymbol{\omega} = \begin{bmatrix} \omega_R & \omega_L \end{bmatrix}^T$, and $\omega_R = \dot{\theta}_R$ and $\omega_L = \dot{\theta}_L$ be the right wheel and left wheel velocities of the WMR. The difference between $\dot{\theta}_R$ and $\dot{\theta}_L$ determines the robot's angular velocity and it's direction. Matrix $\mathbf{S}(\boldsymbol{q})$ is selected as [41]

$$\mathbf{S}(\boldsymbol{q}) = \begin{bmatrix} \frac{r}{2}\cos(\phi) & \frac{r}{2}\cos(\phi) \\ \frac{r}{2}\sin(\phi) & \frac{r}{2}\sin(\phi) \\ \frac{r}{2b} & -\frac{r}{2b} \\ 1 & 0 \\ 0 & 1 \end{bmatrix} \tag{2.37}$$

If the vector $\boldsymbol{\omega} = \begin{bmatrix} \omega_R & \omega_L \end{bmatrix}^T$ is considered as a velocity control input vector for kinematic control design, the kinematic model of a WMR platform is described

in the form of (2.37) or

$$\begin{bmatrix} \dot{x} \\ \dot{y} \\ \dot{\phi} \\ \dot{\theta}_r \\ \dot{\theta}_l \end{bmatrix} = \begin{bmatrix} \frac{r}{2}\cos(\phi) & \frac{r}{2}\cos(\phi) \\ \frac{r}{2}\sin(\phi) & \frac{r}{2}\sin(\phi) \\ \frac{r}{2b} & -\frac{r}{2b} \\ 1 & 0 \\ 0 & 1 \end{bmatrix} \begin{bmatrix} \omega_R \\ \omega_L \end{bmatrix} \tag{2.38}$$

Among five state variables, $x, y, \phi, \theta_R, \theta_L$, in (2.32), the vector of state variables $\begin{bmatrix} \theta_R & \theta_L \end{bmatrix}^T$ relates explicitly to the control input vector $\begin{bmatrix} \omega_R & \omega_L \end{bmatrix}^T$, see (2.38). Therefore, only three state variables, namely x, y, ϕ are considered. Let v be the linear velocity, ω is the angular velocity of the WMR at the point P_0. Hence, the relationship between ω_R, ω_L and v, ω is defined as follows

$$\begin{bmatrix} \omega_R \\ \omega_L \end{bmatrix} = \begin{bmatrix} \frac{1}{r} & \frac{b}{r} \\ \frac{1}{r} & -\frac{b}{r} \end{bmatrix} \begin{bmatrix} v \\ \omega \end{bmatrix} \tag{2.39}$$

For the preparation of control design at dynamic level later, i.e., torque control inputs applied to the right and left actuators, the wheel velocities ω_R and ω_L are converted to the linear, v, and angular, ω, velocities by using the relationship [41]:

$$\mathbf{v} = \mathbf{B}^{-1}\boldsymbol{\omega}, \tag{2.40}$$

where $\mathbf{v} = [v \quad \omega]^T$, $\mathbf{B} = \frac{1}{r}\begin{bmatrix} 1 & b \\ 1 & -b \end{bmatrix}$. The generalized form of kinematic model for the WMR is obtained by substituting (2.39) into (2.38) without consideration of two states $\begin{bmatrix} \theta_R & \theta_L \end{bmatrix}^T$ as follows

$$\begin{cases} \dot{x} = v\cos(\phi) \\ \dot{y} = v\sin(\phi) \\ \dot{\phi} = \omega \end{cases} . \tag{2.41}$$

2.2.2 Dynamics of the WMR

In addition to the kinematic model, this section aims to derive the dynamic model. This model describes the dynamic relations between configuration coordinates and the torques generated by the actuators for the overall control design purpose. Through the Lagrange formulation, the derivation of the dynamic equations of the WMR is achieved.

Lagrangian dynamics

The equations of motion for a mechanical system can be generated in several different ways. In this research, the Lagrangian formulation, which is the difference between the kinetic and potential energy of the system, is used [17, 154, 155]

$$L(\boldsymbol{q}, \dot{\boldsymbol{q}}) = T(\boldsymbol{q}, \dot{\boldsymbol{q}}) - V(\boldsymbol{q}), \tag{2.42}$$

where T is the kinetic energy, a function of the configuration and of the velocity, and V is the potential energy, a function of configuration only. The Lagrange's equation of motion can be written simply in the matrix form [17, 155]

$$\frac{d}{dt}\frac{\partial L}{\partial \dot{\boldsymbol{q}}} - \frac{\partial L}{\partial \boldsymbol{q}} = \boldsymbol{\tau}, \tag{2.43}$$

where $\boldsymbol{\tau}$ denotes the external torque vector. As the motion of a WMR system is confined to a flat plane, i.e., the XOY plane, the potential energy of the system in the Lagrangian formulation is neglected. Hence, the equation (2.43) becomes:

$$L = T = T_1 + T_2 + T_3, \tag{2.44}$$

where T_1 is the kinetic part of the robot platform; T_2 and T_3 are the kinetic parts of the two wheels. All those parts comprise translational and rotational components and are calculated by

$$\begin{aligned} T_1 &= \frac{1}{2}m_c(\dot{x}_c^2 + \dot{y}_c^2) + \frac{1}{2}I_c\dot{\phi}^2 \\ T_2 &= \frac{1}{2}m_w(\dot{x}_R^2 + \dot{y}_R^2) + \frac{1}{2}I_m\dot{\phi}^2 + \frac{1}{2}I_w\dot{\theta}^2 \\ T_3 &= \frac{1}{2}m_w(\dot{x}_L^2 + \dot{y}_L^2) + \frac{1}{2}I_m\dot{\phi}^2 + \frac{1}{2}I_w\dot{\theta}^2 \end{aligned} \tag{2.45}$$

where m_c is mass of the robot platform; m_w is mass of the wheel; I_c is moment of inertia of the robot with respect to the middle point P_0. I_w is moment of inertia of each wheel and the actuator about the wheel axis. I_m is moment of inertia of each wheel and the actuator about the wheel diameter.

Dynamic equations

In general, the kinetic energy $T(\boldsymbol{q}, \dot{\boldsymbol{q}})$ is described in vector form as [39, 155]

$$T = \frac{1}{2}\dot{\boldsymbol{q}}^T\mathbf{M}(\boldsymbol{q})\dot{\boldsymbol{q}}. \tag{2.46}$$

where $\mathbf{M}(\boldsymbol{q})$ is the $(n \times n)$ symmetric, definite positive inertia matrix. The components required in Lagrangian equation (2.23) are now calculated by

$$\begin{aligned} \frac{\partial L}{\partial \dot{\boldsymbol{q}}} &= \frac{\partial T}{\partial \dot{\boldsymbol{q}}} = \mathbf{M}(\boldsymbol{q})\dot{\boldsymbol{q}} \\ \frac{d}{dt}\frac{\partial L}{\partial \dot{\boldsymbol{q}}} &= \mathbf{M}(\boldsymbol{q})\ddot{\boldsymbol{q}} + \dot{\mathbf{M}}(\boldsymbol{q})\dot{\boldsymbol{q}} \\ \frac{\partial L}{\partial \boldsymbol{q}} &= \frac{1}{2}\frac{\partial}{\partial \boldsymbol{q}}\big(\dot{\boldsymbol{q}}^T\mathbf{M}(\boldsymbol{q})\dot{\boldsymbol{q}}\big). \end{aligned} \tag{2.47}$$

Substituting those components of (2.31) into (2.23) yields the dynamic equation of the WMR under the constraints given by (2.34)

$$\mathbf{M}(\boldsymbol{q})\ddot{\boldsymbol{q}} + \mathbf{C}(\boldsymbol{q}, \dot{\boldsymbol{q}})\dot{\boldsymbol{q}} + \mathbf{D}\dot{\boldsymbol{q}} = \boldsymbol{\tau}, \tag{2.48}$$

where $\mathbf{D}$ has been denoted to be the damping matrix and the *Coriolis/Centripetal* term is calculated by

$$\mathbf{C}(\boldsymbol{q}, \dot{\boldsymbol{q}})\dot{\boldsymbol{q}} = \dot{\mathbf{M}}(\boldsymbol{q})\dot{\boldsymbol{q}} - \frac{1}{2}\frac{\partial}{\partial \boldsymbol{q}}(\dot{\boldsymbol{q}}^T\mathbf{M}(\boldsymbol{q})\dot{\boldsymbol{q}}). \tag{2.49}$$

It is noted that only frictional terms $\mathbf{D}\dot{\boldsymbol{q}}$ are considered and the gravity terms are excluded in the dynamic equation (2.48) above since the potential energy is neglected. With appropriate definitions of (2.51), the equation (2.48) can be rewritten as the final standard form of the dynamical equation for our control purposes later [17, 41, 155]

$$\begin{bmatrix} \dot{v} \\ \dot{\omega} \end{bmatrix} = \bar{\mathbf{C}} \begin{bmatrix} \omega^2 \\ -v\omega \end{bmatrix} - \bar{\mathbf{D}} \begin{bmatrix} v \\ \omega \end{bmatrix} + \bar{\mathbf{B}}\boldsymbol{\tau}, \tag{2.50}$$

with $\boldsymbol{\tau} = [\tau_v \quad \tau_\omega]^T$ denotes the control input torques applied to the wheels.
The detailed representation of $\mathbf{M}$, $\mathbf{C}(\dot{\boldsymbol{q}})$, $\mathbf{D}$ matrices in (2.48) are similar to those

in [6, 53]. Matrices $\bar{\mathbf{C}}$, $\bar{\mathbf{D}}$ and $\bar{\mathbf{B}}$ in (2.50) are re-arranged and defined as follows

$$
\begin{aligned}
&\mathbf{M} = \begin{bmatrix} m_{11} & m_{12} \\ m_{12} & m_{11} \end{bmatrix}, \quad \mathbf{C}(\dot{\boldsymbol{q}}) = \begin{bmatrix} 0 & c\dot{\phi} \\ -c\dot{\phi} & 0 \end{bmatrix}, \quad \mathbf{D} = \begin{bmatrix} d_{11} & 0 \\ 0 & d_{22} \end{bmatrix}, \\
&c = \frac{r^2}{2b} m_c a, \quad m_{11} = \frac{r^2}{4b^2}(mb^2 + I) + I_w, \quad m_{12} = \frac{r^2}{4b^2}(mb^2 - I), \\
&m = m_c + 2m_w, \qquad I = m_c a^2 + 2m_w b^2 + I_c + 2I_m, \\
&\bar{\mathbf{M}} = \mathbf{B}^{-1}\mathbf{M}\mathbf{B} = \begin{bmatrix} m_{11} + m_{12} & 0 \\ 0 & m_{11} - m_{12} \end{bmatrix} =: \begin{bmatrix} \bar{m}_{11} & 0 \\ 0 & \bar{m}_{22} \end{bmatrix}, \\
&\bar{\mathbf{C}} = \bar{\mathbf{M}}^{-1}\mathbf{B}^{-1}\mathbf{C}(\dot{\boldsymbol{q}})\mathbf{B} = \begin{bmatrix} \frac{bc}{(m_{11}+m_{12})} & 0 \\ 0 & \frac{c}{b(m_{11}-m_{12})} \end{bmatrix} =: \begin{bmatrix} \bar{c}_1 & 0 \\ 0 & \bar{c}_2 \end{bmatrix}, \\
&\bar{\mathbf{D}} = \bar{\mathbf{M}}^{-1}\mathbf{B}^{-1}\mathbf{D}\mathbf{B} = \begin{bmatrix} \frac{(d_{11}+d_{22})}{2(m_{11}+m_{12})} & \frac{b(d_{11}-d_{22})}{2(m_{11}+m_{12})} \\ \frac{(d_{11}-d_{22})}{2b(m_{11}-m_{12})} & \frac{(d_{11}+d_{22})}{2(m_{11}-m_{12})} \end{bmatrix} =: \begin{bmatrix} \bar{d}_{11} & \bar{d}_{12} \\ \bar{d}_{21} & \bar{d}_{22} \end{bmatrix}, \\
&\bar{\mathbf{B}} = \bar{\mathbf{M}}^{-1}\mathbf{B}^{-1} = \begin{bmatrix} \frac{r}{2(m_{11}+m_{12})} & \frac{r}{2(m_{11}+m_{12})} \\ \frac{r}{2b(m_{11}-m_{12})} & \frac{-r}{2b(m_{11}-m_{12})} \end{bmatrix} =: \begin{bmatrix} \bar{b}_{11} & \bar{b}_{12} \\ \bar{b}_{21} & \bar{b}_{22} \end{bmatrix}.
\end{aligned}
\tag{2.51}
$$

Properties of the dynamic equation of motion

Note that the WMR dynamics is under-actuated, see (2.41) and (2.50), since there are three inputs in terms of generalized coordinates $\boldsymbol{q} = \begin{bmatrix} x & y & \phi \end{bmatrix}^T$, whereas there are only two actual control inputs applied to the left and right wheels of the WMR, $\boldsymbol{\tau} = \begin{bmatrix} \tau_v & \tau_\omega \end{bmatrix}^T$.
The WMR dynamics enjoys the following properties [17, 39, 155]:

- $\mathbf{M}$ is symmetric and positive definite matrix.
- $\mathbf{M}$ is bounded by positive constants, i.e., $m_1 \leq \|\mathbf{M}\| \leq m_2$.
- $\dot{\mathbf{M}} - 2\mathbf{C}$ is a skew-symmetric matrix.

2.3 Motion planning of the WMR

This section describes briefly control problems for a WMR moving on the plane. While path planning problem in robotics covers a large range, this research only concentrates on two matters of the WMR's workspace: fully structured environment and partially unstructured environment. In the first issue, the path is fully known by a reference path/trajectory. Hence, the task is to generate motion control algorithms for a WMR to approach the reference path/trajectory and reach

to its designed destination. In the second issue, the reference is also predefined. However, the workspace is not fully known in advance, i.e., obstacles exist within the area. The WMR is required to avoid colliding with obstacles while it still keeps tracking the reference.

2.3.1 Motion control

At first, the consideration is restricted to the obstacle-free workspace. Reference trajectory/path and final destination are predefined. Based on the classification in [13, 48, 156], control designs will deal with three basic classes of problems.

- *Point-to-point stabilization:* The vehicle must reach the desired goal configuration starting from a given initial configuration.
- *Trajectory tracking:* In this task, the vehicle is forced to reach and follow a time parameterized reference trajectory in the Cartesian space starting from a given initial configuration (on or off the trajectory). The work can be considered as a tracking task of an actual vehicle and a virtual moving reference vehicle.
- *Path following:* The task is relaxed to be a variant of the standard *Trajectory tracking*, in which the virtual reference vehicle is not necessarily provided. The primary control objective is that the controller forces the vehicle's heading angle to steer it along to a predefined geometric path at desired speed profile without a timing law of motion.

2.3.2 Potential field method

As obstacles exist in the workspace, the path planning problem needs to be solved. In particular, the WMR must have a capability to avoid collision with the obstacles while it still keeps the ultimate objective of following its reference path/trajectory and reaching its destination. There has been plenty of noticeable techniques for solving this problem for different purposes in the literature. Those are Road maps, i.e., Voronoi diagram [109, 157], Cell decomposition [109], Potential fields [109, 113, 114, 158], Vector field histograms [159, 160] to name a few. Readers are advised to refer to mentioned documents and reference therein for further interests. This research only aims to adopt one of these effective methods for the control objective. The potential field method intends to facilitate goal

convergence and obstacle avoidance for the WMR in a static or dynamic environment. The principal idea of the potential field method is that the workspace of the WMR is filled with an artificial potential field in which the vehicle is attracted to its goal location and is repulsed away from the obstacles [109, 113, 159].
Originally, the formulation of artificial potential fields was proposed in [108]. Based on this idea, other works have been developed [2, 113, 116, 125, 126, 161] with notable improvements and contributions. In general, the main ideas of this method can be represented mathematically as follows

$$\mathbf{U}(\boldsymbol{q}) = \mathbf{U}_{att}(\boldsymbol{q}) + \mathbf{U}_{rep}(\boldsymbol{q}), \tag{2.52}$$

where $\mathbf{U}(\boldsymbol{q})$ is the total potential field; $\mathbf{U}_{att}(\boldsymbol{q})$ is the attractive potential field, and $\mathbf{U}_{rep}(\boldsymbol{q})$ is the repulsive potential field. They are differentiable real-valued functions and their values can be considered as energy. Hence gradients of these potential functions are forces. Then the potential forces can be calculated by

$$\mathbf{F}(\boldsymbol{q}) = \mathbf{F}_{att}(\boldsymbol{q}) + \mathbf{F}_{rep}(\boldsymbol{q}), \tag{2.53}$$

where gradients of each potential field components are respective forces $\mathbf{F}(\boldsymbol{q}) = -\nabla\mathbf{U}(\boldsymbol{q})$, $\mathbf{F}_{att}(\boldsymbol{q}) = -\nabla\mathbf{U}_{att}(\boldsymbol{q})$, $\mathbf{F}_{rep}(\boldsymbol{q}) = -\nabla\mathbf{U}_{rep}(\boldsymbol{q})$. The attractive force $\mathbf{F}_{att}(\boldsymbol{q})$ tends to drive the vehicle to the target position. It should be monotonically increasing with relative distance from the destination. Meanwhile, the repulsive force $\mathbf{F}_{rep}(\boldsymbol{q})$ tends to push it away from the obstacles. The strength of the repulsive force depends on the vehicle's proximity to the obstacle. The closer the vehicle is to an obstacle, the stronger the repulsive force should be. This idea plays a key role when one chooses a suitable repulsive potential function which is usually defined in terms of the relative distance between the vehicle and the closest obstacle. The combination of attractive and repulsive forces drives the WMR from the starting point to the destination while it is capable of avoiding obstacles [154].

2.3.3 Odometric localization

The implementation of proposed feedback controllers requires the availability of the WMR configuration at each instant time. Normally, the WMR is equipped with incremental encoders that measure the rotation of the two wheels instead of position and orientation of the vehicle while these two types of variables are controlled in control algorithms. Therefore, it is necessary to devise a localization

procedure that estimates in real-time the WMR configuration.

Assume that at the sampling time t_k, the robot configuration $\boldsymbol{q}(t_k) = \boldsymbol{q}_k$ is known. Incremental encoders measure angular displacements of the right wheel, $\Delta\phi_R$, and the left wheel, $\Delta\phi_L$, during the sampling time interval $T_s = t_{k+1} - t_k$. Then the linear and angular displacements are calculated by [13]

$$\begin{aligned} \Delta s &= \frac{r}{2}(\Delta\phi_R + \Delta\phi_L) \\ \Delta\phi &= \frac{r}{d}(\Delta\phi_R - \Delta\phi_L) \end{aligned} \tag{2.54}$$

Values of linear velocity v_k and angular velocity ω_k can be reconstructed as

$$v_k = \frac{\Delta s}{T_s}, \qquad \omega_k = \frac{\Delta\phi}{T_s} \tag{2.55}$$

As a result, the value of the configuration variables $\boldsymbol{q}_{k+1}$ at the sample time t_{k+1} can be obtained by applying the Euler method for numerical integration of the kinematic model [13, 162]

$$\begin{aligned} x_{k+1} &= x_k + v_k T_s \cos(\phi_k), \\ y_{k+1} &= y_k + v_k T_s \sin(\phi_k), \\ \phi_{k+1} &= \phi_k + \omega_k T_s. \end{aligned} \tag{2.56}$$

2.4 Conclusions

Related concepts, mathematical tools, and control techniques that will be applied throughout this research are covered in this chapter. Some preliminary results are also included. The WMR dynamics model is constructed as a preparation of control design tasks in subsequent chapters. While the path planning problem dealing with obstacles in robotics covers a large range, only the potential field is focused on as a particular interest in this research.

Chapter 3

State-feedback path-following control design using level curve approach

The purpose of this chapter is to formulate a new global state-feedback control algorithm for the path-following problem of the WMR. The control design algorithm relies on the level curve approach reported in [88], Lyapunov's direct method [57], and the standard backstepping technique [58]. Under certain assumptions, the proposed control scheme forces the position of the dynamic model of a WMR to satisfy the reference path's equation and to move along the path at a desired linear velocity. The designed controllers ensure the error between actual and reference paths, and that of position and heading angle globally asymptotically converge to zero. Virtual controls and torque control inputs driving the WMR are guaranteed to be bounded. Results are supported through rigorous Lyapunov-based stability analysis, numerical demonstrations and experiments.

3.1 Problem statement

3.1.1 Mobile robot dynamics

To facilitate the subsequent control development and stability analysis, the mathematical model of a WMR moving in the Cartesian space is considered. This model is combined with kinematic and dynamic models (2.41), (2.50), respec-

tively, developed in Chapter 2:

$$\begin{cases} \dot{x} = v\cos(\phi) \\ \dot{y} = v\sin(\phi) \\ \dot{\phi} = \omega \end{cases}, \tag{3.1}$$
$$\begin{bmatrix} \dot{v} \\ \dot{\omega} \end{bmatrix} = \bar{\mathbf{C}} \begin{bmatrix} \omega^2 \\ -v\omega \end{bmatrix} - \bar{\mathbf{D}} \begin{bmatrix} v \\ \omega \end{bmatrix} + \bar{\mathbf{B}}\boldsymbol{\tau},$$

where matrices $\bar{\mathbf{C}}$, $\bar{\mathbf{D}}$ and $\bar{\mathbf{B}}$ are described by (2.51) in Chapter 2.

3.1.2 Control objective

For the concerns of particular level curve approach, the following assumptions on the reference path and measurements of the WMR's state variables are stated. These assumptions will simplify the control design and associated stability analysis.

Assumption 3.1.1

The reference path is described by the equation:

$$y_d = -f(x_d), \tag{3.2}$$

where $f(x_d)$ is an analytical single-valued function of x_d, and is differentiable with respect to x_d three times, and satisfies the following conditions for all $x_d \in \mathbb{R}$:

$$|f_{x_d}| \leq L_1, \quad |f_{x_d x_d}| \leq L_2, \quad |f_{x_d x_d x_d}| \leq L_3, \tag{3.3}$$

where $f_{x_d} = \frac{\partial f(x_d)}{\partial x_d}$, $f_{x_d x_d} = \frac{\partial^2 f(x_d)}{\partial x_d^2}$, $f_{x_d x_d x_d} = \frac{\partial^3 f(x_d)}{\partial x_d^3}$, and L_1, L_2, and L_3 are nonnegative constants. Moreover, $f(x_d)$, $f_{x_d}(x_d)$, $f_{x_d x_d}(x_d)$, and $f_{x_d x_d x_d}(x_d)$ are bounded if their argument x_d is bounded.

Assumption 3.1.2

There exist strictly positive constants ϵ_1, ϵ_2, and ϵ_3 such that the desired linear velocity $v_d(t)$ is at least two times differentiable with respect to t and its the first and second derivatives $\dot{v}_d(t)$, $\ddot{v}_d(t)$ are bounded.

$$|v_d(t)| \leq \epsilon_1 := v_M, \quad |\dot{v}_d(t)| \leq \epsilon_2, \quad |\ddot{v}_d(t)| \leq \epsilon_3, \qquad \forall t \geq 0. \tag{3.4}$$

In addition, $v_d(t)$ does not converge to zero, i.e., velocity $v_d(t)$ satisfies the following PE conditions (3.4) and (3.5) in Assumption 3.1.2.

$$\lim_{t\to\infty} v_d^2(t) \neq 0. \tag{3.5}$$

Assumption 3.1.3

All physical state variables of the WMR are measurable for feedback.

Remark. 1. According to [1], the equation of reference path (3.2) satisfying two first conditions in (3.3) covers various paths in practice, including straight, sinusoidal, and polynomial paths. However, the author has clarified that the reference path equation (3.2) might not include closed paths such as a circular path and the paths with $f(x_d)$ described a fractional polynomial of x_d, for example $y_d = 1/x_d^2$. In case a close reference path must be addressed, individual sub-paths, which are separated from the close path, can be considered provided that each sub-path satisfies the equation (3.2) and the two conditions. Together conditions with respect to the reference path in (3.2) and its derivatives are imposed by [1], an additional assumption of $|f_{x_d x_d x_d}| \leq L_3$ is made in (3.3). Thus, they hold for a class of reference paths covering linear, circular, sinusoidal paths, and their combination. In particular, boundedness of the virtual control in (3.27), and other parts in (3.32) are guaranteed under Assumption 3.1.1. Hence, the goal in (3.7) can be achieved for a certain class of reference paths. Readers are advised to see the Remark 2.1 in [1] for further discussion on the reference path.

2. The scope of this research aims to investigate the path-following problem solely. Therefore, condition (3.5) on the desired linear velocity $v_d(t)$ makes the solution of the path-following problem feasible. This also implies the stabilization problem not to be included.

3. The desired angular velocity ω_d is derived from the reference heading angle ϕ_d,

$$\begin{aligned} \phi_d &= \arctan(f_{x_d}), \\ \omega_d &= \dot{\phi}_d = \frac{1}{1 + f_{x_d}^2} f_{x_d x_d} \dot{x}_d. \end{aligned} \tag{3.6}$$

Control objective

Under assumptions made above, a proper control input vector $\boldsymbol{\tau} = \begin{bmatrix} \tau_v & \tau_\omega \end{bmatrix}^T$ is designed for the dynamics model given by (3.1) such that the controllers drive

the current position of the WMR to follow asymptotically to a position on a reference path and to force the WMR to move along the path tangentially at a desired linear velocity $v_d(t)$. Also, virtual controls and torque control inputs are bounded by constants. The overall control objective can be described as follows:

$$\begin{aligned} &\lim_{t\to\infty} \|\Gamma(x(t), y(t)) - \Gamma(x_d(t), y_d(t))\| = 0, \\ &|\tau_v(t)| \leq \tau_{vM}, \quad |\tau_\omega(t)| \leq \tau_{\omega M} \quad \forall t \geq t_0, \end{aligned} \tag{3.7}$$

where $\Gamma(x_d(t), y_d(t))$ and $\Gamma(x(t), y(t))$ are defined below by (3.8) and (3.10), respectively. τ_{vM} and $\tau_{\omega M}$ are strictly positive constants denoted for maximum values of torque control inputs.

3.2 Control design

3.2.1 Level curve approach

To facilitate the control design, this section re-introduces the level curve approach which has been recently developed in [1, 88, 133]. By defining

$$\Gamma(x_d, y_d) = y_d + f(x_d), \tag{3.8}$$

reference path equation (3.2) can be represented as follows

$$\Gamma(x_d, y_d) = 0. \tag{3.9}$$

Because of the assumption of $f(x_d)$ to be a single-valued function of x_d, it is obvious that coordinates of the current point (x, y) are not equal to those of a reference point (x_d, y_d) if the function $\Gamma(x, y)$ is not equal to zero, see (3.8) and (3.9). As can be seen from figure 3.1 that the reference path lies in the $O_E X_E Y_E$ plane so $\Gamma(x_d, y_d) = 0$, i.e., the equation (3.9) holds. The point $O_b(x, y)$, which is on the real trajectory of the WMR, will tend to the desired point $O_d(x_d, y_d)$ on the reference path, i.e., $\Gamma(x_d, y_d) = 0$, if

$$\Gamma(x, y) = y + f(x) \tag{3.10}$$

goes to zero. As a result, the control objective becomes to designing control inputs so that $\Gamma(x, y)$ globally asymptotically goes to zero, and the WMR moves along the path tangentially at the desired linear velocity $v_d(t)$ [1].

The kinematic model (3.1) of the WMR system is of a cascade system, which offers a procedure of designing the control input vector $\mathbf{v} = \begin{bmatrix} v & \omega \end{bmatrix}^T$ in two steps.

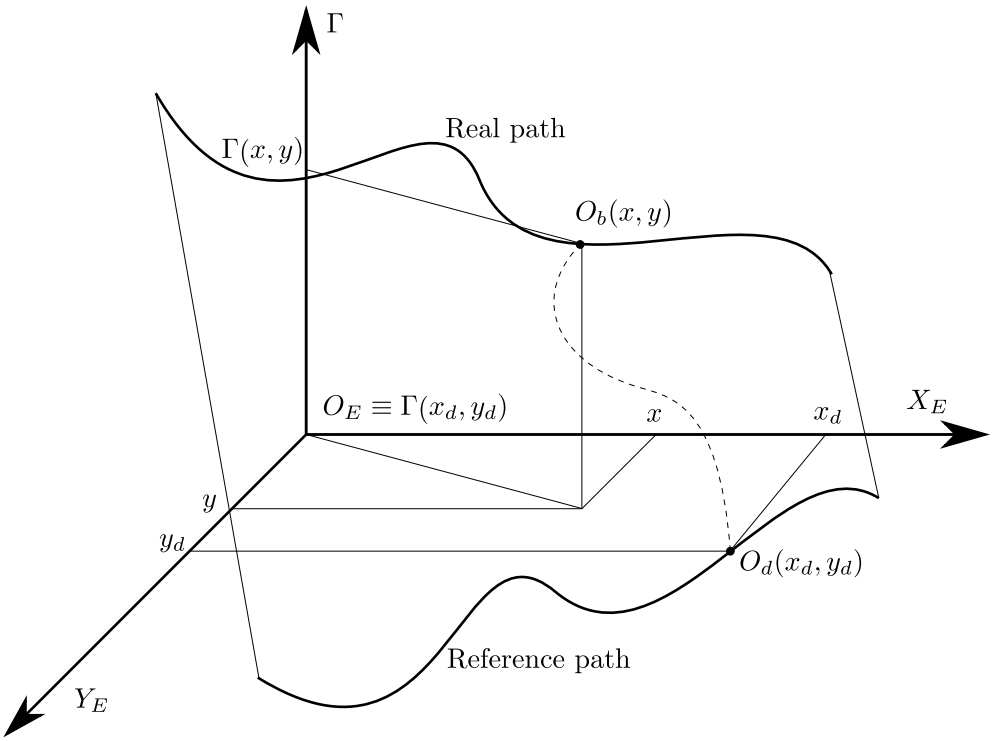

Figure 3.1: Illustration of the level curve approach [1]

Firstly, the virtual control α_ϕ, in the representation of heading angle $\phi = \phi_e + \alpha_\phi$, will be designed to stabilize $\Gamma(x, y)$ at the origin, where ϕ_e is an error between ϕ and α_ϕ. Next, the angular velocity is written as $\omega = \omega_e + \alpha_\omega$, where α_w is referred to as the virtual control of ω, and ω_e is an error between ω and α_ω. Stabilization of ϕ_e at the origin can be achieved by designing α_ω.

3.2.2 Design step 1

Followed by the work of the authors in [1], this chapter aims to design a global state-feedback path-following controller at the dynamic level. While the design procedure in this step is similar to that in [1], the difference is the choice of the virtual control α_ϕ, as represented below in (3.18). Firstly, error variables v_e and ϕ_e are defined as follows

$$\begin{aligned} v_e &= v - v_d, \\ \phi_e &= \phi - \alpha_\phi. \end{aligned} \tag{3.11}$$

The virtual control α_ϕ is designed in this step by taking the time derivative both sides of (3.10) along the solutions of (3.1) and using the representation of (3.11) to result in

$$\dot{\Gamma}(x, y) = \dot{y} + f_x \dot{x} = v\big(f_x \cos(\phi) + \sin(\phi)\big),$$

$$= v_d\Big[f_x\cos(\alpha_\phi)+\sin(\alpha_\phi)\Big] + f_x\Omega_{11} + \Omega_{12} + v_e\big(f_x\cos(\phi)+\sin(\phi)\big), \tag{3.12}$$

where, f_x, Ω_{11} and Ω_{12} have been denoted as

$$\begin{aligned} f_x &= \frac{\partial f(x)}{\partial x}, \\ \Omega_{11} &= v_d\Big((\cos(\phi_e)-1)\cos(\alpha_\phi) - \sin(\alpha_\phi)\sin(\phi_e)\Big), \\ \Omega_{12} &= v_d\Big((\cos(\phi_e)-1)\sin(\alpha_\phi) + \cos(\alpha_\phi)\sin(\phi_e)\Big). \end{aligned} \tag{3.13}$$

It is important to note that the arrangement of Ω_{11} and Ω_{12} guarantees the boundedness of themselves with respect to their variables. To design the virtual control α_ϕ that can globally and asymptotically stabilize $\Gamma(x,y)$ at the origin based on the Lyapunov's direct method, the following Lyapunov function candidate is considered

$$V_1 = \sqrt{1+\Gamma^2(x,y)} - 1, \tag{3.14}$$

which is positive definite and radially unbounded in $\Gamma(x,y)$, and equal to zero when $\Gamma(x,y)=0$. Then the time derivative of V_1 along the solutions of (3.12) is given by

$$\begin{aligned} \dot{V}_1 = {} & \frac{\Gamma}{\sqrt{1+\Gamma^2}} v_d\sqrt{1+f_x^2}\Big(\frac{f_x}{\sqrt{1+f_x^2}}\cos(\alpha_\phi) + \frac{f_x}{\sqrt{1+f_x^2}}\sin(\alpha_\phi)\Big) \\ & + \frac{\Gamma}{\sqrt{1+\Gamma^2}}\big(f_x\Omega_{11}+\Omega_{12}\big) + \frac{\Gamma}{\sqrt{1+\Gamma^2}} v_e\big(f_x\cos(\phi)+\sin(\phi)\big). \end{aligned} \tag{3.15}$$

Now defining $\sin(\delta) = \frac{f_x}{\sqrt{1+f_x^2}}$ and $\cos(\delta) = \frac{1}{\sqrt{1+f_x^2}}$, then δ is obtained by

$$\delta = \arctan(f_x). \tag{3.16}$$

Substituting denotations of $\sin(\delta)$ and $\cos(\delta)$ into (3.15) yields

$$\begin{aligned} \dot{V}_1 = {} & \frac{\Gamma}{\sqrt{1+\Gamma^2}} v_d\sqrt{1+f_x^2}\big(\sin(\alpha_\phi)+\delta\big) \\ & + \frac{\Gamma}{\sqrt{1+\Gamma^2}}\big(f_x\Omega_{11}+\Omega_{12}\big) + \frac{\Gamma}{\sqrt{1+\Gamma^2}} v_e\big(f_x\cos(\phi)+\sin(\phi)\big). \end{aligned} \tag{3.17}$$

From (3.17), the virtual control α_ϕ is chosen by

$$\alpha_\phi = \arcsin\big(-\frac{k_1 v_d\Gamma}{\sqrt{1+f_x^2}\sqrt{1+k_1^2 v_d^2\Gamma^2}}\big) - \delta, \tag{3.18}$$

where k_1 is a positive constant. It is clearly seen that the value of α_ϕ is well-defined for all $(v_d, f_x, \Gamma) \in \mathbb{R}^2$, i.e., $-1 \le \arcsin(\bullet) \le 1$. The angle δ is the angle between the curve $y=-f(x)$ and the O_EX_E axis. Therefore, the WMR

approaches the reference path and moves along the path tangentially at desired linear velocity v_d provided that our proposed controllers ensure convergence of $\phi_e(t), v_e(t)$, and $\Gamma(x(t), y(t))$ to zero [1]. Substituting (3.18) into (3.17) gives

$$\dot{V}_1 = -\frac{k_1 v_d^2 \Gamma^2}{\sqrt{1+\Gamma^2}\sqrt{1+k_1^2 v_d^2 \Gamma^2}} + \frac{\Gamma}{\sqrt{1+\Gamma^2}}\big(f_x \Omega_{11} + \Omega_{12}\big) + v_e \Psi_{11}, \tag{3.19}$$

where, Ψ_{11} has been denoted as

$$\Psi_{11} = \frac{\Gamma}{\sqrt{1+\Gamma^2}}\big(f_x \cos(\phi) + \sin(\phi)\big). \tag{3.20}$$

This equation will be used in the next step so that the second term will be canceled out. On the other hand, substituting (3.18) into (3.12) results in

$$\dot{\Gamma}(x,y) = -\frac{k_1 v_d^2 \Gamma}{\sqrt{1+k_1^2 v_d^2 \Gamma^2}} + f_x \Omega_{11} + \Omega_{12} + v_e\big(f_x \cos(\phi) + \sin(\phi)\big). \tag{3.21}$$

3.2.3 Design step 2

As can be seen from (3.18) that α_ϕ is a smooth function of Γ, v_d, and f_x, differentiating both sides of the second equation in (3.11) along the solutions of (3.1) and (3.12) yields

$$\begin{aligned}\dot{\phi}_e = \omega - v_d\Big[\frac{\partial \alpha_\phi}{\partial \Gamma}\big(f_x \cos(\phi) + \sin(\phi)\big) + \frac{\partial \alpha_\phi}{\partial f_x} f_{xx} \cos(\phi)\Big] - \frac{\partial \alpha_\phi}{\partial v_d}\dot{v}_d \\ - v_e\Big[\frac{\partial \alpha_\phi}{\partial \Gamma}\big(f_x \cos(\phi) + \sin(\phi)\big) + \frac{\partial \alpha_\phi}{\partial f_x} f_{xx} \cos(\phi)\Big],\end{aligned} \tag{3.22}$$

where $f_{xx} = \frac{\partial^2 f}{\partial x^2}$ is the second order partial derivative of f with respect to x. To stabilize ϕ_e at the origin, the virtual control α_ω is defined by

$$\omega_e = \omega - \alpha_\omega. \tag{3.23}$$

Next, the following Lyapunov function candidate is considered

$$V_2 = V_1 + \frac{1}{2}\phi_e^2, \tag{3.24}$$

which is positive definite and radially unbounded in $(\Gamma(x,y), \phi_e)$, see (3.14) for the details of equation V_1, and is equal to zero when $\Gamma(x,y) = 0$ and $\phi_e = 0$. After taking the time derivative both sides of (3.24) along the solutions of (3.19), (3.22), the following expression is obtained

$$\begin{aligned}\dot{V}_2 = -\frac{k_1 v_d^2 \Gamma^2}{\sqrt{1+\Gamma^2}\sqrt{1+k_1^2 v_d^2 \Gamma^2}} + \phi_e\Big[\frac{\Gamma\big(f_x \bar{\Omega}_{11} + \bar{\Omega}_{12}\big)}{\sqrt{1+\Gamma^2}} + \alpha_\omega \\ - v_d\Big(\frac{\partial \alpha_\phi}{\partial \Gamma}\big(f_x \cos(\phi) + \sin(\phi)\big) + \frac{\partial \alpha_\phi}{\partial f_x} f_{xx} \cos(\phi)\Big) - \frac{\partial \alpha_\phi}{\partial v_d}\dot{v}_d\Big]\end{aligned}$$

$$+ v_e\Psi_{12} + \omega_e\Psi_{22}, \tag{3.25}$$

where the denotations below have been used

$$\begin{aligned}\Psi_{12} &= \Psi_{11} - \Big(\frac{\partial\alpha_\phi}{\partial\Gamma}\big(f_x\cos(\phi)+\sin(\phi)\big) + \frac{\partial\alpha_\phi}{\partial f_x}f_{xx}\cos(\phi)\Big)\phi_e,\\ \Psi_{22} &= \phi_e.\end{aligned} \tag{3.26}$$

From the definition of Ω_{11} and Ω_{12} in (3.13), it shows that $\sin(\phi_e)/\phi_e = \int_0^1 \cos(s\phi_e)ds$ and $(\cos(\phi_e)-1)/\phi_e = -\int_0^1 \sin(s\phi_e)ds$ are smooth for all $\phi_e \in \mathbb{R}$. Hence, the terms $\bar{\Omega}_{11} = \Omega_{11}/\phi_e$ and $\bar{\Omega}_{12} = \Omega_{12}/\phi_e$ in (3.25) are well-defined [3, 22]. Hence, the virtual control α_ω in (3.25) is chosen by

$$\begin{aligned}\alpha_\omega = -k_2\frac{\phi_e}{\sqrt{1+\phi_e^2}} - \frac{\Gamma\big(f_x\bar{\Omega}_{11}+\bar{\Omega}_{12}\big)}{\sqrt{1+\Gamma^2}} + v_d\Big(\frac{\partial\alpha_\phi}{\partial\Gamma}\big(f_x\cos(\phi)+\sin(\phi)\big)\\ + \frac{\partial\alpha_\phi}{\partial f_x}f_{xx}\cos(\phi)\Big) + \frac{\partial\alpha_\phi}{\partial v_d}\dot{v}_d,\end{aligned} \tag{3.27}$$

where k_2 is a positive constant. Now substituting (3.27) into (3.25) gives

$$\dot{V}_2 = -\frac{k_1 v_d^2\Gamma^2}{\sqrt{1+\Gamma^2}\sqrt{1+k_1^2v_d^2\Gamma^2}} - \frac{k_2\phi_e^2}{1+\phi_e^2} + v_e\Psi_{12} + \omega_e\Psi_{22}. \tag{3.28}$$

It can be clearly seen from this equation that if the linear velocity $v_e = 0$ and the angular velocity $\omega_e = 0$, i.e., to be considered as actual controls at kinematic level, $(\Gamma(x,y),\phi_e)$ are globally and asymptotically stable at the origin. From the control design above, the closed-loop system for the WMR at this stage can be rewritten by substituting the equations of (3.11) into the first and the second equations in (3.1), and (3.27), (3.23) into (3.22) as follows

$$\begin{aligned}\dot{x} &= (v_e+v_d)\cos(\phi_e+\alpha_\phi),\\ \dot{y} &= (v_e+v_d)\sin(\phi_e+\alpha_\phi),\\ \dot{\phi}_e &= -k_2\frac{\phi_e}{\sqrt{1+\phi_e^2}} - \frac{\Gamma}{\sqrt{1+\Gamma^2}}\big(f_x\bar{\Omega}_{11}+\bar{\Omega}_{12}\big) + \omega_e\\ &\quad - v_e\Big[\frac{\partial\alpha_\phi}{\partial\Gamma}\big(f_x\cos(\phi)+\sin(\phi)\big) + \frac{\partial\alpha_\phi}{\partial f_x}f_{xx}\cos(\phi)\Big].\end{aligned} \tag{3.29}$$

3.2.4 Design step 3

It can be seen from (3.27) that α_ω is a smooth function of $(v_d, \dot{v}_d, \Gamma, \phi, f_x, f_{xx})$. Therefore, taking differentiation both sides of the first equation of (3.11) and (3.23) gives

$$\begin{aligned}\dot{v}_e &= \dot{v} - \dot{v}_d,\\ \dot{\omega}_e &= \dot{\omega} - \dot{\alpha}_\omega.\end{aligned} \tag{3.30}$$

Substituting those equations of (3.30) into the last equation of (3.1) to achieve the following expression

$$\begin{bmatrix}\dot{v}_e\\ \dot{\omega}_e\end{bmatrix} = \bar{\mathbf{C}}\begin{bmatrix}\omega^2\\ -v\omega\end{bmatrix} - \bar{\mathbf{D}}\begin{bmatrix}v\\ \omega\end{bmatrix} + \bar{\mathbf{B}}\boldsymbol{\tau} - \begin{bmatrix}\Delta_1\\ \Delta_2\end{bmatrix}, \tag{3.31}$$

with $\Delta = [\Delta_1, \Delta_2]^T$ and $\Delta_2 = \Delta_{21} + \Delta_{22}$, and they have been denoted by

$$\begin{aligned}
\Delta_1 &= \dot{v}_d\\
\Delta_{21} &= v_d\Big[\frac{\partial \alpha_\omega}{\partial \Gamma}\big(f_x\cos(\phi)+\sin(\phi)\big) + \frac{\partial \alpha_\omega}{\partial f_x}f_{xx}\cos(\phi) + \frac{\partial \alpha_\omega}{\partial f_{xx}}f_{xxx}\cos(\phi)\Big]\\
&\quad + \frac{\partial \alpha_\omega}{\partial v_d}\dot{v}_d + \frac{\partial \alpha_\omega}{\partial \dot{v}_d}\ddot{v}_d + \frac{\partial \alpha_\omega}{\partial \phi}\alpha_\omega,\\
\Delta_{22} &= v_e\Big[\frac{\partial \alpha_\omega}{\partial \Gamma}\big(f_x\cos(\phi)+\sin(\phi)\big) + \frac{\partial \alpha_\omega}{\partial f_x}f_{xx}\cos(\phi) + \frac{\partial \alpha_\omega}{\partial f_{xx}}f_{xxx}\cos(\phi)\Big]\\
&\quad + \frac{\partial \alpha_\omega}{\partial \phi}\omega_e.
\end{aligned} \tag{3.32}$$

To design the actual control input torques $\boldsymbol{\tau} = \begin{bmatrix}\tau_v & \tau_\omega\end{bmatrix}^T$ applied to the wheels, the following Lyapunov function candidate is considered

$$V_3 = V_2 + \frac{1}{2}\begin{bmatrix}v_e & \omega_e\end{bmatrix}\bar{\mathbf{C}}^{-\mathbf{1}}\begin{bmatrix}v_e\\ \omega_e\end{bmatrix}, \tag{3.33}$$

which is positive definite and radially unbounded in $(\Gamma(x,y), \phi_e, v_e, \omega_e)$, see (3.14) and (3.24) for the equations of V_1 and V_2, respectively. After differentiating both sides of (3.33) along the solutions of (3.28) and (3.31), the following expression can be achieved

$$\begin{aligned}
\dot{V}_3 = &-\frac{k_1 v_d^2\Gamma^2}{\sqrt{1+\Gamma^2}\sqrt{1+k_1^2 v_d^2\Gamma^2}} - \frac{k_2\phi_e^2}{1+\phi_e^2} + \begin{bmatrix}v_e & \omega_e\end{bmatrix}\bar{\mathbf{C}}^{-\mathbf{1}}\Bigg\{\bar{\mathbf{C}}\begin{bmatrix}\omega^2\\ -v\omega\end{bmatrix}\\
&- \bar{\mathbf{D}}\begin{bmatrix}v\\ \omega\end{bmatrix} + \bar{\mathbf{B}}\boldsymbol{\tau} - \begin{bmatrix}\Delta_1\\ \Delta_2\end{bmatrix} + \bar{\mathbf{C}}\begin{bmatrix}\Psi_{12}\\ \Psi_{22}\end{bmatrix}\Bigg\},
\end{aligned} \tag{3.34}$$

see (3.20) and (3.26) for the details of Ψ_{12} and Ψ_{22}. For the convenience of calculation, $\dot{V}_3$ can be rearranged as

$$\dot{V}_3 = -\frac{k_1 v_d^2\Gamma^2}{\sqrt{1+\Gamma^2}\sqrt{1+k_1^2 v_d^2\Gamma^2}} - \frac{k_2\phi_e^2}{1+\phi_e^2} + \Pi_1 + \Pi_2, \tag{3.35}$$

where, Π_1 and Π_2 have been denoted for

$$\begin{aligned}
\Pi_1 = v_e\bar{c}_1^{-1}\dot{v}_e &= v_e\omega_e^2 + 2\alpha_\omega v_e\omega_e + \alpha_\omega^2 v_e - \bar{\bar{d}}_{11}v_e^2 - \bar{\bar{d}}_{11}v_d v_e - \bar{\bar{d}}_{12}v_e\omega_e - \bar{\bar{d}}_{12}\alpha_\omega v_e\\
&\quad - \frac{1}{\bar{c}_1}v_e\Delta_1 + v_e\Psi_{12} + \bar{\bar{b}}_{11}\tau_v v_e + \bar{\bar{b}}_{12}\tau_\omega v_e,
\end{aligned} \tag{3.36}$$

$$\Pi_2 = \omega_e \bar{c}_2^{-1}\dot{\omega}_e = -v_e\omega_e^2 - v_d\omega_e^2 - \alpha_\omega v_e\omega_e - v_d\alpha_\omega\omega_e - \bar{\bar{d}}_{21}v_e\omega_e - \bar{\bar{d}}_{21}v_d\omega_e - \bar{\bar{d}}_{22}\omega_e^2$$
$$- \bar{\bar{d}}_{22}\alpha_\omega\omega_e - \frac{1}{\bar{c}_2}\omega_e(\Delta_{21}+\Delta_{22}) + \omega_e\Psi_{22} + \bar{\bar{b}}_{21}\tau_v\omega_e + \bar{\bar{b}}_{22}\tau_\omega\omega_e, \tag{3.37}$$

In these equations (3.36) and (3.37), coefficients are denoted as follows: $\bar{\bar{d}}_{11} = \frac{\bar{d}_{11}}{\bar{c}_1}; \bar{\bar{d}}_{12} = \frac{\bar{d}_{12}}{\bar{c}_1}; \bar{\bar{b}}_{11} = \frac{\bar{b}_{11}}{\bar{c}_1}; \bar{\bar{b}}_{12} = \frac{\bar{b}_{12}}{\bar{c}_1}; \bar{\bar{d}}_{21} = \frac{\bar{d}_{21}}{\bar{c}_2}; \bar{\bar{d}}_{22} = \frac{\bar{d}_{22}}{\bar{c}_2}; \bar{\bar{b}}_{21} = \frac{\bar{b}_{21}}{\bar{c}_2}; \bar{\bar{b}}_{22} = \frac{\bar{b}_{22}}{\bar{c}_2}$.
Regarding some coupling terms in (3.32), (3.36) and (3.37), we apply the Young's inequality represented in Chapter 2 to yield

$$\begin{aligned}
\frac{\mu}{\bar{c}_2}v_e\omega_e &\le \frac{|\mu|}{\bar{c}_2}\big(\kappa v_e^2 + \frac{1}{4\kappa}\omega_e^2\big)\\
\alpha_\omega v_e\omega_e &\le 2|\alpha_\omega|\big(\kappa v_e^2 + \frac{1}{2}\omega_e^2\big),\\
(\bar{\bar{d}}_{12}+\bar{\bar{d}}_{21})v_e\omega_e &\le \bar{\bar{d}}_{12}\big(\kappa v_e^2 + \frac{1}{4\kappa}\omega_e^2\big),
\end{aligned} \tag{3.38}$$

where, κ is a positive constant and $\mu = \Big[\frac{\partial\alpha_\omega}{\partial\Gamma}\big(f_x\cos(\phi)+\sin(\phi)\big) + \frac{\partial\alpha_\omega}{\partial f_x}f_{xx}\cos(\phi) + \frac{\partial\alpha_\omega}{\partial f_{xx}}f_{xxx}\cos(\phi)\Big]$. After substituting results of (3.38) back into (3.32), (3.36), and (3.37) and then into (3.35), the following expression is achieved

$$\begin{aligned}
\dot{V}_3 \le &-\frac{k_1 v_d^2\Gamma^2}{\sqrt{1+\phi_e^2}\sqrt{1+\Gamma^2}\sqrt{1+k_1^2v_d^2\Gamma^2}} - \frac{k_2\phi_e^2}{1+\phi_e^2}\\
&+ \Big[v_e\big(\Lambda_1 + (\bar{\bar{b}}_{11}\tau_v + \bar{\bar{b}}_{12}\tau_\omega)\big) + \omega_e\big(\Lambda_2 + (\bar{\bar{b}}_{21}\tau_v + \bar{\bar{b}}_{22}\tau_\omega)\big)\Big]\\
&- \Big[v_e^2\Lambda_3 + \omega_e^2\Lambda_4\Big],
\end{aligned} \tag{3.39}$$

where, the below denotations have been used

$$\begin{aligned}
\Lambda_1 &= \alpha_\omega^2 - \bar{\bar{d}}_{11}v_d - \bar{\bar{d}}_{12}\alpha_\omega - \frac{1}{\bar{c}_1}\Delta_1 + \Psi_{12},\\
\Lambda_2 &= -v_d\alpha_\omega - \bar{\bar{d}}_{21}v_d - \bar{\bar{d}}_{22}\alpha_\omega - \frac{1}{\bar{c}_2}\Delta_{21} + \Psi_{22},\\
\Lambda_3 &= \bar{\bar{d}}_{11} - |\alpha_\omega| - \frac{\bar{\bar{d}}_{12}}{2} - \frac{|\alpha_\omega|}{2} - \frac{\bar{\bar{d}}_{21}}{2} - \frac{|\mu|}{2\bar{c}_2},\\
\Lambda_4 &= |v_d| + \bar{\bar{d}}_{22} - |\alpha_\omega| - \frac{\bar{\bar{d}}_{12}}{2} - \frac{|\alpha_\omega|}{2} - \frac{\bar{\bar{d}}_{21}}{2} - \frac{|\mu|}{2\bar{c}_2} - \frac{1}{\bar{c}_2}\Big|\frac{\partial\alpha_\omega}{\partial\phi}\Big|.
\end{aligned} \tag{3.40}$$

It is straightforward to derive the conditions such that the terms Λ_3 and Λ_4 in (3.40) are nonnegative definite as follows

$$\begin{aligned}
\bar{\bar{d}}_{11} &\ge \frac{3}{2}|\alpha_\omega| + \frac{1}{2}(\bar{\bar{d}}_{12}+\bar{\bar{d}}_{21}) + \frac{|\mu|}{2\bar{c}_2},\\
|v_d| + \bar{\bar{d}}_{22} &\ge \frac{3}{2}|\alpha_\omega| + \frac{1}{2}(\bar{\bar{d}}_{12}+\bar{\bar{d}}_{21}) + \frac{|\mu|}{2\bar{c}_2} + \frac{1}{\bar{c}_2}\Big|\frac{\partial\alpha_\omega}{\partial\phi}\Big|,
\end{aligned} \tag{3.41}$$

where the upper bound of $|\alpha_\omega|$ in (3.27) is estimated by employing conditions (3.3), (3.4), and associated results calculated in (3.54), (3.55) and (3.56). Besides,

results of (3.57), (3.58), and (3.59) are used for upper bound estimation of $|\mu|$. The upper bound of $\left|\frac{\partial \alpha_\omega}{\partial \phi}\right|$ is estimated in (3.62). Hence, the following expression of upper bounds is obtained

$$\begin{aligned} |\alpha_\omega| &\leq k_2 + 2(L_1+1) + \epsilon_1\big(k_1\epsilon_1(L_1+1) + L_2\big) + k_1\epsilon_2 = \chi_1, \\ |\mu| &\leq 2(L_1+1)^2 + (2+k_1\epsilon_1^2)L_2\sqrt{1+L_1^2} + \epsilon_1 L_3(1+L_1^2) = \chi_2, \end{aligned} \tag{3.42}$$

where, χ_1 and χ_2 are positive constants. There always exist parameters ϵ_1, ϵ_2, k_1, k_2, L_1, L_2, and L_3 such that those conditions in (3.42) satisfied with $\bar{c}_1$, $\bar{c}_2$, $\bar{d}_{11}$, $\bar{d}_{12}$, $\bar{d}_{21}$, and $\bar{d}_{22}$ are defined in (2.51). Since the terms Λ_3 and Λ_4 are positive definite as long as conditions (3.38) and (3.42) hold. The actual torque control vector $\boldsymbol{\tau} = \begin{bmatrix} \tau_v & \tau_\omega \end{bmatrix}^T$ is chosen as follows

$$\begin{aligned} \tau_v &= \frac{-\bar{\bar{b}}_{22}}{\bar{\bar{b}}_{11}\bar{\bar{b}}_{22} - \bar{\bar{b}}_{12}\bar{\bar{b}}_{21}}\big(k_3\sigma(v_e) + \Lambda_1\big) + \frac{\bar{\bar{b}}_{12}}{\bar{\bar{b}}_{11}\bar{\bar{b}}_{22} - \bar{\bar{b}}_{12}\bar{\bar{b}}_{21}}\big(k_4\sigma(\omega_e) + \Lambda_2\big), \\ \tau_\omega &= \frac{\bar{\bar{b}}_{21}}{\bar{\bar{b}}_{11}\bar{\bar{b}}_{22} - \bar{\bar{b}}_{12}\bar{\bar{b}}_{21}}\big(k_3\sigma(v_e) + \Lambda_1\big) - \frac{\bar{\bar{b}}_{11}}{\bar{\bar{b}}_{11}\bar{\bar{b}}_{22} - \bar{\bar{b}}_{12}\bar{\bar{b}}_{21}}\big(k_4\sigma(\omega_e) + \Lambda_2\big). \end{aligned} \tag{3.43}$$

where k_3 and k_4 are positive constants. It can easily seen that actual controls τ_v and τ_ω are well-defined since:

$$\begin{aligned} \bar{\bar{\mathbf{B}}} &= \begin{bmatrix} \bar{c}_1^{-1} & 0 \\ 0 & \bar{c}_2^{-1} \end{bmatrix} \begin{bmatrix} \bar{b}_{11} & \bar{b}_{12} \\ \bar{b}_{21} & \bar{b}_{22} \end{bmatrix} = \begin{bmatrix} \bar{\bar{b}}_{11} & \bar{\bar{b}}_{12} \\ \bar{\bar{b}}_{21} & \bar{\bar{b}}_{22} \end{bmatrix}, \\ det(\bar{\bar{\mathbf{B}}}) &= \bar{\bar{b}}_{11}\bar{\bar{b}}_{22} - \bar{\bar{b}}_{12}\bar{\bar{b}}_{21} = -\frac{r^2}{2bc^2} \neq 0. \end{aligned} \tag{3.44}$$

where, all these terms $\bar{c}_1, \bar{c}_2, \bar{b}_{11}, \bar{b}_{12}, \bar{b}_{21}$ and $\bar{b}_{22}$ are defined in (2.51). Selection of control vector $\boldsymbol{\tau} = \begin{bmatrix} \tau_v & \tau_\omega \end{bmatrix}^T$ in (3.43) turns the derivative of V_3 in (3.39) into

$$\dot{V}_3 \leq -\frac{k_1 v_d^2 \Gamma^2}{\sqrt{1+\phi_e^2}\sqrt{1+\Gamma^2}\sqrt{1+k_1^2 v_d^2 \Gamma^2}} - \frac{k_2\phi_e^2}{1+\phi_e^2} - k_3\sigma(v_e)v_e - k_4\sigma(\omega_e)\omega_e. \tag{3.45}$$

From (3.14), (3.24), and (3.33), V_3 is positive definite and radially unbounded, and its derivative, $\dot{V}_3$, given by (3.45) is negative definite. These properties are utilized in the next section as the stability analysis is concerned. Finally, the closed-loop system for the WMR can be rewritten by substituting the first equation of (3.11) into (3.1), two equations of (3.23), (3.27) into (3.22), and equations of (3.43) into

(3.31) as follows

$$
\begin{aligned}
\dot{x} &= (v_e + v_d)\cos(\phi_e + \alpha_\phi), \\
\dot{y} &= (v_e + v_d)\sin(\phi_e + \alpha_\phi), \\
\dot{\phi}_e &= -\frac{k_2\phi_e}{\sqrt{1+\phi_e^2}} - \frac{\Gamma\big(f_x\bar{\Omega}_{11} + \bar{\Omega}_{12}\big)}{\sqrt{1+\Gamma^2}} + \omega_e \\
&\quad - v_e\Big[\frac{\partial\alpha_\phi}{\partial\Gamma}\big(f_x\cos(\phi) + \sin(\phi)\big) + \frac{\partial\alpha_\phi}{\partial f_x}f_{xx}\cos(\phi)\Big], \\
\begin{bmatrix}\dot{v}_e \\ \dot{\omega}_e\end{bmatrix} &= \bar{\mathbf{C}}\begin{bmatrix}\omega^2 \\ -v\omega\end{bmatrix} - \bar{\mathbf{D}}\begin{bmatrix}v \\ \omega\end{bmatrix} - \begin{bmatrix}(k_3\sigma(v_e) + \Lambda_1) \\ (k_4\sigma(\omega_e) + \Lambda_2)\end{bmatrix} - \begin{bmatrix}\Delta_1 \\ \Delta_2\end{bmatrix}.
\end{aligned}
\tag{3.46}
$$

The control design has been completed and the results are summarized in the following theorem.

Theorem 3.2.1. *Consider the nonholonomic WMR system described by (3.1). Under the assumptions 3.1.1, 3.1.2, and 3.1.3, the torque control vector $\boldsymbol{\tau}$ given in (3.43) solves the control objective (3.7) provided that control gains k_1, k_2, k_3, and k_4 and conditions in (3.41) are satisfied. In particular, the following results hold for all initial conditions $\Gamma(x(t_0), y(t_0)) \in \mathbb{R}$, $\phi_e(t_0) \in \mathbb{R}$ and $(v_e(t_0), \omega_e(t_0)) \in \mathbb{R}^2$:*

1. *The closed-loop system (3.46) is forward complete, and is globally stable at the origin.*
2. *The WMR asymptotically follows the reference path and moves along the path tangentially at a desired linear velocity v_d.*
3. *All the virtual controls and torque control inputs are bounded.*

3.3 Stability analysis

In this section, the proof of Theorem 3.2.1 is represented. In the sequel, the closed-loop is firstly shown to be forward complete [163]. Next, the path-following errors $\Gamma(x(t), y(t))$ and $\phi_e(t)$ is proven to globally asymptotically converge to the origin. Finally, all the virtual and actual controls are proven to be bounded.

3.3.1 Proof of forward completeness of the closed-loop system

In order to prove the closed-loop system (3.46) to be forward complete, V_1 in (3.14) is substituted into V_2 in (3.24) and then into V_3 in (3.33) to achieve the

full description of equation V_3 as follows

$$V_3 = \sqrt{1+\Gamma^2(x,y)} + \sqrt{1+\phi_e^2} - 2 + \frac{1}{2}\begin{bmatrix} v_e & \omega_e \end{bmatrix} \bar{\mathbf{C}}^{-1} \begin{bmatrix} v_e \\ \omega_e \end{bmatrix}, \tag{3.47}$$

which is positive definite and radially unbounded in $(|\Gamma(x,y)|, |\phi_e|, \|\mathbf{v}_e\|)$. On the other hand, the equation (3.45) indicates that $\dot{V}_3 \leq 0$ for all $\Gamma(x,y) \in \mathbb{R}$, $\phi_e \in \mathbb{R}$, $f_x \in \mathbb{R}$ and $\mathbf{v}_e \in \mathbb{R}^2$. Integrating both sides of the inequality $\dot{V}_3 \leq 0$ from t_0 to t results in $V_3(t) - V_3(t_0) \leq 0$, i.e.,

$$\begin{aligned} &\sqrt{1+\Gamma^2(x(t),y(t))} + \sqrt{1+\phi_e^2(t)} + \frac{1}{2}\begin{bmatrix} v_e(t) & \omega_e(t) \end{bmatrix} \bar{\mathbf{C}}^{-1} \begin{bmatrix} v_e(t) \\ \omega_e(t) \end{bmatrix} \\ &\leq \sqrt{1+\Gamma^2(x(t_0),y(t_0))} + \sqrt{1+\phi_e^2(t_0)} + \frac{1}{2}\begin{bmatrix} v_e(t_0) & \omega_e(t_0) \end{bmatrix} \bar{\mathbf{C}}^{-1} \begin{bmatrix} v_e(t_0) \\ \omega_e(t_0) \end{bmatrix} \end{aligned} \tag{3.48}$$

Obviously, the right-hand side of the inequality (3.48) is bounded, so that the left-hand side of (3.48) must be also bounded for all $t \geq t_0 \geq 0$. This in turn implies the boundedness of the terms $|\Gamma(x(t),y(t))|, |\phi_e(t)|, \|\mathbf{v}_e(t)\|$ for all $t \geq t_0 \geq 0$. It can be also seen from the first equation of (3.29), i.e., $\dot{x} = (v_d + v_e)\cos(\phi)$, that all components are bounded for all $t \geq t_0 \geq 0$, $x(t)$ then exists for all $t \geq t_0 \geq 0$. Existence of $x(t)$ implies that of $f_x(x(t))$, $f_{xx}(x(t))$ and $f_{xxx}(x(t))$ because the function $f_x(x(t))$ is a single-valued function of $x(t)$, $f_{xx}(x(t))$, $f_{xxx}(x(t))$ are bounded if their argument $x(t)$ is bounded, see the assumption 3.1.2. As a result, the solutions $|\Gamma(x(t),y(t))|, |\phi_e(t)|, \|\mathbf{v}_e(t)\|, f_x(x(t)), f_{xx}(x(t))$ and $f_{xxx}(x(t))$ of the closed-loop system (3.46) satisfy to be global existence and uniqueness for all $t \geq t_0 \geq 0$ by Theorem 2.1.2. This implies the forward completeness of the closed-loop system (3.46).

Furthermore, V_3 is positive definite and radially unbounded in $(|\Gamma(x(t),y(t))|, |\phi_e(t)|, \|\mathbf{v}_e(t)\|)$, and $\dot{V}_3 \leq 0$, the closed-loop system (3.46) is globally stable at the origin by Theorem 4.2 in [57].

3.3.2 Proof of asymptotic convergence of path-following errors to zero

To prove that the WMR follows the reference path described by (3.9) and its position $(x(t), y(t))$ and heading angle $\phi(t)$ globally asymptotically track their reference trajectories $(x_d(t), y_d(t))$ and $\phi_d(t)$, it is sufficient to prove that $\Gamma(x(t),y(t)), \phi_e(t)$,

and $\mathbf{v}_e(t)$ globally asymptotically converge to the origin. Since V_3 is positive definite and radially unbounded, and $\dot{V_3} \leq 0$, see (3.45)

$$\dot{V_3} \leq -W_3 \leq 0, \tag{3.49}$$

where W_3 is a positive definite function and have been denoted as

$$W_3 = \frac{k_1 v_d^2 \Gamma^2}{\sqrt{1+\phi_e^2}\sqrt{1+\Gamma^2}\sqrt{1+k_1^2 v_d^2 \Gamma^2}} + \frac{k_2 \phi_e^2}{1+\phi_e^2} + k_3 \sigma(v_e) v_e + k_4 \sigma(\omega_e)\omega_e. \tag{3.50}$$

Integrating both sides of (3.49) from t_0 to t results in

$$\int_{t_0}^{t} W_3(\tau) d\tau \leq V_3(t_0) - V_3(t) \leq V_3(t_0), \tag{3.51}$$

where,

$$\begin{aligned} V_3(t_0) =& \sqrt{1+\Gamma^2(x(t_0), y(t_0))} + \sqrt{1+\phi_e^2(t_0)} - 2 \\ &+ \frac{1}{2} \begin{bmatrix} v_e(t_0) & \omega_e(t_0) \end{bmatrix} \bar{\mathbf{C}}^{-1} \begin{bmatrix} v_e(t_0) \\ \omega_e(t_0) \end{bmatrix}. \end{aligned} \tag{3.52}$$

It is seen that the right-hand side of (3.51) exists and is bounded. On the other hand, W_3 satisfies to be a uniformly continuous function. Hence, by applying the Barbalat's Lemma in [57], $\lim_{t\to\infty} W_3(t) = 0$ is obtained.
Due to the condition (3.5) imposed on $v_d^2(t)$, which in turn means

$$\begin{aligned} &\lim_{t\to\infty} \frac{\Gamma^2(x(t), y(t))}{\sqrt{1+\phi_e^2(t)}\sqrt{1+\Gamma^2(x(t), y(t))}} = 0, \\ &\lim_{t\to\infty} \frac{\phi_e^2(t)}{1+\phi_e^2(t)} = 0, \\ &\lim_{t\to\infty} \left[k_3 \sigma(v_e(t)) v_e(t) + k_4 \sigma(\omega_e(t)) \omega_e(t) \right] = 0. \end{aligned} \tag{3.53}$$

Moreover, $\Gamma(x(t), y(t))$, $\phi_e(t)$, $v_e(t)$ and $\omega_e(t)$ are proven to be bounded for all $t \geq t_0 \geq 0$ in the previous section. From the definition of the smooth saturation function $\sigma(x)$ in Chapter 2, it can be conluded that Γ, ϕ_e, v_e, and ω_e in (3.53) globally asymptotically converge to the origin.

3.3.3 Boundedness of virtual and actual controls

In this section, the boundedness of virtual, and actual controls α_ϕ, α_ω, and $\boldsymbol{\tau} = \begin{bmatrix} \tau_v & \tau_\omega \end{bmatrix}^T$, see (3.18), (3.27), and (3.43), are calculated. First, it is easily seen that α_ϕ is bounded because of its representation in (3.16), and (3.18). Regarding α_ω in (3.27), it shows that if the upper bounds of the parts $\frac{\partial \alpha_\phi}{\partial \Gamma}$, $\frac{\partial \alpha_\phi}{\partial f_x}$, and $\frac{\partial \alpha_\phi}{\partial v_d}$ are

estimated, the boundedness of α_ω is guaranteed. As such, the upper bounds of these parts are calculated as follows

$$\begin{aligned}\Big|\frac{\partial\alpha_\phi}{\partial\Gamma}\Big| &= \Big|\frac{1}{\sqrt{1-\Big(\frac{-k_1v_d\Gamma}{\sqrt{(1+f_x^2)(1+k_1^2v_d^2\Gamma^2)}}\Big)^2}}\Big(\frac{-k_1v_d\Gamma}{\sqrt{(1+f_x^2)(1+k_1^2v_d^2\Gamma^2)}}\Big)'_\Gamma\Big| \\ &= \frac{k_1|v_d|}{\sqrt{1+(1+k_1^2v_d^2\Gamma^2)f_x^2}(1+k_1^2v_d^2\Gamma^2)} \leq \frac{k_1|v_d|}{\sqrt{1+L_1^2}} \leq k_1\epsilon_1. \end{aligned} \tag{3.54}$$

$$\begin{aligned}\Big|\frac{\partial\alpha_\phi}{\partial f_x}\Big| &= \Big|\frac{1}{\sqrt{1-\Big(\frac{-k_1v_d\Gamma}{\sqrt{(1+f_x^2)(1+k_1^2v_d^2\Gamma^2)}}\Big)^2}}\Big(\frac{-k_1v_d\Gamma}{\sqrt{(1+f_x^2)(1+k_1^2v_d^2\Gamma^2)}}\Big)'_{f_x}\Big| \\ &= \frac{k_1|v_d\Gamma f_x|}{\sqrt{1+f_x^2+k_1^2v_d^2\Gamma^2f_x^2}}\frac{1}{1+f_x^2} \leq \frac{1}{1+L_1^2} \leq 1, \end{aligned} \tag{3.55}$$

$$\begin{aligned}\Big|\frac{\partial\alpha_\phi}{\partial v_d}\Big| &= \Big|\frac{1}{\sqrt{1-\Big(\frac{-k_1v_d\Gamma}{\sqrt{(1+f_x^2)(1+k_1^2v_d^2\Gamma^2)}}\Big)^2}}\Big(\frac{-k_1v_d\Gamma}{\sqrt{(1+f_x^2)(1+k_1^2v_d^2\Gamma^2)}}\Big)'_{v_d}\Big| \\ &= \frac{k_1|\Gamma|}{(1+k_1^2v_d^2\Gamma^2)\sqrt{1+(1+k_1^2v_d^2\Gamma^2)f_x^2}} \leq \frac{k_1|\Gamma|}{(1+k_1^2v_d^2\Gamma^2)\sqrt{1+L_1^2}} \leq k_1. \end{aligned} \tag{3.56}$$

Because those terms f_x, f_{xx}, $v_d(t)$, $\dot{v}_d(t)$ have been assumed to be bounded, i.e., see conditions (3.3), and (3.4), the boundedness of the virtual control α_ω in (3.27) is guaranteed. The upper bound of α_ω can be estimated by using of results in (3.54), (3.55), and (3.56) as it has already shown in (3.42).

It is seen from (3.43) that the actual control vector $\boldsymbol{\tau} = \begin{bmatrix}\tau_v & \tau_\omega\end{bmatrix}^T$ is bounded if the boundedness of the parts Λ_1 and Λ_2 is ensured, i.e., see (3.40). Specifically, the terms $\frac{\partial\alpha_\omega}{\partial\Gamma}$, $\frac{\partial\alpha_\omega}{\partial f_x}$, $\frac{\partial\alpha_\omega}{\partial f_{xx}}$, $\frac{\partial\alpha_\omega}{\partial v_d}$, $\frac{\partial\alpha_\omega}{\partial\dot{v}_d}$, and $\frac{\partial\alpha_\omega}{\partial\phi}$, which appear in Δ_{21}, i.e., see (3.32), must be bounded. For that reason, upper bounds of these terms can be found by

$$\Big|\frac{\partial\alpha_\omega}{\partial\Gamma}\Big| = \Big|\Big(\frac{\Gamma\big(f_x\bar{\Omega}_{11}+\bar{\Omega}_{12}\big)}{\sqrt{(1+\Gamma^2)}}\Big)'_\Gamma\Big| = \Big|\frac{\big(f_x\bar{\Omega}_{11}+\bar{\Omega}_{12}\big)}{(1+\Gamma^2)^{\frac{3}{2}}}\Big| \leq 2(L_1+1). \tag{3.57}$$

$$\begin{aligned}\Big|\frac{\partial\alpha_\omega}{\partial f_x}\Big| &= \Big|\Big(\frac{\Gamma\big(f_x\bar{\Omega}_{11}+\bar{\Omega}_{12}\big)}{\sqrt{(1+\Gamma^2)}}\Big)'_{f_x}\Big| + \Big|\Big(v_d\frac{\partial\alpha_\phi}{\partial\Gamma}(f_x\cos(\phi)+\sin(\phi))\Big)'_{f_x}\Big| \\ &\leq \Big|\frac{\Gamma\bar{\Omega}_{11}}{\sqrt{1+\Gamma^2}}\Big| + \Big|v_d\frac{\partial\alpha_\phi}{\partial\Gamma}\cos(\phi)\Big| \leq 2+k_1\epsilon_1^2. \end{aligned} \tag{3.58}$$

$$\Big|\frac{\partial\alpha_\omega}{\partial f_{xx}}\Big| = \Big|\Big(v_d\frac{\partial\alpha_\phi}{\partial f_x}f_{xx}\cos(\phi)\Big)'_{f_{xx}}\Big| = \Big|v_d\frac{\partial\alpha_\phi}{\partial f_x}\cos(\phi)\Big| \leq \epsilon_1. \tag{3.59}$$

$$\begin{aligned}\Big|\frac{\partial\alpha_\omega}{\partial v_d}\Big| &= \Big|\Big(v_d\frac{\partial\alpha_\phi}{\partial\Gamma}\big(f_x\cos(\phi)+\sin(\phi)\big)+v_d\frac{\partial\alpha_\phi}{\partial f_x}f_{xx}\cos(\phi)\Big)'_{v_d}\Big| \\ &= \Big|\frac{\partial\alpha_\phi}{\partial\Gamma}\big(f_x\cos(\phi)+\sin(\phi)\big)+\frac{\partial\alpha_\phi}{\partial f_x}f_{xx}\cos(\phi)\Big| \\ &\le k_1\epsilon_1(L_1+1)+L_2\sqrt{1+L_1^2}. \end{aligned} \tag{3.60}$$

$$\Big|\frac{\partial\alpha_\omega}{\partial\dot v_d}\Big| = \Big|\Big(\frac{\partial\alpha_\phi}{\partial v_d}\dot v_d\Big)'_{\dot v_d}\Big| = \Big|\frac{\partial\alpha_\phi}{\partial v_d}\Big| \le k_1. \tag{3.61}$$

$$\begin{aligned}\Big|\frac{\partial\alpha_\omega}{\partial\phi}\Big| &= \Big|\Big(v_d\frac{\partial\alpha_\phi}{\partial\Gamma}\big(f_x\cos(\phi)+\sin(\phi)\big)+v_d\frac{\partial\alpha_\phi}{\partial f_x}f_{xx}\cos(\phi)\Big)'_{\phi}\Big| \\ &= \Big|v_d\Big(\frac{\partial\alpha_\phi}{\partial\Gamma}\big(f_x\sin(\phi)+\cos(\phi)\big)+\frac{\partial\alpha_\phi}{\partial f_x}f_{xx}\sin(\phi)\Big)\Big| \\ &\le \epsilon_1(k_1\epsilon_1(L_1+1)+L_2). \end{aligned} \tag{3.62}$$

In the previous subsection, boundness of $\phi_e(t)$, $v_e(t)$ and $\omega_e(t)$ has been proven for all $t \ge t_0 \ge 0$ and $\lim_{t\to\infty}\big(\phi_e(t),\, v_e(t), \omega_e(t)\big) = 0$. Thus, the boundedness of Ψ_{22} and Δ_{22} are not necessary to evaluate, and only upper bounds of Ψ_{11}, Ψ_{12}, Δ_1, and Δ_{21} are needed to estimate, see (3.20), (3.26), and (3.32). For convenience, Θ_1 and Θ_2 are denoted as the upper bounds of Δ_1 and Δ_{21}, respectively. Those values can be calculated as follows

$$\begin{aligned}&|\Psi_{12}| = |\Psi_{11}| \le L_1+1, \\ &|\Delta_1| \le \epsilon_2 := \Theta_1, \\ &|\Delta_{21}| \le \epsilon_1\big[2(L_1+1)^2+(k_1\epsilon_1^2+2)L_2+\epsilon_1^2L_3(1+L_1^2)\big] \\ &\qquad + k_1\epsilon_1(L_1+1)+L_2\epsilon_2+k_1\epsilon_3 \\ &\qquad + \epsilon_1(k_1\epsilon_1(L_1+1)+L_2)\chi_1 := \Theta_2, \end{aligned} \tag{3.63}$$

where χ_1 is the denotation of the upper bound of α_ω in (3.42). By using results in (3.42) and (3.63) the upper bounded values of the parts Λ_1 and Λ_2 are calculated as

$$\begin{aligned}&|\Lambda_1| \le \chi_1^2+\bar{\bar d}_{11}\epsilon_1+\bar{\bar d}_{12}\chi_1+\frac{\Theta_1}{\bar c_1}+(L_1+1)(k_1\epsilon_1+1)+L_1+1, \\ &|\Lambda_2| \le \epsilon_1\chi_1+\bar{\bar d}_{12}\epsilon_1+\bar{\bar d}_{22}\chi_1+\frac{\Theta_2}{\bar c_2}. \end{aligned} \tag{3.64}$$

From notations of $\bar b$, $\bar c$ in (2.51), $\bar{\bar b}_{11}, \bar{\bar b}_{12}$ in (4.44), and $\bar{\bar b}_{21}, \bar{\bar b}_{22}$ in (4.45), absolute values of the following representations can be obtained by the simple calculation below

$$\begin{aligned}&\Big|\frac{\bar{\bar b}_{11}}{\bar{\bar b}_{11}\bar{\bar b}_{22}-\bar{\bar b}_{12}\bar{\bar b}_{21}}\Big| = \frac{c}{r}; \qquad \Big|\frac{\bar{\bar b}_{12}}{\bar{\bar b}_{11}\bar{\bar b}_{22}-\bar{\bar b}_{12}\bar{\bar b}_{21}}\Big| = \frac{c}{r}; \\ &\Big|\frac{\bar{\bar b}_{21}}{\bar{\bar b}_{11}\bar{\bar b}_{22}-\bar{\bar b}_{12}\bar{\bar b}_{21}}\Big| = \frac{bc}{r}; \qquad \Big|\frac{\bar{\bar b}_{22}}{\bar{\bar b}_{11}\bar{\bar b}_{22}-\bar{\bar b}_{12}\bar{\bar b}_{21}}\Big| = \frac{bc}{r}. \end{aligned} \tag{3.65}$$

Now, employing (3.64), (3.65), the bounds of τ_v and τ_ω can be calculated from (3.43) as follows

$$\begin{aligned}
|\tau_v| &\leq \frac{bc}{r}\Big(k_3 + \big(\chi_1^2 + \bar{\bar{d}}_{11}\epsilon_1 + \bar{\bar{d}}_{12}\chi_1 + \frac{\Theta_1}{\bar{c}_1} + (L_1+1)(k_1\epsilon_1+1) + L_1 + 1\big)\Big) \\
&\quad + \frac{c}{r}\Big(k_4 + \big(\epsilon_1\chi_1 + \bar{\bar{d}}_{12}\epsilon_1 + \bar{\bar{d}}_{22}\chi_1 + \frac{\Theta_2}{\bar{c}_2}\big)\Big) := \tau_{vM}, \\
|\tau_\omega| &\leq \frac{bc}{r}\Big(k_3 + \big(\chi_1^2 + \bar{\bar{d}}_{11}\epsilon_1 + \bar{\bar{d}}_{12}\chi_1 + \frac{\Theta_1}{\bar{c}_1} + (L_1+1)(k_1\epsilon_1+1) + L_1 + 1\big)\Big) \\
&\quad - \frac{c}{r}\Big(k_4 + \big(\epsilon_1\chi_1 + \bar{\bar{d}}_{12}\epsilon_1 + \bar{\bar{d}}_{22}\chi_1 + \frac{\Theta_2}{\bar{c}_2}\big)\Big) := \tau_{\omega M}.
\end{aligned} \tag{3.66}$$

It is seen from (3.42), (3.63), (3.64), (3.65), and (3.66) that torque control vector $\boldsymbol{\tau} = \begin{bmatrix}\tau_v & \tau_\omega\end{bmatrix}^T$ depends on the system's parameters in (2.51), predefined constants in assumptions 3.1.1, 3.1.2, and control gains k_1, k_2, k_3, and k_4. Therefore, the boundedness of $\boldsymbol{\tau}$ can be predetermined.

3.4 Simulation results

In this section, two simulation examples are implemented to illustrate the effectiveness of the proposed control laws (3.43). Numerical simulation is carried out by using the physical parameters of the WMR which is taken from [6]. The parameters are summarized in Table 3.1 below. In the first example, the WMR is forced to follow to a tanh-shape reference path. In the second example, the behaviour of the WMR to follow a sine-shape reference path is shown. Both results show the correctness of the proposed control laws.

Specifications for two reference paths are selected as follows: $x_d = x$, $y_d = -2\tanh(0.1x_d)$ and $x_d = x$, $y_d = -2\sin(0.1x_d)$. These reference paths are regular and conditions in (3.3) hold for both cases. For example, in the second reference path, i.e., $f(x_d) = 2\sin(0.1x_d)$, $L_1 = 0.2$, $L_2 = 0.02$, and $L_3 = 0.002$ are satisfied.

The linear velocity in both cases is chosen as $v_d = 0.5 + sin(0.2t)(m/s)$. This selection of v_d satisfies conditions in (3.4) and (3.5), i.e., $|v_d(t)| \leq 1.5 = \epsilon_1$, $|\dot{v}_d(t)| \leq 0.2 = \epsilon_2$, and $|\ddot{v}_d(t)| \leq 0.04 = \epsilon_3$, and $|v_d(t)|^2 = 2.25$.

The initial configuration of the WMR and other design parameters for virtual controls (3.18), (3.27) and actual controls (3.43) are included in Table 3.2 below. By substituting the given control gains, constants, and design parameters to conditions in (3.41), a simple calculation shows that these conditions hold with $\bar{\bar{d}}_{11} = 49.4 \geq 11.86$ and $|v_d| + \bar{\bar{d}}_{22} = 1.5 + 27.7 \geq 16.95$.

Table 3.1: List of the WMR physical parameters [6]

Parameters	Definition	Value
r	radius of the wheel	$0.15m$
b	half width of the robot	$0.75m$
a	distance between the center of mass (CoM) P_C and the middle point P_0	$0.3m$
m	total mass	$32kg$
m_w	mass of the wheel with a motor	$1kg$
m_c	mass of robot body	$30kg$
d_{11}	damping coefficient	5
d_{22}	damping coefficient	5
I_c	moment of inertia of the body about the vertical axis through CoM	$15.625kgm^2$
I_w	moment of inertia of the wheel with a motor about the wheel axis	$0.005kgm^2$
I_m	moment of inertia of the wheel with a motor about the wheel diameter	$0.0025kgm^2$
R_{safe}	radius of physical safety region of the WMR	$0.075m$
$R_{sensing}$	radius of sensing region of the WMR	$0.35m$

Table 3.2: Values of design parameters

Parameters	Meaning	Values
$\begin{bmatrix} x(0) \\ y(0) \\ \phi(0) \end{bmatrix}$	initial configuration of the actual WMR	$\begin{bmatrix} -20 \\ 1.5 \\ 0.25 \end{bmatrix}$
k_1	control gain of the virtual control α_ϕ in (3.18)	0.85
k_2	control gain of the virtual control α_ω in (3.27)	0.85
k_3	control gain of actual controllers in (3.41)	4
k_4	control gain of actual controllers in (3.41)	4
h	time step used in Euler method for numerical computation	0.005

Trajectories of the WMR following two reference paths are shown in figures 3.2 and 3.4. The WMR starts approaching smoothly to the desired paths and follows nicely to the destination. Errors in position and orientation, i.e., x_e, y_e

and ϕ_e, and errors in velocities, i.e., v_e and ω_e, in both cases are plotted in figure 3.3 and 3.5. These errors tend to zero asymptotically when time goes to infinity. Correspondingly, τ_v and τ_ω applied to two wheels stay in a certain range of value.

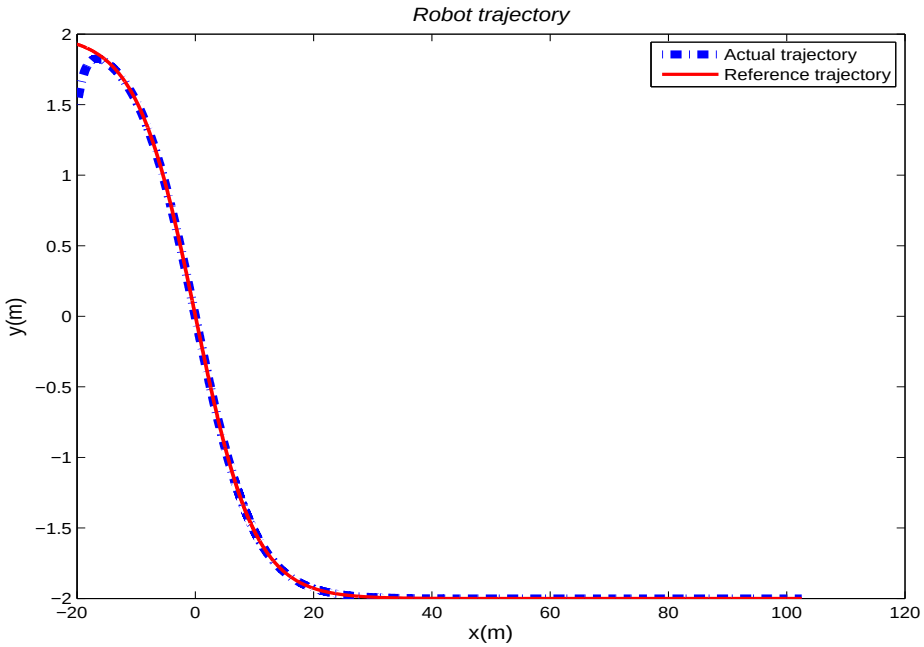

Figure 3.2: Path-following of the WMR to the tanh-shape reference path.

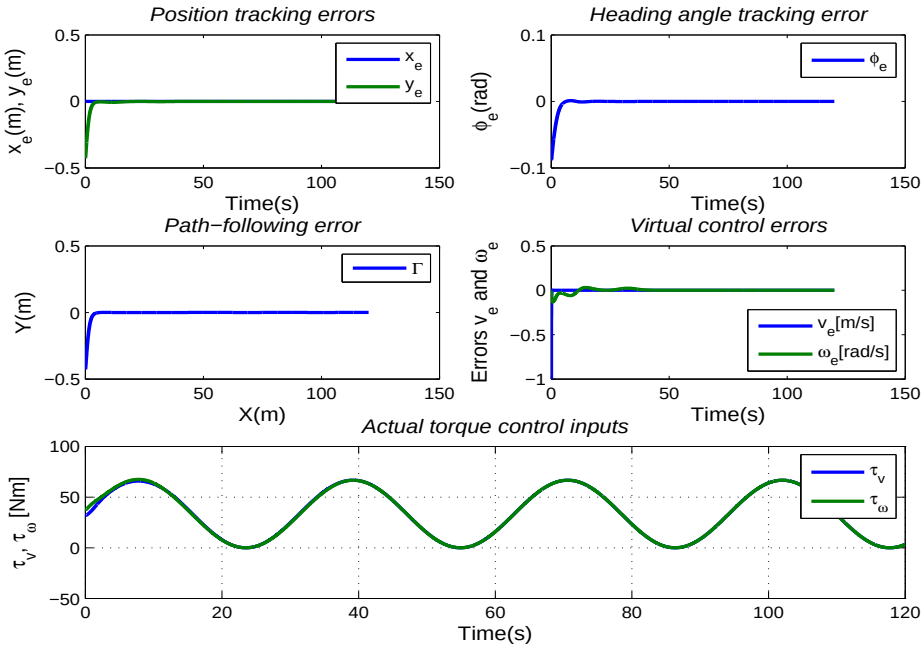

Figure 3.3: Position tracking errors (first row-left); Heading angle tracking error (first row-right); Path-following error (second row-left); Virtual control errors (second row-right); Actual torque control inputs (third row).

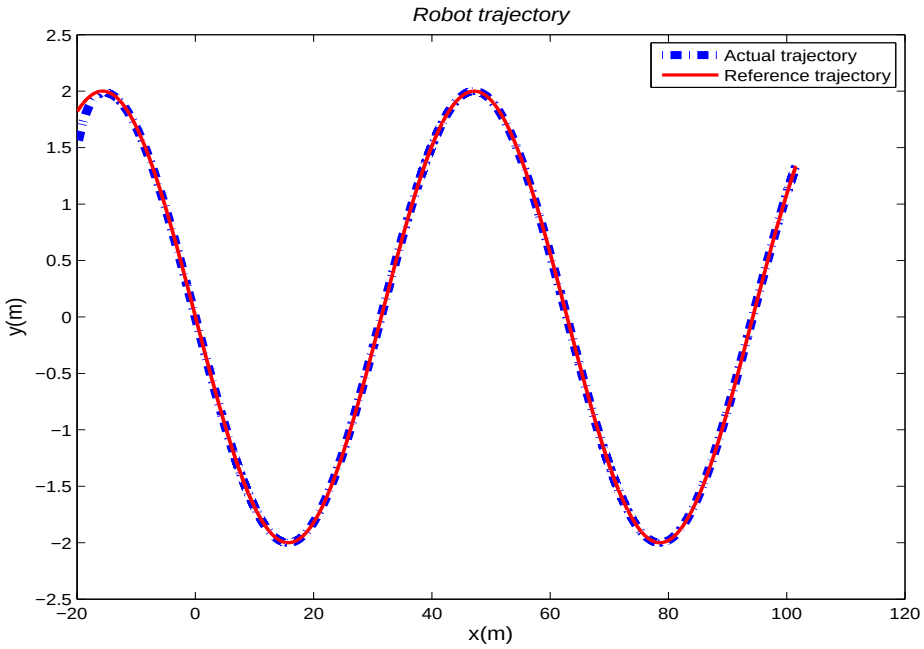

Figure 3.4: Path-following of the WMR to the sine-shape reference path.

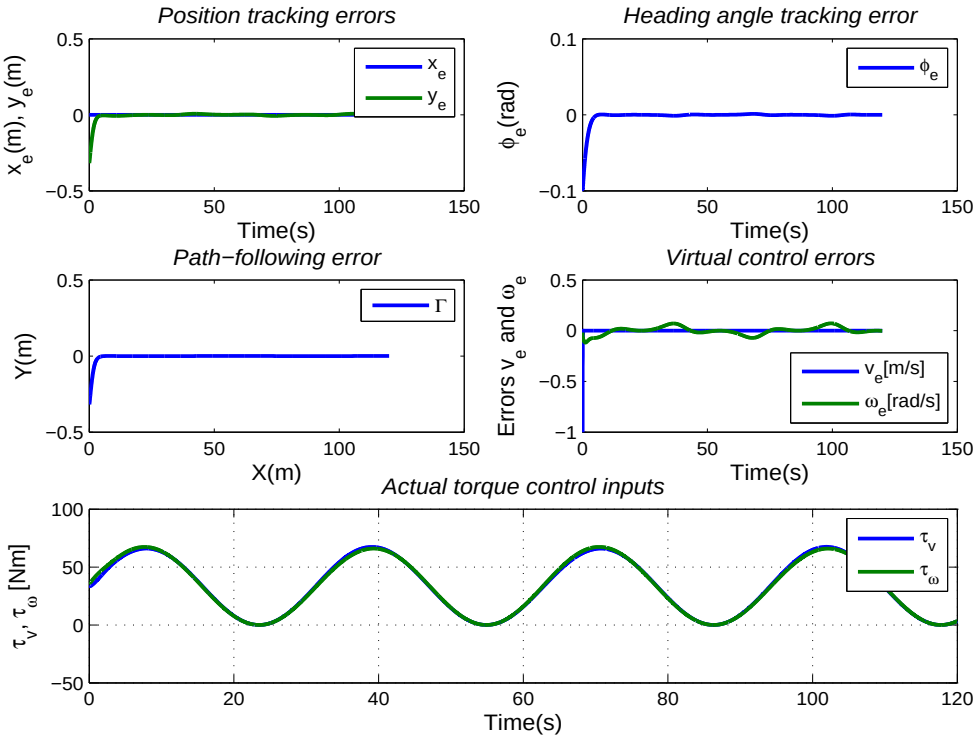

Figure 3.5: Position tracking errors (first row-left); Heading angle tracking error (first row-right); Path-following error (second row-left); Virtual control errors (second row-right); Actual torque control inputs (third row).

3.5 Experimental verification

This experiment demonstrates the correctness of the proposed control laws in (3.18), (3.27) at kinematic stage. Realtime values of designed controllers are numerically calculated by Matlab on a host computer. These values are then transfered to the WMR via a wireless communication (bluetooth) protocol.

3.5.1 Experimental platform

This section describes the Khepera III robot which is developed for researching and educational purposes by K-Team (http://k-team.com). This ready-to-use platform is used for the experimental demonstration of the designed controllers in this chapter.

Figure 3.6: Khepera III mobile robot [7].

Features

Brief introduction of some main features is taken from the Khepera III User manual, version 3.5, February 2013 [7].

Explanation of parts numbered in the figure 3.7 is as follows

1. Infrared sensors.
2. Ultrasonic sensors.
3. Main serial connector.
4. USB miniAB connector.
5. Power jack connector.

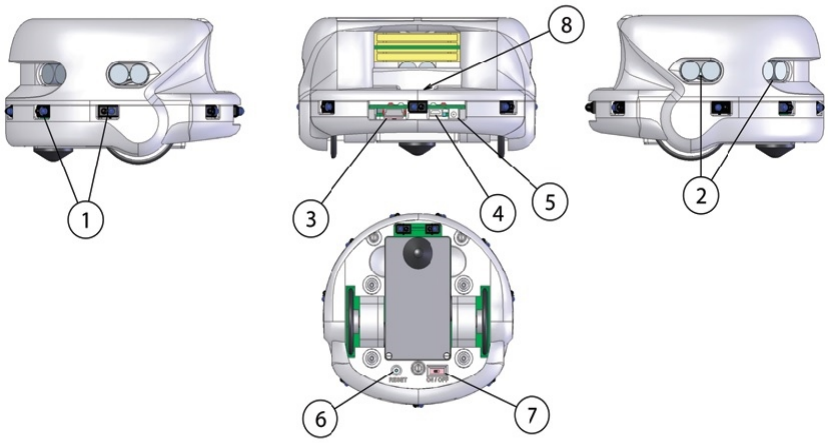

Figure 3.7: Overview of the Khepera III mobile robot [7].

6. Reset.

7. On/Off.

8. Cable unroller connector.

Communication

Khepera III provides 2 types of communication between the host computer station and the robot, i.e., serial and bluetooth protocols.
Serial communication mode can be used in standalone(only Khepera III without any extended hardware). A standard RS232 cable is used to link the host computer to the interface module of Khepera III. RS232 signal is converted into TTL level signal by the interface module for mutual communication between two devices. In this experimental work, this communication protocol is not used. Instead, a bluetooth protocol is used.
The class of Khepera III is equipped a bluetooth device with firmware 2.0 or higher. Configuration of the bluetooth communication mode is set as follows: 115200bps, 8 data bits, 1 stop bit, no parity, no hardware control, and security code: 0000. The procedure of establishment and validation of the bluetooth communication between a host computer anf Khepera III is described as follows [7]

- Connecting bluetooth dongle to the host computer (or active bluetooth communication mode in laptop).

- Verifying that the connection is securized and that a COM port is reserved for the bluetooth serial communication.

- Making sure the power of Khepera III in ON status (Green LED is on). Checking the appearance of Khepera III with a logo on "View device in range". The name KHIII and serial number which is the same as the label on the bottom also appear.
- Entering "0000"security code for creating a connection. Program assigns a COM port to the device.
- Opening a terminal with the assigned COM port and the configuration above.
- Resetting Khepera III by pressing the reset button on the bottom.
- Testing the OS system of Khepera III by using the command $\boldsymbol{B}$ to validate the communication. Returned information should be: $\boldsymbol{b, 3, 0}$.
- Applying any program, i.e., Matlab, to control remotely Khepera III.

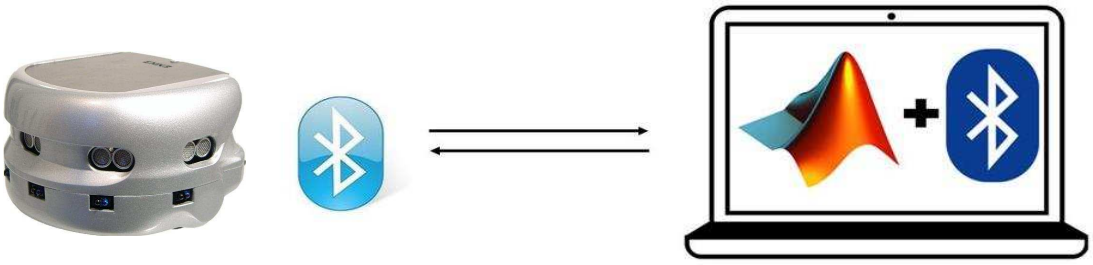

Figure 3.8: Communication between host computer and Khepera III via bluetooth protocol.

Sensing devices

For obstacle avoidance purpose, Khepera III is equipped with two types of sensing devices. Those include infrared proximity sensors and ultrasonic sensors. Diagrams of sensing devices are shown in Figures 3.9 and 3.10 below.
Khepera III has been equipped with 9 sensors around its body and 2 on the bottom. These sensors allow to measure ambient light and the light reflected by obstacles.

- Measurement of normal ambient light is made by using the receiver part of the device only, without the emitter part. For every $33ms$, a new measurement is created. During the period of $33ms$, 11 sensors are read in a

sequential way every $3ms$. The value returned at a given time is the result of the last measurement.

- Measurement of the light reflected by obstacles is measured by emitting light using the emitter part. The returned value is the difference between the measurement created by emitting light and the measured ambient light. For every $33ms$, a new measurement is made. During the period of $33ms$, 11 sensors are read in a sequential way every $3ms$. The value returned at a given time is the result of the last measurement.

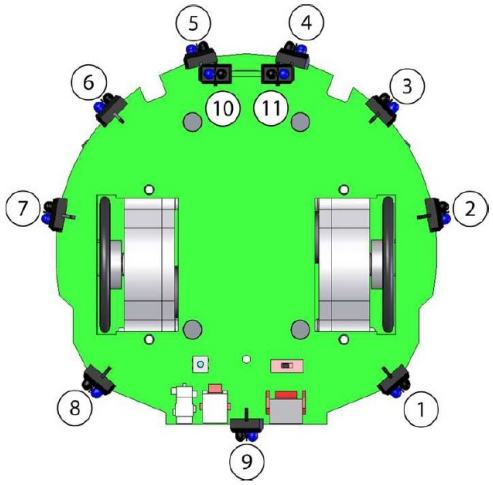

Figure 3.9: Bottom view of the infrared sensors [7].

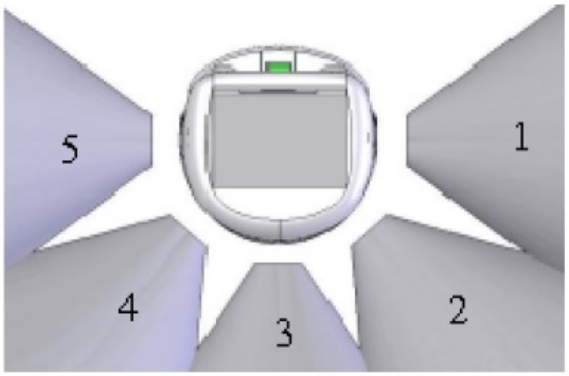

Figure 3.10: Position of 5 pairs ultrasonic sensors [7].

There are 5 pairs of ultrasonic devices placed around the Khepera III and are positioned and numbered as illustrated in Figure 3.10. Each pair of ultrasonic

devices is composed of one transmitter and one receiver. The ultrasonic devices are powered by a 20Vdc source. The norminal frequency of these transducers is 40kHz +/-1kHz. By default, there has been maximum 3 echos, sensor number 3 (front) is active, timeout is set to see from $20cm$ to $4m$. Each measurement returns the number of found echos, the distance in cm of each echo, the amplitude of each, and the time stamp when the echo was sent. The value returned by the command, is the white noise measured before an ultrasonic wave was sent. Then the real amplitude of each echo will be its amplitude minus the white noise.
Other information and specification of Khepera III can be found in [7] in detail.

3.5.2 Experimental results

Two experiments are performed to demonstrate the effectiveness of the proposed kinematic controllers. They are applied to Khepera III to force it to follow two different reference paths including tanh-shape and sine-shape.
Experiment 1: Parameters of reference path and velocity, initial configuration values, and constants of controllers are given by:
Reference path: $y_d = \tanh(x_d)$. Reference velocity: $v_d(t) = 0.12 + 0.015\sin(0.1t)$ satisfies conditions in Assumption 3.1.2.
Initial configuration values of Khepera III: $(x_0, y_0, \phi_0) = (-1.95, 0.585, 0)$. Constants of designed controllers in (3.18), (3.27) are selected by $k_1 = 0.95$ and $k_2 = 1$.

Figure 3.11 illustrates the experimental result of the tanh-shape path following of Khepera III under designed controllers (3.18) and (3.27). Figure 3.12 consists of 5 different subfigures. Two subfigures in the first row are position tracking, heading angle tracking errors. They depict very small change between the configuration of virtual reference robot and that of Khepera III. Subfigure of path-following error reflects the effectiveness of the method as this error changes very litle. The subfigure of control inputs shows that values of two control inputs are in the range of a certain bound during experimental time. Hence, the control objective is guaranteed. Figure 3.13 shows a series of snapshot which are taken from the experimental video.
Experiment 2: Parameters of reference path and velocity, initial values of the WMR, and constants of controllers are chosen as follows:
Reference path: $y_d = 0.78\sin(2x_d)$. Reference velocity: $v_d(t) = 0.14{+}0.01\sin(0.1t)$ satisfies conditions in Assumption 3.1.2.

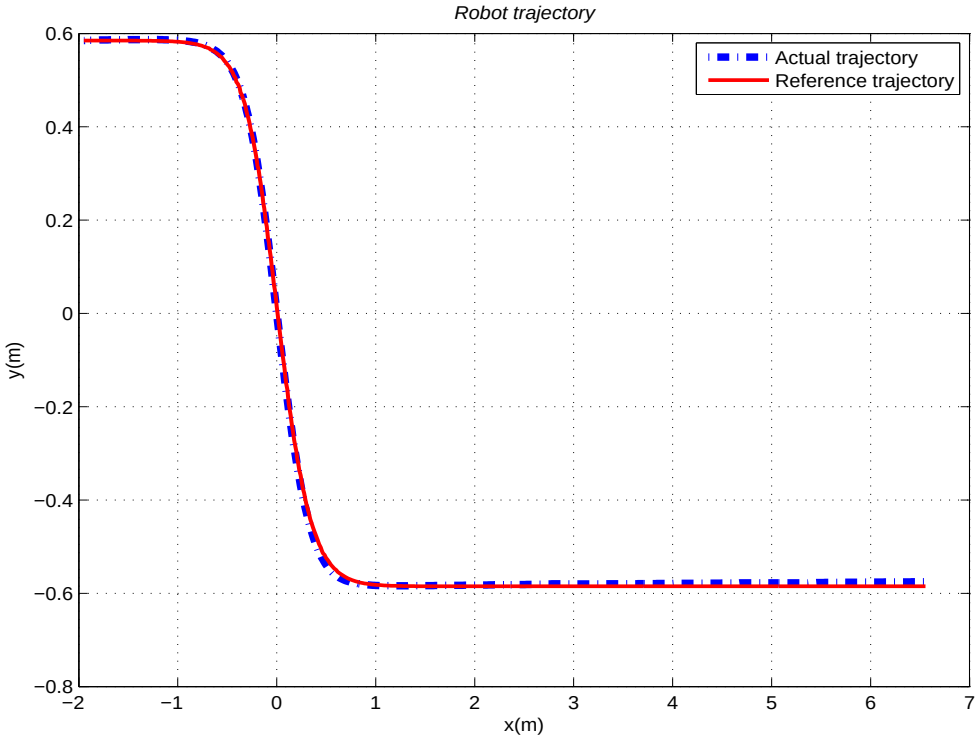

Figure 3.11: The WMR follows the tanh-shape path under the proposed controllers.

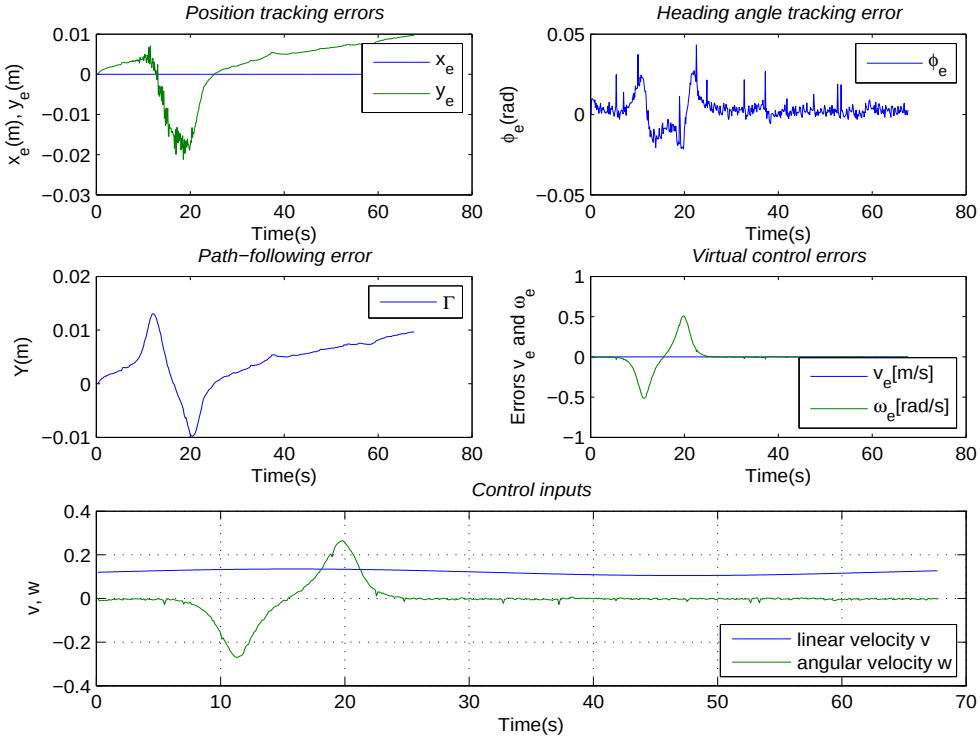

Figure 3.12: Errors and control inputs at kinematic control stage.

Initial configuration values of Khepera III: $(x_0, y_0, \phi_0) = (-0.39, 0, 0)$. Constants

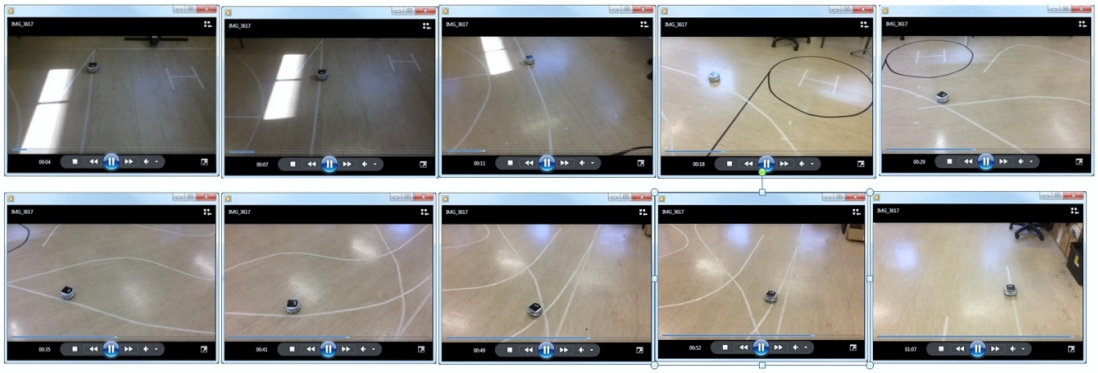

Figure 3.13: Demonstration of WMR following the tanh-shape reference path (Each subfigure is successively extracted from the movie file at different time frames).

of designed controllers in (3.18), (3.27) are set by $k_1 = 0.75$ and $k_2 = 0.95$.

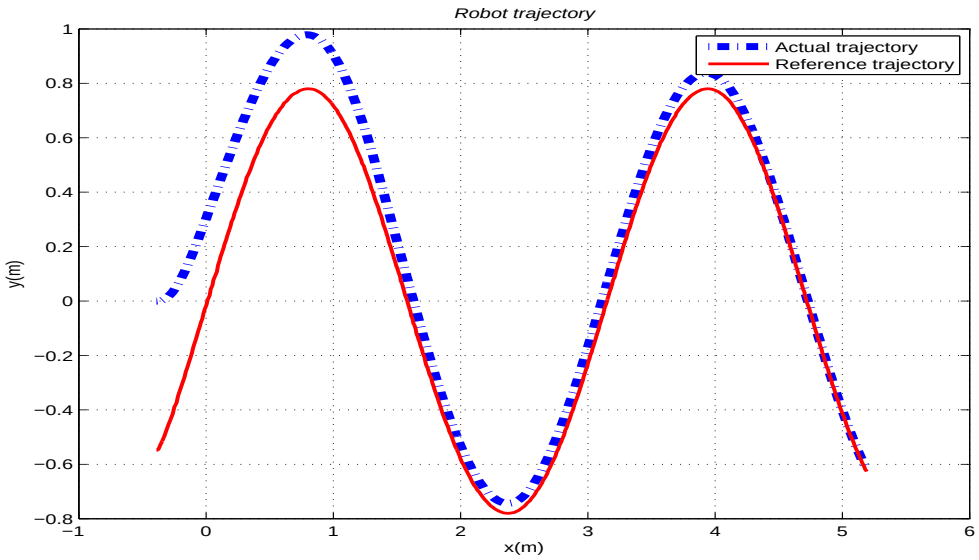

Figure 3.14: Khepera III follows the sine-shape path.

Illustration of the experimental result of the sine-shape path following of Khepera III is given in Figure 3.14. Similar to *Experiment 1*, figure 3.15 consists of 5 subfigures of errors and control inputs. With regards to the configuration, all errors, i.e., x_e, y_e, ϕ_e, approach to zero as time increases. While v_e does not change, the error of ω_e reflects the move of Khepera III following the sine-shape. The subfigure of control inputs shows that values of two control inputs are constrained by a certain bound. Hence, the control objective is guaranteed. Figure 3.16 also represents a series of snapshot which are taken from the experimental video.

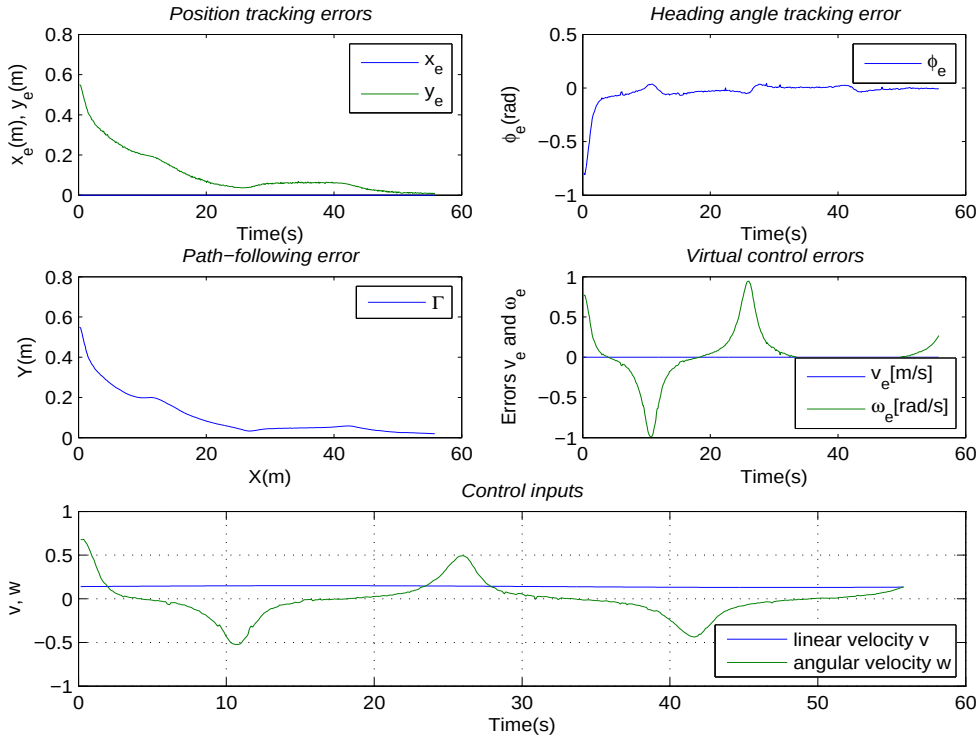

Figure 3.15: Errors and control inputs at kinematic control stage.

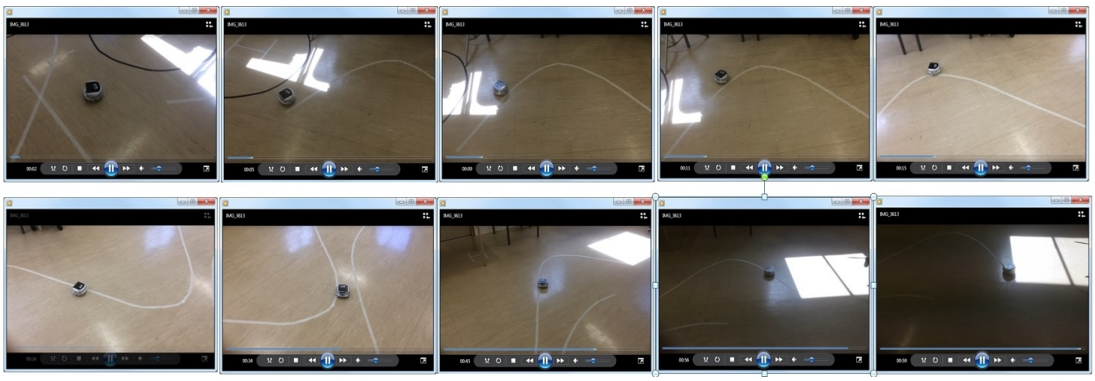

Figure 3.16: Demonstration of the WMR following the sine-shape reference path (Each subfigure is successively extracted from the movie file at different time frames).

3.6 Conclusions

In this chapter, the global state-feedback path-following control laws for the WMR system have been designed constructively at torque level. Following the works in [1], the level curve approach, Lyapunov's direct method, and the standard backstepping technique are deployed to obtain the control objective in (3.7). The position of the WMR is driven to that of the reference path and remains on the path, i.e., position of the WMR satisfies the equation of the reference path.

Hence, globally asymptotic convergence to zero of errors in terms of the path, position, and orientation is ensured. Under the proper selection of Lyapunov functions in control design, the boundedness of virtual controls and torque control inputs are guaranteed. The global stability of the overall system at the origin has been analyzed by applying the Lyapunov's stability and Babarlat's lemma. Finally, the simulation and experimental results demonstrated the feasibility of proposed control schemes.

Chapter 4

Combined path tracking and obstacle avoidance control

This chapter addresses a combined control algorithm for the WMR system to track a desired path while it is capable of avoiding any stationary obstacle along the path. For the path tracking problem, position and orientation of the WMR are forced to converge to those of the reference geometric path parameterized by a time-dependent path parameter. Also, the WMR's velocity should approach the desired linear velocity. To deal with the obstacle avoidance problem, the local potential function represented in [3] is utilized to formulate an effective tool. The smooth step functions are introduced to the local potential function for the continuity of control modes. The Lyapunov's direct method [57], and the standard backstepping technique [58] are used to construct controllers for both problems of path tracking and obstacle avoidance. The rigorous Lyapunov analysis is presented to prove the system's stability. Numerical simulations are shown in the last section for the illustration of the correctness of the proposed control design.

4.1 Problem statement

4.1.1 Mobile robot dynamics

To facilitate the subsequent control development and stability analysis, the mathematical model of a WMR moving in the Cartesian space is considered. This model is combined with kinematic and dynamic models (2.41), (2.50), respec-

tively, developed in Chapter 2:

$$\begin{cases} \dot{x} = v\cos(\phi) \\ \dot{y} = v\sin(\phi) \\ \dot{\phi} = \omega \end{cases}, \qquad \begin{bmatrix} \dot{v} \\ \dot{\omega} \end{bmatrix} = \bar{\mathbf{C}} \begin{bmatrix} \omega^2 \\ -v\omega \end{bmatrix} - \bar{\mathbf{D}} \begin{bmatrix} v \\ \omega \end{bmatrix} + \bar{\mathbf{B}}\boldsymbol{\tau}, \tag{4.1}$$

where matrices $\bar{\mathbf{C}}$, $\bar{\mathbf{D}}$ and $\bar{\mathbf{B}}$ are described by (2.51) in Chapter 2.

4.1.2 Control objective

In general, control design of motion planning problem for the WMR can be described as: given the desired position $\boldsymbol{q}_d(s(t))$ and desired velocity $\dot{\boldsymbol{q}}_d(s(t))$, design a control law for the linear velocity $v(t)$ and angular velocity $\omega(t)$ at kinematic level, or/and torque input vector $\boldsymbol{\tau} = \begin{bmatrix} \tau_v & \tau_\omega \end{bmatrix}^T$ applied to the wheels at the dynamic level, which drives the WMR to move. These velocities must track smoothly the velocity control inputs and the reference path while at the same time satisfying the control objective [13]. Assuming that the immediate point $(x(t), y(t))$ represents the coordinates of the point P_C of the actual WMR's body in figure 2.2. This point must track the reference path generated by the virtual reference vehicle for $\forall t \geq t_0 \geq 0$.

For the particular problem of path tracking and obstacle avoidance, the following assumptions on the reference path, sensing capability, and measurements of the WMR's state variables are stated. These assumptions will simplify the control design and associated stability analysis.

Assumption 4.1.1

The reference path $\boldsymbol{q}_d(s(t)) = \begin{bmatrix} x_d(s(t)) & y_d(s(t)) \end{bmatrix}^T$ *is parameterized by a path parameter* s *which is a time-dependent variable. Let* s_d *be the desired value of the path parameter* s*, and the first derivative of* $s_d(t)$ *is bounded by a strictly positive constants* ϵ_0 *and* ϵ_1*,*

$$\epsilon_0 \leq |\dot{s}_d(t)| \leq \epsilon_1, \qquad \forall t \geq 0. \tag{4.2}$$

Moreover, the vector $\boldsymbol{q}_d(s)$ *is regular and differentiable with respect to* s *at least two times and satisfies the bounded conditions*

$$\begin{aligned} &x_d'^2(s) + y_d'^2(s) \geq \epsilon_2, \qquad \forall s \in \mathbb{R}, \\ &\|\dot{\boldsymbol{q}}_d\| \leq \epsilon_3, \quad \|\ddot{\boldsymbol{q}}_d\| \leq \epsilon_4, \end{aligned} \tag{4.3}$$

where $x'_d(s) = \frac{\partial x_d}{\partial s}$ and $y'_d(s) = \frac{\partial y_d}{\partial s}$, and ϵ_2, ϵ_3 and ϵ_4 are strictly positive constants.

Assumption 4.1.2

The desired linear velocity $v_d(t) = \sqrt{x'^2_d(s) + y'^2_d(s)}\dot{s}(t)$ *is differentiable and its derivatives with respect to t up to second-order are bounded, i.e., there exist strictly positive constants* ϵ_5, ϵ_6, *and* ϵ_7 *such that* $v_d(t)$, $\dot{v}_d(t)$, *and* $\ddot{v}_d(t)$ *satisfy the following conditions*

$$|v_d(t)| \leq \epsilon_5, \qquad |\dot{v}_d(t)| \leq \epsilon_6, \qquad |\ddot{v}_d(t)| \leq \epsilon_7. \tag{4.4}$$

In addition, the desired linear velocity $v_d(t)$ *does not converge to zero, i.e.,* $v_d(t)$ *satisfies the following PE condition*

$$|v_d(t)| \geq \delta, \tag{4.5}$$

where, δ *is a strictly positive constant.*

Assumption 4.1.3

All physical state variables of the WMR are measurable for feedback. The WMR has a physical safety ball with a radius R_{safe}, *and sensing circular area,* R_{sen}, *denotes the radius of the region in which it can detect the presence of an obstacle.*

Assumption 4.1.4

The obstacle is static and it is considered as a convex polygon whose position, $\boldsymbol{q}_{obs} = \begin{bmatrix} x_{obs} & y_{obs} \end{bmatrix}^T$, *and distance of influence,* R_{obs} *can be accurately measured.*

Assumption 4.1.5

There exist a strictly positive constant ϵ_8 *such that at the initial time* t_0, *the WMR initializes at a location* $\boldsymbol{q}(t_0) = [\ x(t_0) \quad y(t_0)\ ]^T$ *where it keeps a safe distance from any obstacle with coordinates* $\boldsymbol{q}_{obs} = \begin{bmatrix} x_{obs} & y_{obs} \end{bmatrix}^T$ *near by*

$$\|\boldsymbol{q}(t_0) - \boldsymbol{q}_{obs}\| \geq \epsilon_8, \tag{4.6}$$

where, $\epsilon_8 \geq (R_{safe} + R_{obs}) + \delta^*$, and δ^* is a strictly positive constant defined later in Control objective section.

Remark. 1. The goal in this chapter is to solve the path tracking and obstacle avoidance problems. Hence, the PE condition (4.5) on the desired linear velocity $v_d(t)$ makes the solution of the path tracking problem feasible. The WMR can move either forward or backward. This also implies that the stabilization problem is excluded from the consideration.

2. Let $P(x_d, y_d)$ be a point of the reference path in the coordinate frame XOY, which is rotated horizontally about the angle ϕ_d. The coordinates of P in the rotating frame X_ROY_R are also illustrated in the figure 4.1. The figure shows that [8]

$$tan(\phi_d) = \frac{(OC - OB)}{(OE - OF)} = \frac{y'_d(s)}{x'_d(d)}.$$

The desired orientation $\phi_d(s)$ and desired angular velocity $\omega_d(t)$ of the virtual reference model are derived as follows

$$\begin{aligned} \phi_d(s) &= \arctan\Big(\frac{y'_d(s)}{x'_d(s)}\Big), \\ \omega_d(t) &= \dot{\phi}_d(s(t)) = \frac{y''_d(s)x'_d(s) - x''_d(s)y'_d(s)}{x'^2_d(s) + y'^2_d(s)}\dot{s}(t), \end{aligned} \tag{4.7}$$

where, the 2^{nd} order partial derivative notations are used: $x''_d(s) = \frac{\partial^2 x_d}{\partial s^2}$ and $y''_d(s) = \frac{\partial^2 y_d}{\partial s^2}$, and $\omega_d(t)$ is well-defined by the condition in (4.3).

3. The condition in Assumption 4.1.5 is necessary for the WMR to avoid colliding with any obstacle in the workspace at the initial time t_0.

Control objective

Under assumptions made above, the overall control objective is to solve the path tracking and obstacle avoidance problems for the WMR dynamics model given by (4.1). As such, designed controllers drive the current configuration of the WMR to asymptotically track to its reference path $\boldsymbol{q}_d(s(t))$ and $\phi_d(s(t))$ at a desired linear velocity $v_d(t)$ while it is able to avoid any obstacle presented within the detecting range of sensing equipment. Moreover, there are no switching modes in the controllers. Mathematically, a proper control input vector $\boldsymbol{\tau} = \begin{bmatrix} \tau_v & \tau_\omega \end{bmatrix}^T$ is sought to ensure that:

1. $\lim_{t\to\infty} \|\boldsymbol{q}(t) - \boldsymbol{q}_d(s(t))\| = 0, \qquad \lim_{t\to\infty} |\phi(t) - \phi_d(s(t))| = 0,$
2. $\|\boldsymbol{q}(t) - \boldsymbol{q}_{obs}\| - (R_{safe} + R_{obs}) \geq \delta^*, \qquad \forall t \geq t_0,$

where δ^* is a strictly positive constant.

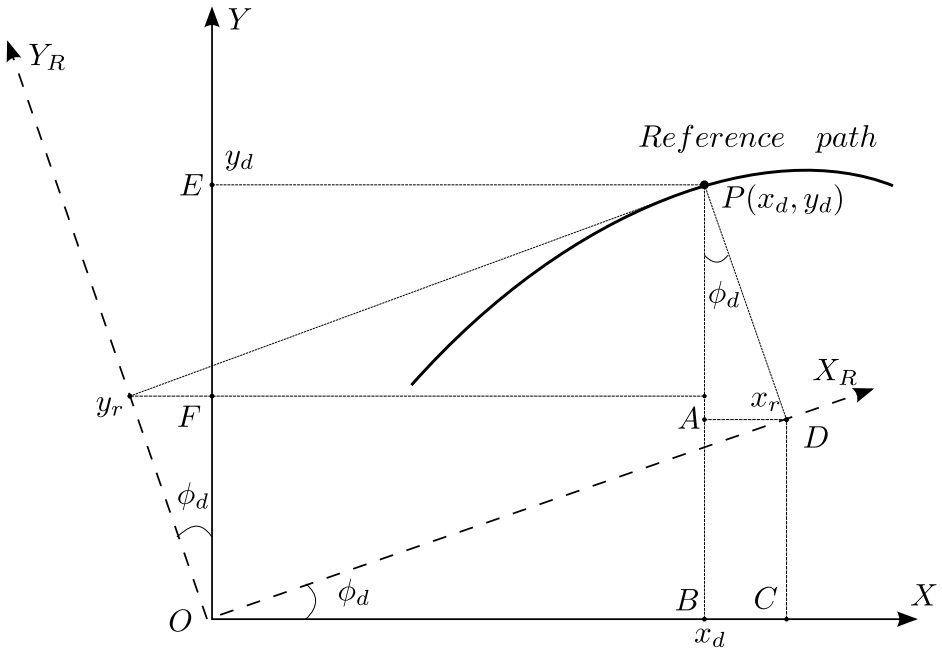

Figure 4.1: Illustration of the reference heading angle ϕ_d

.

4.2 Control design

4.2.1 Design step 1

This control design is inspired by the novel results represented in [2,3] of bounded controllers for mobile robots with limited sensing ranges. First, state-feedback path tracking controllers are designed at kinematic level. Since the kinematic control results are differentiable, the standard backstepping technique [58] can be applied to design controllers associated with the dynamic model in the next step. Let error variables v_e and ϕ_e be defined as

$$\begin{aligned} v_e &= v - \alpha_v, \\ \phi_e &= \phi - \alpha_\phi. \end{aligned} \tag{4.8}$$

For the convenience of solving the obstacle avoidance problem together with path tracking task addressed in control objective, an alternative representation for the position (x, y) and orientation ϕ is adopted for the kinematic model in (4.1). This representation of kinematic parameters is different from the common one in the literature, for example, [39, 41, 47, 76]. Hence the first two equations of (4.1) can be modified according to the definition of (4.8)

$$\dot{\boldsymbol{q}} = \boldsymbol{u} + \boldsymbol{\Lambda}_1 + \boldsymbol{\Lambda}_2, \tag{4.9}$$

where $\dot{\boldsymbol{q}} = \begin{bmatrix} \dot{x} & \dot{y} \end{bmatrix}^T$ and $\boldsymbol{u}$, $\boldsymbol{\Lambda}_1$ and $\boldsymbol{\Lambda}_2$ have been denoted as

$$\begin{aligned} \boldsymbol{u} &= \alpha_v \begin{bmatrix} \cos(\alpha_\phi) \\ \sin(\alpha_\phi) \end{bmatrix}, \\ \boldsymbol{\Lambda}_1 &= \alpha_v \begin{bmatrix} (\cos(\phi_e) - 1)\cos(\alpha_\phi) - \sin(\alpha_\phi)\sin(\phi_e) \\ (\cos(\phi_e) - 1)\sin(\alpha_\phi) + \cos(\alpha_\phi)\sin(\phi_e) \end{bmatrix}, \\ \boldsymbol{\Lambda}_2 &= v_e \begin{bmatrix} \cos(\phi) \\ \sin(\phi) \end{bmatrix}. \end{aligned} \tag{4.10}$$

Based on the control objective, this designing task comprises two sub-tasks, namely, path tracking and obstacle avoidance. In terms of geometric issue, the Cartesian coordinate $\boldsymbol{q}(x, y)$ is forced to reach and track the reference geometric path $\boldsymbol{q}_d\big(x_d(s), y_d(s)\big)$. In terms of dynamic issue, the actual velocity of the WMR $\dot{\boldsymbol{q}}(t)$ should approach the desired linear velocity $v_d(t)$. The task of forcing the WMR to follow a predefined path while having an effective capability of avoiding static obstacles on the path motivates the author to propose a new control algorithm to solve the problem completely.

To achieve both goals of path tracking and obstacle avoidance, the potential field method presented in Section 2.4.2, Chapter 2, are deployed. This combined task can be accomplished by considering the following function

$$\varphi = \gamma + \beta, \tag{4.11}$$

where γ and β are the goal and obstacle avoidance function of the WMR. Equation (4.11) is a particular form of the general equation (2.51). For the path tracking matter, the following Lyapunov function candidate is considered

$$\gamma = \frac{1}{2}\|\boldsymbol{q} - \boldsymbol{q}_d\|^2, \tag{4.12}$$

which is positive definite and radially unbounded, and equal to zero when $x(t) \to x_d$ and $y(t) \to y_d$ as $t \to \infty$. This Lyapunov function plays as a goal function, which is normally mentioned in the literature, for example, [2, 109, 113, 119, 125, 164] for the problem of path planning and collision avoidance.

For the obstacle avoidance matter, a collision function β should be selected in such a way that it is activated whenever the proximity sensors i.e., ultrasound, infrared, detect obstacles in their sensing range and force the WMR to stay away, and equal to infinity whenever it collides with the obstacle. This function β is then deactivated, i.e., is equal to zero, when the obstacle is out of detection

region. Following the work in [3], this function is chosen as:

$$\beta = \frac{1 - h\big(\frac{\|\boldsymbol{q}-\boldsymbol{q}_{obs}\|^2}{2}, \frac{(R_{safe}+R_{obs})^2}{2}, \frac{R_{sen}^2}{2}\big)}{h\big(\frac{\|\boldsymbol{q}-\boldsymbol{q}_{obs}\|^2}{2}, \frac{(R_{safe}+R_{obs})^2}{2}, \frac{R_{sen}^2}{2}\big)}, \tag{4.13}$$

where $h(\frac{\|\boldsymbol{q}-\boldsymbol{q}_{obs}\|^2}{2}, \frac{(R_{safe}+R_{obs})^2}{2}, \frac{R_{sen}^2}{2})$ is the smooth step function introduced in Definition 2.1.3 in Chapter 2. Notations of $\frac{\|\boldsymbol{q}-\boldsymbol{q}_{obs}\|^2}{2}$, $\frac{(R_{safe}+R_{obs})^2}{2}$, and $\frac{R_{sen}^2}{2}$ corresponds to parameters x, a, and b in the Definition 2.1.3, respectively. The function β is a function of $\|\boldsymbol{q} - \boldsymbol{q}_{obs}\|^2/2$ and possesses the following properties [2, 3]:

1. $\beta = 0$, $\beta' = 0$, and $\beta'' = 0$ if $\|\boldsymbol{q} - \boldsymbol{q}_{obs}\| \geq R_{sen}$,
2. $\beta > 0$ if $(R_{safe} + R_{obs}) < \|\boldsymbol{q} - \boldsymbol{q}_{obs}\| < R_{sen}$,
3. $\beta = \infty$, $\beta' = \infty$ if $\|\boldsymbol{q} - \boldsymbol{q}_{obs}\| = (R_{safe} + R_{obs})$,
4. $\beta|_{\|\boldsymbol{q}\|=\|\boldsymbol{q}_d\|} = 0$, $\beta'|_{\|\boldsymbol{q}\|=\|\boldsymbol{q}_d\|} = 0$, $\beta''|_{\|\boldsymbol{q}\|=\|\boldsymbol{q}_d\|} \geq 0$,
5. β is a smooth function with respect to $\|\boldsymbol{q} - \boldsymbol{q}_{obs}\|$ for all $(R_{safe} + R_{obs}) < \|\boldsymbol{q} - \boldsymbol{q}_{obs}\| < R_{sen}$,
6. $\beta \leq \mu_1$, $|\beta'| \leq \mu_2$, and $|\beta''(\boldsymbol{q}-\boldsymbol{q}_{obs})^T(\boldsymbol{q}-\boldsymbol{q}_{obs})| \leq \mu_3$, for all $(R_{safe}+R_{obs}) < \|\boldsymbol{q} - \boldsymbol{q}_{obs}\| < R_{sen}$,

where μ_1, μ_2, and μ_3 are positive constants. The terms β' and β'' are the first and second derivatives of β with respect to $\|\boldsymbol{q} - \boldsymbol{q}_{obs}\|^2/2$ denoted as

$$\begin{aligned} \beta' &= \frac{\partial \beta}{\partial(\|\boldsymbol{q} - \boldsymbol{q}_{obs}\|^2/2)}, \\ \beta'' &= \frac{\partial^2 \beta}{\partial(\|\boldsymbol{q} - \boldsymbol{q}_{obs}\|^2/2)^2}. \end{aligned} \tag{4.14}$$

Remark. 1. There are many functions that satisfy all properties of β mentioned above, for example, [2, 3, 5]. The selection of this particular function β in (4.13) is because it contributes a remarkable property, i.e., $\beta' < 0$, which facilitates to stability analysis of the WMR system under the proposed controllers in this work.

2. Based on observation of real situations, the priority of the WMR's movement can be intuitively explained as follows: under certain initial conditions, the actual WMR tracks a time-varying/time-invariant reference path. The relative distance between the actual WMR and the virtual reference, i.e., $\|\boldsymbol{q} - \boldsymbol{q}_d\|$, is considered at first. This implies the first part of the potential

field-type function (4.11) defined by (4.12) to take charge the priority. This also means no obstacle within the sensing range and property 1 of function β is true. Next, if the actual WMR moves in a detecting area of a potential obstacle, the controller will prioritize to obstacle avoidance function which is represented by second part of (4.11) and particularly chosen by (4.13) in this work. The property 2 of function β is true. At this priority stage, the relative distance $\|\boldsymbol{q} - \boldsymbol{q}_{obs}\|$ is taken into consideration.

3. Properties 1, 2, 3 and 4 imply that β is a continuous differentiable, and positive definite function which satisfies to be a Lyapunov's function candidate for control design and stability analysis purposes. Function β is guaranteed to be zero when the WMR is at the desired location and to be infinity when a collision between it and the obstacle occurs. Property 4 and the function γ given in (4.12) ensure the minimum value of the potential function φ given in (4.11) when the WMR is at its desired location. Property 5 is utilized to deal with the obstacle avoidance problem under the WMRs' limited sensing range for continuous systems instead of techniques for switched, non-smooth, and discontinuous systems. Property 6 is used to prove the stability of the closed feedback system.

Taking the time derivative both sides of equation(4.11) while using the representation of (4.12) and (4.13) along the solutions of (4.9) yields

$$\begin{aligned}\dot{\varphi} &= (\boldsymbol{q} - \boldsymbol{q}_d)^T(\dot{\boldsymbol{q}} - \frac{\partial \boldsymbol{q}_d}{\partial s}\dot{s}) + \beta'(\boldsymbol{q} - \boldsymbol{q}_{obs})^T(\dot{\boldsymbol{q}} - \frac{\partial \boldsymbol{q}_d}{\partial s}\dot{s}) + \beta'(\boldsymbol{q} - \boldsymbol{q}_{obs})^T\frac{\partial \boldsymbol{q}_d}{\partial s}\dot{s} \\ &= \Big((\boldsymbol{q} - \boldsymbol{q}_d) + \beta'(\boldsymbol{q} - \boldsymbol{q}_{obs})\Big)^T(\boldsymbol{u} + \boldsymbol{\Lambda}_1 + \boldsymbol{\Lambda}_2 - \frac{\partial \boldsymbol{q}_d}{\partial s}\dot{s}) + \beta'(\boldsymbol{q} - \boldsymbol{q}_{obs})^T\frac{\partial \boldsymbol{q}_d}{\partial s}\dot{s}.\end{aligned} \tag{4.15}$$

For a compact representation, the following notations are used

$$\begin{cases} \boldsymbol{\Omega} = [\Omega_x \quad \Omega_y]^T = \Big((\boldsymbol{q} - \boldsymbol{q}_d) + \beta'(\boldsymbol{q} - \boldsymbol{q}_{obs})\Big), \\ \Omega_x = (x - x_d) + \beta'(x - x_{obs}), \\ \Omega_y = (y - y_d) + \beta'(y - y_{obs}). \end{cases} \tag{4.16}$$

By applying the idea of differential and bounded functions described in Chapter 2, a bounded control $\boldsymbol{u}$ is selected for the equation (4.15) as follows

$$\boldsymbol{u} = -v_d^2\mathbf{K}\Psi(\boldsymbol{\Omega}) + \frac{\partial \boldsymbol{q}_d}{\partial s}\dot{s}, \tag{4.17}$$

$$\dot{s} = -\lambda\big(\beta'(\boldsymbol{q} - \boldsymbol{q}_{obs})^T\frac{\partial \boldsymbol{q}_d}{\partial s}\big) + \dot{s}_d, \tag{4.18}$$

where, s_d is considered as an additional control to provide the continuity of the path parameter s. $\mathbf{K} = diag(k_1, k_2)$ is a diagonal positive constant matrix, λ is a strictly positive constant. $\Psi(\mathbf{\Omega})$ is the vector of bounded functions of $\mathbf{\Omega} = [\Omega_x \quad \Omega_y]^T$ and has been denoted by

$$\Psi(\mathbf{\Omega}) = \Big[\Psi(\Omega_x) \quad \Psi(\Omega_y)\Big]^T. \tag{4.19}$$

Now, substituting (4.17) and (4.18) into (4.15) results in

$$\begin{aligned}\dot{\varphi} = &-v_d^2 \mathbf{\Omega}^T \mathbf{K} \Psi(\mathbf{\Omega}) - \lambda\big(\beta'(\boldsymbol{q} - \boldsymbol{q}_{obs})^T \frac{\partial \boldsymbol{q}_d}{\partial s}\big)^2 + \mathbf{\Omega}^T(\mathbf{\Lambda}_1 + \mathbf{\Lambda}_2) \\ &+ \beta'(\boldsymbol{q} - \boldsymbol{q}_{obs})^T \frac{\partial \boldsymbol{q}_d}{\partial s}\dot{s}_d.\end{aligned} \tag{4.20}$$

The description of $\boldsymbol{u}$ in (4.10) is used to calculate the virtual control α_ϕ from the bounded control $\boldsymbol{u}$ selected in (4.17)

$$\begin{bmatrix}\alpha_v \cos(\alpha_\phi) \\ \alpha_v \sin(\alpha_\phi)\end{bmatrix} = \begin{bmatrix}-k_1 v_d^2 \Psi(\Omega_x) \\ -k_2 v_d^2 \Psi(\Omega_y)\end{bmatrix} + \begin{bmatrix}v_d \cos(\phi_d) \\ v_d \sin(\phi_d)\end{bmatrix}, \tag{4.21}$$

where the part $\frac{\partial \boldsymbol{q}_d}{\partial s}\dot{s}$ in (4.17) can be described as follows [3, 13]

$$\begin{aligned}\frac{\partial x_d}{\partial s}\dot{s} = x_d'\dot{s} = x_d' \frac{\sqrt{x_d'^2 + y_d'^2}}{\sqrt{x_d'^2 + y_d'^2}}\dot{s} = v_d \cos(\phi_d), \\ \frac{\partial y_d}{\partial s}\dot{s} = y_d'\dot{s} = y_d' \frac{\sqrt{x_d'^2 + y_d'^2}}{\sqrt{x_d'^2 + y_d'^2}}\dot{s} = v_d \sin(\phi_d),\end{aligned} \tag{4.22}$$

with $x_d'^2 + y_d'^2 > \epsilon_2$, $v_d = \sqrt{x_d'^2 + y_d'^2}\dot{s}$, and $\phi_d = \arctan(\frac{y_d'}{x_d'})$, see (4.3), (4.4), and (4.7), respectively.

Multiplying both sides of the first row of (4.21) with $\cos(\phi_d)$ and both sides of the second row of (4.21) with $\sin(\phi_d)$ then adding the two resulting equations together to achieve

$$\alpha_v \cos(\alpha_\phi - \phi_d) = -k_1 v_d^2 \Psi(\Omega_x)\cos(\phi_d) - k_2 v_d^2 \Psi(\Omega_y)\sin(\phi_d) + v_d. \tag{4.23}$$

On the other hand, multiplying both sides of the first row of (4.21) with $\sin(\phi_d)$ and both of the second row of (4.21) with $\cos(\phi_d)$ then subtracting the two resulting equations to give

$$\alpha_v \sin(\alpha_\phi - \phi_d) = k_1 v_d^2 \Psi(\Omega_x)\sin(\phi_d) - k_2 v_d^2 \Psi(\Omega_y)\cos(\phi_d). \tag{4.24}$$

From (4.23) and (4.24), α_ϕ can be solved by deviding (4.24) to (4.23)

$$\alpha_\phi = \arctan\Big[\frac{k_1 v_d \Psi(\Omega_x)\sin(\phi_d) - k_2 v_d \Psi(\Omega_y)\cos(\phi_d)}{-k_1 v_d \Psi(\Omega_x)\cos(\phi_d) - k_2 v_d \Psi(\Omega_y)\sin(\phi_d) + 1}\Big] + \phi_d. \tag{4.25}$$

Owing to the Assumption 4.1.2 for $v_d(t)$ in (4.4) and the property of a differential bounded function in Chapter 2, i.e., $|v_d(t)| \leq \epsilon_5$, $|\Psi(\Omega_x)| \leq M_1$ and $|\Psi(\Omega_y)| \leq M_1$. Hence, the value of virtual control α_ϕ in (4.25) is well-defined if the positive constants are chosen in such a way that

$$k_1 + k_2 < \frac{1}{\epsilon_5 M_1} \tag{4.26}$$

Also, from (4.21), it is straightforward to obtain α_v as follows

$$\alpha_v = \cos(\alpha_\phi)\big(- k_1 v_d^2 \Psi(\Omega_x) + v_d \cos(\phi_d)\big) + \sin(\alpha_\phi)\big(- k_2 v_d^2 \Psi(\Omega_y) + v_d \sin(\phi_d)\big). \tag{4.27}$$

The equation of $\dot{\varphi}$ in (4.20) will be used in the next step. On the other hand, after substituting (4.17) into (4.9), the following expression can be obtained

$$\dot{\boldsymbol{q}} = -v_d^2 \mathbf{K} \Psi(\boldsymbol{\Omega}) + \frac{\partial \boldsymbol{q}_d}{\partial s}\dot{s} + \boldsymbol{\Lambda}_1 + \boldsymbol{\Lambda}_2. \tag{4.28}$$

Remark. As $\boldsymbol{\Omega}$ defined in (4.16) and $\frac{\partial \boldsymbol{q}_d}{\partial s}\dot{s}$ represented in (4.22) are substituted into (4.17), the control $\boldsymbol{u}$ can be rewritten as

$$\boldsymbol{u} = -v_d^2 \begin{bmatrix} k_1 & 0 \\ 0 & k_2 \end{bmatrix} \begin{bmatrix} \Psi\big((x - x_d) + \beta'(x - x_{obs})\big) \\ \Psi\big((y - y_d) + \beta'(y - y_{obs})\big) \end{bmatrix} + \begin{bmatrix} v_d \cos(\phi_d) \\ v_d \sin(\phi_d) \end{bmatrix}. \tag{4.29}$$

Similar to other control designs for the problem of path planning and collision avoidance, for example, [2,3,109,113,119,125,164], it can be seen from (4.29) that the argument of Ψ consists of two parts. The first part, $(x - x_d)$ or $(y - y_d)$, referred to as the attractive force which drives the WMR to its reference path through the means of virtual control α_ϕ. The second part, $\beta'(x - x_{obs})$ or $\beta'(y - y_{obs})$, referred to as the repulsive force which takes the responsibility of obstacle avoidance task.

4.2.2 Design step 2

At this step, the design focuses on stabilizing ϕ at the origin by considering ω as an immediate control. As such, the error variable ω_e is defined as

$$\omega_e = \omega - \alpha_\omega \tag{4.30}$$

where α_ω is the virtual control of ω. It can also be seen from (4.25) that α_ϕ is a smooth function of v_d, ϕ_d, $\boldsymbol{q}_d$, and $\boldsymbol{q}$. After taking the time derivative both sides of the second equation of (4.8) along the solutions of (4.1) and using the equation (4.30), the following expression is obtained

$$\begin{aligned} \dot{\phi}_e &= \dot{\phi} - \dot{\alpha}_\phi \\ &= \omega_e + \alpha_\omega - \Big(\frac{\partial \alpha_\phi}{\partial v_d}\dot{v}_d + \frac{\partial \alpha_\phi}{\partial \phi_d}\dot{\phi}_d + \frac{\partial \alpha_\phi}{\partial \boldsymbol{q}_d}\frac{\partial \boldsymbol{q}_d}{\partial s}\dot{s} + \frac{\partial \alpha_\phi}{\partial \boldsymbol{q}}(\boldsymbol{u} + \boldsymbol{\Lambda}_1 + \boldsymbol{\Lambda}_2)\Big). \end{aligned} \tag{4.31}$$

Now, the following Lyapunov's function candidate is considered

$$V_2 = \varphi + \frac{1}{2}\phi_e^2. \tag{4.32}$$

Taking differentiation both sides of (4.32) along the solutions of (4.20), and (4.31) gives

$$\begin{aligned}
\dot{V}_2 &= \dot{\varphi} + \phi_e\dot{\phi}_e \\
&= -v_d^2\boldsymbol{\Omega}^T\mathbf{K}\Psi(\boldsymbol{\Omega}) - \lambda\big(\beta'(\boldsymbol{q}-\boldsymbol{q}_{obs})^T\frac{\partial \boldsymbol{q}_d}{\partial s}\big)^2 + \boldsymbol{\Omega}^T(\boldsymbol{\Lambda}_1+\boldsymbol{\Lambda}_2) \\
&\quad + \beta'(\boldsymbol{q}-\boldsymbol{q}_{obs})^T\frac{\partial \boldsymbol{q}_d}{\partial s}\dot{s}_d \\
&\quad + \phi_e\Big[\omega_e + \alpha_\omega - \Big(\frac{\partial \alpha_\phi}{\partial v_d}\dot{v}_d + \frac{\partial \alpha_\phi}{\partial \phi_d}\dot{\phi}_d + \frac{\partial \alpha_\phi}{\partial \boldsymbol{q}_d}\frac{\partial \boldsymbol{q}_d}{\partial s}\dot{s} + \frac{\partial \alpha_\phi}{\partial \boldsymbol{q}}(\boldsymbol{u}+\boldsymbol{\Lambda}_1+\boldsymbol{\Lambda}_2)\Big)\Big] \\
&= -v_d^2\boldsymbol{\Omega}^T\mathbf{K}\Psi(\boldsymbol{\Omega}) - \lambda\big(\beta'(\boldsymbol{q}-\boldsymbol{q}_{obs})^T\frac{\partial \boldsymbol{q}_d}{\partial s}\big)^2 + \beta'(\boldsymbol{q}-\boldsymbol{q}_{obs})^T\frac{\partial \boldsymbol{q}_d}{\partial s}\dot{s}_d \\
&\quad + \phi_e\Big[\omega_e + \alpha_\omega + \frac{\boldsymbol{\Omega}^T\boldsymbol{\Lambda}_1}{\phi_e} - \Big(\frac{\partial \alpha_\phi}{\partial v_d}\dot{v}_d + \frac{\partial \alpha_\phi}{\partial \phi_d}\dot{\phi}_d + \frac{\partial \alpha_\phi}{\partial \boldsymbol{q}_d}\frac{\partial \boldsymbol{q}_d}{\partial s}\dot{s} + \frac{\partial \alpha_\phi}{\partial \boldsymbol{q}}(\boldsymbol{u}+\boldsymbol{\Lambda}_1)\Big)\Big] \\
&\quad + \boldsymbol{\Omega}^T\boldsymbol{\Lambda}_2 - \phi_e\frac{\partial \alpha_\phi}{\partial \boldsymbol{q}}\boldsymbol{\Lambda}_2.
\end{aligned} \tag{4.33}$$

Since $\sin(\phi_e)/\phi_e = \int_0^1 \cos(s\phi_e)ds$ and $(\cos(\phi_e)-1)/\phi_e = -\int_0^1 \sin(s\phi_e)ds$ are smooth for all $\phi_e \in \mathbb{R}$, the term $\boldsymbol{\Lambda}_1/\phi_e$ in (4.33) is well-defined [3, 22]. From the expression of $\dot{V}_2$, the virtual control α_ω is selected as follows

$$\alpha_\omega = -k_3\sigma(\phi_e) - \frac{\boldsymbol{\Omega}^T\boldsymbol{\Lambda}_1}{\phi_e} + \frac{\partial \alpha_\phi}{\partial v_d}\dot{v}_d + \frac{\partial \alpha_\phi}{\partial \phi_d}\dot{\phi}_d + \frac{\partial \alpha_\phi}{\partial \boldsymbol{q}_d}\frac{\partial \boldsymbol{q}_d}{\partial s}\dot{s} + \frac{\partial \alpha_\phi}{\partial \boldsymbol{q}}(\boldsymbol{u}+\boldsymbol{\Lambda}_1), \tag{4.34}$$

where k_3 is a positive constant and $\sigma(\bullet)$ is a smooth saturation function defined in Chapter 2. Now substituting (4.34) into (4.33) yields

$$\begin{aligned}
\dot{V}_2 &= -v_d^2\boldsymbol{\Omega}^T\mathbf{K}\Psi(\boldsymbol{\Omega}) - \lambda\big(\beta'(\boldsymbol{q}-\boldsymbol{q}_{obs})^T\frac{\partial \boldsymbol{q}_d}{\partial s}\big)^2 - k_3\sigma(\phi_e)\phi_e + \begin{bmatrix}\Phi_{12} & \Phi_{22}\end{bmatrix}\begin{bmatrix}v_e \\ \omega_e\end{bmatrix} \\
&\quad + \beta'(\boldsymbol{q}-\boldsymbol{q}_{obs})^T\frac{\partial \boldsymbol{q}_d}{\partial s}\dot{s}_d,
\end{aligned} \tag{4.35}$$

where Φ_{12} and Φ_{22} have been denoted as

$$\begin{aligned}
\Phi_{12} &= \boldsymbol{\Omega}^T\begin{bmatrix}\cos(\phi) \\ \sin(\phi)\end{bmatrix} - \phi_e\frac{\partial \alpha_\phi}{\partial \boldsymbol{q}}\begin{bmatrix}\cos(\phi) \\ \sin(\phi)\end{bmatrix}, \\
\Phi_{22} &= \phi_e.
\end{aligned} \tag{4.36}$$

From the control design above, the closed-loop system for the WMR at the kinematic level can be rewritten by substituting (4.34) into (4.31)

$$\begin{aligned}
\dot{\boldsymbol{q}} &= -v_d^2\mathbf{K}\Psi(\boldsymbol{\Omega}) + \frac{\partial \boldsymbol{q}_d}{\partial s}\dot{s} + \boldsymbol{\Lambda}_1 + \boldsymbol{\Lambda}_2, \\
\dot{\phi}_e &= -k_3\sigma(\phi_e) - \frac{\boldsymbol{\Omega}^T\boldsymbol{\Lambda}_1}{\phi_e} - \frac{\partial \alpha_\phi}{\partial \boldsymbol{q}}\boldsymbol{\Lambda}_2 + \omega_e.
\end{aligned} \tag{4.37}$$

4.2.3 Design step 3

Using the representation in (4.9), the kinematics and dynamics of a nonholonomic WMR in (4.1) can be rewritten as

$$\begin{aligned} &\begin{cases} \dot{\boldsymbol{q}} = \boldsymbol{u} + \boldsymbol{\Lambda}_1 + \boldsymbol{\Lambda}_2, \\ \dot{\phi} = \omega \end{cases}, \\ &\begin{bmatrix} \dot{v} \\ \dot{\omega} \end{bmatrix} = \bar{\mathbf{C}} \begin{bmatrix} \omega^2 \\ -v\omega \end{bmatrix} - \bar{\mathbf{D}} \begin{bmatrix} v \\ \omega \end{bmatrix} + \bar{\mathbf{B}}\boldsymbol{\tau}, \end{aligned} \tag{4.38}$$

where the matrices $\bar{\mathbf{C}}$, $\bar{\mathbf{D}}$ and $\bar{\mathbf{B}}$ are described in (2.51). With the choice of α_ω in (4.34), it is a differentiable and smooth function with respect to its variables. Hence, taking differentiation both sides of the first equation of (4.8) and (4.30) yields

$$\begin{aligned} \dot{v}_e &= \dot{v} - \dot{\alpha}_v, \\ \dot{\omega}_e &= \dot{\omega} - \dot{\alpha}_\omega. \end{aligned} \tag{4.39}$$

Substituting those equations in (4.39) into the last equation of (4.38) gives

$$\begin{bmatrix} \dot{v}_e \\ \dot{\omega}_e \end{bmatrix} = \bar{\mathbf{C}} \begin{bmatrix} \omega^2 \\ -v\omega \end{bmatrix} - \bar{\mathbf{D}} \begin{bmatrix} v \\ \omega \end{bmatrix} + \bar{\mathbf{B}}\boldsymbol{\tau} - \begin{bmatrix} \Delta_1 \\ \Delta_2 \end{bmatrix}, \tag{4.40}$$

where $\Delta_1 = \Delta_{11} + \Delta_{12}$ and $\Delta_2 = \Delta_{21} + \Delta_{22}$, and

$$\begin{aligned} \Delta_{11} &= \frac{\partial \alpha_v}{\partial v_d}\dot{v}_d + \frac{\partial \alpha_v}{\partial \phi_d}\dot{\phi}_d + \frac{\partial \alpha_v}{\partial \boldsymbol{q}_d}\frac{\partial \boldsymbol{q}_d}{\partial s}\dot{s} + \frac{\partial \alpha_v}{\partial \boldsymbol{q}}(\boldsymbol{u} + \boldsymbol{\Lambda}_1), \\ \Delta_{12} &= \frac{\partial \alpha_v}{\partial \boldsymbol{q}}\boldsymbol{\Lambda}_2, \\ \Delta_{21} &= \frac{\partial \alpha_\omega}{\partial v_d}\dot{v}_d + \frac{\partial \alpha_\omega}{\partial \dot{v}_d}\ddot{v}_d + \frac{\partial \alpha_\omega}{\partial \phi_d}\dot{\phi}_d + \frac{\partial \alpha_\omega}{\partial \dot{\phi}_d}\ddot{\phi}_d + \frac{\partial \alpha_\omega}{\partial \boldsymbol{q}_d}\frac{\partial \boldsymbol{q}_d}{\partial s}\dot{s} \\ &\quad + \frac{\partial \alpha_\omega}{\partial \dot{\boldsymbol{q}}_d}\frac{\partial^2 \boldsymbol{q}_d}{\partial s^2}\dot{s} + \frac{\partial \alpha_\omega}{\partial \boldsymbol{q}}(\boldsymbol{u} + \boldsymbol{\Lambda}_1) + \frac{\partial \alpha_\omega}{\partial \phi}\alpha_\omega, \\ \Delta_{22} &= \frac{\partial \alpha_\omega}{\partial \boldsymbol{q}}\boldsymbol{\Lambda}_2 + \frac{\partial \alpha_\omega}{\partial \phi}\omega_e. \end{aligned} \tag{4.41}$$

To design control input torque vector $\boldsymbol{\tau} = \begin{bmatrix} \tau_1 & \tau_2 \end{bmatrix}^T$, the following Lyapunov function candidate is considered

$$V_3 = V_2 + \frac{1}{2}\begin{bmatrix} v_e & \omega_e \end{bmatrix} \bar{\mathbf{C}}^{-1} \begin{bmatrix} v_e \\ \omega_e \end{bmatrix}, \tag{4.42}$$

which is positive definite and radially unbounded in x_e, y_e, v_e, ω_e, see (4.11), (4.12), (4.13) for the equation of φ, and (4.32) for the equation of V_2, respectively. After

taking the time derivative both sides of (4.42) along the solutions of (4.35) and (4.40), the following expression is achieved

$$\dot{V}_3 = -v_d^2 \boldsymbol{\Omega}^T \mathbf{K} \Psi(\boldsymbol{\Omega}) - \lambda \big(\beta'(\boldsymbol{q} - \boldsymbol{q}_{obs})^T \frac{\partial \boldsymbol{q}_d}{\partial s}\big)^2 - k_3 \sigma(\phi_e)\phi_e + \beta'(\boldsymbol{q} - \boldsymbol{q}_{obs})^T \frac{\partial \boldsymbol{q}_d}{\partial s} \dot{s}_d + \begin{bmatrix} v_e & \omega_e \end{bmatrix} \bar{\mathbf{C}}^{-\mathbf{1}} \Bigg\{ \bar{\mathbf{C}} \begin{bmatrix} \omega^2 \\ -v\omega \end{bmatrix} - \bar{\mathbf{D}} \begin{bmatrix} v \\ \omega \end{bmatrix} + \bar{\mathbf{B}} \boldsymbol{\tau} - \begin{bmatrix} \Delta_1 \\ \Delta_2 \end{bmatrix} + \bar{\mathbf{C}} \begin{bmatrix} \Phi_{12} \\ \Phi_{22} \end{bmatrix} \Bigg\}, \tag{4.43}$$

where Φ_{12} and Φ_{22} are shown in (4.36). For the convenience of calculation, $\dot{V}_3$ can be rearranged as

$$\begin{aligned} \dot{V}_3 = & -v_d^2 \boldsymbol{\Omega}^T \mathbf{K} \Psi(\boldsymbol{\Omega}) - \lambda \big(\beta'(\boldsymbol{q} - \boldsymbol{q}_{obs})^T \frac{\partial \boldsymbol{q}_d}{\partial s}\big)^2 - k_3 \sigma(\phi_e)\phi_e \\ & + \beta'(\boldsymbol{q} - \boldsymbol{q}_{obs})^T \frac{\partial \boldsymbol{q}_d}{\partial s} \dot{s}_d + \Pi_1 + \Pi_2, \end{aligned} \tag{4.44}$$

where Π_1 and Π_2 have been denoted as,

$$\begin{aligned} \Pi_1 = & \, v_e \bar{c}_1^{-1} \dot{v}_e + v_e \Phi_{12} = v_e \omega_e^2 + 2\alpha_\omega v_e \omega_e + \alpha_\omega^2 v_e - \bar{\bar{d}}_{11} v_e^2 - \bar{\bar{d}}_{11} \alpha_v v_e - \bar{\bar{d}}_{12} v_e \omega_e \\ & - \bar{\bar{d}}_{12} \alpha_\omega v_e - \frac{1}{\bar{c}_1} v_e \Delta_1 + v_e \Phi_{12} + \bar{\bar{b}}_{11} \tau_v v_e + \bar{\bar{b}}_{12} \tau_\omega v_e, \end{aligned} \tag{4.45}$$

$$\begin{aligned} \Pi_2 = & \, \omega_e \bar{c}_2^{-1} \dot{\omega}_e + \omega_e \Phi_{22} \\ = & -v_e \omega_e^2 - \alpha_v \omega_e^2 - \alpha_\omega v_e \omega_e - \alpha_v \alpha_\omega \omega_e - \bar{\bar{d}}_{21} v_e \omega_e - \bar{\bar{d}}_{21} \alpha_v \omega_e - \bar{\bar{d}}_{22} \omega_e^2 \\ & - \bar{\bar{d}}_{22} \alpha_\omega \omega_e - \frac{1}{\bar{c}_2} \omega_e \Delta_2 + \omega_e \Phi_{22} + \bar{\bar{b}}_{21} \tau_v \omega_e + \bar{\bar{b}}_{22} \tau_\omega \omega_e, \end{aligned} \tag{4.46}$$

In (4.45) and (4.46), coefficients have been denoted as follows: $\bar{\bar{d}}_{11} = \frac{\bar{d}_{11}}{\bar{c}_1}; \bar{\bar{d}}_{12} = \frac{\bar{d}_{12}}{\bar{c}_1}; \bar{\bar{b}}_{11} = \frac{\bar{b}_{11}}{\bar{c}_1}; \bar{\bar{b}}_{12} = \frac{\bar{b}_{12}}{\bar{c}_1}; \bar{\bar{d}}_{21} = \frac{\bar{d}_{21}}{\bar{c}_2}; \bar{\bar{d}}_{22} = \frac{\bar{d}_{22}}{\bar{c}_2}; \bar{\bar{b}}_{21} = \frac{\bar{b}_{21}}{\bar{c}_2}; \bar{\bar{b}}_{22} = \frac{\bar{b}_{22}}{\bar{c}_2}$.
Coefficients $\bar{\bar{d}}_{11}$ and $\bar{\bar{d}}_{22}$ in (4.44) and (4.45) are useful damping elements. This property is used to dominate other associated coupling terms after applying the Young's inequality below

$$\begin{aligned} & \alpha_\omega v_e \omega_e \leq |\alpha_\omega| \big(\kappa v_e^2 + \frac{1}{4\kappa} \omega_e^2\big), \\ & (\bar{\bar{d}}_{12} + \bar{\bar{d}}_{21}) v_e \omega_e \leq (\bar{\bar{d}}_{12} + \bar{\bar{d}}_{21}) \big(\kappa v_e^2 + \frac{1}{4\kappa} \omega_e^2\big), \end{aligned} \tag{4.47}$$

where κ is a positive constant and α_ω is represented in (4.34). The absolute value $|\alpha_\omega|$ in (4.47) is valid because all parts of α_ω are bounded. Now substituting results of (4.47) back into (4.45), (4.46) and then into (4.44) yields

$$\begin{aligned} \dot{V}_3 \leq & -v_d^2 \boldsymbol{\Omega}^T \mathbf{K} \Psi(\boldsymbol{\Omega}) - \lambda \big(\beta'(\boldsymbol{q} - \boldsymbol{q}_{obs})^T \frac{\partial \boldsymbol{q}_d}{\partial s}\big)^2 - k_3 \sigma(\phi_e)\phi_e \\ & - \Big[v_e^2 \Upsilon_3 + \omega_e^2 \Upsilon_4\Big] + \beta'(\boldsymbol{q} - \boldsymbol{q}_{obs})^T \frac{\partial \boldsymbol{q}_d}{\partial s} \dot{s}_d \end{aligned}$$

$$+\Big[v_e\big(\Upsilon_1+(\bar{\bar{b}}_{11}\tau_v+\bar{\bar{b}}_{12}\tau_\omega)\big)+\omega_e\big(\Upsilon_2+(\bar{\bar{b}}_{21}\tau_v+\bar{\bar{b}}_{22}\tau_\omega)\big)\Big], \tag{4.48}$$

where constants Υ_1, Υ_2, Υ_3, and Υ_4 have been denoted as

$$\begin{aligned}
\Upsilon_1 &= \alpha_\omega^2-\bar{\bar{d}}_{11}\alpha_v-\bar{\bar{d}}_{12}\alpha_\omega-\frac{1}{\bar{c}_1}\Delta_1+\Phi_{12},\\
\Upsilon_2 &= -\alpha_v\alpha_\omega-\bar{\bar{d}}_{21}\alpha_v-\bar{\bar{d}}_{22}\alpha_\omega-\frac{1}{\bar{c}_2}\Delta_2+\Phi_{22},\\
\Upsilon_3 &= (1-\epsilon^*)\bar{\bar{d}}_{11}-\kappa(\bar{\bar{d}}_{12}+\bar{\bar{d}}_{21}+|\alpha_\omega|),\\
\Upsilon_4 &= (1-\epsilon^*)\bar{\bar{d}}_{22}+|\alpha_v|-\frac{1}{4\kappa}(\bar{\bar{d}}_{12}+\bar{\bar{d}}_{21}).
\end{aligned} \tag{4.49}$$

Noting from (4.48) and (4.49) that only $(1-\epsilon^*)\bar{\bar{d}}_{11}$ and $(1-\epsilon^*)\bar{\bar{d}}_{22}$ are used for the domination to guarantee the terms Υ_3 and Υ_4 to be strictly positive while $\epsilon^*\bar{\bar{d}}_{11}$ and $\epsilon^*\bar{\bar{d}}_{22}$ are kept for stability analysis later. ϵ^* is a positive constant and it is chosen to satisfy $0<\epsilon^*<1$ and the positive constant κ is selected as $\frac{1}{2}$. Hence, the conditions below must hold

$$\begin{aligned}
(1-\epsilon^*)\bar{\bar{d}}_{11} &> \frac{1}{2}(\bar{\bar{d}}_{12}+\bar{\bar{d}}_{21}+|\alpha_\omega|),\\
(1-\epsilon^*)\bar{\bar{d}}_{22} &> \frac{1}{2}(\bar{\bar{d}}_{12}+\bar{\bar{d}}_{21})+|\alpha_v|,
\end{aligned} \tag{4.50}$$

where the bounds of $|\alpha_v|$ in (4.27), and $|\alpha_\omega|$ in (4.34) can be calculated by employing conditions (4.4), the property of a differential bounded function $\Psi(\bullet)$ in Chapter 2, and property 6 of function β in (4.11). There always exist parameters ϵ_i, for $i=0,1,\ldots,6$, and k_j, for $j=1,\ldots,3$ such that two conditions in (4.49) hold with $\bar{c}_1$, $\bar{c}_2$, $\bar{d}_{11}$, $\bar{d}_{12}$, $\bar{d}_{21}$, and $\bar{d}_{22}$ are defined in (2.51). Hence, the torque control inputs τ_v and τ_ω are chosen as follows

$$\begin{aligned}
\tau_v &= \frac{-\bar{\bar{b}}_{22}}{\bar{\bar{b}}_{11}\bar{\bar{b}}_{22}-\bar{\bar{b}}_{12}\bar{\bar{b}}_{21}}\big(k_4\sigma(v_e)+\Upsilon_1\big)+\frac{\bar{\bar{b}}_{12}}{\bar{\bar{b}}_{11}\bar{\bar{b}}_{22}-\bar{\bar{b}}_{12}\bar{\bar{b}}_{21}}\big(k_5\sigma(\omega_e)+\Upsilon_2\big),\\
\tau_\omega &= \frac{\bar{\bar{b}}_{21}}{\bar{\bar{b}}_{11}\bar{\bar{b}}_{22}-\bar{\bar{b}}_{12}\bar{\bar{b}}_{21}}\big(k_4\sigma(v_e)+\Upsilon_1\big)-\frac{\bar{\bar{b}}_{11}}{\bar{\bar{b}}_{11}\bar{\bar{b}}_{22}-\bar{\bar{b}}_{12}\bar{\bar{b}}_{21}}\big(k_5\sigma(\omega_e)+\Upsilon_2\big).
\end{aligned} \tag{4.51}$$

where k_4, and k_5 are positive constants.

Remark. It can easily be seen that actual controls τ_v and τ_ω are well-defined since:

$$\begin{aligned}
\bar{\bar{\mathbf{B}}} &= \begin{bmatrix}\bar{c}_1^{-1} & 0\\ 0 & \bar{c}_2^{-1}\end{bmatrix}\begin{bmatrix}\bar{b}_{11} & \bar{b}_{12}\\ \bar{b}_{21} & \bar{b}_{22}\end{bmatrix}=\begin{bmatrix}\bar{\bar{b}}_{11} & \bar{\bar{b}}_{12}\\ \bar{\bar{b}}_{21} & \bar{\bar{b}}_{22}\end{bmatrix},\\
det(\bar{\bar{\mathbf{B}}}) &= \bar{\bar{b}}_{11}\bar{\bar{b}}_{22}-\bar{\bar{b}}_{12}\bar{\bar{b}}_{21}=-\frac{r^2}{2bc^2}\neq 0.
\end{aligned} \tag{4.52}$$

where all these terms $\bar{c}_1,\bar{c}_2,\bar{b}_{11},\bar{b}_{12},\bar{b}_{21}$ and $\bar{b}_{22}$ are defined in (2.51).

After substituting the control vector $\boldsymbol{\tau} = \begin{bmatrix} \tau_v & \tau_\omega \end{bmatrix}^T$ designed in (4.50) into (4.47), the expression of $\dot{V}_3$ is given by

$$\begin{aligned}
\dot{V}_3 \leq & -v_d^2 \boldsymbol{\Omega}^T \mathbf{K} \Psi(\boldsymbol{\Omega}) - \lambda \big(\beta'(\boldsymbol{q} - \boldsymbol{q}_{obs})^T \frac{\partial \boldsymbol{q}_d}{\partial s}\big)^2 - k_3 \sigma(\phi_e)\phi_e - k_4 \sigma(v_e) v_e - k_5 \sigma(\omega_e)\omega_e \\
& - \Big[v_e^2 \Upsilon_3 + \omega_e^2 \Upsilon_4\Big] + \beta'(\boldsymbol{q} - \boldsymbol{q}_{obs})^T \frac{\partial \boldsymbol{q}_d}{\partial s} \dot{s}_d - \epsilon^* \lambda_{min}(\bar{\mathbf{D}}) v_e^2 - \epsilon^* \lambda_{min}(\bar{\mathbf{D}}) \omega_e^2 \\
\leq & -v_d^2 \boldsymbol{\Omega}^T \mathbf{K} \Psi(\boldsymbol{\Omega}) - \lambda \big(\beta'(\boldsymbol{q} - \boldsymbol{q}_{obs})^T \frac{\partial \boldsymbol{q}_d}{\partial s}\big)^2 - k_3 \sigma(\phi_e)\phi_e - k_4 \sigma(v_e) v_e - k_5 \sigma(\omega_e)\omega_e \\
& + \beta'(\boldsymbol{q} - \boldsymbol{q}_{obs})^T \frac{\partial \boldsymbol{q}_d}{\partial s} \dot{s}_d - \epsilon^* \lambda_{min}(\bar{\mathbf{D}}) v_e^2 - \epsilon^* \lambda_{min}(\bar{\mathbf{D}}) \omega_e^2. \qquad (4.53)
\end{aligned}$$

Provided that the conditions in (4.50) are satisfied, the inequality in (4.53) is achieved. From (4.11), (4.12), (4.13), (4.32), and (4.42), it can be seen that V_3 is positive definite and radially unbounded. This property is used in the next section of stability analysis. As a result, the closed-loop system at dynamic level for the WMR can be rewritten by using the closed-loop system at the kinematic level (4.37), and substituting (4.51) into (4.40) as follows

$$\begin{aligned}
\dot{\boldsymbol{q}} &= -v_d^2 \mathbf{K} \Psi(\boldsymbol{\Omega}) + \frac{\partial \boldsymbol{q}_d}{\partial s} \dot{s} + \boldsymbol{\Lambda}_1 + \boldsymbol{\Lambda}_2, \\
\dot{\phi}_e &= -k_3 \sigma(\phi_e) - \frac{\boldsymbol{\Omega}^T \boldsymbol{\Lambda}_1}{\phi_e} - \frac{\partial \alpha_\phi}{\partial \boldsymbol{q}} \boldsymbol{\Lambda}_2 + \omega_e, \\
\begin{bmatrix} \dot{v}_e \\ \dot{\omega}_e \end{bmatrix} &= \bar{\mathbf{C}} \begin{bmatrix} \omega^2 \\ -v\omega \end{bmatrix} - \bar{\mathbf{D}} \begin{bmatrix} v \\ \omega \end{bmatrix} - \begin{bmatrix} (k_4 \sigma(v_e) + \Upsilon_1) \\ (k_5 \sigma(\omega_e) + \Upsilon_2) \end{bmatrix} - \begin{bmatrix} \Delta_1 \\ \Delta_2 \end{bmatrix}.
\end{aligned} \qquad (4.54)$$

The control design has been completed and the control objective is achieved. The results are summarized in the following theorem.

Theorem 4.2.1. *Consider the nonholonomic WMR system described by (4.38) and the reference path is regular. Under the Assumptions 4.1.1, 4.1.2, 4.1.3, 4.1.4, and 4.1.5, the torque control vector $\boldsymbol{\tau}$ given by (4.51) solves the control objective provided that control gains k_1, k_2 are satisfied the condition (4.26), k_3, k_4, k_5, and $\kappa \in \mathbb{R}_+$, and conditions (4.50) hold. In particular, the following results hold for all initial conditions $(x(t_0), y(t_0)) \in \mathbb{R}^2$, $\phi_e(t_0) \in \mathbb{R}$ and $(v_e(t_0), \omega_e(t_0)) \in \mathbb{R}^2$:*

1. *The closed-loop system (4.54) is forward complete and globally converges to the origin.*

2. *The WMR globally asymptotically moves along the path tangentially with a desired linear velocity v_d.*

3. *No collisions between the WMR and obstacles have been guaranteed for all $t \geq t_0 \geq 0$.*

4.3 Stability analysis

Stability analysis in this chapter follows techniques used in [3]. The difference here is that this proof is given to the closed-loop system of the single WMR and obstacles without collisions and forward completeness, instead of a group of mobile robots working in the scheme of formation control. Also, a particular investigation for the forward completeness is included. Properties of equilibrium and saddle points are clarified similarly. Hence, Theorem 4.2.1 is proven in two steps. First, no collision between the WMR and obstacles is proven and the closed-loop system is forward complete [163]. In the second step, stability properties of equilibrium points are carefully investigated.

4.3.1 Proof of forward completeness of closed-loop system and no collisions

The inequality (4.53) can be represented alternatively as

$$\dot{V}_3 \leq -v_d^2 \boldsymbol{\Omega}^T \mathbf{K} \Psi(\boldsymbol{\Omega}) - W_3 - \lambda \big(\beta'(\boldsymbol{q} - \boldsymbol{q}_{obs})^T \frac{\partial \boldsymbol{q}_d}{\partial s}\big)^2 + \beta'(\boldsymbol{q} - \boldsymbol{q}_{obs})^T \frac{\partial \boldsymbol{q}_d}{\partial s} \dot{s}_d. \tag{4.55}$$

where W_3 is denoted by

$$W_3 = k_3 \sigma(\phi_e)\phi_e + k_4 \sigma(v_e) v_e + k_5 \sigma(\omega_e)\omega_e + \epsilon^* \lambda_{min}(\bar{\mathbf{D}}) v_e^2 + \epsilon^* \lambda_{min}(\bar{\mathbf{D}}) \omega_e^2. \tag{4.56}$$

W_3 is a nonnegative-valued, radially unbounded, smooth function for all $\phi_e(t) \in \mathbb{R}$, and $\mathbf{v}_e(t) = [v_e(t) \quad \omega_e(t)]^T \in \mathbb{R}^2$.

Case 1: ***The obstacle is outside of the WMR's sensing detection range or*** $\|\boldsymbol{q} - \boldsymbol{q}_{obs}\| > R_{sen}$**.**

Case 1 implies that the collision function β defined in (4.13) is inactive and there is no collision. Property 1 of the function β holds, i.e., $\beta = 0$ and $\beta' = 0$. The inequality (4.53) can be replaced as follows

$$\begin{aligned} \dot{V}_3 \leq & - v_d^2 (\boldsymbol{q} - \boldsymbol{q}_d)^T \mathbf{K} \Psi((\boldsymbol{q} - \boldsymbol{q}_d)) - k_3 \sigma(\phi_e)\phi_e - k_4 \sigma(v_e) v_e - k_5 \sigma(\omega_e)\omega_e \\ & - \epsilon^* \lambda_{min}(\bar{\mathbf{D}}) v_e^2 - \epsilon^* \lambda_{min}(\bar{\mathbf{D}}) \omega_e^2 \leq -W_3^* \leq 0. \end{aligned} \tag{4.57}$$

This is because function W_3^* in the right-hand side of (4.57) is a nonnegative-valued, radially unbounded, smooth function for all $\boldsymbol{q}(t) - \boldsymbol{q}_d(t) \in \mathbb{R}^2$, $\phi_e(t) \in \mathbb{R}$,

and $\mathbf{v}_e(t) = [v_e(t) \quad \omega_e(t)]^T \in \mathbb{R}^2$. Integrating both sides of the inequality (4.57) from t_0 to t results in

$$\int_{t_0}^{t} V_3(\tau)d\tau = V_3(t) - V_3(t_0) \leq 0, \tag{4.58}$$

this means $V_3(t_0) - V_3(t) \geq 0$, for all $t \geq t_0$. Using function V_3 defined in (4.42) with its components in (4.11), (4.12), (4.13) and (4.32) gives

$$\begin{aligned} &\gamma(t) + \sqrt{1+\phi_e^2(t)} - 1 + \frac{1}{2}\mathbf{v}_e^T(t)\bar{\mathbf{C}}^{-1}\mathbf{v}_e(t) \\ &\leq \gamma(t_0) + \sqrt{1+\phi_e^2(t_0)} - 1 + \frac{1}{2}\mathbf{v}_e^T(t_0)\bar{\mathbf{C}}^{-1}\mathbf{v}_e(t_0), \end{aligned} \tag{4.59}$$

for all $t \geq t_0 \geq 0$. From the definitions of γ, ϕ_e and $\mathbf{v}_e$, the right-hand side of the inequality (4.59) is obviously bounded by a positive constant depending on the initial conditions. Boundedness of the right-hand side of (4.59) means that the left-hand side of this inequality must also be bounded. Furthermore, boundedness of the left-hand side of the inequality (4.59) also implies that of $(x_e(t), y_e(t)), \phi_e(t)$, and $\mathbf{v}_e(t)$ for all $t \geq t_0 \geq 0$. This leads to the implication that $x_e(t), y_e(t), \phi_e(t), v_e(t)$, and $\omega_e(t)$ do not escape to infinity in finite time. Therefore, the solutions of the closed-loop system (4.54) exist globally for all $t \geq t_0 \geq 0$ by Theorem 2.1.2, and this system is forward complete.

Case 2: ***The obstacle is inside the WMR's sensing detection range or*** $R_{safe} + R_{obs} < \|\boldsymbol{q} - \boldsymbol{q}_{obs}\| < R_{sen}$**.**

Case 2 addresses the situation when the vehicle approaches closely to an obstacle which is within the detection range of the WMR. As the obstacle avoidance is only considered in this case, the parts γ in (4.11) and W_3 in (4.56) can be neglected in this analysis. The expression of (4.55) becomes

$$\dot{V}_3 \leq -v_d^2\boldsymbol{\Omega}^T\mathbf{K}\Psi(\boldsymbol{\Omega}) - \lambda\big(\beta'(\boldsymbol{q} - \boldsymbol{q}_{obs})^T\frac{\partial \boldsymbol{q}_d}{\partial s}\big)^2 + \beta'(\boldsymbol{q} - \boldsymbol{q}_{obs})^T\frac{\partial \boldsymbol{q}_d}{\partial s}\dot{s}_d. \tag{4.60}$$

From the notation of $\boldsymbol{\Omega}$ in (4.16), the relative distances, $\|\boldsymbol{q} - \boldsymbol{q}_d\|$ and $\|\boldsymbol{q} - \boldsymbol{q}_{obs}\|$ are bounded by upper bounds, i.e., $\|\boldsymbol{q} - \boldsymbol{q}_d\| \leq \epsilon^*$ and $\|\boldsymbol{q} - \boldsymbol{q}_{obs}\| \leq \bar{\epsilon}^*$, where, ϵ^* and $\bar{\epsilon}^*$ are nonnegative bounded constants. Hence, the inequality (4.60) becomes

$$\begin{aligned} \dot{V}_3 \leq &- v_d^2\big(\epsilon^* + \beta'\|\boldsymbol{q} - \boldsymbol{q}_{obs}\|\big)\mathbf{K}\Psi\big(\epsilon^* + \beta'\|\boldsymbol{q} - \boldsymbol{q}_{obs}\|\big) - \lambda\big(\epsilon_3\beta'\|\boldsymbol{q} - \boldsymbol{q}_{obs}\|\big)^2 \\ &+ |v_d|\beta'\|\boldsymbol{q} - \boldsymbol{q}_{obs}\|. \end{aligned} \tag{4.61}$$

Due to the fact that $\beta' = f(\frac{1}{\|\boldsymbol{q}-\boldsymbol{q}_{obs}\|^2})$, see (4.12), as the WMR moves inside the ball $\bar{\mathbf{B}}(R(\epsilon^*, \bar{\epsilon}^*))$, the part $\|\boldsymbol{q} - \boldsymbol{q}_d\|$ is then dominated by $\beta'\|\boldsymbol{q} - \boldsymbol{q}_{obs}\|$, or

$\epsilon^* + \beta' \|\boldsymbol{q} - \boldsymbol{q}_{obs}\| \leq \beta' \|\boldsymbol{q} - \boldsymbol{q}_{obs}\|$. In other words, if the WMR is close to the obstacle, calculation in terms of obstacle avoidance, $\|\boldsymbol{q} - \boldsymbol{q}_{obs}\|$, significantly outweighs the reference tracking, $\|\boldsymbol{q} - \boldsymbol{q}_d\|$. Obviously, the collision avoidance task is prioritized during this period of time. Therefore, only the term $\|\boldsymbol{q} - \boldsymbol{q}_{obs}\|$ in the right-hand side of (4.60) is taken into consideration, instead of both $\|\boldsymbol{q} - \boldsymbol{q}_d\|$ and $\|\boldsymbol{q} - \boldsymbol{q}_{obs}\|$. Moreover, for all $(\boldsymbol{q} - \boldsymbol{q}_{obs}) \in \mathbb{R}^2$ and $\beta' \sim \frac{1}{\|\boldsymbol{q} - \boldsymbol{q}_{obs}\|^2}$, this explanation implies that

$$\dot{V}_3 \leq -v_d^2 \lambda^* \beta^{*'} \mathbf{K} \Psi(\lambda^* \beta^{*'}) - \lambda \big(\epsilon_3 \lambda^* \beta^{*'}\big)^2 + |v_d| \lambda^* \beta^{*'}, \tag{4.62}$$

where, $\beta' \|\boldsymbol{q} - \boldsymbol{q}_{obs}\| \leq \lambda^* \beta^{*'}$ and $\beta^{*'} \sim \frac{1}{\|\boldsymbol{q} - \boldsymbol{q}_{obs}\|}$, and λ^* is a positive constant. Function $\tanh(\bullet)$ is selected as a particular function of the general bounded function $\Psi(\bullet)$, it shows that

$$|\lambda^* \beta^{*'}| - \lambda^* \beta^{*'} \tanh(\lambda^* \beta^{*'}) \leq \delta, \tag{4.63}$$

where δ is a constant. Substituting inequality (4.63) into (4.62) obtains

$$\begin{aligned} \dot{V}_3 &\leq -\lambda_{min}(\mathbf{K}) v_d^2 (\lambda^* \beta^{*'}) \tanh(\lambda^* \beta^{*'}) - \lambda \big(\beta' \bar{\epsilon}^* \epsilon_3\big)^2 + |v_d| \big(\lambda^* \beta^{*'} \tanh(\lambda^* \beta^{*'}) + \delta\big) \\ &\leq -\lambda^* \beta^{*'} \big(\lambda_{min}(\mathbf{K}) v_d^2 - |v_d|\big) \tanh(\lambda^* \beta^{*'}) - \lambda \big(\beta' \bar{\epsilon}^* \epsilon_3\big)^2 + |v_d| \delta, \end{aligned} \tag{4.64}$$

where $\lambda_{min}(\bullet)$ is the minimum eigenvalue of $(\bullet)$. Therefore, by selecting appropriately the control design constants of $\mathbf{K}$ such that

$$\lambda_{min}(\mathbf{K}) v_d^2 - |v_d| > 0, \tag{4.65}$$

the inequality (4.64) results in

$$\dot{V}_3 \leq -\lambda^* \beta^{*'} \tanh(\lambda^* \beta^{*'}) + |v_d| \delta \leq -c_1 V_3 + c_2, \tag{4.66}$$

where c_1 and c_2 are some positive constants. The above inequality (4.66) shows that the closed-loop system (4.54) is forward complete.

Properties 2 and 6 of function $\beta(t)$ holds as the condition $(R_{safe} + R_{obs}) < \|\boldsymbol{q} - \boldsymbol{q}_{obs}\| < R_{sen}$ is satisfied, i.e., $0 < \beta(t) \leq \mu_1$, μ_1 is a positive constant, depending on initial conditions for all $t \geq t_0 \geq 0$. Hence, there are no collisions between the WMR and obstacle for all $t \geq t_0 \geq 0$. By combining conclusions of Case 1 and Case 2, the solutions of the closed-loop system (4.54) exist globally for all $t \geq t_0 \geq 0$ by Theorem 4.2.1, and this system is forward complete.

4.3.2 Properties of equilibrium points

As proven in the previous section there are no collisions between the WMR and obstacle within the workspace, and all state variables are bounded for all $t \geq$

$t_0 \geq 0$. In this part, Lemma 2.1.10 (Barbalat-like Lemma) will be used to find the equilibrium points, which the trajectory of the closed-loop system (4.54) converge to. Two conditions of the Barbalat-like Lemma are checked for satisfaction. Considering (4.55) and denoting the right-hand side of the inequality as a function W_4.

$$\dot{V}_3 \leq -W_4 \tag{4.67}$$

where W_4 is denoted by

$$\begin{aligned} W_4 =& v_d^2 \boldsymbol{\Omega}^T \mathbf{K} \Psi(\boldsymbol{\Omega}) + \lambda \big(\beta'(\boldsymbol{q} - \boldsymbol{q}_{obs})^T \frac{\partial \boldsymbol{q}_d}{\partial s}\big)^2 - \beta'(\boldsymbol{q} - \boldsymbol{q}_{obs})^T \frac{\partial \boldsymbol{q}_d}{\partial s} \dot{s}_d + k_3 \sigma(\phi_e)\phi_e \\ &+ k_4 \sigma(v_e) v_e + k_5 \sigma(\omega_e)\omega_e + \epsilon^* \lambda_{min}(\bar{\mathbf{D}}) v_e^2 + \epsilon^* \lambda_{min}(\bar{\mathbf{D}}) \omega_e^2. \end{aligned} \tag{4.68}$$

W_4 is a nonnegative-valued, radially unbounded, smooth function for all $\phi_e(t) \in \mathbb{R}$, and $\mathbf{v}_e(t) = [v_e(t) \quad \omega_e(t)]^T \in \mathbb{R}^2$. To verify the first condition of the Lemma 2.1.10, each part of the right-hand side of (4.68) is denoted and investigated. Denoting $\boldsymbol{\Omega}^T \mathbf{K} \Psi(\boldsymbol{\Omega}) = A$ then taking the derivative of A with respect to t gives

$$|\dot{A}| = |2 v_d \dot{v}_d \big(\boldsymbol{\Omega}^T \mathbf{K} \Psi(\boldsymbol{\Omega})\big) + v_d^2 \big(\dot{\boldsymbol{\Omega}}^T \mathbf{K} \Psi(\boldsymbol{\Omega}) + \boldsymbol{\Omega}^T \mathbf{K} \Psi'(\boldsymbol{\Omega}) \dot{\boldsymbol{\Omega}}\big)| \tag{4.69}$$

Now, each part of the right-hand side of (4.69) is examinated as

$$|\dot{A}_1| = |2 v_d \dot{v}_d \boldsymbol{\Omega}^T \mathbf{K} \Psi(\boldsymbol{\Omega})| \leq k_{11}^* A, \tag{4.70}$$

where $|v_d| \leq \epsilon_5$ and $|\dot{v}_d| \leq \epsilon_6$ are bounded terms, see Assumption in (4.4), and $k_{11}^* = 2\epsilon_5 \epsilon_6$ is a positive constant. Next, the last two parts of (4.69) are considered as

$$|\dot{A}_2| = |v_d^2 \dot{\boldsymbol{\Omega}}^T \mathbf{K} \Psi(\boldsymbol{\Omega})| = |v_d^2 \big((1 + \beta')\mathbf{I} + \beta''(\boldsymbol{q} - \boldsymbol{q}_{obs})^T (\boldsymbol{q} - \boldsymbol{q}_{obs})\big) \mathbf{K} \Psi(\boldsymbol{\Omega})| \tag{4.71}$$

$$|\dot{A}_3| = |v_d^2 \boldsymbol{\Omega}^T \mathbf{K} \Psi'(\boldsymbol{\Omega}) \dot{\boldsymbol{\Omega}}| = |v_d^2 \boldsymbol{\Omega}^T \mathbf{K} \Psi'(\boldsymbol{\Omega}) \big((1 + \beta')\mathbf{I} + \beta''(\boldsymbol{q} - \boldsymbol{q}_{obs})^T (\boldsymbol{q} - \boldsymbol{q}_{obs})\big)| \tag{4.72}$$

In the last section, $\|\boldsymbol{q}(t)\|$ has already proven to be bounded and greater than a positive constant for all $t \geq t_0 \geq 0$. Properties of differentiable and bounded function $\Psi(\bullet)$ defined in Chapter 2 and function β in (4.11) can be used for the calculation of the part $\dot{\boldsymbol{\Omega}}$ above. They include $|\Psi'(\boldsymbol{\Omega})| = \left|\frac{d\Psi(\boldsymbol{\Omega})}{d\boldsymbol{\Omega}}\right| \leq M_3$, $|\beta'| \leq \mu_2$, and $|\beta''(\boldsymbol{q} - \boldsymbol{q}_{obs})^T (\boldsymbol{q} - \boldsymbol{q}_{obs})| \leq \mu_3$. Substituting these properties into (4.71) and (4.72) results in

$$\begin{aligned} |\dot{A}_2| &\leq v_d^2 \big(1 + \mu_2 + \mu_3\big) \mathbf{K} \Psi(\|\boldsymbol{\Omega}\|) \leq k_{12}^* \boldsymbol{\Omega}^T \mathbf{K} \Psi(\boldsymbol{\Omega}) = k_{12}^* A \\ |\dot{A}_3| &\leq v_d^2 \|\boldsymbol{\Omega}^T\| \mathbf{K} M_3 \big(1 + \mu_2 + \mu_3\big) \leq k_{13}^* \boldsymbol{\Omega}^T \mathbf{K} \Psi(\boldsymbol{\Omega}) = k_{13}^* A \end{aligned} \tag{4.73}$$

where $k_{12}^* = (1+\mu_2+\mu_3)\epsilon_5^2$ and $k_{13}^* = M_3\epsilon_5^2(1+\mu_2+\mu_3)$ are positive constants. Denoting $\lambda\big(\beta'(\boldsymbol{q}-\boldsymbol{q}_{obs})^T\frac{\partial \boldsymbol{q}_d}{\partial s}\big)^2 = B$ then taking derivative of B with respect to t gives

$$\begin{aligned}|\dot{B}| =&\Big|2\lambda\big(\beta'(\boldsymbol{q}-\boldsymbol{q}_{obs})^T\frac{\partial \boldsymbol{q}_d}{\partial s}\big)\Big((\beta''(\boldsymbol{q}-\boldsymbol{q}_{obs})^T(\boldsymbol{q}-\boldsymbol{q}_{obs})\frac{\partial \boldsymbol{q}_d}{\partial s}\big)\\ &+\beta'(\boldsymbol{q}-\boldsymbol{q}_{obs})^T\frac{\partial^2 \boldsymbol{q}_d}{\partial s^2}\dot{s}+\beta'\big(\frac{\partial \boldsymbol{q}_d}{\partial s}\big)^T\dot{\boldsymbol{q}}\Big)\Big|\end{aligned} \tag{4.74}$$

First, two following parts of the right-hand side of (4.74) are examinated

$$\begin{aligned}|\dot{B}_1| &= \Big|2\lambda\big(\beta'(\boldsymbol{q}-\boldsymbol{q}_{obs})^T\frac{\partial \boldsymbol{q}_d}{\partial s}\big)\big(\beta''(\boldsymbol{q}-\boldsymbol{q}_{obs})^T(\boldsymbol{q}-\boldsymbol{q}_{obs})\frac{\partial \boldsymbol{q}_d}{\partial s}\big)\Big| \le 2\mu_3 B = k_{13}^* B,\\ |\dot{B}_2| &= \Big|2\lambda\big(\beta'(\boldsymbol{q}-\boldsymbol{q}_{obs})^T\frac{\partial \boldsymbol{q}_d}{\partial s}\big)\big(\beta'(\boldsymbol{q}-\boldsymbol{q}_{obs})^T\frac{\partial^2 \boldsymbol{q}_d}{\partial s^2}\dot{s}\big)\Big| \le 2\epsilon_6 B = k_{23}^* B.\end{aligned} \tag{4.75}$$

where $\beta''(\boldsymbol{q}-\boldsymbol{q}_{obs})^T(\boldsymbol{q}-\boldsymbol{q}_{obs}) \le \mu_3$, $\frac{\partial^2 \boldsymbol{q}_d}{\partial s^2}\dot{s} \le \epsilon_1\epsilon_3$, see (4.2), (4.3), and $k_{13}^* = 2\mu_3$, $k_{23}^* = 2\epsilon_6$ are positive constants. The last part of (4.74) is considered by substituting $\dot{\boldsymbol{q}}$ in (4.54) into it to give

$$|\dot{B}_3| =\Big|2\lambda\big(\beta'(\boldsymbol{q}-\boldsymbol{q}_{obs})^T\frac{\partial \boldsymbol{q}_d}{\partial s}\big)\beta'\big(\frac{\partial \boldsymbol{q}_d}{\partial s}\big)^T\big(v_d^2\mathbf{K}\Psi(\boldsymbol{\Omega})+\frac{\partial \boldsymbol{q}_d}{\partial s}\dot{s}+\boldsymbol{\Lambda}_1+\boldsymbol{\Lambda}_2\big)\Big| \tag{4.76}$$

Before calculating the boundedness of all terms in (4.76). The upper boundedness of α_v in (4.24) and $\boldsymbol{\Lambda}_1$ in (4.10) are evaluated as follows

$$\begin{aligned}&\alpha_v \le (k_1\epsilon_5^2M_1+\epsilon_5)+(k_2\epsilon_5^2M_1+\epsilon_5) \le 2(k_{12max}\epsilon_5^2M_1+\epsilon_5) \le k_{12max}^*,\\ &\|\boldsymbol{\Lambda}_1\| \le 2\alpha_v \le 2k_{12max}^*,\end{aligned} \tag{4.77}$$

where, $|v_d| \le \epsilon_5$, see (4.4), $|\Psi(\bullet)| \le M_1$, see Property 1 of Differentiable and bounded function in Chapter 2, and $k_{12max}^* = max(k_1,k_2)$ is a positive constant. Now, each part of the right-hand side in (4.76) is considered one by one.

$$\begin{aligned}|\dot{B}_{31}| = \big|2\lambda\big(\beta'(\boldsymbol{q}-\boldsymbol{q}_{obs})^T\frac{\partial \boldsymbol{q}_d}{\partial s}\big)\beta'\big(\frac{\partial \boldsymbol{q}_d}{\partial s}\big)^T v_d^2\mathbf{K}\Psi(\boldsymbol{\Omega})\big| &\le k_{31}^* v_d^2\boldsymbol{\Omega}^T\mathbf{K}\Psi(\boldsymbol{\Omega})\\ &\le k_{31}^* A.\end{aligned} \tag{4.78}$$

$$|\dot{B}_{32}| = \Big|2\lambda\big(\beta'(\boldsymbol{q}-\boldsymbol{q}_{obs})^T\frac{\partial \boldsymbol{q}_d}{\partial s}\big)\beta'\big(\frac{\partial \boldsymbol{q}_d}{\partial s}\big)^T\frac{\partial \boldsymbol{q}_d}{\partial s}\dot{s}\Big| \le 2\epsilon_5 B = k_{32}^* B, \tag{4.79}$$

$$\tag{4.80}$$

where $\frac{\partial \boldsymbol{q}_d}{\partial s}\dot{s} = v_d \le \epsilon_5$, see (4.4), and $k_{32}^* = 2\epsilon_5$ is a positive constant.

$$|\dot{B}_{33}| = \Big|2\lambda\big(\beta'(\boldsymbol{q}-\boldsymbol{q}_{obs})^T\frac{\partial \boldsymbol{q}_d}{\partial s}\big)\beta'\big(\frac{\partial \boldsymbol{q}_d}{\partial s}\big)^T\boldsymbol{\Lambda}_1\Big| \le 4k_{12max}^* \le k_{33}^* B, \tag{4.81}$$

where the upper bound of $\mathbf{\Lambda}_1$ found in (4.77) is applied, and $k_{33}^* = 4k_{12max}^*$ is a positive constant. Next, substituting $\mathbf{\Lambda}_2$ in (4.10) and completing squares yield

$$\begin{aligned}
|\dot{B}_{34}| &= \Big|2\lambda\big(\beta'(\boldsymbol{q}-\boldsymbol{q}_{obs})^T\frac{\partial \boldsymbol{q}_d}{\partial s}\big)\beta'\big(\frac{\partial \boldsymbol{q}_d}{\partial s}\big)^T\begin{bmatrix}\cos(\phi)\\ \sin(\phi)\end{bmatrix}v_e\Big| \\
&\leq 2\lambda\kappa\Big(\big(\beta'(\boldsymbol{q}-\boldsymbol{q}_{obs})^T\frac{\partial \boldsymbol{q}_d}{\partial s}\big)\beta'\big(\frac{\partial \boldsymbol{q}_d}{\partial s}\big)^T\begin{bmatrix}\cos(\phi)\\ \sin(\phi)\end{bmatrix}\Big)^2 + 2\lambda\frac{1}{4\kappa}v_e^2 \\
&\leq k_{34}^* B + 2\lambda\frac{1}{4\kappa}v_e^2
\end{aligned} \tag{4.82}$$

$k_{34}^* = 2\lambda\kappa$ is a positive constant. Let's denote $k_3\sigma(\phi_e)\phi_e = C$. Taking derivative of C with respect to t and substituting $\dot{\phi}_e$ in (4.54) give

$$\begin{aligned}
|\dot{C}| &= k_3\Big|\frac{d\sigma(\phi_e)}{d\phi_e}\phi_e + \sigma(\phi_e)\Big||\dot{\phi}_e| \\
&= k_3\Big|\frac{d\sigma(\phi_e)}{d\phi_e}\phi_e + \sigma(\phi_e)\Big||k_3\sigma(\phi_e) + \frac{\mathbf{\Omega}^T\mathbf{\Lambda}_1}{\phi_e} + \frac{\partial\alpha_\phi}{\partial\boldsymbol{q}}\mathbf{\Lambda}_2 + \omega_e|
\end{aligned} \tag{4.83}$$

Now, each part of the right-hand side of (4.72) is examinated

$$|\dot{C}_1| = k_3\Big|\big(\frac{d\sigma(\phi_e)}{d\phi_e}\phi_e + \sigma(\phi_e)\big)k_3\sigma(\phi_e)\Big| \leq 2k_3^2\sigma(\phi_e)\phi_e = k_{31}^* C \tag{4.84}$$

where properties of smooth saturation functions in Definition (2.1.2), i.e., $\big|\frac{d\sigma(\phi_e)}{d\phi_e}\big| \leq 1$, $|\sigma(\phi_e)| \leq 1$ have been applied, and $k_{31}^* = 2k_3^2$ is a positive constant.

$$\begin{aligned}
|\dot{C}_2| = k_3\Big|\big(\frac{d\sigma(\phi_e)}{d\phi_e}\phi_e + \sigma(\phi_e)\big)\frac{\mathbf{\Omega}^T\mathbf{\Lambda}_1}{\phi_e}\Big| &\leq 4k_3k_{12max}^*\|\mathbf{\Omega}\| \leq k_{32}^*\mathbf{\Omega}^T\Psi(\mathbf{\Omega}) \\
&\leq k_{32}^* A,
\end{aligned} \tag{4.85}$$

where the part $\frac{\mathbf{\Lambda}_1}{\phi_e}$ is well-defined and bounded by a positive constant $2k_{12max}^*$, see (4.8) and (4.77). This includes the bounded control element α_v designed in (4.24), and $k_{32}^* = 4k_3k_{12max}^*$ is a positive constant.

From the designed control function α_ϕ in (4.22), it can be easily derived its partial derivatives with respect to variables through simple calculation below. A denotation $\alpha_\phi = \arctan(\frac{Nu}{De}) + \phi_d$ is used for compact representation.

$$\begin{aligned}
\Big|\frac{\partial\alpha_\phi}{\partial v_d}\Big| &= \Big|\frac{1}{1+\big(\frac{Nu}{De}\big)^2}\big(\frac{Nu}{De}\big)'_{v_d}\Big| \\
&\leq \frac{(k_1+k_2)M_1((k_1\epsilon_5M_1 + k_2\epsilon_5M_1 + 1) + (k_1+k_2)M_1(k_1\epsilon_5M_1 + k_2\epsilon_5M_1)}{(k_1\epsilon_5M_1 + k_2\epsilon_5M_1 + 1)^2} \\
&\leq \delta^*,
\end{aligned} \tag{4.86}$$

where, δ^* is a positive constant, $|v_d| \leq \epsilon_5$, see (4.4), $|\Psi(\bullet)| \leq M_1$, see property 1 of Differentiable and bounded function in Chapter 2, and

$$|(Nu)'_{v_d}| = |k_1\Psi(\Omega_x)\sin(\phi_d) - k_2\Psi(\Omega_y)\cos(\phi_d)| \leq (k_1+k_2)M_1,$$
$$|(De)'_{v_d}| = |-k_1\Psi(\Omega_x)\cos(\phi_d) - k_2\Psi(\Omega_y)\sin(\phi_d)| \leq (k_1+k_2)M_1.$$

$$\begin{aligned}\Big|\frac{\partial\alpha_\phi}{\partial\phi_d}\Big| &= \Big|\frac{1}{1+\left(\frac{Nu}{De}\right)^2}\Big(\frac{Nu}{De}\Big)'_{\phi_d}\Big|,\\ &\leq \frac{(k_1+k_2)\epsilon_5M_1(k_1\epsilon_5M_1+k_2\epsilon_5M_1+1)+(k_1\epsilon_5M_1+k_2\epsilon_5M_1)^2}{(k_1\epsilon_5M_1+k_2\epsilon_5M_1+1)^2}+1\\ &\leq \delta^{**},\end{aligned} \tag{4.87}$$

where, δ^{**} is a positive constant, and

$$|(Nu)'_{\phi_d}| = |k_1v_d\Psi(\Omega_x)\cos(\phi_d) + k_2v_d\Psi(\Omega_y)\sin(\phi_d)| \leq (k_1+k_2)\epsilon_5M_1$$
$$|(De)'_{\phi_d}| = |k_1v_d\Psi(\Omega_x)\sin(\phi_d) - k_2v_d\Psi(\Omega_y)\cos(\phi_d)| \leq (k_1+k_2)\epsilon_5M_1.$$

$$\Big\|\frac{\partial\alpha_\phi}{\partial\boldsymbol{q}_d}\Big\| = \frac{1}{1+\left(\frac{Nu}{De}\right)^2}\Big\|\Big(\frac{Nu}{De}\Big)'_{\boldsymbol{q}_d}\Big\| \leq \left\|\begin{bmatrix}\frac{k_1\epsilon_5M_3(2k_1\epsilon_5M_3+2k_2\epsilon_5M_3+1)}{(k_1\epsilon_5M_3+k_2\epsilon_5M_3+1)^2}\\ \frac{k_2\epsilon_5M_3(2k_1\epsilon_5M_3+2k_2\epsilon_5M_3+1)}{(k_1\epsilon_5M_3+k_2\epsilon_5M_3+1)^2}\end{bmatrix}^T\right\| \leq \delta^{***}, \tag{4.88}$$

where, δ^{***} is a positive constant, $|\frac{\partial\Psi(\bullet)}{\partial\bullet}| \leq M_3$, see Property 4 of Differentiable and bounded function in Chapter 2, and

$$\begin{aligned}|\Big(\frac{Nu}{De}\Big)'_{x_d}| &= \Big|\frac{k_1v_d\frac{\partial\Psi(\boldsymbol{\Omega})}{\partial\Omega_x}\frac{\partial\Omega_x}{\partial x_d}\sin(\phi_d)(De)+k_1v_d\frac{\partial\Psi(\boldsymbol{\Omega})}{\partial\Omega_x}\frac{\partial\Omega_x}{\partial x_d}\cos(\phi_d)(Nu)}{(De)^2}\Big|\\ &\leq \frac{k_1\epsilon_5M_3(2k_1\epsilon_5M_3+2k_2\epsilon_5M_3+1)}{(k_1\epsilon_5M_3+k_2\epsilon_5M_3+1)^2},\\ |\Big(\frac{Nu}{De}\Big)'_{y_d}| &= \Big|\frac{-k_2v_d\frac{\partial\Psi(\boldsymbol{\Omega})}{\partial\Omega_y}\frac{\partial\Omega_y}{\partial y_d}\cos(\phi_d)(De)+k_2v_d\frac{\partial\Psi(\boldsymbol{\Omega})}{\partial\Omega_y}\frac{\partial\Omega_y}{\partial y_d}\cos(\phi_d)(Nu)}{(De)^2}\Big|\\ &\leq \frac{k_2\epsilon_5M_3(2k_1\epsilon_5M_3+2k_2\epsilon_5M_3+1)}{(k_1\epsilon_5M_3+k_2\epsilon_5M_3+1)^2}.\end{aligned}$$

$$\begin{aligned}\Big|\frac{\partial\alpha_\phi}{\partial\boldsymbol{q}}\Big| &= \frac{1}{1+\left(\frac{Nu}{De}\right)^2}\Big\|\Big(\frac{Nu}{De}\Big)'_{\boldsymbol{q}}\Big\|\\ &\leq \left\|\begin{bmatrix}\frac{k_1\epsilon_5M_3(1+\mu_2+\mu_3)(2k_1\epsilon_5M_3+2k_2\epsilon_5M_3+1)}{(k_1\epsilon_5M_3+k_2\epsilon_5M_3+1)^2}\\ \frac{k_2\epsilon_5M_3(1+\mu_2+\mu_3)(2k_1\epsilon_5M_3+2k_2\epsilon_5M_3+1)}{(k_1\epsilon_5M_3+k_2\epsilon_5M_3+1)^2}\end{bmatrix}^T\right\| \leq \delta^{****},\end{aligned} \tag{4.89}$$

where, $|\frac{\partial\Psi(\bullet)}{\partial\bullet}| \leq M_3$, $|\beta'| \leq \mu_2$, $|\beta''(\boldsymbol{q}-\boldsymbol{q}_{obs})^T(\boldsymbol{q}-\boldsymbol{q}_{obs})| \leq \mu_3$, and δ^{****} is a positive constant, and

$$|\Big(\frac{Nu}{De}\Big)'_{x}| = \Big|\frac{k_1v_d\frac{\partial\Psi(\boldsymbol{\Omega})}{\partial\Omega_x}\frac{\partial\Omega_x}{\partial x}\sin(\phi_d)(De)+k_1v_d\frac{\partial\Psi(\boldsymbol{\Omega})}{\partial\Omega_x}\frac{\partial\Omega_x}{\partial x}\cos(\phi_d)(Nu)}{(De)^2}\Big|$$

$$\leq \frac{k_1\epsilon_5 M_3(1+\mu_2+\mu_3)(2k_1\epsilon_5 M_3+2k_2\epsilon_5 M_3+1)}{(k_1\epsilon_5 M_3+k_2\epsilon_5 M_3+1)^2},$$

$$|\big(\frac{Nu}{De}\big)'_y| = \big|\frac{-k_2 v_d \frac{\partial\Psi(\boldsymbol{\Omega})}{\partial\Omega_y}\frac{\partial\Omega_y}{\partial y}\cos(\phi_d)(De)+k_2 v_d \frac{\partial\Psi(\boldsymbol{\Omega})}{\partial\Omega_y}\frac{\partial\Omega_y}{\partial y}\sin(\phi_d)(Nu)}{(De)^2}\big|$$

$$\leq \frac{k_2\epsilon_5 M_3(1+\mu_2+\mu_3)(2k_1\epsilon_5 M_3+2k_2\epsilon_5 M_3+1)}{(k_1\epsilon_5 M_3+k_2\epsilon_5 M_3+1)^2}.$$

To calculate the upper bound of $|\dot{C}_3|$ below, $\boldsymbol{\Lambda}_2$ in (4.8) and result of (4.87) are used to give

$$\begin{aligned}|\dot{C}_3| = k_3\Big|\big(\frac{d\sigma(\phi_e)}{d\phi_e}\phi_e+\sigma(\phi_e)\big)\frac{\partial\alpha_\phi}{\partial\boldsymbol{q}}\boldsymbol{\Lambda}_2\Big| &\leq k_3\Big|\big(\frac{d\sigma(\phi_e)}{d\phi_e}\phi_e+\sigma(\phi_e)\big)\frac{\partial\alpha_\phi}{\partial\boldsymbol{q}}\begin{bmatrix}\cos(\phi)\\ \sin(\phi)\end{bmatrix}v_e\\ &\leq k_3\delta^{****}\Big|\frac{d\sigma(\phi_e)}{d\phi_e}\phi_e+\sigma(\phi_e)\Big||v_e|\\ &\leq k_3\delta^{****}\kappa\Big(\frac{d\sigma(\phi_e)}{d\phi_e}\phi_e+\sigma(\phi_e)\Big)^2+\frac{1}{4\kappa}v_e^2\\ &\leq k_{33}^* C+\frac{1}{4\kappa}v_e^2,\end{aligned} \tag{4.90}$$

where, $\big|\frac{\partial\alpha_\phi}{\partial\boldsymbol{q}}\begin{bmatrix}\cos(\phi)\\ \sin(\phi)\end{bmatrix}\big| \leq \delta^{****}$, $k_{33}^* = 4k_3\delta^{****}\kappa$ is a positive constant. Completing squares the last part yields

$$\begin{aligned}|\dot{C}_4| = k_3\Big|\big(\frac{d\sigma(\phi_e)}{d\phi_e}\phi_e+\sigma(\phi_e)\big)\omega_e\Big| &\leq k_3\kappa\Big(\frac{d\sigma(\phi_e)}{d\phi_e}\phi_e+\sigma(\phi_e)\Big)^2+\frac{1}{4\kappa}\omega_e^2\\ &\leq k_{34}^* C+\frac{1}{4\kappa}\omega_e^2,\end{aligned} \tag{4.91}$$

where $k_{34}^* = 4k_3\kappa$ is a positive constant. Similarly, let's denote $k_4\sigma(v_e)v_e = D$ and $k_5\sigma(\omega_e)\omega_e = E$. Taking derivative of D and E with respect to t and the substituting $\dot{v}_e$ and $\dot{\omega}_e$ in (4.54) give

$$\begin{aligned}|\dot{D}| &= |k_4\big(\frac{d\sigma(v_e)}{dv_e}v_e+\sigma(v_e)\big)\dot{v}_e|\\ &= \big|k_4\big(\frac{d\sigma(v_e)}{dv_e}v_e+\sigma(v_e)\big)\big(\bar{c}_{11}(\alpha_\omega^2+2\alpha_\omega\omega_e+\omega_e^2)-\bar{d}_{11}(\alpha_v+v_e)\\ &\quad -\bar{d}_{12}(\alpha_\omega+\omega_e)-k_4\sigma(v_e)-\Upsilon_1-\Delta_1\big)\big|.\end{aligned} \tag{4.92}$$

$$\begin{aligned}|\dot{E}| &= |k_5\big(\frac{d\sigma(\omega_e)}{d\omega_e}\omega_e+\sigma(\omega_e)\big)\dot{\omega}_e|\\ &= \big|k_5\big(\frac{d\sigma(\omega_e)}{d\omega_e}\omega_e+\sigma(\omega_e)\big)\big(-\bar{c}_{22}(\alpha_v\alpha_\omega+v_e\alpha_\omega+\omega_e\alpha_v+v_e\omega_e)-\bar{d}_{21}(\alpha_v+v_e)\\ &\quad -\bar{d}_{22}(\alpha_\omega+\omega_e)-k_5\sigma(\omega_e)-\Upsilon_2-\Delta_2\big)\big|.\end{aligned} \tag{4.93}$$

$$
\begin{aligned}
|\dot{F}| &= |2\epsilon^* \lambda_{min}(\bar{\mathbf{D}}) v_e \dot{v}_e| \\
&= \big|2\epsilon^* \lambda_{min}(\bar{\mathbf{D}}) v_e \big(\bar{c}_{11}(\alpha_\omega^2 + 2\alpha_\omega \omega_e + \omega_e^2) + \bar{d}_{11}(\alpha_v + v_e) + \bar{d}_{12}(\alpha_\omega + \omega_e) \\
&\quad + k_4 \sigma(v_e) + \Upsilon_1 + \Delta_1\big)\big|. \qquad (4.94)
\end{aligned}
$$

$$
\begin{aligned}
|\dot{G}| &= |2\epsilon^* \lambda_{min}(\bar{\mathbf{D}}) \omega_e \dot{\omega}_e| \\
&= \big|2\epsilon^* \lambda_{min}(\bar{\mathbf{D}}) \omega_e \big(\bar{c}_{22}(\alpha_v \alpha_\omega + v_e \alpha_\omega + \omega_e \alpha_v + v_e \omega_e) + \bar{d}_{21}(\alpha_v + v_e) \\
&\quad + \bar{d}_{22}(\alpha_\omega + \omega_e) + k_5 \sigma(\omega_e) + \Upsilon_2 + \Delta_2\big)\big|. \qquad (4.95)
\end{aligned}
$$

Now the right-hand side of $|\dot{D}|$, $|\dot{E}|$, $|\dot{F}|$, and $|\dot{G}|$ will be calculated in details to find out the upper boundedness. First, substituting α_ω designed in (4.31) into the first part of $|\dot{D}|$ in (4.92) yields

$$
\begin{aligned}
|\dot{D}_1| = \big|k_4 \bar{c}_{11} \big(\frac{d\sigma(v_e)}{dv_e} v_e + \sigma(v_e)\big) \big(- k_3 \sigma(\phi_e) - \frac{\mathbf{\Omega}^T \mathbf{\Lambda}_1}{\phi_e} + \frac{\partial \alpha_\phi}{\partial v_d} \dot{v}_d + \frac{\partial \alpha_\phi}{\partial \phi_d} \dot{\phi}_d \\
+ \frac{\partial \alpha_\phi}{\partial \boldsymbol{q}_d} \frac{\partial \boldsymbol{q}_d}{\partial s} \dot{s} + \frac{\partial \alpha_\phi}{\partial \boldsymbol{q}} (\boldsymbol{u} + \mathbf{\Lambda}_1)\big)^2\big| \qquad (4.96)
\end{aligned}
$$

Expanding(4.94) and taking one by one for upper boundedness give

$$
|\dot{D}_{11}| = \big|k_4 \bar{c}_{11} \big(\frac{d\sigma(v_e)}{dv_e} v_e + \sigma(v_e)\big) \big(k_3 \sigma(\phi_e)\big)^2\big| \leq 2k_3^2 k_4 \bar{c}_{11} D = k_{411}^* D. \qquad (4.97)
$$

where the similar approach in (4.84) has been used. $k_{411}^* = 2k_3^2 k_4$ is a positive constant.

$$
\begin{aligned}
|\dot{D}_{12}| &= \big|k_4 \bar{c}_{11} \big(\frac{d\sigma(v_e)}{dv_e} v_e + \sigma(v_e)\big) \Big(\frac{\mathbf{\Omega}^T \mathbf{\Lambda}_1}{\phi_e}\Big)^2\big| \leq 2k_4 k_{12max}^2 \bar{c}_{11} \|\mathbf{\Omega}\|^2 \\
&\leq k_{412}^* \mathbf{\Omega}^T \Psi(\mathbf{\Omega}) \leq k_{412}^* A, \qquad (4.98)
\end{aligned}
$$

where the similar approach in (4.85) has been used, and $k_{412}^* = 2k_4 k_{12max}^2 \bar{c}_{11}$ is a positive constant. By substituting results in (4.86), (4.87), and (4.88) and the boundedness of the terms $\dot{v}_d$, $\frac{\partial \boldsymbol{q}_d}{\partial s} \dot{s}$, and $\dot{\phi}_d$, given by (4.2), (4.3), (4.4), and (4.7), the results below can be easily obtained

$$
|\dot{D}_{13}| = \big|k_4 \bar{c}_{11} \big(\frac{d\sigma(v_e)}{dv_e} v_e + \sigma(v_e)\big) \big(\frac{\partial \alpha_\phi}{\partial v_d} \dot{v}_d\big)^2\big| \leq k_{413}^* D. \qquad (4.99)
$$

$$
|\dot{D}_{14}| = \big|k_4 \bar{c}_{11} \big(\frac{d\sigma(v_e)}{dv_e} v_e + \sigma(v_e)\big) \big(\frac{\partial \alpha_\phi}{\partial \phi_d} \dot{\phi}_d\big)^2\big| \leq k_{414}^* D. \qquad (4.100)
$$

$$
|\dot{D}_{15}| = \big|k_4 \bar{c}_{11} \big(\frac{d\sigma(v_e)}{dv_e} v_e + \sigma(v_e)\big) \big(\frac{\partial \alpha_\phi}{\partial \boldsymbol{q}_d} \frac{\partial \boldsymbol{q}_d}{\partial s} \dot{s}\big)^2\big| \leq k_{415}^* D. \qquad (4.101)
$$

where $k^*_{413} = 2k_4\bar{c}_{11}(\delta^*\epsilon_6)^2$, $k^*_{414} = 2k_4\bar{c}_{11}(\delta^{**}\frac{\epsilon_4}{\epsilon_3}\epsilon_1)^2$, and $k^*_{415} = 2k_4\bar{c}_{11}(\delta^{***}\epsilon_5)^2$ are positive constants. Next, substituting $\boldsymbol{u}$ in (4.15) and $\boldsymbol{\Lambda}_1$ in (4.8) into $\dot{D}_{16}$ below and completing squares yield

$$\begin{aligned}|\dot{D}_{16}| &= \big|k_4\bar{c}_{11}\big(\frac{d\sigma(v_e)}{dv_e}v_e + \sigma(v_e)\big)\Big(\frac{\partial\alpha_\phi}{\partial\boldsymbol{q}}(\boldsymbol{u}+\boldsymbol{\Lambda}_1)\Big)^2\big| \\ &\leq \big|k_4\bar{c}_{11}\big(\frac{d\sigma(v_e)}{dv_e}v_e + \sigma(v_e)\big)\Big(\frac{\partial\alpha_\phi}{\partial\boldsymbol{q}}\Big)^2\big((1+2\kappa)\boldsymbol{u}^2 + (1+\frac{1}{2\kappa})\boldsymbol{\Lambda}_1^2\big)\big| \quad (4.102)\end{aligned}$$

$|\dot{D}_{16}|$ is expanded to two separated parts $|\dot{D}_{161}|$ and $|\dot{D}_{162}|$ for the upper bound investigation as follows

$$\begin{aligned}|\dot{D}_{161}| &= \big|k_4(1+2\kappa)\bar{c}_{11}\big(\frac{d\sigma(v_e)}{dv_e}v_e + \sigma(v_e)\big)\Big(\frac{\partial\alpha_\phi}{\partial\boldsymbol{q}}\Big)^2\boldsymbol{u}^2\big| \\ &= \big|k_4(1+2\kappa)\bar{c}_{11}\big(\frac{d\sigma(v_e)}{dv_e}v_e + \sigma(v_e)\big)\Big(\frac{\partial\alpha_\phi}{\partial\boldsymbol{q}}\Big)^2\big(v_d^2\mathbf{K}\Psi(\boldsymbol{\Omega}) + \frac{\partial\boldsymbol{q}_d}{\partial s}\dot{s}\big)^2\big| \\ &\leq \big|k_4(1+2\kappa)\bar{c}_{11}\big(\frac{d\sigma(v_e)}{dv_e}v_e + \sigma(v_e)\big)\Big(\frac{\partial\alpha_\phi}{\partial\boldsymbol{q}}\Big)^2\big(v_d^2\mathbf{K}\Psi(\boldsymbol{\Omega}) + \epsilon_5\big)^2\big| \\ &\leq k^*_{161}v_d^2\boldsymbol{\Omega}^T\mathbf{K}\Psi(\boldsymbol{\Omega}) = k^*_{161}A. \quad (4.103)\end{aligned}$$

where, $|\frac{\partial\alpha_\phi}{\partial\boldsymbol{q}}| \leq \delta^{****}$ in (4.87) hasd been used. $k^*_{161} = 2k_4(1+2\kappa)\bar{c}_{11}\lambda_{min}(\mathbf{K})(\epsilon_5\delta^{****})^2$ is a positive constant.

$$|\dot{D}_{162}| = \big|k_4(1+\frac{1}{2\kappa})\bar{c}_{11}\big(\frac{d\sigma(v_e)}{dv_e}v_e + \sigma(v_e)\big)\Big(\frac{\partial\alpha_\phi}{\partial\boldsymbol{q}}\Big)^2\boldsymbol{\Lambda}_1^2\big| \leq k^*_{162}D \quad (4.104)$$

where, $\boldsymbol{\Lambda}_1 \leq 2k^*_{12max}$ in (4.77) has been used. $k^*_{162} = 2k_4(1+\frac{1}{2\kappa})\bar{c}_{11}(2k^*_{12max}\delta^{****})^2$ is positive constant. Now the next part of $|\dot{D}|$ is considered by completing squares

$$\begin{aligned}|\dot{D}_2| &= \big|2k_4\bar{c}_{11}\big(\frac{d\sigma(v_e)}{dv_e}v_e + \sigma(v_e)\big)\alpha_\omega\omega_e\big| \leq \kappa\Big(2k_4\bar{c}_{11}\big(\frac{d\sigma(v_e)}{dv_e}v_e + \sigma(v_e)\big)\alpha_\omega\Big)^2 + \frac{1}{4\kappa}\omega_e^2 \\ &\leq k^*_{421}A + k^*_{422}D + \frac{1}{4\kappa}\omega_e^2. \quad (4.105)\end{aligned}$$

where results found for $\dot{D}_1$ above are applied to give positive constants k^*_{421} and k^*_{422}.

$$|\dot{D}_3| = \big|k_4\bar{c}_{11}\big(\frac{d\sigma(v_e)}{dv_e}v_e + \sigma(v_e)\big)\omega_e^2\big| \leq 2k_4\bar{c}_{11}\omega_e^2 = k^*_{43}\omega_e^2. \quad (4.106)$$

where k^*_{43} is a positive constant. Next, the boundedness of α_v in (4.77) is used to find the upper bound below

$$|\dot{D}_4| = \big|k_4\bar{d}_{11}\big(\frac{d\sigma(v_e)}{dv_e}v_e + \sigma(v_e)\big)\alpha_v\big| \leq 2k_4k^*_{12max}\bar{d}_{11} = k^*_{44}D. \quad (4.107)$$

$$|\dot{D}_5| = \big|k_4\bar{d}_{11}\big(\frac{d\sigma(v_e)}{dv_e}v_e + \sigma(v_e)\big)v_e\big| \leq 2k_4\bar{d}_{11}v_e = k^*_{45}D. \quad (4.108)$$

where k_{44}^* and k_{45}^* are positive constants. Next, the upper bound of $\dot{D}_6$ below can be found by substituting α_ω in (4.31) and using results found for $\dot{D}_1$ above to give

$$|\dot{D}_6| = \big|k_4\bar{d}_{12}\big(\frac{d\sigma(v_e)}{dv_e}v_e + \sigma(v_e)\big)\alpha_\omega\big| \leq k_{461}^* A + k_{462}^* D. \tag{4.109}$$

where k_{461}^* and k_{462}^* are positive constants. Considering $\dot{D}_7$ below by completing squares

$$\begin{aligned}|\dot{D}_7| = \big|k_4\bar{d}_{12}\big(\frac{d\sigma(v_e)}{dv_e}v_e + \sigma(v_e)\big)\omega_e\big| &\leq k_4\kappa\bar{d}_{12}\big(\frac{d\sigma(v_e)}{dv_e}v_e + \sigma(v_e)\big)^2 + \frac{1}{4\kappa}\omega_e^2 \\ &\leq k_{47}^* D + \frac{1}{4\kappa}\omega_e^2. \end{aligned}\tag{4.110}$$

$$|\dot{D}_8| = \big|k_4\big(\frac{d\sigma(v_e)}{dv_e}v_e + \sigma(v_e)\big)k_4\sigma(v_e)\big| \leq 2k_4^2\sigma(v_e)v_e = k_{48}^* D. \tag{4.111}$$

where $k_{47}^* = 4k_4\kappa\bar{d}_{12}$ and $k_{48}^* = 2k_4^2$ are positive constants. Now the definition of Υ_1 in (4.48) is substituted into the next part of the right-hand side of D to yield

$$\begin{aligned}|\dot{D}_9| &= \big|k_4\big(\frac{d\sigma(v_e)}{dv_e}v_e + \sigma(v_e)\big)\Upsilon_1\big| \\ &= \big|k_4\big(\frac{d\sigma(v_e)}{dv_e}v_e + \sigma(v_e)\big)(\alpha_\omega^2 + \bar{\bar{d}}_{11}\alpha_v + \bar{\bar{d}}_{12}\alpha_\omega + \frac{1}{\bar{c}_1}\Delta_1 + \Phi_{12})\big| \end{aligned}\tag{4.112}$$

applying results obtained above, it can be easily estimated the boundedness of the terms below

$$|\dot{D}_{91}| = \big|k_4\big(\frac{d\sigma(v_e)}{dv_e}v_e + \sigma(v_e)\big)\alpha_\omega^2\big| \leq k_{4911}^* A + k_{4912}^* D, \tag{4.113}$$

$$|\dot{D}_{92}| = \big|k_4\big(\frac{d\sigma(v_e)}{dv_e}v_e + \sigma(v_e)\big)\bar{\bar{d}}_{11}\alpha_v\big| \leq k_{492}^* D, \tag{4.114}$$

$$|\dot{D}_{93}| = \big|k_4\big(\frac{d\sigma(v_e)}{dv_e}v_e + \sigma(v_e)\big)\bar{\bar{d}}_{12}\alpha_\omega\big| \leq k_{4931}^* A + k_{4932}^* D, \tag{4.115}$$

where k_{4911}^*, k_{4912}^*, k_{492}^*, k_{4931}^*, and k_{4932}^* are positive constants. Substituting Δ_1 in (4.40) into the part $\dot{D}_{94}$ below gives

$$\begin{aligned}|\dot{D}_{94}| &= \big|k_4\big(\frac{d\sigma(v_e)}{dv_e}v_e + \sigma(v_e)\big)\frac{1}{\bar{c}_1}\Delta_1\big| \\ &= \big|\frac{k_4}{\bar{c}_1}\big(\frac{d\sigma(v_e)}{dv_e}v_e + \sigma(v_e)\big)\big(\frac{\partial\alpha_v}{\partial v_d}\dot{v}_d + \frac{\partial\alpha_v}{\partial\phi_d}\dot{\phi}_d + \frac{\partial\alpha_v}{\partial\boldsymbol{q}_d}\frac{\partial\boldsymbol{q}_d}{\partial s}\dot{s} + \frac{\partial\alpha_v}{\partial\boldsymbol{q}}(\boldsymbol{u} + \boldsymbol{\Lambda}_1), \\ &\quad + \frac{\partial\alpha_v}{\partial\boldsymbol{q}}\boldsymbol{\Lambda}_2)\big|. \end{aligned}\tag{4.116}$$

From the designed control function α_v in (4.24), it can be easily derived its partial derivatives with respect to variables through simple calculation below.

$$\big|\frac{\partial\alpha_v}{\partial v_d}\big| = \big|\cos(\alpha_\phi)\big(-2k_1v_d\Psi(\Omega_x) + \cos(\phi_d)\big) + \sin(\alpha_\phi)\big(-2k_2v_d\Psi(\Omega_y)$$

$$+\sin(\phi_d)\big)\big| \leq 2k_1\epsilon_5 M_1 + 2k_2\epsilon_5 M_1 + 2. \tag{4.117}$$

$$\big|\frac{\partial \alpha_v}{\partial \phi_d}\big| = \big| - v_d\cos(\alpha_\phi)\sin(\phi_d) + v_d\sin(\alpha_\phi)\cos(\phi_d)\big| \leq 2v_d \leq 2\epsilon_5. \tag{4.118}$$

$$\big\|\frac{\partial \alpha_v}{\partial \boldsymbol{q}_d}\big\| = \big\| \begin{bmatrix} -\cos(\alpha_\phi)k_1 v_d^2 \frac{\partial \Psi(\boldsymbol{\Omega})}{\partial \Omega_x}\frac{\partial \Omega_x}{\partial x_d} \\ -\sin(\alpha_\phi)k_2 v_d^2 \frac{\partial \Psi(\boldsymbol{\Omega})}{\partial \Omega_y}\frac{\partial \Omega_y}{\partial y_d} \end{bmatrix}^T \big\| \leq \lambda_{min}(\mathbf{K})\epsilon_5^2 M_3. \tag{4.119}$$

$$\big\|\frac{\partial \alpha_v}{\partial \boldsymbol{q}}\big\| = \big\| \begin{bmatrix} -\cos(\alpha_\phi)k_1 v_d^2 \frac{\partial \Psi(\boldsymbol{\Omega})}{\partial \Omega_x}\frac{\partial \Omega_x}{\partial x} \\ -\sin(\alpha_\phi)k_2 v_d^2 \frac{\partial \Psi(\boldsymbol{\Omega})}{\partial \Omega_y}\frac{\partial \Omega_y}{\partial y} \end{bmatrix}^T \big\| \leq \lambda_{min}(\mathbf{K})\epsilon_5^2 M_3(1+\mu_2+\mu_3). \tag{4.120}$$

where, $|v_d| \leq \epsilon_5$, $|\frac{\partial \Psi(\bullet)}{\partial(\bullet)}| \leq M_3$, $|\beta'| \leq \mu_2$, and $|\beta''(\boldsymbol{q}-\boldsymbol{q}_{obs})^T(\boldsymbol{q}-\boldsymbol{q}_{obs})| \leq \mu_3$ have been used. $\lambda_{min}(\mathbf{K})$ is minimum eigenvalue of matrix $\mathbf{K}$. Applying the results in (4.117), (4.118), (4.119), and (4.120) to obtain upper bounds for the terms below

$$|\dot{D}_{941}| = \big|\frac{k_4}{\bar{c}_1}\big(\frac{d\sigma(v_e)}{dv_e}v_e + \sigma(v_e)\big)\frac{\partial \alpha_v}{\partial v_d}\dot{v}_d\big| \leq k^*_{4941} D, \tag{4.121}$$

where, $|\dot{v}_d| \leq \epsilon_6$, $k^*_{4941} = 2\frac{k_4}{\bar{c}_1}\epsilon_6(2k_1\epsilon_5 M_1 + 2k_2\epsilon_5 M_1 + 2)$ is a positive constant.

$$|\dot{D}_{942}| = \big|\frac{k_4}{\bar{c}_1}\big(\frac{d\sigma(v_e)}{dv_e}v_e + \sigma(v_e)\big)\frac{\partial \alpha_v}{\partial \phi_d}\dot{\phi}_d\big| \leq k^*_{4942} D, \tag{4.122}$$

where, $|\dot{\phi}_d| \leq \frac{\epsilon_4}{\epsilon_3}\epsilon_1$, $k^*_{4942} = 4\frac{k_4}{\bar{c}_1}\frac{\epsilon_4}{\epsilon_3}\epsilon_1\epsilon_5$ is a positive constant.

$$|\dot{D}_{943}| = \big|\frac{k_4}{\bar{c}_1}\big(\frac{d\sigma(v_e)}{dv_e}v_e + \sigma(v_e)\big)\frac{\partial \alpha_v}{\partial \boldsymbol{q}_d}\frac{\partial \boldsymbol{q}_d}{\partial s}\dot{s}\big| \leq k^*_{4943} D. \tag{4.123}$$

where, $|\frac{\partial \boldsymbol{q}_d}{\partial s}\dot{s}| = |v_d| \leq \epsilon_5$, $k^*_{4943} = 2\frac{k_4}{\bar{c}_1}\lambda_{min}(\mathbf{K})\epsilon_5^3 M_3$ is a positive constant. Applying the similar approach to (4.103) and (4.104) results in

$$|\dot{D}_{944}| = \big|\frac{k_4}{\bar{c}_1}\big(\frac{d\sigma(v_e)}{dv_e}v_e + \sigma(v_e)\big)\frac{\partial \alpha_v}{\partial \boldsymbol{q}}\big(v_d^2\mathbf{K}\Psi(\boldsymbol{\Omega}) + \frac{\partial \boldsymbol{q}_d}{\partial s}\dot{s}\big)\big| \leq k^*_{4944} A, \tag{4.124}$$

$$|\dot{D}_{945}| = \big|\frac{k_4}{\bar{c}_1}\big(\frac{d\sigma(v_e)}{dv_e}v_e + \sigma(v_e)\big)\frac{\partial \alpha_v}{\partial \boldsymbol{q}}\boldsymbol{\Lambda}_1\big| \leq k^*_{4945} D. \tag{4.125}$$

where, $k^*_{4944} = 2\frac{k_4}{\bar{c}_1}\lambda_{min}(\mathbf{K})\epsilon_5^2 M_3(1+\mu_2+\mu_3)$, $k^*_{4945} = 4\frac{k_4}{\bar{c}_1}\lambda_{min}(\mathbf{K})\epsilon_5^2 M_3(1+\mu_2+\mu_3)k^*_{12max}$ are positive constants. Substituting $\boldsymbol{\Lambda}_2$ in (4.8) into the last part of $|\dot{D}_{94}|$ in (4.116) and completing squares yield

$$|\dot{D}_{946}| = \big|\frac{k_4}{\bar{c}_1}\big(\frac{d\sigma(v_e)}{dv_e}v_e + \sigma(v_e)\big)\frac{\partial \alpha_v}{\partial \boldsymbol{q}}\begin{bmatrix}\cos(\phi)\\ \sin(\phi)\end{bmatrix}v_e\big| \leq k^*_{9446} D + \frac{1}{4\kappa}|v_e|^2, \tag{4.126}$$

where, $|\frac{\partial \alpha_v}{\partial \boldsymbol{q}} \begin{bmatrix}\cos(\phi)\\ \sin(\phi)\end{bmatrix}| \leq \|\frac{\partial \alpha_v}{\partial \boldsymbol{q}}\| \leq \lambda_{min}(\mathbf{K})\epsilon_5^2 M_3(1+\mu_2+\mu_3)$, and $k^*_{4946} = 2\kappa\frac{k_4}{\bar{c}_1}\lambda_{min}(\mathbf{K})\epsilon_5^2 M_3(1+\mu_2+\mu_3)$ is a positive constant. Substituting Φ_{12} in (4.33) into the last part of $\dot{D}_9$ gives

$$\begin{aligned}|\dot{D}_{11}| &= \big|k_4\big(\frac{d\sigma(v_e)}{dv_e}v_e + \sigma(v_e)\big)\Phi_{12}\big| \\ &= \big|k_4\big(\frac{d\sigma(v_e)}{dv_e}v_e + \sigma(v_e)\big)\big(\boldsymbol{\Omega}^T \begin{bmatrix}\cos(\phi)\\ \sin(\phi)\end{bmatrix} - \phi_e\frac{\partial \alpha_\phi}{\partial \boldsymbol{q}}\begin{bmatrix}\cos(\phi)\\ \sin(\phi)\end{bmatrix}\big)\big| \\ &\leq 2k_4\|\boldsymbol{\Omega}\| + 2k_4\|\frac{\partial \alpha_\phi}{\partial \boldsymbol{q}}\||\phi_e| \leq k^*_{4111}A + k^*_{4112}C, \end{aligned} \tag{4.127}$$

where, $k^*_{4111} = 2k_4$, $k^*_{4112} = 2k_4\lambda_{min}(\mathbf{K})\epsilon_5^2 M_3(1+\mu_2+\mu_3)$ are positive constants. Next, the boundedness of $\dot{E}$ in (4.93) is calculated by considering each part in the right-hand side below

$$\begin{aligned}|\dot{E}| \leq \big|k_5\big(\frac{d\sigma(\omega_e)}{d\omega_e}\omega_e + \sigma(\omega_e)\big)\big|\big(\bar{c}_{22}(\alpha_v\alpha_\omega + v_e\alpha_\omega + \omega_e\alpha_v + v_e\omega_e)\big) + \bar{d}_{21}(\alpha_v + v_e) \\ + \bar{d}_{22}(\alpha_\omega + \omega_e) + k_5\sigma(\omega_e) + \Upsilon_2 + \Delta_2\big|. \end{aligned} \tag{4.128}$$

Using the upper bound of α_v in (4.77) and substituting α_ω in (4.31) into $\dot{E}_1$ below yields

$$\begin{aligned}|\dot{E}_1| &= \big|k_5\big(\frac{d\sigma(\omega_e)}{d\omega_e}\omega_e + \sigma(\omega_e)\big)\big|\bar{c}_{22}\alpha_v\alpha_\omega\big| \\ &\leq \big|k_5k^*_{12max}\bar{c}_{22}\big(\frac{d\sigma(\omega_e)}{d\omega_e}\omega_e + \sigma(\omega_e)\big)\big| - k_3\sigma(\phi_e) - \frac{\boldsymbol{\Omega}^T\boldsymbol{\Lambda}_1}{\phi_e} \\ &\quad + \frac{\partial \alpha_\phi}{\partial v_d}\dot{v}_d + \frac{\partial \alpha_\phi}{\partial \phi_d}\dot{\phi}_d + \frac{\partial \alpha_\phi}{\partial \boldsymbol{q}_d}\frac{\partial \boldsymbol{q}_d}{\partial s}\dot{s} + \frac{\partial \alpha_\phi}{\partial \boldsymbol{q}}(\boldsymbol{u} + \boldsymbol{\Lambda}_1)\big| \end{aligned} \tag{4.129}$$

$\dot{E}_1$ is expanded to parts for convenient boundedness examination as follows

$$\begin{aligned}|\dot{E}_{11}| = \big|k_5k^*_{12max}\bar{c}_{22}\big(\frac{d\sigma(\omega_e)}{d\omega_e}\omega_e + \sigma(\omega_e)\big)\big|\big|k_3\sigma(\phi_e)\big| \leq 2k_5k^*_{12max}\bar{c}_{22}k_3\sigma(\phi_e) \\ \leq k^*_{511}\sigma(\phi_e)\phi_e = k^*_{511}E. \end{aligned} \tag{4.130}$$

$$\begin{aligned}|\dot{E}_{12}| &= \big|k_5k^*_{12max}\bar{c}_{22}\big(\frac{d\sigma(\omega_e)}{d\omega_e}\omega_e + \sigma(\omega_e)\big)\big|\big|\frac{\boldsymbol{\Omega}^T\boldsymbol{\Lambda}_1}{\phi_e}\big| \\ &\leq 4k_5k^*_{12max}\bar{c}_{22}\|\boldsymbol{\Omega}\| \leq 4k_5k^*_{12max}\bar{c}_{22}\boldsymbol{\Omega}^T\Psi(\boldsymbol{\Omega}) \leq k^*_{512}A. \end{aligned} \tag{4.131}$$

where, $k^*_{511} = 2k_5k^*_{12max}\bar{c}_{22}k_3$ and $k^*_{512} = 4k_5k^*_{12max}\bar{c}_{22}$ are positive constants. Applying the calculation in (4.86), (4.87), (4.88), and (4.89) the upper bounds for the parts below can be easily estimated

$$|\dot{E}_{13}| = \big|k_5k^*_{12max}\bar{c}_{22}\big(\frac{d\sigma(\omega_e)}{d\omega_e}\omega_e + \sigma(\omega_e)\big)\frac{\partial \alpha_\phi}{\partial v_d}\dot{v}_d\big| \leq k^*_{513}E, \tag{4.132}$$

$$|\dot{E}_{14}| = \big|k_5 k^*_{12max}\bar{c}_{22}\big(\frac{d\sigma(\omega_e)}{d\omega_e}\omega_e + \sigma(\omega_e)\big)\big|\frac{\partial\alpha_\phi}{\partial\phi_d}\dot{\phi}_d\big| \leq k^*_{514}E, \tag{4.133}$$

$$|\dot{E}_{15}| = \big|k_5 k^*_{12max}\bar{c}_{22}\big(\frac{d\sigma(\omega_e)}{d\omega_e}\omega_e + \sigma(\omega_e)\big)\big|\frac{\partial\alpha_\phi}{\partial\boldsymbol{q}_d}\frac{\partial\boldsymbol{q}_d}{\partial s}\dot{s}\big| \leq k^*_{515}E, \tag{4.134}$$

where, $k^*_{513} = 2k_5 k^*_{12max}\bar{c}_{22}k_3\delta^*\epsilon_6$, $k^*_{514} = 2k_5 k^*_{12max}\bar{c}_{22}k_3\delta^{**}\frac{\epsilon_4}{\epsilon_3}\epsilon_1$, $k^*_{515} = 2k_5 k^*_{12max}\bar{c}_{22}k_3\delta^{***}\epsilon_5$ are positive constants. Applying the similar approach to (4.103) and (4.104) results in

$$|\dot{E}_{16}| = \big|k_5 k^*_{12max}\bar{c}_{22}\big(\frac{d\sigma(\omega_e)}{d\omega_e}\omega_e + \sigma(\omega_e)\big)\big|\frac{\partial\alpha_\phi}{\partial\boldsymbol{q}}\boldsymbol{u}\big| \leq k^*_{516}A, \tag{4.135}$$

$$|\dot{E}_{17}| = \big|k_5 k^*_{12max}\bar{c}_{22}\big(\frac{d\sigma(\omega_e)}{d\omega_e}\omega_e + \sigma(\omega_e)\big)\big|\frac{\partial\alpha_\phi}{\partial\boldsymbol{q}}\boldsymbol{\Lambda}_1\big| \leq k^*_{517}E, \tag{4.136}$$

where, $k^*_{516} = 2k_5 k^*_{12max}\bar{c}_{22}k_3\delta^{****}$ and $k^*_{517} = 4k_5(k^*_{12max})^2\bar{c}_{22}k_3\delta^{****}$ are positive constants. Completing squares

$$|\dot{E}_2| = \big|k_5\big(\frac{d\sigma(\omega_e)}{d\omega_e}\omega_e + \sigma(\omega_e)\big)\bar{c}_{22}v_e\alpha_\omega\big| \leq \big|k_5\bar{c}_{22}\big(\frac{d\sigma(\omega_e)}{d\omega_e}\omega_e + \sigma(\omega_e)\big)(\kappa\alpha_\omega^2 + \frac{1}{4\kappa}v_e^2)\big|. \tag{4.137}$$

$\dot{E}_2$ is expanded to two parts i.e., $\dot{E}_{21}$ and $\dot{E}_{22}$ for boundedness examination as follows

$$|\dot{E}_{21}| = \big|k_5\kappa\bar{c}_{22}\big(\frac{d\sigma(\omega_e)}{d\omega_e}\omega_e + \sigma(\omega_e)\big)\alpha_\omega^2\big| \leq k^*_{5211}A + k^*_{5212}E, \tag{4.138}$$

$$|\dot{E}_{22}| = \big|k_5\frac{1}{4\kappa}\bar{c}_{22}\big(\frac{d\sigma(\omega_e)}{d\omega_e}\omega_e + \sigma(\omega_e)\big)v_e^2\big| \leq k^*_{522}v_e^2, \tag{4.139}$$

where, the similar calculation of $\dot{D}_1$ in (4.96) is applied to that of $|\dot{E}_{21}|$. The upper bounds of $\dot{E}_{21}$ are written in compact form of $k^*_{5211}A$ and $k^*_{5212}E$. $k^*_{522} = \frac{1}{2\kappa}k_5\bar{c}_{22}$. k^*_{5211}, k^*_{5212}, and k^*_{522} are positive constants.

$$|\dot{E}_3| = \big|k_5\big(\frac{d\sigma(\omega_e)}{d\omega_e}\omega_e + \sigma(\omega_e)\big)\bar{c}_{22}\alpha_v\omega_e\big| \leq k^*_{53}\omega_e \leq k^*_{53}E, \tag{4.140}$$

where, $|\alpha_v| \leq k^*_{12max}$ in (4.77), $k^*_{53} = 2k_5 k^*_{12max}\bar{c}_{22}$ is a positive constant. Completing squares

$$\begin{aligned}|\dot{E}_4| = \big|k_5\big(\frac{d\sigma(\omega_e)}{d\omega_e}\omega_e + \sigma(\omega_e)\big)\bar{c}_{22}v_e\omega_e\big| &\leq \big|k_5\big(\frac{d\sigma(\omega_e)}{d\omega_e}\omega_e + \sigma(\omega_e)\big)\bar{c}_{22}\big(\kappa v_e^2 + \frac{1}{4\kappa}\omega_e^2\big)\big| \\ &\leq k^*_{541}v_e^2 + k^*_{542}\omega_e^2,\end{aligned} \tag{4.141}$$

where, $k^*_{541} = 2k_5\kappa\bar{c}_{22}$ and $k^*_{542} = \frac{1}{2\kappa}k_5\bar{c}_{22}$ are positive constants. Similar to the calculation in (4.107), (4.108), (4.109), and (4.110), upper bounds of the terms belows can be easily estimated

$$|\dot{E}_5| = \big|k_5\big(\frac{d\sigma(\omega_e)}{d\omega_e}\omega_e + \sigma(\omega_e)\big)\bar{d}_{21}\alpha_v\big| \leq 2k_5\bar{d}_{21}k^*_{12max}E = k^*_{55}E, \tag{4.142}$$

$$|\dot{E}_6| = \big|k_5\big(\frac{d\sigma(\omega_e)}{d\omega_e}\omega_e + \sigma(\omega_e)\big)\bar{d}_{21}v_e\big| \leq 2k_5\bar{d}_{21}v_e \leq k^*_{56}E, \tag{4.143}$$

$$|\dot{E}_7| =\leq \big|k_5\big(\frac{d\sigma(\omega_e)}{d\omega_e}\omega_e + \sigma(\omega_e)\big)\bar{d}_{22}\alpha_\omega\big| \leq k^*_{571}A + k^*_{572}E, \tag{4.144}$$

$$|\dot{E}_8| \leq \big|k_5\big(\frac{d\sigma(\omega_e)}{d\omega_e}\omega_e + \sigma(\omega_e)\big)\bar{d}_{22}\omega_e\big| \leq 2k_5\bar{d}_{22}\omega_e \leq k^*_{58}E, \tag{4.145}$$

where, the similar calculation of $\dot{D}_1$ in (4.96) is applied to that of $|\dot{E}_7|$. The upper bounds of $\dot{E}_7$ are written in compact form of $k^*_{571}A$ and $k^*_{572}E$. $k^*_{55} = 2k_5\bar{d}_{21}k^*_{12max}$, $k^*_{56} = 2k_5\bar{d}_{21}$, k^*_{571}, k^*_{572}, and $k^*_{58} = 2k_5\bar{d}_{22}$ are positive constants.

$$|\dot{E}_9| = \big|k_5\big(\frac{d\sigma(\omega_e)}{d\omega_e}\omega_e + \sigma(\omega_e)\big)k_5\sigma(\omega_e)\big| \leq k^*_{59}E, \tag{4.146}$$

where, $k^*_{59} = 2k_5^2$. Substituting Υ_2 in (4.49) into the part $\dot{E}_{10}$ below gives

$$\begin{aligned}|\dot{E}_{10}| &= \big|k_5\big(\frac{d\sigma(\omega_e)}{d\omega_e}\omega_e + \sigma(\omega_e)\big)\Upsilon_2\big| \\ &= \big|k_5\big(\frac{d\sigma(\omega_e)}{d\omega_e}\omega_e + \sigma(\omega_e)\big)\big(-\alpha_v\alpha_\omega - \bar{\bar{d}}_{21}\alpha_v - \bar{\bar{d}}_{22}\alpha_\omega - \frac{1}{\bar{c}_2}\Delta_2 + \Phi_{22}\big)\big|\end{aligned} \tag{4.147}$$

The boundedness of $\dot{E}_{10}$ is investigated by expanding the right-hand side to separated parts and examinating each part for the upper bound. Considering the first three parts and applying previous results gives

$$|\dot{E}_{101}| = \big|k_5\big(\frac{d\sigma(\omega_e)}{d\omega_e}\omega_e + \sigma(\omega_e)\big)\alpha_v\alpha_\omega\big| \leq k^*_{51012}A + k^*_{51012}E, \tag{4.148}$$

$$|\dot{E}_{102}| = \big|k_5\big(\frac{d\sigma(\omega_e)}{d\omega_e}\omega_e + \sigma(\omega_e)\big)\bar{\bar{d}}_{21}\alpha_v\big| \leq k^*_{5102}E, \tag{4.149}$$

$$|\dot{E}_{103}| = \big|k_5\big(\frac{d\sigma(\omega_e)}{d\omega_e}\omega_e + \sigma(\omega_e)\big)\bar{\bar{d}}_{22}\alpha_\omega\big| \leq k^*_{51031}A + k^*_{51032}E, \tag{4.150}$$

where, $|\alpha_v| \leq k^*_{12max}$ in (4.77), results of $\dot{D}_1$ have been applied. $k^*_{5102} = 2k_5k^*_{12max}\bar{\bar{d}}_{21}$, k^*_{51011}, k^*_{51012}, k^*_{51031}, and k^*_{51032} are positive constants and written in compact representation. Substituting Δ_2 in (4.40) into the part $\dot{D}_{104}$ below yields

$$|\dot{E}_{104}| = \big|k_5\big(\frac{d\sigma(\omega_e)}{d\omega_e}\omega_e + \sigma(\omega_e)\big)\frac{1}{\bar{c}_2}\Delta_2\big| \tag{4.151}$$

$$\begin{aligned}&= \big|k_5\big(\frac{d\sigma(\omega_e)}{d\omega_e}\omega_e + \sigma(\omega_e)\big)\frac{1}{\bar{c}_2}\big(\frac{\partial\alpha_\omega}{\partial v_d}\dot{v}_d + \frac{\partial\alpha_\omega}{\partial\dot{v}_d}\ddot{v}_d + \frac{\partial\alpha_\omega}{\partial\phi_d}\dot{\phi}_d + \frac{\partial\alpha_\omega}{\partial\dot{\phi}_d}\ddot{\phi}_d + \frac{\partial\alpha_\omega}{\partial\boldsymbol{q}_d}\frac{\partial\boldsymbol{q}_d}{\partial s}\dot{s} \\ &\quad + \frac{\partial\alpha_\omega}{\partial\dot{\boldsymbol{q}}_d}\frac{\partial^2\boldsymbol{q}_d}{\partial s^2}\dot{s} + \frac{\partial\alpha_\omega}{\partial\boldsymbol{q}}(\boldsymbol{u} + \boldsymbol{\Lambda}_1) + \frac{\partial\alpha_\omega}{\partial\phi}\alpha_\omega + \frac{\partial\alpha_\omega}{\partial\boldsymbol{q}}\boldsymbol{\Lambda}_2 + \frac{\partial\alpha_\omega}{\partial\phi}\omega_e\big)\big|,\end{aligned} \tag{4.152}$$

Results obtained in (4.86), (4.87), (4.88), an (4.89) are applied for this calculation.

$$|\dot{E}_{1041}| = \big|k_5\big(\frac{d\sigma(\omega_e)}{d\omega_e}\omega_e + \sigma(\omega_e)\big)\frac{1}{\bar{c}_2}\frac{\partial\alpha_\omega}{\partial v_d}\dot{v}_d\big| \leq k^*_{51041}E, \tag{4.153}$$

where, $|\frac{\partial \alpha_\omega}{\partial v_d}| = |2v_d \frac{\partial \alpha_\phi}{\partial \boldsymbol{q}} \mathbf{K}\Psi(\boldsymbol{\Omega})| \leq 2\epsilon_5 \delta^{****} \lambda_{min}(\mathbf{K}) M_1$, see α_ω in (4.31). $k^*_{51041} = 4\frac{k_5}{\bar{c}_2}\epsilon_5\epsilon_6\delta^{****}\lambda_{min}(\mathbf{K})M_1$ is a positive constant.

$$|\dot{E}_{1042}| = \big|k_5\big(\frac{d\sigma(\omega_e)}{d\omega_e}\omega_e + \sigma(\omega_e)\big)\frac{1}{\bar{c}_2}\frac{\partial \alpha_\omega}{\partial \dot{v}_d}\ddot{v}_d\big| \leq k^*_{51042}E, \tag{4.154}$$

where, $|\frac{\partial \alpha_\omega}{\partial \dot{v}_d}| = |\frac{\partial \alpha_\phi}{\partial v_d}| \leq \delta^*$, see (4.86), $\ddot{v}_d \leq \epsilon_7$, see (4.4). $k^*_{51041} = 2\frac{k_5}{\bar{c}_2}\epsilon_7\delta^*$ is a positive constant.

$$|\dot{E}_{1043}| = \big|k_5\big(\frac{d\sigma(\omega_e)}{d\omega_e}\omega_e + \sigma(\omega_e)\big)\frac{1}{\bar{c}_2}\frac{\partial \alpha_\omega}{\partial \dot{\phi}_d}\ddot{\phi}_d\big| \leq k^*_{51043}E, \tag{4.155}$$

where, $|\frac{\partial \alpha_\omega}{\partial \dot{\phi}_d}| = |\frac{\partial \alpha_\phi}{\partial \phi_d}| \leq \delta^{**}$, see (4.87). $k^*_{51043} = 2\frac{k_5}{\bar{c}_2}\epsilon_7\delta^{**}$ is a positive constant.

$$|\dot{E}_{1044}| = \big|k_5\big(\frac{d\sigma(\omega_e)}{d\omega_e}\omega_e + \sigma(\omega_e)\big)\frac{1}{\bar{c}_2}\frac{\partial \alpha_\omega}{\partial \boldsymbol{q}_d}\frac{\partial \boldsymbol{q}_d}{\partial s}\dot{s}\big| \leq k^*_{51044}E, \tag{4.156}$$

where, $\|\frac{\partial \alpha_\omega}{\partial \boldsymbol{q}_d}\| = \|\frac{\partial \alpha_\phi}{\partial \boldsymbol{q}} v_d^2 \mathbf{K}\frac{\partial \Psi(\boldsymbol{\Omega})}{\partial \boldsymbol{\Omega}}\frac{\partial \boldsymbol{\Omega}}{\partial \boldsymbol{q}_d}\| \leq \delta^{****}\epsilon_5^2\lambda_{min}(\mathbf{K})M_3$, $|\frac{\partial \boldsymbol{q}_d}{\partial s}\dot{s}| = |v_d| \leq \epsilon_5$, see (4.4). $k^*_{51043} = 2\frac{k_5}{\bar{c}_2}\epsilon_5\delta^{****}\epsilon_5^2\lambda_{min}(\mathbf{K})M_3$ is a positive constant.

$$|\dot{E}_{1045}| = \big|k_5\big(\frac{d\sigma(\omega_e)}{d\omega_e}\omega_e + \sigma(\omega_e)\big)\frac{1}{\bar{c}_2}\frac{\partial \alpha_\omega}{\partial \boldsymbol{q}}(\boldsymbol{u} + \boldsymbol{\Lambda}_1)\big| \leq k^*_{510451}A + k^*_{510452}E, \tag{4.157}$$

where, calculation on (4.103) and (4.104) has been applied. $|\frac{\partial \boldsymbol{q}_d}{\partial s}\dot{s}| = |v_d| \leq \epsilon_5$, see (4.4). $\|\frac{\partial \alpha_\omega}{\partial \boldsymbol{q}}\| = \|\frac{\partial \alpha_\phi}{\partial \boldsymbol{q}} v_d^2 \mathbf{K}\frac{\partial \Psi(\boldsymbol{\Omega})}{\partial \boldsymbol{\Omega}}\frac{\partial \boldsymbol{\Omega}}{\partial \boldsymbol{q}}\| \leq \delta^{****}\epsilon_5^2\lambda_{min}(\mathbf{K})M_3(1+\mu_2+\mu_3)$. k^*_{510451} and k^*_{510452} are positive constants. Similarly,

$$|\dot{E}_{1046}| = \big|k_5\big(\frac{d\sigma(\omega_e)}{d\omega_e}\omega_e + \sigma(\omega_e)\big)\frac{1}{\bar{c}_2}\frac{\partial \alpha_\omega}{\partial \boldsymbol{q}}\boldsymbol{\Lambda}_2\big| \leq k^*_{51046}v_e \leq k^*_{51046}D, \tag{4.158}$$

where, $\boldsymbol{\Lambda}_2$ in (4.8) has been substituted. $k^*_{51046} = \delta^{****}\epsilon_5^2\lambda_{min}(\mathbf{K})M_3(1+\mu_2+\mu_3)$ is a positive constant. Other parts are equal to zero. Lastly, substituting Φ_{22} in (4.33) into the part $\dot{D}_{105}$ below yields

$$\begin{aligned}|\dot{E}_{105}| &= \big|k_5\big(\frac{d\sigma(\omega_e)}{d\omega_e}\omega_e + \sigma(\omega_e)\big)\frac{1}{\bar{c}_2}\Phi_{22}\big| = \big|k_5\big(\frac{d\sigma(\omega_e)}{d\omega_e}\omega_e + \sigma(\omega_e)\big)\phi_e\big| \\ &\leq 2k_5\phi_e \leq k^*_{5105}C,\end{aligned} \tag{4.159}$$

where, k^*_{5105} is a positive constant. Calculation for $|\dot{F}|$ and $|\dot{G}|$ in (4.94) and (4.95) are implemented in similar approach of that of $|\dot{D}|$ and $|\dot{E}|$ to achieve the upper bounds for each part of the right-hand side. Hence, results can be written in compact representation as follows

$$|\dot{F}| \leq k^*_{61}A + k^*_{62}v_e^2 + k^*_{63}\omega_e^2, \tag{4.160}$$

$$|\dot{G}| \leq k_{71}^* A + k_{72}^* v_e^2 + k_{73}^* \omega_e^2, \tag{4.161}$$

where, k_{61}^*, k_{62}^*, k_{63}^*, k_{71}^*, k_{72}^*, and k_{73}^* are positive constants.
Finally, the upper bounds of $|\dot{A}|$, $|\dot{B}|$, $|\dot{C}|$, $|\dot{D}|$, $|\dot{E}|$, $|\dot{F}|$ and $|\dot{G}|$ are grouped and added together to result in

$$\begin{aligned}
|\dot{A}| &\leq k_A A, \\
|\dot{B}| &\leq k_B B, \\
|\dot{C}| &\leq k_C C, \\
|\dot{D}| &\leq k_D D, \\
|\dot{E}| &\leq k_E E, \\
|\dot{F}| &\leq k_F v_e^2, \\
|\dot{G}| &\leq k_G \omega_e^2,
\end{aligned} \tag{4.162}$$

or it can be written in the short form as follows

$$|\frac{dW_4}{dt}| \leq k_\Sigma W_4, \tag{4.163}$$

where, $|\frac{dW_4}{dt}| \leq |\dot{A}| + |\dot{B}| + |\dot{C}| + |\dot{D}| + |\dot{E}| + |\dot{F}| + |\dot{G}|$. k_Σ is a positive constant, and W_4 is denoted in (4.68). This concludes that the first condition of the Lemma 2.1.10 (Babarlat-like Lemma) holds.

Now the second condition of the Lemma 2.1.10 is examinated by integrating both sides of (4.67) to yield

$$\int_0^\infty W_4(t)dt \leq -\int_0^\infty \dot{V}_3(t)dt = V_3(t_0) - V_3(\infty) \leq V_3(t_0) \tag{4.164}$$

Based on the construction of the positive definite and radially unbounded function V_3 in (4.41), the right-hand side of the inequality above, i.e., $V_3(t_0)$, is obviously bounded by a positive constant depending on the initial conditions. Therefore, two conditions of Barbalat-like Lemma hold.
Applying Theorem 8.4 in [57] (see Theorem 2.1.8 in Chapter 2), the convergence of $W_4(t)$ in (4.68) exists and is finite by

$$\begin{aligned}
\lim_{t\to\infty} \Big[& v_d^2(t)\boldsymbol{\Omega}^T(t)\mathbf{K}\Psi(\boldsymbol{\Omega}(t)) + \lambda\big(\beta'(t)(\boldsymbol{q}(t) - \boldsymbol{q}_{obs})^T \frac{\partial \boldsymbol{q}_d}{\partial s}\big)^2 - \beta'(t)(\boldsymbol{q}(t) - \boldsymbol{q}_{obs})^T \frac{\partial \boldsymbol{q}_d}{\partial s}\dot{s}_d \\
& + k_3\sigma(\phi_e(t))\phi_e(t) + k_4\sigma(v_e(t))v_e(t) + k_5\sigma(\omega_e(t))\omega_e(t) \\
& + \epsilon^*\lambda_{min}(\bar{\mathbf{D}})v_e^2(t) + \epsilon^*\lambda_{min}(\bar{\mathbf{D}})\omega_e^2(t)\Big] = 0.
\end{aligned} \tag{4.165}$$

By noting that $|v_d(t)| \neq 0$, see the condition (4.4) and (4.5) in Assumption 4.1.2, the limit equation (4.165) implies that

$$\begin{aligned}
&\lim_{t\to\infty}\Big(k_3\sigma(\phi_e(t))\phi_e(t) + k_4\sigma(v_e(t))v_e(t) + k_5\sigma(\omega_e(t))\omega_e(t) \\
&\qquad + \epsilon^*\lambda_{min}(\bar{\mathbf{D}})v_e^2(t) + \epsilon^*\lambda_{min}(\bar{\mathbf{D}})\omega_e^2(t)\Big) = 0, \\
&\lim_{t\to\infty}\Big(\lambda\big(\beta'(t)(\boldsymbol{q}(t)-\boldsymbol{q}_{obs})^T\frac{\partial \boldsymbol{q}_d}{\partial s}\big)^2 - \beta'(t)(\boldsymbol{q}(t)-\boldsymbol{q}_{obs})^T\frac{\partial \boldsymbol{q}_d}{\partial s}\dot{s}_d\Big) = 0, \\
&\lim_{t\to\infty}\boldsymbol{\Omega}(t) = 0.
\end{aligned} \tag{4.166}$$

Due to the construction of the positive definite and radially unbounded function V_3, and the proven boundedness of $(x_e(t), y_e(t))$, $\phi_e(t), v_e(t)$, and $\omega_e(t)$ for all $t \geq t_0 \geq 0$, and the definition of the smooth saturation function $\sigma(\bullet)$ in Chapter 2. Moreover, no collision which has already been proven means $\beta'(t) = 0$ as $t \to \infty$. The first two limits of (4.166) mean those terms globally asymptotically converge to zero. Lastly, from the definition of $\boldsymbol{\Omega}$ in (4.14), $\lim_{t\to\infty}\boldsymbol{\Omega}(t) = 0$ means

$$\lim_{t\to\infty}\Big(\begin{bmatrix}\Omega_x(t)\\ \Omega_y(t)\end{bmatrix}\Big) = \lim_{t\to\infty}\Big(\begin{bmatrix}(x(t)-x_d)\\ (y(t)-y_d)\end{bmatrix} + \beta'(t)\begin{bmatrix}(x(t)-x_{obs})\\ (y(t)-y_{obs})\end{bmatrix}\Big) = 0. \tag{4.167}$$

The equation (4.167) implies that $\boldsymbol{q} = \begin{bmatrix}x(t) & y(t)\end{bmatrix}^T$ approaches either to $\boldsymbol{q}_d = \begin{bmatrix}x_d & y_d\end{bmatrix}^T$ or a vector denoted by $\boldsymbol{q}_c = \begin{bmatrix}x_c & y_c\end{bmatrix}^T$ as $t \to \infty$. This means that the equilibrium points can be $\boldsymbol{q}_d$ or $\boldsymbol{q}_c$. Therefore, it is necessary to investigate the stability properties of these equilibrium points by considering the behavior of the first equation of the closed-loop system (4.54)

$$\dot{\boldsymbol{q}} = -v_d^2\mathbf{K}\Psi(\boldsymbol{\Omega}) + \frac{\partial \boldsymbol{q}_d}{\partial s}\dot{s} + \boldsymbol{\Lambda}_1 + \boldsymbol{\Lambda}_2. \tag{4.168}$$

The system (4.168) is linearized around the equilibrium point, which can be either $\boldsymbol{q}_d = \begin{bmatrix}x_d & y_d\end{bmatrix}^T$ or $\boldsymbol{q}_c = \begin{bmatrix}x_c & y_c\end{bmatrix}^T$, to obtain

$$\dot{\boldsymbol{q}} = -v_d^2\mathbf{K}\frac{\partial \Psi(\boldsymbol{\Omega})}{\partial \boldsymbol{q}}(\boldsymbol{q}-\boldsymbol{q}_{eq}) + \frac{\partial \boldsymbol{q}_d}{\partial s}\dot{s} + \boldsymbol{\Lambda}_1 + \boldsymbol{\Lambda}_2, \tag{4.169}$$

where the general gradient of $\boldsymbol{\Omega}(t)$ with respect to vector $\boldsymbol{q}$ is given by

$$\frac{\partial \Psi(\boldsymbol{\Omega})}{\partial \boldsymbol{q}} = \begin{bmatrix} \frac{\partial \Psi(\boldsymbol{\Omega})}{\partial \Omega_x}\frac{\partial \Omega_x}{\partial x} & \frac{\partial \Psi(\boldsymbol{\Omega})}{\partial \Omega_x}\frac{\partial \Omega_x}{\partial y} \\ \frac{\partial \Psi(\boldsymbol{\Omega})}{\partial \Omega_y}\frac{\partial \Omega_y}{\partial x} & \frac{\partial \Psi(\boldsymbol{\Omega})}{\partial \Omega_y}\frac{\partial \Omega_y}{\partial y}\end{bmatrix} \tag{4.170}$$

The previous section has already proven the forward completeness of the closed-loop system (4.54), and $\lim_{t\to\infty}\phi_e(t) = 0$, $\lim_{t\to\infty}\mathbf{v}_e(t) = 0$, see (4.166). Therefore, it is necessary to prove that $\boldsymbol{q}_d$ is locally asymptotically stable and that $\boldsymbol{q}_c$ is locally unstable. In other words, the actual path $\boldsymbol{q}(t)$ of the WMR approaches the reference path $\boldsymbol{q}_d$ from almost everywhere except from the set denoted by the condition (4.6) and the set denoted by $\boldsymbol{q}_c$ which is unstable.

Proof of asymptotic stability of an desired equilibrium point

In order to show the equilibrium point $\boldsymbol{q}_d(x_d, y_d)$ being locally asymptotically stable, the Jacobian matrix in (4.170) is evaluated at the desired equilibrium point $\boldsymbol{q} = \boldsymbol{q}_d$, i.e., $\frac{\partial \Psi(\boldsymbol{\Omega})}{\partial \boldsymbol{q}}|_{\boldsymbol{q}=\boldsymbol{q}_d}$. Results can be achieved by applying property 4 of the differential bounded function Ψ in Chapter 2 and associated properties of function β described in the previous section, and the first and second derivatives of β, i.e., β' and β'', defined in (4.14)

$$\begin{aligned} &\frac{\partial \Psi(\boldsymbol{\Omega})}{\partial \boldsymbol{\Omega}}|_{\boldsymbol{q}=\boldsymbol{q}_d} = \mathbf{I}_2; \beta'_d = \beta'|_{\boldsymbol{q}=\boldsymbol{q}_d} = 0; \beta''_d = \beta''|_{\boldsymbol{q}=\boldsymbol{q}_d}, \\ &\frac{\partial \boldsymbol{\Omega}}{\partial \boldsymbol{q}}|_{\boldsymbol{q}=\boldsymbol{q}_d} = \mathbf{I}_2 + \beta''_d(\boldsymbol{q} - \boldsymbol{q}_{obs})(\boldsymbol{q} - \boldsymbol{q}_{obs})^T. \end{aligned} \tag{4.171}$$

To investigate the stability behavior of the point $\boldsymbol{q} = \boldsymbol{q}_d$, the following Lyapunov function is considered

$$V_d = \sqrt{1 + \|(\boldsymbol{q} - \boldsymbol{q}_d)\|^2} - 1 \tag{4.172}$$

Taking the time derivative of (4.172) along the solution of (4.169) with $\boldsymbol{q}_{eq}$ replaced by $\boldsymbol{q}_d$ results in

$$\begin{aligned} \dot{V}_d &= -\frac{\mathbf{K} v_d^2 \|\boldsymbol{q} - \boldsymbol{q}_d\|^2}{\sqrt{1 + \|\boldsymbol{q} - \boldsymbol{q}_d\|^2}} - \frac{\mathbf{K} v_d^2 \beta''_d}{\sqrt{1 + \|\boldsymbol{q} - \boldsymbol{q}_d\|^2}} \big((\boldsymbol{q} - \boldsymbol{q}_{obs})^T (\boldsymbol{q} - \boldsymbol{q}_d)\big)^2 \\ &\quad + \frac{(\boldsymbol{q} - \boldsymbol{q}_d)^T}{\sqrt{1 + \|(\boldsymbol{q} - \boldsymbol{q}_d)\|^2}} (\frac{\partial \boldsymbol{q}_d}{\partial s} \dot{s} + \boldsymbol{\Lambda}_1 + \boldsymbol{\Lambda}_2) \\ &\leq -\frac{\mathbf{K} v_d^2 \|\boldsymbol{q} - \boldsymbol{q}_d\|^2}{\sqrt{1 + \|\boldsymbol{q} - \boldsymbol{q}_d\|^2}} + \frac{(\boldsymbol{q} - \boldsymbol{q}_d)^T}{\sqrt{1 + \|(\boldsymbol{q} - \boldsymbol{q}_d)\|^2}} (\frac{\partial \boldsymbol{q}_d}{\partial s} \dot{s} + \boldsymbol{\Lambda}_1 + \boldsymbol{\Lambda}_2) \end{aligned} \tag{4.173}$$

It has been assumed that $\mathbf{K}$ is a positive constant matrix, $v_d^2 \neq 0$, see (4.5), and $\beta''|_{\boldsymbol{q}=\boldsymbol{q}_d} \geq 0$ see property 4 of function β in (4.13). Near the equilibrium point $\boldsymbol{q}_d$ the part $\frac{\partial \boldsymbol{q}_d}{\partial s} \dot{s}$ is always bounded by a strictly positive constant $\zeta = \epsilon_1 \epsilon_3$, see conditions (4.2) and (4.3) in Assumption 4.1.1 for all $t \geq t_0$. Each individual elements of $\boldsymbol{\Lambda}_1(t)$ and $\boldsymbol{\Lambda}_2(t)$ in (4.10) are bounded, see (4.24) and (4.27) for the expression of α_ϕ and α_v, respectively. Also, the boundedness of v_e and ϕ_e have been already stated in the previous section. The first equation of (4.166) implies $\lim_{t \to \infty} \big(\boldsymbol{\Lambda}_1(t) + \boldsymbol{\Lambda}_2(t)\big) = 0$. Thus, it can be concluded by the inequality (4.73) that the equilibrium point $\boldsymbol{q}_d(x_d, y_d)$ is locally asymptotically stable.

Proof of instability of a saddle point

Similarly, the Jacobian matrix in (4.170) is calculated at the critical point $\boldsymbol{q} = \boldsymbol{q}_c$, i.e., $\frac{\partial \Psi(\boldsymbol{\Omega})}{\partial \boldsymbol{q}}|_{\boldsymbol{q}=\boldsymbol{q}_c}$ while using properties of functions β and Ψ to give

$$\begin{aligned} &\frac{\partial \Psi(\boldsymbol{\Omega})}{\partial \boldsymbol{\Omega}}|_{\boldsymbol{q}=\boldsymbol{q}_c} = \mathbf{I}_2; \beta_c' = \beta'|_{\boldsymbol{q}=\boldsymbol{q}_c}; \beta_c'' = \beta''|_{\boldsymbol{q}=\boldsymbol{q}_c}, \\ &\frac{\partial \boldsymbol{\Omega}}{\partial \boldsymbol{q}}|_{\boldsymbol{q}=\boldsymbol{q}_c} = (1+\beta_c')\mathbf{I}_2 + \beta_c''(\boldsymbol{q}-\boldsymbol{q}_{obs})^T(\boldsymbol{q}-\boldsymbol{q}_{obs}). \end{aligned} \tag{4.174}$$

For the purpose of stability evaluation of the linearized system (4.168) at the critical point $\boldsymbol{q}_c(x_c, y_c)$, the following Lyapunov function candidate is considered

$$V_c = \sqrt{1 + \|\boldsymbol{q}-\boldsymbol{q}_c\|^2} - 1. \tag{4.175}$$

Taking the time derivative of (4.175) along the solution of (4.168) with $\boldsymbol{q}_{eq}$ replaced by $\boldsymbol{q}_c$ yields

$$\begin{aligned} \dot{V}_c = &-\frac{\mathbf{K}v_d^2(1+\beta_c')}{\sqrt{1+\|\boldsymbol{q}-\boldsymbol{q}_c\|^2}}\|\boldsymbol{q}-\boldsymbol{q}_c\|^2 - \frac{\mathbf{K}v_d^2\beta_c''}{\sqrt{1+\|\boldsymbol{q}-\boldsymbol{q}_c\|^2}}\big((\boldsymbol{q}-\boldsymbol{q}_{obs})^T(\boldsymbol{q}-\boldsymbol{q}_c)\big)^2 \\ &+ \frac{(\boldsymbol{q}-\boldsymbol{q}_c)^T}{\sqrt{1+\|\boldsymbol{q}-\boldsymbol{q}_c\|^2}}(\frac{\partial \boldsymbol{q}_d}{\partial s}\dot{s} + \boldsymbol{\Lambda}_1 + \boldsymbol{\Lambda}_2). \end{aligned} \tag{4.176}$$

It is observed from the fact that a saddle point emerges only if three points $\boldsymbol{q}$, $\boldsymbol{q}_c$ and $\boldsymbol{q}_{obs}$ are collinear and the point $\boldsymbol{q}_c$ must be in the middle of the two points $\boldsymbol{q}$ and $\boldsymbol{q}_{obs}$. Otherwise, the coordinates of actual mobile robot, $\boldsymbol{q}$, will converge to the reference trajectory, $\boldsymbol{q}_d$, by all means. This refers back to the previous situation of an desired equilibrium point. To investigate stability properties of the critical point $\boldsymbol{q}_c(x_c, y_c)$, each parts of (4.176) will be evaluated carefully. Let $\mathbf{V}$ be a vector space over the field $\mathbb{R}^2$, in which $\|\boldsymbol{q}-\boldsymbol{q}_c\|^2 \geq 0$ for all $[x \quad y]^T, [x_c \quad y_c]^T \in \mathbf{V}$. Firstly, a subspace $\mathbf{V}^* \subset \mathbf{V}$ is defined such that $\boldsymbol{q} = \boldsymbol{q}_c$ for any $x_c \in \mathbf{V}^*$. This assumption also holds for the case of any $y_c \in \mathbf{V}^*$. Therefore, only the case of x_c is needed to prove here. This implies the sum of attractive and repulsive forces at this point to be equal to zero, but each individual forces are nonzero. Moreover, $\mathbf{K}$ is a positive constant matrix, $|v_d(t)| \geq 0$, and $\beta'' \geq 0$ which are already mentioned in the previous section. Hence, $\dot{V}_c$ in (4.176) can be rewritten in subspace $\mathbf{V}^*$ by

$$\dot{V}_c = -\frac{\mathbf{K}v_d^2(1+\beta_c')}{\sqrt{1+\|\boldsymbol{q}-\boldsymbol{q}_c\|^2}}\|\boldsymbol{q}-\boldsymbol{q}_c\|^2 + \frac{(\boldsymbol{q}-\boldsymbol{q}_c)^T}{\sqrt{1+\|\boldsymbol{q}-\boldsymbol{q}_c\|^2}}(\frac{\partial \boldsymbol{q}_d}{\partial s}\dot{s} + \boldsymbol{\Lambda}_1 + \boldsymbol{\Lambda}_2). \tag{4.177}$$

Secondly, another subspace $\mathbf{V}^{**} \subset \mathbf{V} \setminus \mathbf{V}^*$ is defined. This means $\|\boldsymbol{q}-\boldsymbol{q}_c\|^2 > 0$ for all $[x \quad y]^T, [x_c \quad y_c]^T \in \mathbf{V}^{**}$. From the definitions of β in (4.13) and smooth

step function $h(\bullet)$ introduced in Definition (2.1.3) and Lemma (2.1.13), it gives

$$\beta' = \frac{\partial \beta}{\partial h}\frac{\partial h}{\partial \tau}\frac{\partial \tau}{\partial \|\boldsymbol{q}-\boldsymbol{q}_{obs}\|^2/2}. \tag{4.178}$$

Now utilizing some results what have been already calculated in [125] gives

$$\begin{aligned}
&\frac{\partial \beta}{\partial h} = -\frac{1}{h^2(\bullet)},\\
&\frac{\partial h}{\partial \tau} = \big(-h(\bullet)+h^2(\bullet)\big)\big(-\frac{1}{\tau^2}-\frac{1}{(\tau-1)^2}\big),\\
&\frac{\partial \tau}{\partial \|\boldsymbol{q}-\boldsymbol{q}_{obs}\|^2/2} = \frac{1}{R_{sen}^2/2-(R_{safe}+R_{obs})^2/2}
\end{aligned} \tag{4.179}$$

where functions $h(\bullet)$ and τ have been defined as

$$\begin{aligned}
h &= \frac{e^{-\frac{1}{\tau}}}{e^{-\frac{1}{\tau}}+e^{-\frac{1}{1-\tau}}},\\
\tau &= \frac{\|\boldsymbol{q}-\boldsymbol{q}_{obs}\|^2/2-(R_{safe}+R_{obs})^2/2}{R_{sen}^2/2-(R_{safe}+R_{obs})^2/2}.
\end{aligned} \tag{4.180}$$

It is revealed that $\big(-h(\bullet)+h^2(\bullet)\big)<0$ for all $\tau \in \big(\frac{(R_{safe}+R_{obs})^2}{2}, \frac{R_{sen}^2}{2}\big)$ [125]. Thus, by substituting (4.179) into (4.178) it gives $\beta'<0$ for all $\tau \in \big(\frac{(R_{safe}+R_{obs})^2}{2}, \frac{R_{sen}^2}{2}\big)$. Since $\frac{\|\boldsymbol{q}-\boldsymbol{q}_{obs}\|^2}{2}$ is the variable of function $h(\bullet)$, see (4.180), and β' is inversely proportional to square of absolute value of $h(\bullet)$, see (4.179) and (4.180), the smaller the relative distance between the WMR and a potential obstacle is, i.e., $\frac{\|\boldsymbol{q}-\boldsymbol{q}_{obs}\|^2}{2}$, the larger the value of β' for all $\tau \in \big(\frac{(R_{safe}+R_{obs})^2}{2}, \frac{R_{sen}^2}{2}\big)$. There always exists $x_c \in \mathbf{V}^{**}$ such that the part $(1+\beta_c')$ is strictly negative, i.e., there exists a strict positive constant b^* such that $(1+\beta_c')<-b^*$. This assumption also holds for the case of any $y_c \in \mathbf{V}^{**}$. Therefore, it is only necessary to prove for the case of x_c. It can be represented $\dot{V}_c$ of (4.176) in the subspace $\mathbf{V}^{**}$ as follows

$$\dot{V}_c = \frac{-\mathbf{K}v_d^2(1+\beta_c')}{\sqrt{1+\|\boldsymbol{q}-\boldsymbol{q}_c\|^2}}\|\boldsymbol{q}-\boldsymbol{q}_c\|^2 + \frac{(\boldsymbol{q}-\boldsymbol{q}_c)^T}{\sqrt{1+\|\boldsymbol{q}-\boldsymbol{q}_c\|^2}}(\frac{\partial \boldsymbol{q}_d}{\partial s}\dot{s}+\boldsymbol{\Lambda}_1+\boldsymbol{\Lambda}_2). \tag{4.181}$$

Using $(1+\beta_c')<-b^*$ for any $x_c \in \mathbf{V}^{**}$, $\dot{V}_c$ in (4.176) can be expressed by

$$\begin{aligned}
\dot{V}_c &\geq \frac{(b^*\mathbf{K}v_d^2-\kappa)}{\sqrt{1+\|\boldsymbol{q}-\boldsymbol{q}_c\|^2}}\|\boldsymbol{q}-\boldsymbol{q}_c\|^2 - \frac{\|\frac{\partial \boldsymbol{q}_d}{\partial s}\dot{s}+\boldsymbol{\Lambda}_1+\boldsymbol{\Lambda}_2\|^2}{4\kappa\sqrt{1+\|\boldsymbol{q}-\boldsymbol{q}_c\|^2}}\\
&\geq b^*\lambda_{max}(\mathbf{K})v_d^2V_c - \frac{\|\frac{\partial \boldsymbol{q}_d}{\partial s}\dot{s}+\boldsymbol{\Lambda}_1+\boldsymbol{\Lambda}_2\|^2}{4\kappa\sqrt{1+\|\boldsymbol{q}-\boldsymbol{q}_c\|^2}},
\end{aligned} \tag{4.182}$$

where $\kappa>0$ is a strictly positive constant, $\lambda_{max}(\mathbf{K})$ is maximum eigenvalue of constant matrix $\mathbf{K}$, $|v_d(t)| \neq 0$, see Assumption 4.1.2, and the closed-loop system (4.54) is forward complete in the previous section. Moreover, near the

critical point $\boldsymbol{q}_c$ the part $\frac{\partial \boldsymbol{q}_d}{\partial s}\dot{s}$ is always bounded by a strictly positive constant ϵ_0 according to the condition of $\dot{s}(t)$ in (4.2) for all $t \geq t_0$.
For the special case $\|\boldsymbol{q}(t_0) - \boldsymbol{q}_c\| = 0$, there would be no contradiction in terms of (4.182). This case, however, is never observed in practice since the ever-present physical noise would cause $\|\boldsymbol{q}(t^*) - \boldsymbol{q}_c\| \neq 0$ for some $x_c \in \mathbf{V}^{**}$ to be different from 0 at the time $t^* \geq t_0$. The inequality (4.182) can be rewriten as

$$\dot{V}_c \geq \frac{(b^*\mathbf{K}v_d^2 - \kappa)}{\sqrt{1 + \|\boldsymbol{q}^* - \boldsymbol{q}_c\|^2}}\|\boldsymbol{q}^* - \boldsymbol{q}_c\|^2 \geq b^*\lambda_{max}(\mathbf{K})v_d^2 V_c, \tag{4.183}$$

where, $\boldsymbol{q}^* = \boldsymbol{q}(t^*)$, for all time $t \geq t^* \geq t_0 \geq 0$. The last part of (4.182) is ignored here due to the explanation above. Since $\|\boldsymbol{q}(t^*) - \boldsymbol{q}_c\| \neq 0$, the right-hand side of (4.183) is divergent, and so does the left-hand side. As a result, the critical point $\boldsymbol{q}_c$ is unstable based on the Theorem 4.3 in [57]. The proof of Theorem 4.2.1 is completed.

4.4 Simulation results

In this section, some numerical simulations are performed to illustrate the correctness of the designed control laws (4.51). Simulation is carried out by using the physical parameters of the WMR which is taken from [6]. These parameters are summarized in Table 3.1 in Chapter 3. A tanh-shape path is chosen as the reference path with specifications as follows: $x_d = s - 8$, $y_d = -5\tanh(0.2x_d)$, and the path parameter is selected as: $s(t) = t$. This selection of the reference path is regular and satisfies requirements (4.3) and (4.4) in Assumptions 4.1.1. A simple calculation shows the satisfaction as,

$$\begin{aligned}
&\dot{s} = 1 = \epsilon_1; \qquad x_d'^2 + y_d'^2 = 1 + (\tanh(0.2(8-s))^2 - 1)^2 \geq \epsilon_2,\\
&\|\dot{\boldsymbol{q}}_d(s)\| = \sqrt{x_d'^2 + y_d'^2} = \sqrt{1 + (\tanh(0.2(8-s))^2 - 1)^2} \leq \epsilon_3,\\
&\|\ddot{\boldsymbol{q}}_d(s)\| = \sqrt{x_d''^2 + y_d''^2} = \sqrt{(0.4\tanh(0.2(8-s))\tanh(0.2(8-s))^2 - 1)^2} \leq \epsilon_4.
\end{aligned}$$

The PE condition (4.5) is also satisfied

$$|\sqrt{x_d'^2 + y_d'^2}\dot{s}| = |\sqrt{1 + (\tanh(0.2(8-s))^2 - 1)^2}| \geq 0.$$

The design parameters for control laws (4.17), (4.34) and (4.51) in are listed in Table 4.1. Particularly, k_1 and k_2 are chosen properly to satisfy the conditions (4.26) and (4.50). To investigate the obstacle avoidance capability of the proposed controllers, positions of a stationary obstacle in two different scenarios are

Table 4.1: Values of design parameters

Parameters	Meaning	Values
$x(0); y(0); \phi(0)$	initial configuration of the actual WMR	$-10; 1; 0.2$
k_1	control gain 1 of constant matrix $\mathbf{K}$ in (4.17)	1.15
k_2	control gain 2 of constant matrix $\mathbf{K}$ in (4.17)	1.15
k_3	control gain of virtual control α_ϕ in (4.34)	0.85
k_4	control gain of torque controllers in (4.51)	2.5
k_5	control gain of torque controllers in (4.51)	2.5
$x_{obs1}; y_{obs1}$	coordinates of the obstacle in scenario 1	$20; -5.5$
$x_{obs2}; y_{obs2}$	coordinates of the obstacle in scenario 2	$25; -6.5$
h	time step used in Euler method for numerical computation	0.06

set up, i.e., scenario 1 (obstacle is on the path): (x_{obs1}, y_{obs1}), scenario 2 (obstacle is close to the path): (x_{obs2}, y_{obs2}). R_{obs} defined in Assumption 4.1.4 is considered to be zero in simulation only. This means obstacle is a point in the Cartesian plane.

Figures 4.2 and 4.5 depict the tracking journeys of the WMR to the desired paths in both scenarios. At first, the WMR starts approaching the predefined paths smoothly. When it encounters the obstacle on its traveling trajectory, the WMR gets the information of relative distance between the obstacle and itself through on-board sensors. This information will activate the designed obstacle avoidance algorithm if the obstacle enters its sensing range. At this point, the control algorithm forces the WMR to surpass the obstacle to avoid a potential collision. Once, the obstacle is out of the WMR's sensing range, the obstacle avoidance algorithm is inactive automatically due to the advances of the smooth step function. Then, it is able to return to the reference path. Figures 4.3 and 4.5 show the errors in position and orientation in two cases, respectively. Apart from the starting and obstacle avoidance circumstances, such errors tend to zero at steady state. In figures 4.4 and 4.7, errors in velocities in both scenarios track their reference nicely. Correspondingly, τ_v and τ_ω applied to two wheels tend to constant values at steady state.

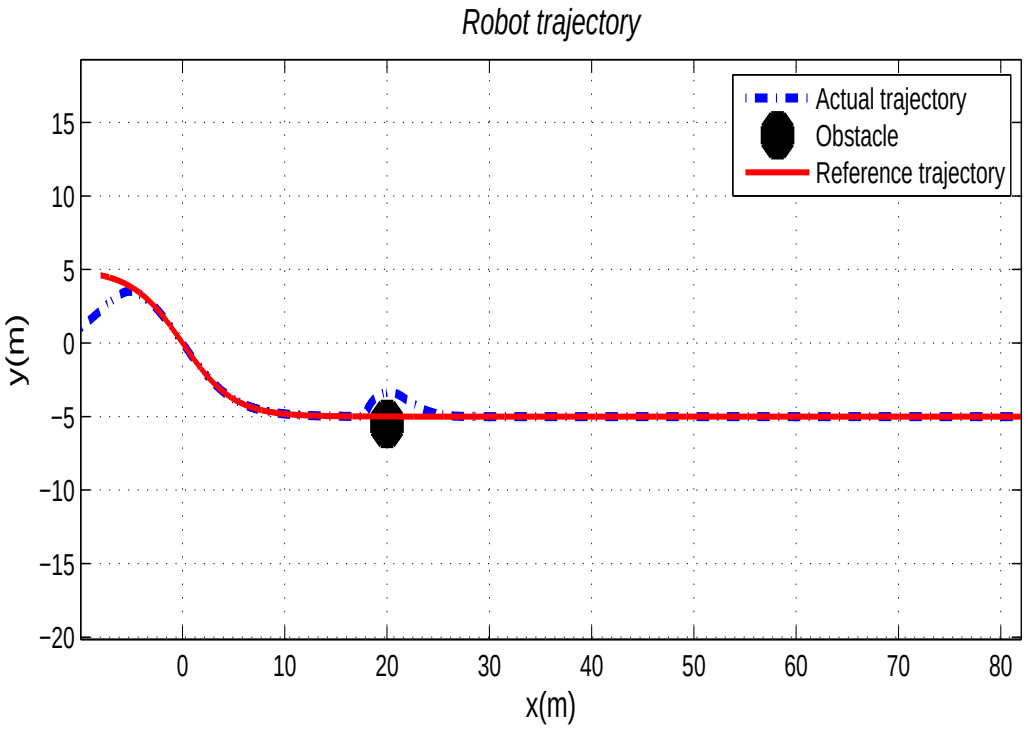

Figure 4.2: Tracking path of the WMR to the tanh-shape reference path in scenario 1 - an obstacle is on the reference path.

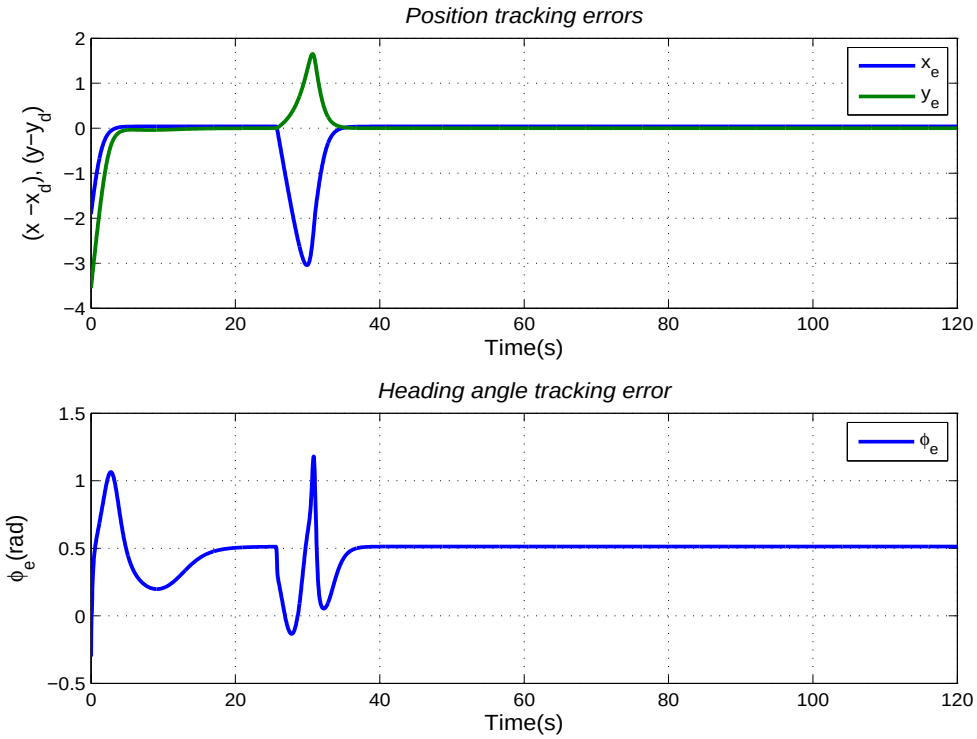

Figure 4.3: Position tracking errors (above); Heading angle tracking error (below).

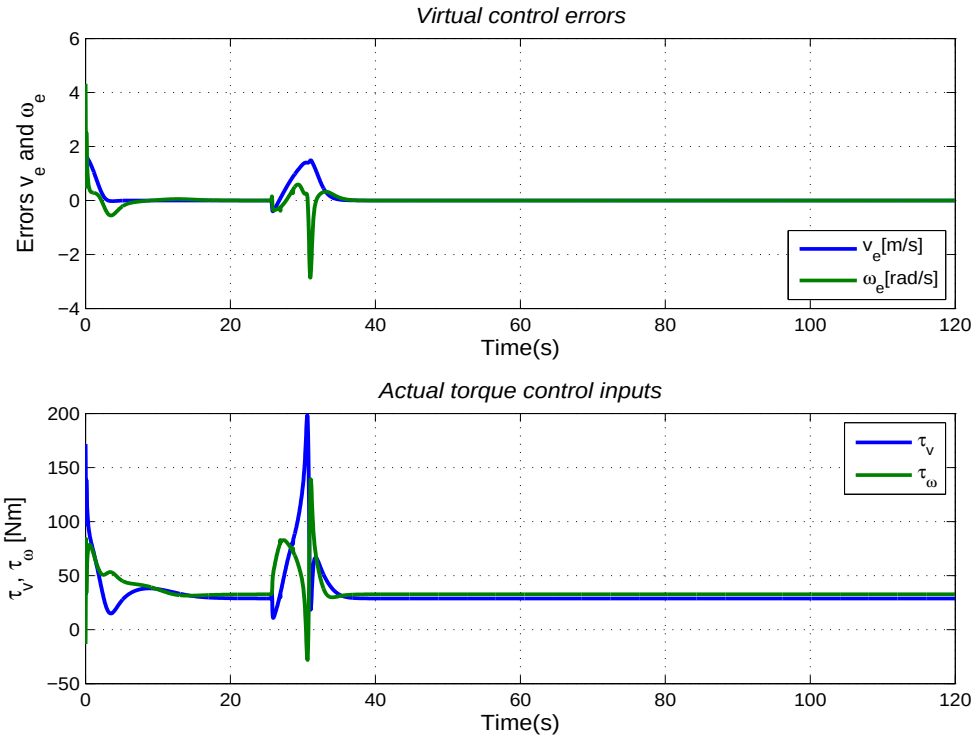

Figure 4.4: Virtual control errors (above); Actual control inputs (below).

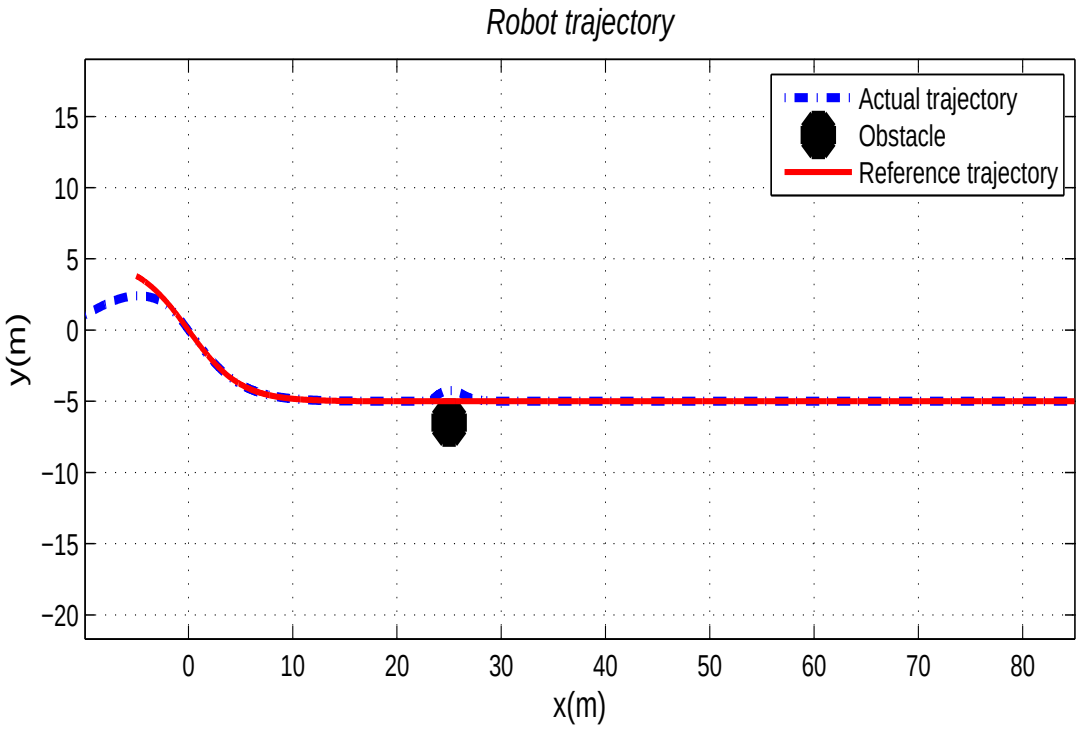

Figure 4.5: Tracking path of the WMR in scenario 2 - an obstacle is close to the reference path

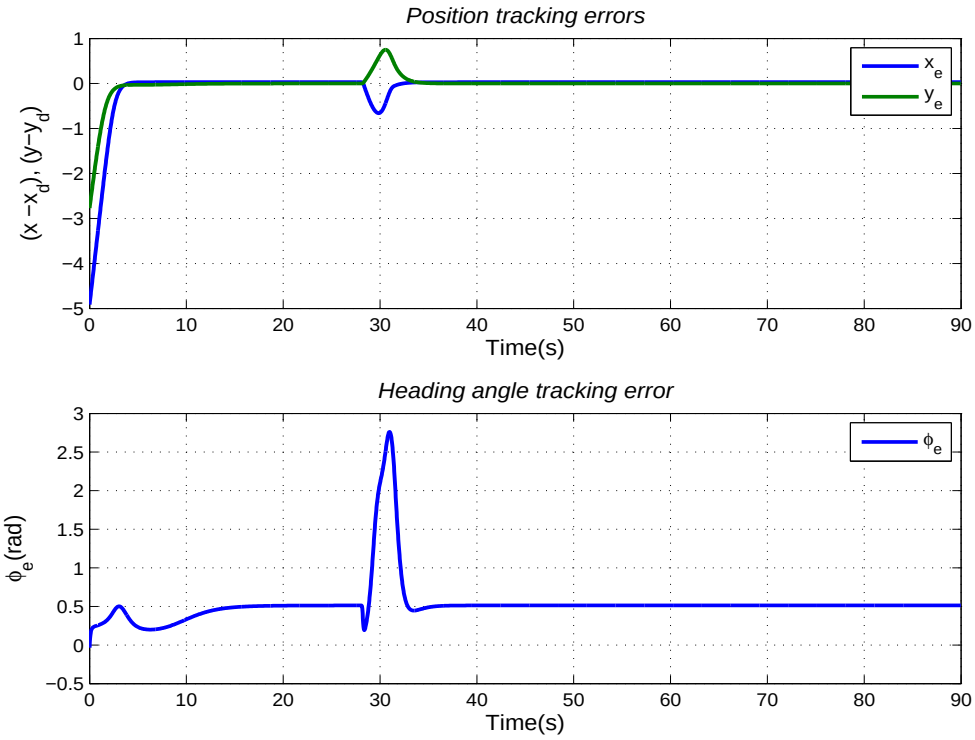

Figure 4.6: Position tracking errors (above); Heading angle error (below).

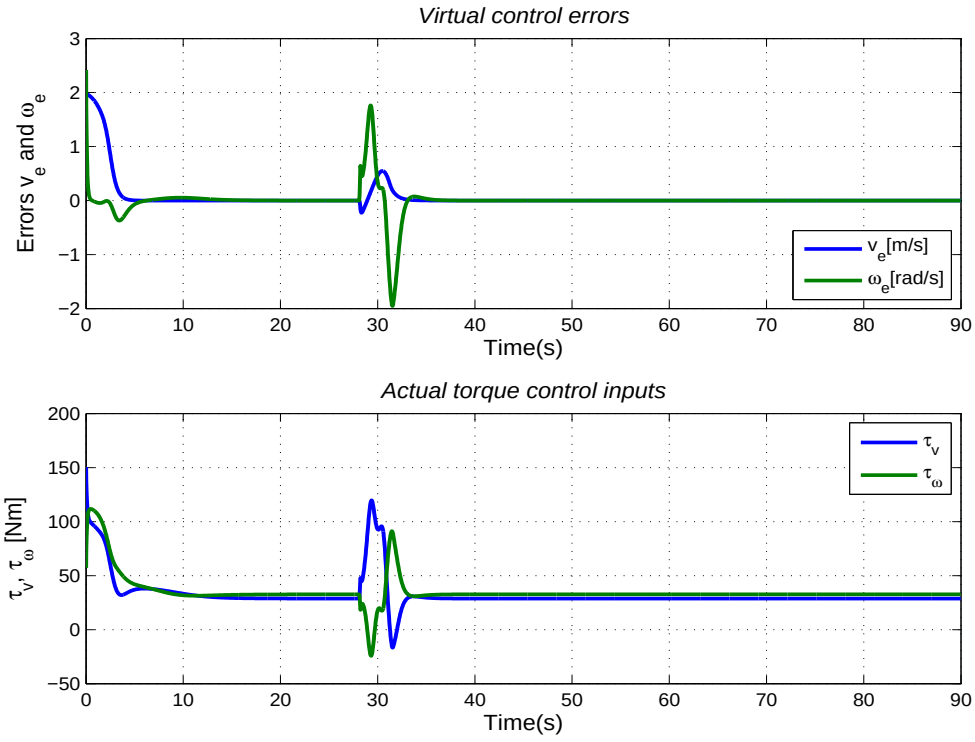

Figure 4.7: Virtual control errors (above); Actual control inputs (below).

4.5 Conclusions

In this chapter, a combined solution for path tracking and obstacle avoidance problems of the WMR has been represented by using the Lyapunov's direct

method and the backstepping technique. By adopting the works in [3], a smooth step function embedded into the local potential function is offered to deal with switching matter in controlling. Through simulation, the proposed controllers have demonstrated that the WMR converges to the reference path from the initial location to the goal while it can avoid any stationary obstacle along its travelling path. Similar to the navigation function in [119, 122], a saddle point emerging in the potential function method is a critical issue. This chapter provided an analytical analysis to prove that only the equilibrium point is locally asymptotically stable while the saddle point is unstable. Thus, the system does not converge to saddle points. However, similarly to conventional artificial potential functions [109, 113] and navigation functions [119, 122, 165], the local potential function built in collision avoidance control algorithm uses the relative distance between the WMR and the obstacle to generate a repulsive force. This might result in very large control efforts if the relative distance of the WMR and the obstacle is sufficiently small. This issue suggests the author do further investigation in the next chapter.

Chapter 5

Bounded position control for path tracking and obstacle avoidance

As stated in the last chapter, the WMR system might encounter very large control efforts if the relative distance between it and an obstacle is sufficiently small. The motivation of this chapter is to examine a new bounded position control algorithm for the problem of path tracking and obstacle avoidance. The nonholonomic kinematics are converted to double integrator dynamics by using a coordinate transformation. Therefore, the technique offers a simplification since only the coordinates of position are directly controlled while the orientation is neglected. This results in an alternative solution for the nonholonomic kinematics problem, i.e., two control inputs v and ω for two state variables x and y. To overcome the difficulties in designing bounded position control, the novel pairwise collision function developed in [4] to deal with the obstacle avoidance problem is deployed. The resulting controllers are capable of handling both path tracking and obstacle avoidance matters smoothly without any switching control scheme. Boundedness in terms of the relative distance between the WMR and obstacle and relative velocity between the WMR and the virtual reference vehicle is achieved. Simulations are represented in the last section for the illustration of the effectiveness of the proposed control design.

5.1 Problem statement

5.1.1 Mobile robot dynamics

To develop the proposed control algorithm and stability analysis, the equations of motion of a WMR moving in the Cartesian space are considered. This is a combination of kinematic and dynamic models, i.e., (2.41), (2.50), respectively, in Chapter 2:

$$\begin{cases} \dot{x} = v\cos(\phi) \\ \dot{y} = v\sin(\phi) \\ \dot{\phi} = \omega \end{cases}, \qquad \begin{bmatrix} \dot{v} \\ \dot{\omega} \end{bmatrix} = \bar{\mathbf{C}} \begin{bmatrix} \omega^2 \\ -v\omega \end{bmatrix} - \bar{\mathbf{D}} \begin{bmatrix} v \\ \omega \end{bmatrix} + \bar{\mathbf{B}}\boldsymbol{\tau}, \tag{5.1}$$

where matrices $\bar{\mathbf{C}}$, $\bar{\mathbf{D}}$ and $\bar{\mathbf{B}}$ are described by (2.51) in Chapter 2.

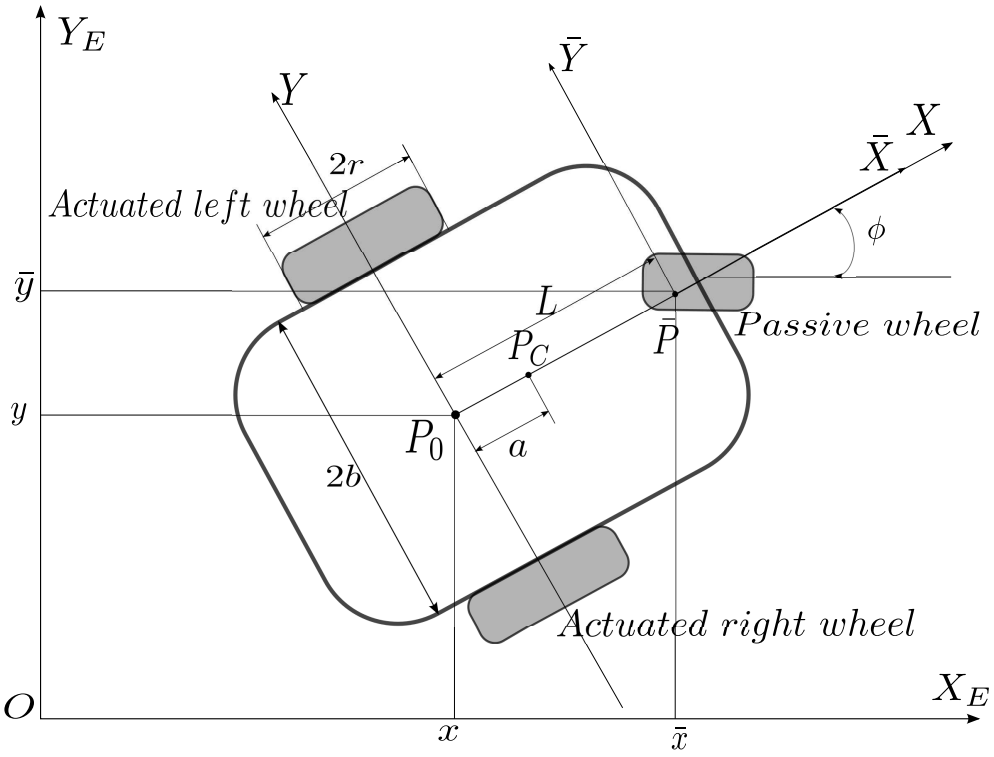

Figure 5.1: Description on Cartesian plane of reference point $\bar{P}$ on the WMR.

The main task is to design the control input vector $\boldsymbol{\tau} = \begin{bmatrix} \tau_1 & \tau_2 \end{bmatrix}^T$ applied to both actuated left and right wheels that forces the WMR to asymptotically move along the path tangentially with a desired linear velocity v_d, while it can avoid collisions to obstacles presented within its sensing range on the reference path. Let $\bar{P}$ be a new virtual reference point on the axis of symmetry displaced through

a distance L from P_0. Instead of controlling directly coordinates $\boldsymbol{q} = \begin{bmatrix} x & y \end{bmatrix}^T$ of the inertial position P_0 on the WMR, the following coordinate transformation of the kinematic model of (5.1) is introduced

$$\begin{aligned} \bar{x} &= x + L\cos(\phi), \\ \bar{y} &= y + L\sin(\phi), \end{aligned} \tag{5.2}$$

with $L \neq 0$, is an offset distance of P_0 along the main axis of the WMR. The coordinate transformation (5.2) presents the definition of coordinates $\bar{\boldsymbol{q}} = \begin{bmatrix} \bar{x} & \bar{y} \end{bmatrix}^T$ of $\bar{P}$. In [62], this virtual point is mentioned as the "hand position". This coordinate transformation is similar to that in [61, 136] to provide the input-output linearized and decoupled systems of mobile manipulators. Eventually, a new kinematic model is obtained by taking the differentiation of both sides of (5.2) with respect to time and using the two first equations of (5.1) to give

$$\begin{aligned} \dot{\bar{x}} &= \dot{x} - L\omega\sin(\phi) = v\cos(\phi) - L\omega\sin(\phi), \\ \dot{\bar{y}} &= \dot{y} + L\omega\cos(\phi) = v\sin(\phi) + L\omega\cos(\phi). \end{aligned} \tag{5.3}$$

By taking differentiation of both sides of (5.3) one more time, the inputs of a second-order dynamic system appeare in the following equations

$$\begin{bmatrix} \ddot{\bar{x}} \\ \ddot{\bar{y}} \end{bmatrix} = \begin{bmatrix} \cos(\phi) & -L\sin(\phi) \\ \sin(\phi) & L\cos(\phi) \end{bmatrix} \begin{bmatrix} \dot{v} \\ \dot{\omega} \end{bmatrix} + \begin{bmatrix} -v\omega\sin(\phi) - L\omega^2\sin(\phi) \\ v\omega\cos(\phi) - L\omega^2\cos(\phi) \end{bmatrix}. \tag{5.4}$$

From (5.3) and (5.4), the equations of the WMR dynamics (5.1) can be represented in the vector form of the second-order dynamics as follows

$$\begin{cases} \dot{\bar{\boldsymbol{q}}} = \bar{\boldsymbol{p}}, \\ \ddot{\bar{\boldsymbol{q}}} = \dot{\bar{\boldsymbol{p}}} = \mathbf{G}\boldsymbol{\tau} + \mathbf{A} = \boldsymbol{u}, \end{cases} \tag{5.5}$$

where $\boldsymbol{u} = \begin{bmatrix} u_1 & u_2 \end{bmatrix}^T$ are control inputs and will be designed later. Matrice $\mathbf{G}$ and $\mathbf{A}$ are denoted as

$$\mathbf{G} = \begin{bmatrix} \cos(\phi) & -L\sin(\phi) \\ \sin(\phi) & L\cos(\phi) \end{bmatrix}; \qquad \mathbf{A} = \begin{bmatrix} -v\omega\sin(\phi) - L\omega^2\sin(\phi) \\ v\omega\cos(\phi) - L\omega^2\cos(\phi) \end{bmatrix}. \tag{5.6}$$

A simple calculation shows that $det(\mathbf{G}) = L$ is a non-zero constant because of the assumption $L \neq 0$ in (5.2). Therefore, the matrix $\mathbf{G}$ is invertible. Based on the proposed coordinate transformations (5.2), the system dynamics (5.5) can avoid a potential singularity which is carefully mentioned in [13], i.e., when the linear velocity of the WMR is equal to zero. Furthermore, by converting equations of dynamics (5.1) to the form of second-order dynamics (5.5), it provides a convenient form that are employed for designing the proposed bounded position control later.

5.1.2 Control objective

As concerns the bounded position control for path tracking and collision avoidance, the following assumptions are made to the reference path, sensing capability and measurements of the WMR's state variables. Let s_d be the desired value of the path parameter s, and the first derivative of $s_d(t)$ is bounded by strictly positive constants ϵ_0 and ϵ_1.

Assumption 5.1.1

The reference path $\boldsymbol{q}_d(s(t)) = \begin{bmatrix} x_d(s(t)) & y_d(s(t)) \end{bmatrix}^T$ *is parameterized by a path parameter* s *which is a time-dependent variable. Let* s_d *be the desired value of the path parameter* s*, and the first derivative of* $s_d(t)$ *is bounded by strictly positive constants* ϵ_0 *and* ϵ_1*.*

$$\epsilon_0 \leq |\dot{s}_d(t)| \leq \epsilon_1, \qquad \forall t \geq 0. \tag{5.7}$$

Moreover, the vector $\boldsymbol{q}_d(s)$ *is regular and differentiable with respect to* s *at least two times and satisfies the bounded conditions*

$$\begin{aligned} &x_d'^2(s) + y_d'^2(s) \geq \epsilon_2, \qquad \forall s \in \mathbb{R}, \\ &\|\dot{\boldsymbol{q}}_d\| \leq \epsilon_3, \qquad \|\ddot{\boldsymbol{q}}_d\| \leq \epsilon_4, \end{aligned} \tag{5.8}$$

where $x_d'(s) = \frac{\partial x_d}{\partial s}$ and $y_d'(s) = \frac{\partial y_d}{\partial s}$, and ϵ_2, ϵ_3 and ϵ_4 are strictly positive constants.

Assumption 5.1.2

There exists a strictly positive constants ϵ_5 *such that the desired linear velocity* $v_d(t)$ *is bounded*

$$|v_d(t)| = \sqrt{x_d'^2(s) + y_d'^2(s)}|\dot{s}(t)| \leq \epsilon_5, \tag{5.9}$$

In addition, the desired linear velocity $v_d(t)$ *does not converge to zero, i.e.,* $v_d(t)$ *satisfies the following PE condition*

$$|v_d(t)| \geq 0. \tag{5.10}$$

Assumption 5.1.3

Relative position between the WMR and the closest point on an obstacle are accurately measurable for feedback. The WMR has a physical safety ball with a radius

R_{safe}, and sensing circular area, R_{sen}, denotes the radius of the region in which the robot can detect the presence of an obstacle.

Assumption 5.1.4

The obstacle is stationary and it is considered as a convex polygon whose position, $\boldsymbol{q}_{obs} = \begin{bmatrix} x_{obs} & y_{obs} \end{bmatrix}^T$, and distance of influence, R_{obs} can be accutately measured.

Assumption 5.1.5

There exist strictly positive constants ϵ_6 and $\bar{\chi}_0$ such that at the initial time $t_0 \geq 0$, the WMR initializes at a location $\bar{\boldsymbol{q}}(t_0) = \begin{bmatrix} \bar{x}(t_0) & \bar{y}(t_0) \end{bmatrix}^T$ where it keeps a safe distance from any obstacle with coordinates $\boldsymbol{q}_{obs} = \begin{bmatrix} x_{obs} & y_{obs} \end{bmatrix}^T$ near by, the following conditions hold:

$$\begin{aligned} &\|\bar{\boldsymbol{q}}_{RO}(t_0)\| \geq \epsilon_6, \\ &\bar{\boldsymbol{q}}_{RO}^T(t_0)\Big(\mathbf{K}\bar{\boldsymbol{q}}_{RO}(t_0) + \big(1 + \frac{1}{2}\|\bar{\boldsymbol{p}}_{Rd}(t_0)\|^2\big)\bar{\boldsymbol{p}}_{Rd}(t_0)\Big) \geq \bar{\chi}_0, \end{aligned} \tag{5.11}$$

where $\bar{\boldsymbol{q}}_{RO}(t_0) = \bar{\boldsymbol{q}}(t_0) - \boldsymbol{q}_{obs}$, $\bar{\boldsymbol{p}}_{Rd}(t_0) = \bar{\boldsymbol{p}}(t_0) - \frac{\partial \boldsymbol{q}_d}{\partial s}\dot{s}(t_0)$, and $\mathbf{K}$ is a 2×2 diagonal positive-definite matrix.

Remark.

1. The desired linear velocity $v_d(t)$ of the virtual reference vehicle in (5.9) moving on the reference path $\boldsymbol{q}_d(s(t))$ is specified by the derivative of the path parameter $\dot{s}(t)$ in (5.7). This indicates how fast the WMR should move through $\dot{\boldsymbol{q}}_d$. Similar to the previous chapter, this chapter formulates a solution for the path tracking and obstacle avoidance problems. Therefore, condition (5.9) on the desired linear velocity $v_d(t)$ makes the solution of the path tracking problem feasible. Condition (5.10) means that the WMR can move either forward or backward and the stabilization problem is out of consideration.

2. The conditions (5.8) ensures the reference path $\boldsymbol{q}_d$ is regular and the desired velocity v_d which moves along the path $\boldsymbol{q}_d$, is bounded by condition (5.9).

3. The first condition of (5.11) is made in order to avoid any possible collision between the WMR and any obstacle at the initial time t_0. Under the second condition of (5.11), a bounded position control designing for path tracking and collision avoidance is achieved provided that this condition is satisfied. It will be explained clearly in the section of stability analysis.

Control objective

Under assumptions made above, the control objective of this chapter is to formulate bounded position controllers for the problem of path tracking and obstacle avoidance. Fundamentally, the current position of the WMR tracks asymptotically to a position on the reference path and the WMR is forced to move along the path tangentially at a desired linear velocity $v_d(t)$. Obstacle avoidance capability is ensured for all $t \geq t_0 \geq 0$ and there are no switching modes in the controllers. Regarding relative position between the WMR and an obstacle, and relative velocity between the WMR and the virtual reference vehicle, the boundedness of torque control inputs τ_v and τ_ω are guaranteed. Overall control objective can be described as follows:

$$\begin{aligned} &\lim_{t\to\infty} \|\bar{\boldsymbol{q}}(t) - \boldsymbol{q}_d(s(t))\| \leq \delta_1, \\ &\lim_{t\to\infty} \|\boldsymbol{\tau}(t)\| \leq \delta_2, \\ &\|\bar{\boldsymbol{q}}(t) - \boldsymbol{q}_{obs}\| - (R_{safe} + R_{obs}) \geq \delta_3, \end{aligned} \tag{5.12}$$

where δ_1, δ_2 and δ_3 are strictly positive constants.

5.2 Preliminaries

This section re-introduces the motivation example and associated lemmas for a bounded control design technique which is originally introduced by the author in [4]. Based on this technique, a bounded position control algorithm for the problem of path tracking and obstacle avoidance is derived.

5.2.1 Motivation example

To motivate the results, the following second-order system is considered [4]:

$$\begin{cases} \dot{x}_1 = x_2, \\ \dot{x}_2 = u \end{cases} \tag{5.13}$$

where x_1 and x_2 are the states, and u is the control input. The control problem is addressed by designing the control input u to asymptotically stabilize the system (5.13) at the origin for any initial values $(x_1(t_0), x_2(t_0)) \in \mathbb{R}^2$ at the initial time $t_0 \geq 0$ such that $|u(t)| \leq \epsilon$ for all $t \geq t_0$. A solution to the above control problem is given in the following lemmas.

5.2.2 Bounded control for second-order systems

Lemma 5.2.1. *[4]: Let the positive constants k and c be chosen such that $0.5k + c \leq \epsilon$, and let $\sigma(\bullet)$ be a smooth saturation function of $(\bullet)$ defined in Definition 3.1. The bounded control law*

$$u = \frac{1}{1 + 1.5x_2^2}\big(- kx_2 - c\sigma(kx_1 + (1 + 0.5x_2^2)x_2)\big), \tag{5.14}$$

globally asymptotically stabilizes the system at the origin.

Proof: see [4].

Lemma 5.2.2 (Nonzero Convergent Lemma)**.** *[4]: Assume the vector $\boldsymbol{x}(t) \in \mathbb{R}^n$ satisfies the following conditions*

$$\begin{aligned} &\|\boldsymbol{x}(t_0)\| \geq a_0, \\ &\boldsymbol{x}^T(\dot{\boldsymbol{x}} + \mathbf{B}\boldsymbol{x}) \geq a, \forall t \geq t_0 \geq 0, \end{aligned} \tag{5.15}$$

where $t_0 \geq 0$ is the initial time, $\mathbf{B}$ is a symmetric positive definite matrix, and a_0 and a are strictly positive constants. Then

$$\|\boldsymbol{x}(t)\| \geq min\Big(a_0, \sqrt{\frac{a}{\lambda_M(\mathbf{B})}}\Big) \tag{5.16}$$

$\forall t \geq t_0 \geq 0$, where $\lambda_M(\mathbf{B})$ is the maximum eigenvalue of the matrix $\mathbf{B}$.

Proof: see [4].

It is noted that this lemma is used for a first-order system. This result will be applied to develop pairwise collision avoidance functions in the next subsection. The lower bound shown by (5.16) will be applicable to ensure that there are no collision between the vehicle and an obstacle.

5.2.3 Pairwise collision avoidance function

This section adopts the definition and construction of pairwise collision avoidance function that were fully represented in [4]. Lemmas (5.2.1) and (5.2.2) introduced above are applied directly to construct this function. Later, the pairwise collision avoidance is integrated to a potential function designed in (5.20) in order to deal with the obstacle avoidance problem in control design. The original pairwise collision avoidance function β in [4] is modified due to the particular coordinate transformation in (5.2).

Definition 5.2.1. [4] Let the pairwise collision avoidance function $\bar{\beta}$ be a scalar function of $\bar{\chi}$, which is given by

$$\bar{\chi} = \bar{\boldsymbol{q}}_{RO}^T\big(\mathbf{K}\bar{\boldsymbol{q}}_{RO} + \bar{\Delta}\bar{\boldsymbol{p}}_{Rd}\big), \tag{5.17}$$

where $\mathbf{K}$ is defined in (5.11), and

$$\begin{aligned} \bar{\boldsymbol{q}}_{Rd} &= \bar{\boldsymbol{q}} - \boldsymbol{q}_d, \\ \bar{\boldsymbol{q}}_{RO} &= \bar{\boldsymbol{q}} - \boldsymbol{q}_{obs}, \\ \bar{\boldsymbol{p}}_{Rd} &= \bar{\boldsymbol{p}} - \frac{\partial \boldsymbol{q}_d}{\partial s}\dot{s} \\ \bar{\Delta} &= 1 + \frac{1}{2}\|\bar{\boldsymbol{p}}_{Rd}\|^2. \end{aligned} \tag{5.18}$$

The function $\bar{\beta}$ provides an obstacle avoidance capability between the WMR and an obstacle and possesses the following properties:

1. $\bar{\beta} = 0$, $\bar{\beta}' = 0$, $\bar{\beta}'' = 0$, $\forall \bar{\chi} \geq R_{sen}$,
2. $\bar{\beta} > 0$ if $(R_{safe} + R_{obs}) < \bar{\chi} < R_{sen}$, $\bar{\beta}' \leq 0$, $\forall \bar{\chi} \in \mathbb{R}$,
3. $\lim\limits_{\bar{\chi}\to 0} \bar{\beta} = \infty$, $\lim\limits_{\bar{\chi}\to 0} \bar{\beta}' = -\infty$, $\lim\limits_{\bar{\chi}\to 0} \bar{\beta}'' = -\infty$,
4. $\bar{\beta}$ is a smooth, $\forall \bar{\chi} \in (0, \infty)$,

where the terms $\bar{\beta}'$ and $\bar{\beta}''$ are the first and second derivatives of $\bar{\beta}$ with respect to $\bar{\chi}$ denoted as follows

$$\bar{\beta}' = \frac{\partial \bar{\beta}}{\partial \bar{\chi}}; \qquad \bar{\beta}'' = \frac{\partial^2 \bar{\beta}}{\partial \bar{\chi}^2}. \tag{5.19}$$

Following the work in [3, 4], this function is chosen:

$$\bar{\beta} = \frac{1 - h\big(\bar{\chi}, \frac{(R_{safe}+R_{obs})^2}{2}, \frac{R_{sen}^2}{2}\big)}{h\big(\bar{\chi}, \frac{(R_{safe}+R_{obs})^2}{2}, \frac{R_{sen}^2}{2}\big)}, \tag{5.20}$$

where $h_1(\bar{\chi}, \frac{(R_{safe}+R_{obs})^2}{2}, \frac{R_{sen}^2}{2})$ is a smooth step function defined in Definition (2.1.3). In particular, $\bar{\chi}$, $\frac{(R_{safe}+R_{obs})^2}{2}$, and $\frac{R_{sen}^2}{2}$ are variable and parameters corresponding to x, a, and b, respectively, defined in the Lemma (2.1.13) in Chapter 2.

Remark. 1. Being different from local potential functions in the previous chapter, this pairwise collision function is a function of both relative position between the WMR and the obstacle, and relative velocity between the actual WMR and the virtual reference vehicle, see (5.17).

2. For the obstacle avoidance matter, the pairwise collision avoidance function $\bar{\beta}$ should be selected in such a way that it is activated whenever the proximity sensors i.e., ultrasound, infrared, detect any obstacle in the sensing range and force the WMR to stay away, and equal to infinity whenever the WMR collides with an obstacle. This is an explanation of properties 2 and 3. This function $\bar{\beta}$ then is deactivated, i.e., is equal to zero, when the obstacle is out of detection region. This clarifies for property 1.

3. The construction of the proposed pairwise collision avoidance function using the mentioned smooth step function facilitates the smoothness between values of $\frac{(R_{safe}+R_{obs})^2}{2}$ and $\frac{R_{sen}^2}{2}$. Property 4 is required in order to deal with the obstacle avoidance problem under the WMR's limited sensing range for continuous systems instead of techniques for switched, non-smooth, and discontinuous systems. This is one of the main control objective.

4. Properties 1, 2, 3 and 4 imply that $\bar{\beta}$ is a continuous differentiable, and positive definite function which satisfies to be a Lyapunov's function candidate for control design and stability analysis purposes. The construction of this particular pairwise collision avoidance function $\bar{\beta}$ in (5.20) using (5.17) and (5.18) is different from that developed in, for example, [3], because the relative velocity $\bar{\boldsymbol{p}}_{Rd}$ of the WMR and the virtual reference one is included.

5.3 Control design

Instead of using the standard backstepping technique [58], the control design procedure in this chapter borrows the novel bounded control design for second-order dynamic systems in [4], including the pairwise collision function. In this method, the relative distance between the WMR and an obstacle must be known. This technique also requires information of the relative velocity between the actual WMR and the virtual reference vehicle. Using the coordinate transformation (5.2), definitions of $\bar{\boldsymbol{q}}_{Rd}$ and $\bar{\boldsymbol{p}}_{Rd}$ in (5.18), the Lyapunov-based potential function V is considered:

$$V = \frac{1}{2}\|2\mathbf{K}\bar{\boldsymbol{q}}_{Rd} + \bar{\Delta}\bar{\boldsymbol{p}}_{Rd}\|^2 + \bar{\beta}. \tag{5.21}$$

where the matrix $\mathbf{K}$, the function $\bar{\Delta}$ and the pairwise collision avoidance function $\bar{\beta}$ are defined in (5.11), (5.17), (5.18), and (5.20) respectively. This potential function comprises of two separated parts. The first part puts a penalty on the relative position error, i.e., $\bar{\boldsymbol{q}}_{Rd}$, and the relative velocity error, i.e., $\bar{\boldsymbol{p}}_{Rd}$.

The second part is the function $\bar{\beta}$ solving the obstacle avoidance problem. In general, this function should play as a combination of a goal function and a collision avoidance function, which is normally mentioned in the literature, for example, [2, 109, 113, 115, 120, 164] for problems of path planning and collision avoidance.

Differentiating both sides of equation (5.21) along the solutions of (5.5) and using the representations of (5.17), (5.18), and (5.20) yields

$$\begin{aligned}
\dot{V} &= \big(2\mathbf{K}\bar{\boldsymbol{q}}_{Rd} + \bar{\Delta}\bar{\boldsymbol{p}}_{Rd}\big)^T\big(2\mathbf{K}\bar{\boldsymbol{p}}_{Rd} + \dot{\bar{\Delta}}\bar{\boldsymbol{p}}_{Rd} + \bar{\Delta}(\dot{\bar{\boldsymbol{p}}} - \frac{\partial^2\boldsymbol{q}_d}{\partial s^2}\dot{s})\big) + \bar{\beta}'\dot{\bar{\chi}},\\
&= \big(2\mathbf{K}\bar{\boldsymbol{q}}_{Rd} + \bar{\Delta}\bar{\boldsymbol{p}}_{Rd}\big)^T\big(2\mathbf{K}\bar{\boldsymbol{p}}_{Rd} + \bar{\boldsymbol{p}}_{Rd}\bar{\boldsymbol{p}}_{Rd}^T(\dot{\bar{\boldsymbol{p}}} - \frac{\partial^2\boldsymbol{q}_d}{\partial s^2}\dot{s}) + \bar{\Delta}(\dot{\bar{\boldsymbol{p}}} - \frac{\partial^2\boldsymbol{q}_d}{\partial s^2}\dot{s})\big)\\
&\quad + \bar{\beta}'\bar{\boldsymbol{q}}_{RO}^T\big(2\mathbf{K}\bar{\boldsymbol{p}}_{Rd} + (\bar{\boldsymbol{p}}_{Rd}\bar{\boldsymbol{p}}_{Rd}^T + \bar{\Delta}\mathbf{I}_2)(\dot{\bar{\boldsymbol{p}}} - \frac{\partial^2\boldsymbol{q}_d}{\partial s^2}\dot{s})\big) + 2\bar{\beta}'\bar{\boldsymbol{q}}_{RO}^T\mathbf{K}\frac{\partial\boldsymbol{q}_d}{\partial s}\dot{s} + \bar{\beta}'\bar{\boldsymbol{p}}_{Rd}^T\bar{\Delta}\frac{\partial\boldsymbol{q}_d}{\partial s}\dot{s},\\
&= \big(2\mathbf{K}\bar{\boldsymbol{q}}_{Rd} + \bar{\Delta}\bar{\boldsymbol{p}}_{Rd} + \bar{\beta}'\bar{\boldsymbol{q}}_{RO}\big)^T\Big(2\mathbf{K}\bar{\boldsymbol{p}}_{Rd} + (\bar{\boldsymbol{p}}_{Rd}\bar{\boldsymbol{p}}_{Rd}^T + \bar{\Delta}\mathbf{I}_2)(\boldsymbol{u} - \frac{\partial^2\boldsymbol{q}_d}{\partial s^2}\dot{s})\Big)\\
&\quad + \bar{\beta}'\big(\bar{\Delta}\|\bar{\boldsymbol{p}}_{Rd}\|^2 + 2\bar{\boldsymbol{q}}_{RO}^T\mathbf{K}\frac{\partial\boldsymbol{q}_d}{\partial s}\dot{s} + \bar{\boldsymbol{p}}_{Rd}^T\bar{\Delta}\frac{\partial\boldsymbol{q}_d}{\partial s}\dot{s}\big).
\end{aligned} \tag{5.22}$$

For a compact representation, the following notation is used

$$\boldsymbol{\Omega} = \big(2\mathbf{K}\bar{\boldsymbol{q}}_{Rd} + \bar{\Delta}\bar{\boldsymbol{p}}_{Rd} + \bar{\beta}'\bar{\boldsymbol{q}}_{RO}\big), \tag{5.23}$$

where $\boldsymbol{\Omega}^T = [\Omega_{\bar{x}} \quad \Omega_{\bar{y}}]$. Owing to one of the important properties of the pairwise collision avoidance function $\bar{\beta}$ detailed in Definition 5.2.1, that is $\bar{\beta}' \leq 0$ for all $\bar{\chi} \in \mathbb{R}$, the following time derivative equation of function V is deduced as

$$\begin{aligned}
\dot{V} &= \boldsymbol{\Omega}^T\big(2\mathbf{K}\bar{\boldsymbol{p}}_{Rd} + (\bar{\boldsymbol{p}}_{Rd}\bar{\boldsymbol{p}}_{Rd}^T + \bar{\Delta}\mathbf{I}_2)(\boldsymbol{u} - \frac{\partial^2\boldsymbol{q}_d}{\partial s^2}\dot{s})\big)\\
&\quad + \bar{\beta}'\big(\bar{\Delta}\|\bar{\boldsymbol{p}}_{Rd}\|^2 + 2\bar{\boldsymbol{q}}_{RO}^T\mathbf{K}\frac{\partial\boldsymbol{q}_d}{\partial s}\dot{s} + \bar{\boldsymbol{p}}_{Rd}^T\bar{\Delta}\frac{\partial\boldsymbol{q}_d}{\partial s}\dot{s}\big).
\end{aligned} \tag{5.24}$$

By applying the fundamental idea of bounded control design for second-order systems described in Section 3.3, a bounded control $\boldsymbol{u}$ in the equation (5.24) is chosen by

$$(\bar{\mathbf{p}}_{Rd}\bar{\mathbf{p}}_{Rd}^T + \bar{\Delta}\mathbf{I}_2)(\boldsymbol{u} - \frac{\partial^2\boldsymbol{q}_d}{\partial s^2}\dot{s}) = -2\mathbf{K}\bar{\mathbf{p}}_{Rd} - \mathbf{C}\sigma(\boldsymbol{\Omega}), \tag{5.25}$$

where the function $\sigma(\boldsymbol{\Omega})$ is in the form of the smooth saturation function defined in Definition (2.1.2), Chapter 2. $\mathbf{C} = diag(c_1, c_2)$ is a diagonal positive constant matrix. Then Lemma 5.2.2 can be used to propose the control vector $\boldsymbol{u}$ as follows

$$\boldsymbol{u} = \frac{1}{(\bar{\boldsymbol{p}}_{Rd}\bar{\boldsymbol{p}}_{Rd}^T + \bar{\Delta}\mathbf{I}_2)}\big(-2\mathbf{K}\bar{\boldsymbol{p}}_{Rd} - \mathbf{C}\sigma(\boldsymbol{\Omega}) + \frac{\partial^2\boldsymbol{q}_d}{\partial s^2}\dot{s}\big). \tag{5.26}$$

It is noted that the part $(\bar{\boldsymbol{p}}_{Rd}\bar{\boldsymbol{p}}_{Rd}^T + \bar{\Delta}\mathbf{I}_2)$ is positive definite for all $\bar{\boldsymbol{p}}_{Rd} \in \mathbb{R}^2$ because of the definition of $\bar{\Delta}$ in (5.17). Therefore, all parts of $\boldsymbol{u}$ are bounded. Upper

bounded values of $\sigma(\bullet)$ and $\frac{\partial^2 \boldsymbol{q}_d}{\partial s^2}\dot{s}$ can be found in Definition (2.1.2) and (5.7), respectively. Eventually, the boundedness of control vector $\boldsymbol{u}$ can be calculated by

$$\|\boldsymbol{u}(t)\| \leq \big(2\lambda_M(\mathbf{K}) + \lambda_M(\mathbf{C}) + \epsilon_1\epsilon_4\big) \leq \delta, \tag{5.27}$$

where $\lambda_M(\bullet)$ is the maximum eigenvalue of $(\bullet)$, ϵ_1, ϵ_4 are upper bounds of $\dot{s}$ and $\frac{\partial^2 \boldsymbol{q}_d}{\partial s^2}$, see ((5.7)) and (5.8), respectively. δ is a strictly positive constant. There always exist positive-definite matrices $\mathbf{K}$, $\mathbf{C}$ and the constant δ such that the condition $\|\boldsymbol{u}(t)\| \leq \delta$ in (5.27) is satisfied for all $t \geq t_0 \geq 0$. Substituting the control $\boldsymbol{u}$ given in (5.26) into (5.5) obtains the closed-loop system

$$\begin{cases} \dot{\bar{\boldsymbol{q}}} = \bar{\boldsymbol{p}}, \\ \dot{\bar{\boldsymbol{p}}} = \frac{1}{(\bar{\boldsymbol{p}}_{Rd}\bar{\boldsymbol{p}}_{Rd}^T + \bar{\Delta}\mathbf{I}_2)}\big(- 2\mathbf{K}\bar{\boldsymbol{p}}_{Rd} - \mathbf{C}\sigma(\boldsymbol{\Omega}) + \frac{\partial^2 \boldsymbol{q}_d}{\partial s^2}\dot{s}\big). \end{cases} \tag{5.28}$$

The control vector $\boldsymbol{u}$ designed in (5.26) results in the time derivative of V in (5.25) as

$$\dot{V} = -\boldsymbol{\Omega}^T\mathbf{C}\sigma(\boldsymbol{\Omega}) + \bar{\beta}'\big(\bar{\Delta}\|\bar{\boldsymbol{p}}_{Rd}\|^2 + 2\bar{\boldsymbol{q}}_{RO}^T\mathbf{K}\frac{\partial \boldsymbol{q}_d}{\partial s}\dot{s} + \bar{\boldsymbol{p}}_{Rd}^T\bar{\Delta}\frac{\partial \boldsymbol{q}_d}{\partial s}\dot{s}\big). \tag{5.29}$$

Next, the torque control vector $\boldsymbol{\tau}$ is derived. As such, the immediate control vector $\boldsymbol{u}$ in (5.26) is substituted into the second equation of the closed-loop system defined in (5.5) to obtain torque control input vector $\boldsymbol{\tau} = \begin{bmatrix} \tau_v & \tau_\omega \end{bmatrix}^T$

$$\begin{bmatrix} \tau_v \\ \tau_\omega \end{bmatrix} = \mathbf{G}^{-1}\big(\boldsymbol{u} - \mathbf{A}\big), \tag{5.30}$$

where $\mathbf{G}$ is an invertible matrix and $\mathbf{A}$ is the column vector which is defined in (5.6). Noting that the actual torque control vector $\boldsymbol{\tau}$, which is applied directly to the left and right wheels of the WMR, can be easily obtained through (5.1). From the dynamics model in (5.1), the coordinate transformation given in (5.2) and the closed-loop system obtained in (5.28), they give

$$\begin{aligned} \dot{\boldsymbol{q}} &= \dot{\bar{\boldsymbol{q}}} - L\omega\begin{bmatrix} \cos(\phi) \\ \sin(\phi) \end{bmatrix}, \\ \dot{\phi} &= \omega, \\ \dot{\bar{\boldsymbol{q}}} &= \bar{\boldsymbol{p}}, \\ \dot{\bar{\boldsymbol{p}}} &= \frac{1}{(\bar{\boldsymbol{p}}_{Rd}\bar{\boldsymbol{p}}_{Rd}^T + \bar{\Delta}\mathbf{I}_2)}\big(- 2\mathbf{K}\bar{\boldsymbol{p}}_{Rd} - \mathbf{C}\sigma(\boldsymbol{\Omega}) + \frac{\partial^2 \boldsymbol{q}_d}{\partial s^2}\dot{s}\big). \end{aligned} \tag{5.31}$$

Remark. As can be seen from (5.30) that the torque control inputs include two different parts. The first part depends on both instantly relative distance between

the WMR and the obstacle, and relative linear velocity between the actual and virtual reference WMRs, i.e., see the representation of immediate control input $\boldsymbol{u}$ in (5.26). The boundedness of the first part is guaranteed as presented in (5.30). Hence, values of torques, i.e., τ_v, τ_ω, are not affected by the relative distance between WMR and the obstacle position when the WMR is close to the obstacle. The second part, which is related to $\mathbf{A}$, depends on states of the system only. State errors will be proved to converge to zero as $t \to \infty$ in the stability analysis section. This implies that actual states will approach to reference states as $t \to \infty$.

From (5.17), (5.18), (5.20), and (5.21), it can be seen that the Lyapunov-based potential function V is positive definite and radially unbounded. These properties are utilized in the next section of stability analysis. The control design has been completed and control objective is obtained. In summary, the results are stated by the following theorem.

Theorem 5.3.1. *Consider the nonholonomic WMR system described by (5.1) and the reference path is regular. Under the Assumptions 5.1.1, 5.1.2, 5.1.3, 5.1.4, and 5.1.5, and coordinate transformation (5.2), the amended system (5.5) which is subject to the torque control vector $\boldsymbol{\tau}$ defined by (5.30) solves the control objective (5.12). In particular, the following results hold for all initial conditions $\boldsymbol{q}(x(t_0), y(t_0)) \in \mathbb{R}^2$, $\phi(t_0) \in \mathbb{R}$ and $(v(t_0), \omega(t_0)) \in \mathbb{R}^2$:*

1. *The closed-loop system (5.31) is forward complete, and it ensures $\lim_{t\to\infty} \|\boldsymbol{q}(t) - \boldsymbol{q}_d(s(t))\| \leq \delta_1$.*
2. *The WMR is forced to track the reference path by bounded torque control input vector: $\|\boldsymbol{\tau}(t)\| \leq \delta_2$ in the sense of equation 5.30.*
3. *No collisions between the WMR and obstacles have been guaranteed for all $t \geq t_0 \geq 0$.*

5.4 Stability analysis

Stability analysis in this chapter follows techniques used in [3, 4]. The difference here is that the author provides a rigorous proof of no collisions and forward completeness for closed-loop system of the single WMR and obstacles instead of a group of mobile robots working together. Properties of equilibrium and saddle points are clarified similarly. Hence, theorem (5.3.1) is proven in two steps. In first

step, the proof shows that there is no collision between the WMR and obstacles and the closed-loop system is forward complete [163]. In the second step, stability properties of equilibrium points are investigated.

5.4.1 Proof of no collisions and forward completeness of closed-loop system

The representation of time derivative of V in (5.29) can be represented alternatively as follows

$$\dot{V} = -\boldsymbol{\Omega}^T \mathbf{C}\sigma(\boldsymbol{\Omega}) + W, \tag{5.32}$$

where, $W = \bar{\beta}'\big(\bar{\Delta}\|\bar{\boldsymbol{p}}_{Rd}\|^2 + 2\bar{\boldsymbol{q}}_{RO}^T\mathbf{K}\frac{\partial \boldsymbol{q}_d}{\partial s}\dot{s} + \bar{\boldsymbol{p}}_{Rd}^T\bar{\Delta}\frac{\partial \boldsymbol{q}_d}{\partial s}\dot{s}\big)$.

Case 1: ***The obstacle is outside of the WMR's sensing detection range or*** $\bar{\chi} > R_{sen}$**.**

Case 1 implies that the collision function $\bar{\beta}$ defined in (5.20) is inactive and there is no collision. Property 1 of the function $\bar{\beta}$ holds, i.e., $\bar{\beta} = 0$ and $\bar{\beta}' = 0$. The equation (5.32) can be replaced by

$$\dot{V} = -\boldsymbol{\Omega}^T \mathbf{C}\sigma(\boldsymbol{\Omega}) \leq 0. \tag{5.33}$$

The inequality $\dot{V} \leq 0$ holds for all $(x, y) \in \mathbb{R}^2$, and $(v, \omega) \in \mathbb{R}^2$ due to the Definition of the Smooth saturation function $\sigma(\bullet)$ in Chapter 2. Integrating both sides of the inequality (5.33) from t_0 to t results in

$$\int_{t_0}^{t} \dot{V}(\tau)d\tau = V(t) - V(t_0) \leq 0, \tag{5.34}$$

this means $V(t) \leq V(t_0)$, for all $t \geq t_0 \geq 0$. With definitions of the function V in (5.21) and its components defined in (5.17), (5.18) and (5.20), it can be expressed in details as

$$\frac{1}{2}\|2\mathbf{K}\bar{\boldsymbol{q}}_{RO}(t) + \bar{\Delta}(t)\bar{\boldsymbol{p}}_{Rd}(t)\|^2 + \bar{\beta}(t) \leq \frac{1}{2}\|2\mathbf{K}\bar{\boldsymbol{q}}_{RO}(t_0) + \bar{\Delta}(t_0)\bar{\boldsymbol{p}}_{Rd}(t_0)\|^2 + \bar{\beta}(t_0), \tag{5.35}$$

for all $t \geq t_0 \geq 0$. In particular, from the conditions (5.11) of Assumption (5.1.2) and the properties 2 and 3 of the pairwise collision avoidance function $\bar{\beta}$, the right-hand side of the inequality (5.35) is bounded by a positive constant depending on the initial conditions. Boundedness of the right-hand side of (5.35) implies that the left-hand side of this inequality must also be bounded. Therefore, the part $\bar{\beta}(t)$, which is a scalar function of $\bar{\chi}(t)$, must be smaller than some

positive constant depending on initial conditions for all $t \geq t_0 \geq 0$. Moreover, definition of $\bar{\chi}(t)$ in (5.17), including (5.18), indicates that it is a smooth function of $\bar{\boldsymbol{q}}_{RO}(t), \bar{\boldsymbol{p}}_{RO}(t), \bar{\boldsymbol{p}}_{Rd}(t)$. The second condition in (5.11) also shows that $\bar{\chi}(t_0) \geq \bar{\chi}_0$. Then $\bar{\chi}(t)$, must be larger than some positive constant depending on initial conditions and the selection of the function $\bar{\beta}(t)$. In other words, we have $\bar{\chi}(t) > (R_{safe} + R_{obs})$ due to the particular choice of function $\bar{\beta}(t)$ in (5.20).

To prove that there are no collisions between the WMR and obstacles for all $t \geq t_0 \geq 0$, the property 2 of the pairwise collision avoidance function $\bar{\beta}$ must hold for all $t \geq t_0 \geq 0$. Since the construction of $\bar{\chi}$ satisfies Lemma (5.2.2), see (5.15), Lemma (5.2.2) is applied to confirm that $\|\bar{\boldsymbol{q}}_{RO}(t)\| > \epsilon$, where ϵ is a strictly positive constant, for all $0 \leq t_0 \leq t \leq \infty$ under the initial condition (5.11). The control objective of collision avoidance is achieved.

As the boundedness of the left-hand side of (5.35) has been already proven, this leads to the implication that of $\bar{\boldsymbol{q}}_{RO}(t), \bar{\boldsymbol{p}}_{Rd}(t)$, and $\bar{\Delta}(t)$. The boundedness of $\bar{\Delta}(t)$ means that of $\bar{\boldsymbol{p}}_{Rd}(t)$, see (5.18). Because $\boldsymbol{q}_d(t)$ and $\boldsymbol{p}_d(t) = \dot{\boldsymbol{q}}_d(t)$ are bounded by Assumption (5.1.2), $\bar{\boldsymbol{q}}(t)$ and $\bar{\boldsymbol{p}}(t)$ are also bounded, see (5.18). This in turn implies that all states do not escape to infinity in finite time. Therefore, the solutions of the closed-loop system (5.35) exist globally for all $t \geq t_0 \geq 0$ by Theorem 2.1.2 and this system is forward complete.

Case 2: ***The obstacle is inside the WMR's sensing detection range or*** $R_{safe} + R_{obs} < \bar{\chi} < R_{sen}$**.**

Case 2 addresses the situation when the vehicle approaches closely to an obstacle which is in within the detection range of the WMR. As the obstacle avoidance is considered, W in (5.32) must be included because $\bar{\beta}' \neq 0$. Expression of $\dot{V}$ in (5.29) is used for the upper boundedness investigation in this section.

In this case, $\bar{\chi}$ satisfies $0 < \bar{\chi} \leq \delta < R_{sen}$, δ is astrictly positive constant. From the definition of function $\bar{\chi}$ in (5.17), it gives

$$\begin{aligned} & \mathbf{K}\|\bar{\boldsymbol{q}}_{RO}\|^2 + \bar{\boldsymbol{q}}_{RO}^T \bar{\Delta} \dot{\bar{\boldsymbol{q}}}_{Rd} \leq \delta \\ \Rightarrow \quad & \bar{\boldsymbol{q}}_{RO}^T \bar{\Delta} \dot{\bar{\boldsymbol{q}}}_{Rd} \leq -\mathbf{K}\|\bar{\boldsymbol{q}}_{RO}\|^2 + \delta. \end{aligned} \tag{5.36}$$

$\bar{\chi} > 0$ implies $\bar{\boldsymbol{q}}_{RO}^T > 0$. Also, $\bar{\Delta} > 0$, see (5.18). Then from (5.36), it gives

$$\dot{\bar{\boldsymbol{q}}} \leq -\lambda_{min}(\mathbf{K}) \frac{\|\bar{\boldsymbol{q}}_{RO}\|^2}{\bar{\boldsymbol{q}}_{RO}^T \bar{\Delta}} + \frac{\delta}{\bar{\boldsymbol{q}}_{RO}^T \bar{\Delta}} + \dot{\bar{\boldsymbol{q}}}_d. \tag{5.37}$$

Considering a Luyapunov function candidate $V_1 = \frac{1}{2}\|\bar{\boldsymbol{q}}_{RO}\|^2$ and taking differentiation both sides along the solution (5.37) results in

$$\dot{V}_1 = \bar{\boldsymbol{q}}_{RO}^T\dot{\bar{\boldsymbol{q}}} \leq -\lambda_{min}(\mathbf{K})\frac{\|\bar{\boldsymbol{q}}_{RO}\|^2}{\bar{\Delta}} + \frac{\delta}{\bar{\Delta}} + \bar{\boldsymbol{q}}_{RO}^T\dot{\bar{\boldsymbol{q}}}_d = -\delta^* V_1 + C_0. \tag{5.38}$$

where, δ^* and C_0 are positive constants. Hence, $V_1(t)$ is bounded because $V_1(t) \leq V_1(t_0)$ for $\forall t \geq t_0$. This in turn implies that $\|\bar{\boldsymbol{q}}_{RO}\|$ is bounded by a positive constant, i.e., $\|\bar{\boldsymbol{q}}_{RO}\| \leq \epsilon_1^*$. From the definition in (5.17) and (5.18), it also gives $\|\bar{\boldsymbol{q}}_{Rd}\| = \|\bar{\boldsymbol{q}} - \boldsymbol{q}_d\|$, and $\|\bar{\boldsymbol{p}}_{Rd}\| = \|\bar{\boldsymbol{p}} - \boldsymbol{p}_d\|$ are bounded by upper bounds, i.e., $\|\bar{\boldsymbol{q}}_{Rd}\| \leq \epsilon_2^*$, and $\|\bar{\boldsymbol{p}}_{Rd}\| \leq \epsilon_3^*$ where, ϵ_2^* and ϵ_3^* are nonnegative bounded constants. Moreover, boundedness $0 < \|\bar{\boldsymbol{q}}_{RO}\| \leq \epsilon_1^*$ indicates no colilsion in this case. Applying these upper bounds to the equation (5.29) yields

$$\begin{aligned}\dot{V} \leq &-\big(2\lambda_{min}(\mathbf{K})\epsilon_2^* + (1+\frac{1}{2}(\epsilon_3^*)^2)\epsilon_3^* + \bar{\beta}'\|\bar{\boldsymbol{q}}_{RO}\|\big)\lambda_{min}(\mathbf{C})\sigma\big(2\lambda_{min}(\mathbf{K})\epsilon_2^* \\ &+ (1+\frac{1}{2}(\epsilon_3^*)^2)\epsilon_3^* + \bar{\beta}'\|\bar{\boldsymbol{q}}_{RO}\|\big) + \bar{\beta}'\big((1+\frac{1}{2}(\epsilon_3^*)^2)(\epsilon_3^*)^2 + 2\lambda_{min}(\mathbf{K})\epsilon_1\epsilon_3\|\bar{\boldsymbol{q}}_{RO}\| \\ &+ \epsilon_3^*(1+\frac{1}{2}(\epsilon_3^*)^2)\epsilon_1\epsilon_3\big).\end{aligned} \tag{5.39}$$

Definitions of $\bar{\beta}$ in (5.20), and $\bar{\beta}'$ in (5.19) show that $\bar{\beta} \sim \frac{1}{\bar{\chi}}$, and $\bar{\beta}' \sim \frac{1}{\bar{\chi}^2}$, where $\bar{\chi} = f(\bar{\boldsymbol{q}}_{RO}, \bar{\boldsymbol{p}}_{Rd})$, see (5.17). As the WMR moves inside the ball $\bar{\mathbf{B}}(R(\epsilon_1^*, \epsilon_2^*))$, the parts $\|\bar{\boldsymbol{q}}_{Rd}\|$ is dominated by $\bar{\beta}'$. Moreover, for all $(\bar{\boldsymbol{q}} - \boldsymbol{q}_{obs})$, $(\boldsymbol{p} - \bar{\boldsymbol{p}}_d) \in \mathbb{R}^2$ and $\bar{\beta}' \sim \frac{1}{\bar{\chi}^2} = \frac{1}{\big(\bar{\boldsymbol{q}}_{RO}(\mathbf{K}\bar{\boldsymbol{q}}_{RO} + \bar{\Delta}\|\bar{\boldsymbol{p}}_{Rd}\|)\big)^2}$, see (5.19)

$$\begin{aligned}&2\lambda_{min}(\mathbf{K})\epsilon_2^* + (1+\frac{1}{2}(\epsilon_3^*)^2)\epsilon_3^* + \bar{\beta}'\|\bar{\boldsymbol{q}}_{RO}\| \leq \lambda_1^*\bar{\beta}^{*'}, \\ &\bar{\beta}'\big((1+\frac{1}{2}(\epsilon_3^*)^2)(\epsilon_3^*)^2 + 2\epsilon_1^*\lambda_{min}(\mathbf{K})\epsilon_1\epsilon_3\|\bar{\boldsymbol{q}}_{RO}\| + \epsilon_3^*(1+\frac{1}{2}(\epsilon_3^*)^2)\epsilon_1\epsilon_3\big) \leq \lambda_2^*\bar{\beta}^{*'},\end{aligned} \tag{5.40}$$

where, $\bar{\beta}'\|\bar{\boldsymbol{q}}_{RO}\| \leq \lambda^*\bar{\beta}^{*'}$ and $\bar{\beta}^{*'} \sim \frac{1}{\bar{\boldsymbol{q}}_{RO}\big((\mathbf{K}\bar{\boldsymbol{q}}_{RO} + \bar{\Delta}\|\bar{\boldsymbol{p}}_{Rd}\|)\big)^2}$, λ_1^* and λ_2^* are positive constants. It can be explained that when the WMR is close to the obstacle, calculation in terms of $\bar{\beta}'$ significantly outweighs than other terms. This reflects the fact that the collision avoidance task is prioritized during this period of time. Hence, the inequality (5.39) becomes

$$\dot{V} \leq -(\lambda_1^*\bar{\beta}^{*'})\mathbf{C}\sigma(\lambda_1^*\bar{\beta}^{*'}) + \lambda_2^*\bar{\beta}^{*'}, \tag{5.41}$$

for all $\bar{\boldsymbol{q}}_{Rd}, \bar{\boldsymbol{q}}_{RO}, \bar{\boldsymbol{p}}_{Rd} \in \mathbb{R}^2$ and $\beta' = f(\frac{1}{\bar{\chi}^2})$. Function $\tanh(\bullet)$ is chosen as a particular function of the general bounded function $\sigma(\bullet)$. It shows that

$$|\lambda^*\bar{\beta}^{*'}| - \lambda^*\bar{\beta}^{*'}\tanh(\lambda^*\bar{\beta}^{*'}) \leq \eta, \tag{5.42}$$

where η is a strictly nonnegative constant. Applying the inequality (5.39) into (5.38) yields

$$\begin{aligned}\dot{V} &\leq -(\lambda_1^*\bar{\beta}^{*'})\lambda_{min}(\mathbf{C})\sigma(\lambda_1^*\bar{\beta}^{*'}) + \lambda_2^*\bar{\beta}^{*'}\tanh(\lambda_2^*\bar{\beta}^{*'}) + \eta \\ &\leq -(\lambda^*\bar{\beta}^{*'})\big(\lambda_{min}(\mathbf{C}) - 1\big)\sigma(\lambda^*\bar{\beta}^{*'}) + \eta, \end{aligned} \tag{5.43}$$

where, $\lambda^* = max(\lambda_1^*, \lambda_2^*)$, $\lambda_{min}(\mathbf{C})$ is minimum eigeinvalue of constant matrix $\mathbf{C}$. Constant matrix $\mathbf{C}$ is chosen properly to satisfy the condition $(\lambda_{min}\mathbf{C} - 1) > 0$. Hence, the inequality (5.40) results in

$$\dot{V} \leq -\lambda^*\bar{\beta}^{*'}\tanh(\lambda^*\bar{\beta}^{*'}) + \delta \leq -c_1 V + \delta, \tag{5.44}$$

where c_1 and δ are some positive constants. The above inequality (5.41) shows that the closed-loop system (5.35) is forward complete.

Properties 2 of function $\beta(t)$ holds as the condition $(R_{safe} + R_{obs}) < \bar{\chi} < R_{sen}$ is satisfied, i.e., $\beta(t) > 0$. Hence, there are no collisions between the WMR and the obstacle for all $t \geq t_0 \geq 0$. By combining conclusions of Case 1 and Case 2, the solutions of the closed-loop system (5.35) exist globally for all $t \geq t_0 \geq 0$ by Theorem 5.3.1, and this system is forward complete.

5.4.2 Properties of equilibrium points

In the previous section, collision avoidance capability of WMR has been proven and all states are bounded for all $t \geq t_0 \geq 0$. Next, it is necessary to find the equilibrium set, which the trajectory of the closed-loop system (5.29) tends to converge and to investigate whether these equilibrium points are asymptotically stable or not. Therefore, Lemma 2.1.10 (Barbalat-like Lemma) will be applied for this purpose. As such, two conditions of the Barbalat-like Lemma are checked for satisfaction. Considering (5.29) and denoting as

$$\dot{V} = -\mathbf{\Omega}^T\mathbf{C}\sigma(\mathbf{\Omega}) + \bar{\beta}'\big(\bar{\Delta}\|\bar{\boldsymbol{p}}_{Rd}\|^2 + 2\bar{\boldsymbol{q}}_{RO}^T\mathbf{K}\frac{\partial \boldsymbol{q}_d}{\partial s}\dot{s} + \bar{\boldsymbol{p}}_{Rd}^T\bar{\Delta}\frac{\partial \boldsymbol{q}_d}{\partial s}\dot{s}\big) = -W_1, \tag{5.45}$$

for the verification of the first condition of Lemma 2.1.10, i.e., $\big|\frac{dW_1}{dt}\big|$. Each part of W_1 in (5.45) is denoted and investigated. It is noted that variable t is omitted in the representation.

Now taking derivative the part $A = \mathbf{\Omega}^T\mathbf{C}\sigma(\mathbf{\Omega})$ with respect to t yields

$$|\dot{A}| = \Big|\frac{d}{dt}\big(\mathbf{\Omega}^T\mathbf{C}\sigma(\mathbf{\Omega})\big)\Big| = \Big|\Big(\frac{\sigma(\mathbf{\Omega})}{\mathbf{\Omega}} + \frac{\partial\sigma(\mathbf{\Omega})}{\partial\mathbf{\Omega}}\Big)^T\mathbf{C}\mathbf{\Omega}\frac{d\mathbf{\Omega}}{dt}\Big| \leq M\Big|\mathbf{C}\mathbf{\Omega}\frac{d\mathbf{\Omega}}{dt}\Big|, \tag{5.46}$$

where, property 4 of the Differentiable and bounded function shown in Chapter 2 has been applied, i.e., $\big|\frac{\sigma(\mathbf{\Omega})}{\mathbf{\Omega}}\big| \leq M_2$ and $\big|\frac{\partial\sigma(\mathbf{\Omega})}{\partial\mathbf{\Omega}}\big| \leq M_3$, and $M = M_2 + M_3$.

The term $\frac{d\boldsymbol{\Omega}}{dt}$ is separated for further calculation using the expression of $\boldsymbol{\Omega} = 2\mathbf{K}\bar{\boldsymbol{q}}_{Rd} + \bar{\Delta}\bar{\boldsymbol{p}}_{Rd} + \bar{\beta}'\bar{\boldsymbol{q}}_{RO}$ and solutions (5.28). Taking derivative both sides gives

$$\Big|\frac{d\boldsymbol{\Omega}}{dt}\Big| = \big|2\mathbf{K}\bar{\boldsymbol{p}}_{Rd} + \big(\bar{\boldsymbol{p}}_{Rd}^T\bar{\boldsymbol{p}}_{Rd} + \bar{\Delta}\mathbf{I}_2\big)\dot{\bar{\boldsymbol{p}}}_{Rd} + \bar{\beta}'\mathbf{I}_2 + \bar{\beta}''\bar{\boldsymbol{q}}_{RO}\big(2\mathbf{K}\bar{\boldsymbol{q}}_{RO} + \bar{\Delta}\bar{\boldsymbol{p}}_{Rd}\big)^T\dot{\bar{\boldsymbol{q}}}_{RO} + \bar{\beta}''\bar{\boldsymbol{q}}_{RO}\bar{\boldsymbol{q}}_{RO}^T\big(\bar{\boldsymbol{p}}_{Rd}^T\bar{\boldsymbol{p}}_{Rd} + \bar{\Delta}\mathbf{I}_2\big)\dot{\bar{\boldsymbol{p}}}_{Rd}\big|. \tag{5.47}$$

Each part of the right-hand side of (5.47) is calculated for upper bounds separately as follows

$$|\dot{A}_1| = |2\mathbf{K}\bar{\boldsymbol{p}}_{Rd} + \bar{\beta}'\mathbf{I}_2| \leq 2\lambda_{min}(\mathbf{K})\epsilon_3^* + \delta^* = k_{A_1}^*, \tag{5.48}$$

where, $k_{A_1}^*$ is a positive constant. $\lambda_{min}(\bullet)$ is minimum eigenvalue of constant matrix $(\bullet)$.

$$|\dot{A}_2| = \big|\big(\bar{\boldsymbol{p}}_{Rd}^T\bar{\boldsymbol{p}}_{Rd} + \bar{\Delta}\mathbf{I}_2\big)(\dot{\bar{\boldsymbol{p}}} - \frac{\partial^2\bar{\boldsymbol{q}}_d}{\partial s^2}\dot{s})\big| \leq \big|2\mathbf{K}\bar{\boldsymbol{p}}_{Rd} + \mathbf{C}\sigma(\boldsymbol{\Omega})\big| + \big|\big(\bar{\boldsymbol{p}}_{Rd}^T\bar{\boldsymbol{p}}_{Rd} + \bar{\Delta}\mathbf{I}_2\big)\frac{\partial^2\bar{\boldsymbol{q}}_d}{\partial s^2}\dot{s}\big|$$
$$\leq 2\lambda_{min}(\mathbf{K})\epsilon_3^* + \mathbf{C}\sigma(\boldsymbol{\Omega}) + (1 + 3/2\epsilon_3^{*2})\epsilon_1\epsilon_4 = k_{A_2}^* + \mathbf{C}\sigma(\boldsymbol{\Omega}). \tag{5.49}$$

where, the solution $\dot{\bar{\boldsymbol{p}}}$ in (5.31) has been used, and $k_2^* = 2\lambda_{min}(\mathbf{K})\epsilon_3^* + (1 + 3/2\epsilon_3^{*2})\epsilon_1\epsilon_4$ is a positive constant.

$$|\dot{A}_3| = \big|\bar{\beta}''\bar{\boldsymbol{q}}_{RO}\big(2\mathbf{K}\bar{\boldsymbol{q}}_{RO} + \bar{\Delta}\bar{\boldsymbol{p}}_{Rd}\big)^T\dot{\bar{\boldsymbol{q}}}_{RO} = \bar{\beta}''\bar{\boldsymbol{q}}_{RO}\big(2\mathbf{K}\bar{\boldsymbol{q}}_{RO} + \bar{\Delta}\bar{\boldsymbol{p}}_{Rd}\big)^T(\bar{\boldsymbol{p}}_{Rd} + \frac{\partial\bar{\boldsymbol{q}}_d}{\partial s}\dot{s})\big|$$
$$\leq \delta^{**}\epsilon_1^*(2\lambda_{min}(\mathbf{K})\epsilon_1^* + (1 + 1/2\epsilon_3^{*2})\epsilon_3^*)(\epsilon_3^* + \epsilon_1\epsilon_3) \leq k_{A_3}^*, \tag{5.50}$$

where, $k_{A_3}^* = \delta^{**}\epsilon_1^*(2\lambda_{min}(\mathbf{K})\epsilon_1^* + (1 + 1/2\epsilon_3^{*2})\epsilon_3^*)(\epsilon_3^* + \epsilon_1\epsilon_3)$ is a positive constant.

$$|\dot{A}_4| = \big|\bar{\beta}''\bar{\boldsymbol{q}}_{RO}\bar{\boldsymbol{q}}_{RO}^T\big(\bar{\boldsymbol{p}}_{Rd}^T\bar{\boldsymbol{p}}_{Rd} + \bar{\Delta}\mathbf{I}_2\big)\dot{\bar{\boldsymbol{p}}}_{Rd}\big| = \big|\bar{\beta}''\bar{\boldsymbol{q}}_{RO}\bar{\boldsymbol{q}}_{RO}^T\dot{A}_2\big| \leq \delta^{**}\epsilon_1^{*2}(k_2^* + \mathbf{C}\sigma(\boldsymbol{\Omega}))$$
$$\leq k_{A_{41}}^* + k_{A_{42}}^*\mathbf{C}\sigma(\boldsymbol{\Omega}), \tag{5.51}$$

where, $k_{A_{41}}^* = \delta^{**}\epsilon_1^{*2}k_2^*$, $k_{A_{42}}^* = \delta^{**}\epsilon_1^{*2}$ are positive constants. Now substituting results of (5.48), (5.4.2), (5.50), and (5.51) into (5.47) results in

$$\Big|\frac{d\boldsymbol{\Omega}}{dt}\Big| \leq k_{A_1}^* + k_{A_2}^* + \mathbf{C}\sigma(\boldsymbol{\Omega}) + k_{A_3}^* + k_{A_{41}}^* + k_{A_{42}}^*\mathbf{C}\sigma(\boldsymbol{\Omega}) = k_A^* + (1 + k_{A_{42}}^*)\mathbf{C}\sigma(\boldsymbol{\Omega}). \tag{5.52}$$

where, $k_A^* = k_{A_1}^* + k_{A_2}^* + k_{A_3}^* + k_{A_{41}}^*$. Substituting (5.52) into (5.46) yields

$$|\dot{A}| \leq M|\mathbf{C}\boldsymbol{\Omega}^T|\big(k_A^* + (1 + k_{A_{42}}^*)\mathbf{C}\sigma(\boldsymbol{\Omega})\big) \leq k_{A_\Sigma}^* A, \tag{5.53}$$

where, $k_{A_\Sigma}^* = \lambda_{min}(\mathbf{C})(k_A^* + 1 + k_{A_{42}}^*)M$. Next, denoting the part $B = \bar{\beta}'\bar{\Delta}\|\bar{\boldsymbol{p}}_{Rd}\|^2$ and taking derivative with respect to t yields

$$|\dot{B}| = \big|\beta''\bar{\Delta}\|\bar{\boldsymbol{p}}_{Rd}\|^2(2\mathbf{K}\bar{\boldsymbol{q}}_{RO} + \bar{\Delta}\bar{\boldsymbol{p}}_{Rd})^T\dot{\bar{\boldsymbol{q}}}_{RO} + \beta''\bar{\Delta}\|\bar{\boldsymbol{p}}_{Rd}\|^2\bar{\boldsymbol{q}}_{RO}^T\big(\bar{\boldsymbol{p}}_{Rd}^T\bar{\boldsymbol{p}}_{Rd} + \bar{\Delta}\mathbf{I}_2\big)\dot{\bar{\boldsymbol{p}}}_{Rd}$$

$$+ \bar{\beta}'\|\bar{\boldsymbol{p}}_{Rd}\|^2\bar{\boldsymbol{p}}_{Rd}^T\dot{\bar{\boldsymbol{p}}}_{Rd} + 2\bar{\beta}'\bar{\Delta}\bar{\boldsymbol{p}}_{Rd}^T\dot{\bar{\boldsymbol{p}}}_{Rd}\big|. \tag{5.54}$$

Each part of the right-hand side of (5.54) is estimated for upper bounds as follows

$$\begin{aligned}|\dot{B}_1| &= \big|\beta''\bar{\Delta}\|\bar{\boldsymbol{p}}_{Rd}\|^2(2\mathbf{K}\bar{\boldsymbol{q}}_{RO} + \bar{\Delta}\bar{\boldsymbol{p}}_{Rd})^T\dot{\bar{\boldsymbol{q}}}_{RO}\big| \\ &= \big|\beta''\bar{\Delta}\|\bar{\boldsymbol{p}}_{Rd}\|^2(2\mathbf{K}\bar{\boldsymbol{q}}_{RO} + \bar{\Delta}\bar{\boldsymbol{p}}_{Rd})^T(\bar{\boldsymbol{p}}_{Rd} + \frac{\partial\bar{\boldsymbol{q}}_d}{\partial s}\dot{s})\big| \le k_{B_1}^*,\end{aligned} \tag{5.55}$$

$$\begin{aligned}|\dot{B}_2| &= \big|\beta''\bar{\Delta}\|\bar{\boldsymbol{p}}_{Rd}\|^2\bar{\boldsymbol{q}}_{RO}^T\big(\bar{\boldsymbol{p}}_{Rd}^T\bar{\boldsymbol{p}}_{Rd} + \bar{\Delta}\mathbf{I}_2\big)\dot{\bar{\boldsymbol{p}}}_{Rd}\big| \\ &= \big|\beta''\bar{\Delta}\|\bar{\boldsymbol{p}}_{Rd}\|^2\bar{\boldsymbol{q}}_{RO}^T\big(\bar{\boldsymbol{p}}_{Rd}^T\bar{\boldsymbol{p}}_{Rd} + \bar{\Delta}\mathbf{I}_2\big)\frac{1}{(\bar{\boldsymbol{p}}_{Rd}\bar{\boldsymbol{p}}_{Rd}^T + \bar{\Delta}\mathbf{I}_2)}\big(-2\mathbf{K}\bar{\boldsymbol{p}}_{Rd} - \mathbf{C}\sigma(\boldsymbol{\Omega})\big)\big| \\ &\le k_{B_2}^* + k_{B_{22}}^*\mathbf{C}\sigma(\boldsymbol{\Omega}),\end{aligned} \tag{5.56}$$

$$\begin{aligned}|\dot{B}_3| &= \big|\bar{\beta}'\|\bar{\boldsymbol{p}}_{Rd}\|^2\bar{\boldsymbol{p}}_{Rd}^T\dot{\bar{\boldsymbol{p}}}_{Rd}\big| = \big|\bar{\beta}'\|\bar{\boldsymbol{p}}_{Rd}\|^2\bar{\boldsymbol{p}}_{Rd}^T\frac{1}{(\bar{\boldsymbol{p}}_{Rd}\bar{\boldsymbol{p}}_{Rd}^T + \bar{\Delta}\mathbf{I}_2)}\big(-2\mathbf{K}\bar{\boldsymbol{p}}_{Rd} - \mathbf{C}\sigma(\boldsymbol{\Omega})\big)\big| \\ &\le k_{B_{31}}^* + k_{B_{32}}^*\mathbf{C}\sigma(\boldsymbol{\Omega}),\end{aligned} \tag{5.57}$$

$$\begin{aligned}|\dot{B}_4| &= \big|2\bar{\beta}'\bar{\Delta}\bar{\boldsymbol{p}}_{Rd}^T\dot{\bar{\boldsymbol{p}}}_{Rd}\big| = \big|2\bar{\beta}'\bar{\Delta}\bar{\boldsymbol{p}}_{Rd}^T\frac{1}{(\bar{\boldsymbol{p}}_{Rd}\bar{\boldsymbol{p}}_{Rd}^T + \bar{\Delta}\mathbf{I}_2)}\big(-2\mathbf{K}\bar{\boldsymbol{p}}_{Rd} - \mathbf{C}\sigma(\boldsymbol{\Omega})\big)\big| \\ &\le k_{B_{41}}^* + k_{B_{42}}^*\mathbf{C}\sigma(\boldsymbol{\Omega}),\end{aligned} \tag{5.58}$$

where, $k_{B_1}^*$, $k_{B_{21}}^*$, $k_{B_{22}}^*$, $k_{B_{31}}^*$, $k_{B_{32}}^*$, $k_{B_{41}}^*$, and $k_{B_{42}}^*$ are positive constants. Upper bounds of all individual parts found in the previous sections have been applied, and definition of $\dot{\bar{\boldsymbol{p}}}$ in (5.31) has been substituted. Substituting (5.55), (5.56), (5.57), and (5.58) into (5.54) yields

$$|\dot{B}| \le k_B^* + (k_{B_{22}}^* + k_{B_{32}}^* + k_{B_{42}}^*)\mathbf{C}\sigma(\boldsymbol{\Omega}) \le k_B^*B + (k_{B_{22}}^* + k_{B_{32}}^* + k_{B_{42}}^*)A, \tag{5.59}$$

where, $k_B^* = k_{B_1}^* + k_{B_{21}}^* + k_{B_{31}}^* + k_{B_{41}}^*$. Next, denoting the part $C = 2\bar{\beta}'\bar{\boldsymbol{q}}_{RO}^T\mathbf{K}\frac{\partial\boldsymbol{q}_d}{\partial s}\dot{s}$ and taking derivative with respect to t yields

$$\begin{aligned}|\dot{C}| = 2\big|&\beta''\bar{\boldsymbol{q}}_{RO}^T\mathbf{K}\frac{\partial\boldsymbol{q}_d}{\partial s}\dot{s}(2\mathbf{K}\bar{\boldsymbol{q}}_{RO} + \bar{\Delta}\bar{\boldsymbol{p}}_{Rd})^T(\bar{\boldsymbol{p}}_{Rd} + \frac{\partial\boldsymbol{q}_d}{\partial s}\dot{s}) \\ &+ \beta''\bar{\boldsymbol{q}}_{RO}^T\mathbf{K}\frac{\partial\boldsymbol{q}_d}{\partial s}\dot{s}\big(\bar{\boldsymbol{p}}_{Rd}^T\bar{\boldsymbol{p}}_{Rd} + \bar{\Delta}\mathbf{I}_2\big)(\dot{\bar{\boldsymbol{p}}} + \frac{\partial^2\boldsymbol{q}_d}{\partial s^2}\dot{s}) + \bar{\beta}'(\frac{\partial\boldsymbol{q}_d}{\partial s}\dot{s})^T\mathbf{K}(\bar{\boldsymbol{p}}_{Rd} + \frac{\partial\boldsymbol{q}_d}{\partial s}\dot{s}) \\ &+ \bar{\beta}'\bar{\boldsymbol{q}}_{RO}^T\mathbf{K}\frac{\partial^2\boldsymbol{q}_d}{\partial s^2}\dot{s}\big|\end{aligned} \tag{5.60}$$

Similar to calculation of $|\dot{B}|$, upper bounds of all individual parts found in the previous sections are used, and definition of $\dot{\bar{\boldsymbol{p}}}$ in (5.31) is substituted. Each part of the right-hand side of (5.54) is estimated for upper bounds as follows

$$|\dot{C}_1| = 2\big|\beta''\bar{\boldsymbol{q}}_{RO}^T\mathbf{K}\frac{\partial\boldsymbol{q}_d}{\partial s}\dot{s}(2\mathbf{K}\bar{\boldsymbol{q}}_{RO} + \bar{\Delta}\bar{\boldsymbol{p}}_{Rd})^T(\bar{\boldsymbol{p}}_{Rd} + \frac{\partial\boldsymbol{q}_d}{\partial s}\dot{s})\big| \le k_{C_1}^*, \tag{5.61}$$

$$|\dot{C}_2| = 2\big|\beta''\bar{\boldsymbol{q}}_{RO}^T\mathbf{K}\frac{\partial \boldsymbol{q}_d}{\partial s}\dot{s}\big(\bar{\boldsymbol{p}}_{Rd}^T\bar{\boldsymbol{p}}_{Rd} + \bar{\Delta}\mathbf{I}_2\big)\big(\dot{\bar{\boldsymbol{p}}} + \frac{\partial^2 \boldsymbol{q}_d}{\partial s^2}\dot{s}\big)\big| \leq k_{C_{21}}^* + k_{C_{22}}^*\mathbf{C}\sigma(\boldsymbol{\Omega}), \tag{5.62}$$

$$|\dot{C}_3| = 2\big|\bar{\beta}'(\frac{\partial \boldsymbol{q}_d}{\partial s}\dot{s})^T\mathbf{K}(\bar{\boldsymbol{p}}_{Rd} + \frac{\partial \boldsymbol{q}_d}{\partial s}\dot{s})\big| \leq k_{C_3}^*, \tag{5.63}$$

$$|\dot{C}_4| = 2\big|\bar{\beta}'\bar{\boldsymbol{q}}_{RO}^T\mathbf{K}\frac{\partial^2 \boldsymbol{q}_d}{\partial s^2}\dot{s}\big| \leq k_{C_4}^*, \tag{5.64}$$

where, $k_{C_1}^*$, $k_{C_{21}}^*$, $k_{C_{22}}^*$, $k_{C_3}^*$, and $k_{C_4}^*$ are positive constants. Substituting (5.61), (5.62), (5.63), and (5.64) into (5.60) gives

$$|\dot{C}| \leq k_C^* + k_{C_{22}}^*\mathbf{C}\sigma(\boldsymbol{\Omega}) \leq k_C^* C + k_{C_{22}}^* A, \tag{5.65}$$

where, $k_C^* = k_{C_1}^* + k_{C_{21}}^* + k_{C_3}^* + k_{C_4}^*$. Lastly, denoting the part $D = \bar{\beta}'\bar{\boldsymbol{p}}_{Rd}^T\bar{\Delta}\frac{\partial \boldsymbol{q}_d}{\partial s}\dot{s}$ and taking derivative with respect to t yields

$$\begin{aligned}|\dot{D}| = \big|&\beta''\bar{\boldsymbol{p}}_{Rd}^T\bar{\Delta}\frac{\partial \boldsymbol{q}_d}{\partial s}\dot{s}(2\mathbf{K}\bar{\boldsymbol{q}}_{RO} + \bar{\Delta}\bar{\boldsymbol{p}}_{Rd})^T(\bar{\boldsymbol{p}}_{Rd} + \frac{\partial \boldsymbol{q}_d}{\partial s}\dot{s}) \\ &+ \beta''\bar{\boldsymbol{p}}_{Rd}^T\bar{\Delta}\frac{\partial \boldsymbol{q}_d}{\partial s}\dot{s}\big(\bar{\boldsymbol{p}}_{Rd}^T\bar{\boldsymbol{p}}_{Rd} + \bar{\Delta}\mathbf{I}_2\big)\big(\dot{\bar{\boldsymbol{p}}} + \frac{\partial^2 \boldsymbol{q}_d}{\partial s^2}\dot{s}\big) + \bar{\beta}'\bar{\Delta}(\frac{\partial \boldsymbol{q}_d}{\partial s}\dot{s})^T(\dot{\bar{\boldsymbol{p}}} + \frac{\partial^2 \boldsymbol{q}_d}{\partial s^2}\dot{s}) \\ &+ \bar{\beta}'\bar{\boldsymbol{p}}_{Rd}^T\bar{\Delta}\frac{\partial^2 \boldsymbol{q}_d}{\partial s^2}\dot{s}\big|\end{aligned} \tag{5.66}$$

The same approach as above is applied for upper bounds calculation of each part of the right-hand side of (5.66).

$$|\dot{D}_1| = \big|\beta''\bar{\boldsymbol{p}}_{Rd}^T\bar{\Delta}\frac{\partial \boldsymbol{q}_d}{\partial s}\dot{s}(2\mathbf{K}\bar{\boldsymbol{q}}_{RO} + \bar{\Delta}\bar{\boldsymbol{p}}_{Rd})^T(\bar{\boldsymbol{p}}_{Rd} + \frac{\partial \boldsymbol{q}_d}{\partial s}\dot{s})\big| \leq k_{D_1}^*, \tag{5.67}$$

$$|\dot{D}_2| = \big|\beta''\bar{\boldsymbol{p}}_{Rd}^T\bar{\Delta}\frac{\partial \boldsymbol{q}_d}{\partial s}\dot{s}\big(\bar{\boldsymbol{p}}_{Rd}^T\bar{\boldsymbol{p}}_{Rd} + \bar{\Delta}\mathbf{I}_2\big)\big(\dot{\bar{\boldsymbol{p}}} + \frac{\partial^2 \boldsymbol{q}_d}{\partial s^2}\dot{s}\big)\big| \leq k_{D_{21}}^* + k_{D_{22}}^*\mathbf{C}\sigma(\boldsymbol{\Omega}), \tag{5.68}$$

$$|\dot{D}_3| = \big|\bar{\beta}'\bar{\Delta}(\frac{\partial \boldsymbol{q}_d}{\partial s}\dot{s})^T(\dot{\bar{\boldsymbol{p}}} + \frac{\partial^2 \boldsymbol{q}_d}{\partial s^2}\dot{s})\big| \leq k_{D_{31}}^* + k_{D_{32}}^*\mathbf{C}\sigma(\boldsymbol{\Omega}), \tag{5.69}$$

$$|\dot{D}_4| = \big|\bar{\beta}'\bar{\boldsymbol{p}}_{Rd}^T\bar{\Delta}\frac{\partial^2 \boldsymbol{q}_d}{\partial s^2}\dot{s}\big| \leq k_{D_4}^*, \tag{5.70}$$

where, $k_{D_1}^*$, $k_{D_{21}}^*$, $k_{D_{22}}^*$, $k_{D_{31}}^*$, $k_{D_{32}}^*$, and $k_{D_4}^*$ are positive constants. Substituting (5.67), (5.68), (5.69), and (5.70) into (5.66) results in

$$|\dot{D}| \leq k_D^* + (k_{D_{22}}^* + k_{D_{32}}^*)\mathbf{C}\sigma(\boldsymbol{\Omega}) \leq k_D^* D + (k_{D_{22}}^* + k_{D_{32}}^*)A, \tag{5.71}$$

where, $k_D^* = k_{D_1}^* + k_{D_{21}}^* + k_{D_{31}}^* + k_{D_4}^*$. Finally, the upper bounds of $|\dot{A}|$, $|\dot{B}|$, $|\dot{C}|$, and $|\dot{D}|$ are grouped and added together to result in

$$|\frac{dW_1}{dt}| \leq k_\Sigma W_1, \tag{5.72}$$

where, $|\frac{dW_1}{dt}| \leq |\dot{A}| + |\dot{B}| + |\dot{C}| + |\dot{D}|$. k_Σ is a positive constant. Function W_1 has been denoted in (5.45). This concludes that the first condition of the Lemma 2.1.10 (Babarlat-like Lemma) holds.

Now the second condition of the Lemma 2.1.10 is examined by integrating both sides of (5.45) to yield

$$\int_0^\infty W_1(t)dt \leq -\int_0^\infty \dot{V}(t)dt = V(t_0) - V(\infty) \leq V(t_0) \tag{5.73}$$

Based on the construction of the positive definite and radially unbounded function V in (5.21), the right-hand side of the inequality above, i.e., $V(t_0)$, is obviously bounded by a positive constant depending on the initial conditions. It is obvious that conditions (5.72) and (5.73) fulfill two requirements of Barbalat-like lemma (2.1.10) given in [2]. Applying Theorem 8.4 in [57] (see Theorem 2.1.8 in Chapter 2), the convergence of $W_4(t)$ in (5.45) exists and is finite by

$$\lim_{t\to\infty} \Big(\mathbf{\Omega}^T \mathbf{C}\sigma(\mathbf{\Omega}) - \bar{\beta}'\big(\bar{\Delta}\|\bar{\boldsymbol{p}}_{Rd}\|^2 + 2\bar{\boldsymbol{q}}_{RO}^T \mathbf{K} \frac{\partial \boldsymbol{q}_d}{\partial s}\dot{s} + \bar{\boldsymbol{p}}_{Rd}^T \bar{\Delta} \frac{\partial \boldsymbol{q}_d}{\partial s}\dot{s}\big)\Big) = 0. \tag{5.74}$$

The limit equation (5.74) implies that

$$\begin{aligned} &\lim_{t\to\infty} \mathbf{\Omega}^T \mathbf{C}\sigma(\mathbf{\Omega}) = 0, \\ &\lim_{t\to\infty} \bar{\beta}'\big(\bar{\Delta}\|\bar{\boldsymbol{p}}_{Rd}\|^2 + 2\bar{\boldsymbol{q}}_{RO}^T \mathbf{K} \frac{\partial \boldsymbol{q}_d}{\partial s}\dot{s} + \bar{\boldsymbol{p}}_{Rd}^T \bar{\Delta} \frac{\partial \boldsymbol{q}_d}{\partial s}\dot{s}\big) = 0. \end{aligned} \tag{5.75}$$

No collision which has already been proven means $\beta'(t) = 0$ as $t \to \infty$. Therefore, the second limit of (5.75) mean those terms globally asymptotically converge to zero. Besides, property 1 of the saturation function $\sigma(\bullet)$ defined by Definition (2.1.2) implies

$$\lim_{t\to\infty} \mathbf{\Omega}(t) = 0. \tag{5.76}$$

In the previous section, the forward completeness of the closed-loop system (5.31) has been proven, and the boundedness of all states, including $\bar{\boldsymbol{q}}_{Rd}$ and $\bar{\boldsymbol{p}}_{Rd}$ for all $t \geq t_0 \geq 0$. From the definitions of $\mathbf{\Omega} = 2\mathbf{K}\bar{\boldsymbol{q}}_{Rd} + \bar{\Delta}\bar{\boldsymbol{p}}_{Rd} + \bar{\beta}'\bar{\boldsymbol{q}}_{RO}$, the limits (5.76) means

$$\begin{cases} \lim_{t\to\infty} \big(\bar{\boldsymbol{q}}(t) - \boldsymbol{q}_d(t)\big) = \mathbf{0}, \\ \lim_{t\to\infty} \big(\bar{\boldsymbol{p}}(t) - \boldsymbol{p}_d(t)\big) = \mathbf{0}, \end{cases} \tag{5.77}$$

The concern here is restricted to a sufficiently small neighborhood of the equilibrium point such that the higher-order terms are negligible. From (5.31), a linearized system for the two last equations can be represented by

$$\begin{bmatrix} \dot{\bar{\boldsymbol{q}}} \\ \dot{\bar{\boldsymbol{p}}} \end{bmatrix} = \begin{bmatrix} \frac{\partial f_1}{\partial \bar{\boldsymbol{q}}} & \frac{\partial f_1}{\partial \bar{\boldsymbol{p}}} \\ \frac{\partial f_2}{\partial \bar{\boldsymbol{q}}} & \frac{\partial f_2}{\partial \bar{\boldsymbol{p}}} \end{bmatrix} \begin{bmatrix} \bar{\boldsymbol{q}} - \bar{\boldsymbol{q}}_0 \\ \bar{\boldsymbol{p}} - \bar{\boldsymbol{p}}_0 \end{bmatrix} \tag{5.78}$$

where $f_1(\bar{\boldsymbol{q}}, \bar{\boldsymbol{p}})$ and $f_2(\bar{\boldsymbol{q}}, \bar{\boldsymbol{p}})$ are the right-hand side of (5.31), respectively. Each elements of the Jacobian matrix in (5.78) can be calculated by

$$\begin{cases} \frac{\partial f_1}{\partial \bar{\boldsymbol{q}}} = \mathbf{0}, \\ \frac{\partial f_1}{\partial \bar{\boldsymbol{p}}} = \mathbf{I}_2, \\ \frac{\partial f_2}{\partial \bar{\boldsymbol{q}}} = \frac{1}{\bar{\Delta}\mathbf{I}_2 + \bar{\boldsymbol{p}}_{Rd}\bar{\boldsymbol{p}}_{Rd}^T} \Big[-\mathbf{C}\big(2\mathbf{K} + \bar{\beta}'\mathbf{I}_2 + \bar{\beta}''\bar{\boldsymbol{q}}_{RO}\bar{\boldsymbol{q}}_{RO}^T\big)\Big], \\ \frac{\partial f_2}{\partial \bar{\boldsymbol{p}}} = \frac{-3\bar{\boldsymbol{p}}_{Rd}^T}{\big(\bar{\Delta}\mathbf{I}_2 + \bar{\boldsymbol{p}}_{Rd}\bar{\boldsymbol{p}}_{Rd}^T\big)^2}\big(-2\mathbf{K}\bar{\boldsymbol{p}}_{Rd} - \mathbf{C}\sigma(\boldsymbol{\Omega}) + \ddot{\boldsymbol{q}}_d\big) \\ \qquad -\frac{1}{\bar{\Delta}\mathbf{I}_2 + \bar{\boldsymbol{p}}_{Rd}\bar{\boldsymbol{p}}_{Rd}^T}\Big[2\mathbf{K} + \mathbf{C}\big(\bar{\Delta}\mathbf{I}_2 + \bar{\boldsymbol{p}}_{Rd}\bar{\boldsymbol{p}}_{Rd}^T\big)\Big] \end{cases} \tag{5.79}$$

Equilibrium points $(\bar{\boldsymbol{q}}_0, \bar{\boldsymbol{p}}_0)$ could either be $(\boldsymbol{q}_d, \boldsymbol{p}_d)$ or $(\boldsymbol{q}_c, \boldsymbol{p}_c)$. Therefore, it is necessary to prove that desired equilibrium points $(\boldsymbol{q}_d, \boldsymbol{p}_d)$ are locally asymptotically stable and saddle points $(\boldsymbol{q}_c, \boldsymbol{p}_c)$ are locally unstable. Hence, it can be concluded that the actual path of the WMR $\bar{\boldsymbol{q}}(t)$ approaches the reference path $\boldsymbol{q}_d$ from almost everywhere except for the set denoted by the condition (5.11) and the set denoted by $(\boldsymbol{q}_c, \boldsymbol{p}_c)$ which is unstable.

Proof of asymptotic stability of an equilibrium point

To prove the equilibrium points $(\boldsymbol{q}_d, \boldsymbol{p}_d)$ to be locally asymptotically stable, the closed-loop system (5.31) is linearized around a desired equilibrium point by substituting $\bar{\boldsymbol{q}} = \boldsymbol{q}_d$ and $\bar{\boldsymbol{p}} = \dot{\boldsymbol{q}}_d$. Results can be achieved by applying the following associated properties of functions $\bar{\chi}$, $\bar{\beta}$ and its first and second derivatives, i.e., $\bar{\beta}'$ and $\bar{\beta}''$, described in the previous section

$$\begin{aligned} &\bar{\chi}_d = \bar{\chi}|_{\bar{\boldsymbol{q}}=\boldsymbol{q}_d, \bar{\boldsymbol{p}}=\dot{\boldsymbol{q}}_d}; \bar{\beta}|_{\bar{\chi}=\bar{\chi}_d} = 0; \bar{\beta}'|_{\bar{\chi}=\bar{\chi}_d} = 0; \bar{\beta}''|_{\bar{\chi}=\bar{\chi}_d} = 0; \\ &\bar{\Delta}_d = \bar{\Delta}|_{\bar{\boldsymbol{p}}=\dot{\boldsymbol{q}}_d} = 1; (\bar{\boldsymbol{p}}_{Rd}\bar{\boldsymbol{p}}_{Rd}^T + \bar{\Delta}\mathbf{I}_2)|_{\bar{\boldsymbol{p}}=\dot{\boldsymbol{q}}_d} = \mathbf{I}_2. \end{aligned} \tag{5.80}$$

Now $\bar{\boldsymbol{q}}_0 = \boldsymbol{q}_d$ and $\bar{\boldsymbol{p}}_0 = \dot{\boldsymbol{q}}_d = \boldsymbol{p}_d$ are substituted into (5.78) while using notations (5.18) of $\bar{\boldsymbol{q}}_{RO}$, $\bar{\boldsymbol{q}}_{Rd}$, $\dot{\bar{\boldsymbol{q}}}_{Rd}$, $\bar{\Delta}$ and applying results of (5.80) to obtain the Jacobian

matrix's elements at these points

$$\begin{cases} \frac{\partial f_1}{\partial \bar{\boldsymbol{q}}} = \mathbf{0}, \\ \frac{\partial f_1}{\partial \bar{\boldsymbol{p}}} = \mathbf{I}_2, \\ \frac{\partial f_2}{\partial \bar{\boldsymbol{q}}} = -2\mathbf{C}\mathbf{K}, \\ \frac{\partial f_2}{\partial \bar{\boldsymbol{p}}} = -2\mathbf{K} - \mathbf{C}. \end{cases} \tag{5.81}$$

Hence, the linearized closed-loop system (5.78) is achieved at $\bar{\boldsymbol{q}}_0 = \boldsymbol{q}_d$ and $\bar{\boldsymbol{p}}_0 = \boldsymbol{p}_d$ as

$$\begin{cases} \dot{\bar{\boldsymbol{q}}} = \bar{\boldsymbol{p}}_{Rd}, \\ \dot{\bar{\boldsymbol{p}}} = -2\mathbf{K}\bar{\boldsymbol{p}}_{Rd} - \mathbf{C}(2\mathbf{K}\bar{\boldsymbol{q}}_{Rd} + \bar{\boldsymbol{p}}_{Rd}), \end{cases} \tag{5.82}$$

Because positive definite matrice $\mathbf{K}$ and $\mathbf{C}$ have been already defined in (5.11) and (5.25), respectively, it is obvious that the linearized closed-loop system (5.82) is locally asymptotically stable at the origin. Hence, the equilibrium points $(\boldsymbol{q}_d, \boldsymbol{p}_d)$ are locally asymptotically stable.

Proof of instability of a critical point

To facilitate investigation of the instability of the saddle points $(\boldsymbol{q}_c, \dot{\boldsymbol{q}}_c)$, the representations of (5.80) are rewritten by applying $\bar{\boldsymbol{q}} = \boldsymbol{q}_c$ and $\bar{\boldsymbol{p}} = \dot{\boldsymbol{q}}_c$ to result in

$$\bar{\Delta}_c = \bar{\Delta}|_{\bar{\boldsymbol{p}}=\dot{\boldsymbol{q}}_c}; \bar{\chi}_c = \bar{\chi}|_{\bar{\boldsymbol{q}}=\boldsymbol{q}_c, \bar{\boldsymbol{p}}=\dot{\boldsymbol{q}}_c}; \bar{\beta}'_c = \bar{\beta}'|_{\bar{\chi}=\bar{\chi}_c}; \bar{\beta}''_c = \bar{\beta}''|_{\bar{\chi}=\bar{\chi}_c}. \tag{5.83}$$

In this approach, the linearized closed-loop system (5.78) is obtained at $\bar{\boldsymbol{q}} = \boldsymbol{q}_c$ and $\bar{\boldsymbol{p}} = \dot{\boldsymbol{q}}_c$ as follows

$$\begin{cases} \frac{\partial f_1}{\partial \bar{\boldsymbol{q}}} = \mathbf{0}, \\ \frac{\partial f_1}{\partial \bar{\boldsymbol{p}}} = \mathbf{I}_2, \\ \frac{\partial f_2}{\partial \bar{\boldsymbol{q}}} = \frac{1}{\bar{\Delta}_c\mathbf{I}_2 + \bar{\boldsymbol{p}}_{Rd}\bar{\boldsymbol{p}}_{Rd}^T}\Big[-\mathbf{C}\big(2\mathbf{K} + \bar{\beta}'_c\mathbf{I}_2 + \bar{\beta}''_c\bar{\boldsymbol{q}}_{RO}\bar{\boldsymbol{q}}_{RO}^T\big)\Big], \\ \frac{\partial f_2}{\partial \bar{\boldsymbol{p}}} = \frac{-3\bar{\boldsymbol{p}}_{Rd}^T}{\big(\bar{\Delta}_c\mathbf{I}_2 + \bar{\boldsymbol{p}}_{Rd}\bar{\boldsymbol{p}}_{Rd}^T\big)^2}\big(-2\mathbf{K}\bar{\boldsymbol{p}}_{Rd} - \mathbf{C}\sigma(\boldsymbol{\Omega_c}) + \ddot{\boldsymbol{q}}_d\big) \\ \qquad -\frac{1}{\bar{\Delta}_c\mathbf{I}_2 + \bar{\boldsymbol{p}}_{Rd}\bar{\boldsymbol{p}}_{Rd}^T}\Big[2\mathbf{K} + \mathbf{C}\big(\bar{\Delta}_c\mathbf{I}_2 + \bar{\boldsymbol{p}}_{Rd}\bar{\boldsymbol{p}}_{Rd}^T\big)\Big] \end{cases} \tag{5.84}$$

To evaluate the stability of the linearized system (5.78) at the critical points $(\boldsymbol{q}_c, \dot{\boldsymbol{q}}_c)$, the Lyapunov function candidate is considered

$$\bar{V}_c = \frac{\mathbf{C}\mathbf{K}}{\bar{\Delta}_c\mathbf{I}_2 + \bar{\boldsymbol{p}}_{Rd}\bar{\boldsymbol{p}}_{Rd}^T}\|\bar{\boldsymbol{q}} - \boldsymbol{q}_c\|^2 + \frac{1}{2}\|\bar{\boldsymbol{p}} - \boldsymbol{p}_c\|^2. \tag{5.85}$$

Taking the time derivative of (5.85) along the solutions of (5.78) and replacing $(\bar{\boldsymbol{q}}_0, \bar{\boldsymbol{p}}_0)$ by $(\boldsymbol{q}_c, \boldsymbol{p}_c)$, respectively, give

$$\begin{aligned}\dot{\bar{V}}_c = &-\frac{\bar{\beta}_c'\mathbf{C}}{\bar{\Delta}_c\mathbf{I}_2 + \bar{\boldsymbol{p}}_{Rd}\bar{\boldsymbol{p}}_{Rd}^T}\|(\bar{\boldsymbol{q}} - \boldsymbol{q}_c)\|^2 - \frac{\bar{\beta}_c''\mathbf{C}}{\bar{\Delta}_c\mathbf{I}_2 + \bar{\boldsymbol{p}}_{Rd}\bar{\boldsymbol{p}}_{Rd}^T}\big(\bar{\boldsymbol{q}}_{RO}^T(\bar{\boldsymbol{q}} - \boldsymbol{q}_c)\big)^2 \\ &+ \Big[\frac{-3\bar{\boldsymbol{p}}_{Rd}^T\big(-2\mathbf{K}\bar{\boldsymbol{p}}_{Rd} - \mathbf{C}\sigma(\boldsymbol{\Omega}_c) + \ddot{\boldsymbol{q}}_d\big)}{\big(\bar{\Delta}_c\mathbf{I}_2 + \bar{\boldsymbol{p}}_{Rd}\bar{\boldsymbol{p}}_{Rd}^T\big)^2} - \frac{2\mathbf{K} + \mathbf{C}\big(\bar{\Delta}_c\mathbf{I}_2 + \bar{\boldsymbol{p}}_{Rd}\bar{\boldsymbol{p}}_{Rd}^T\big)}{\bar{\Delta}_c\mathbf{I}_2 + \bar{\boldsymbol{p}}_{Rd}\bar{\boldsymbol{p}}_{Rd}^T}\Big]\|\bar{\boldsymbol{p}} - \boldsymbol{p}_c\|^2.\end{aligned} \tag{5.86}$$

It is observed from the fact that a saddle point emerges only if three points $\boldsymbol{q}_c$, $\boldsymbol{q}_{obs}$ and $\boldsymbol{q}_d$ are collinear and the point $\boldsymbol{q}_{obs}$ must be in the middle of the two points $\boldsymbol{q}_c$ and $\boldsymbol{q}_d$. Otherwise, the coordinates of actual mobile robot, $\bar{\boldsymbol{q}}$, will converge to the reference trajectory, $\boldsymbol{q}_d$, by all means. This refers back to the previous situation of the desired equilibrium points. To investigate stability properties of the critical points $\big(\boldsymbol{q}_c(x_c, y_c), \boldsymbol{p}_c(\dot{x}_c, \dot{y}_c)\big)$, each parts of (5.86) will be evaluated carefully.

Let $\mathbf{V}$ be a vector space over the field $\mathbb{R}^2$, in which $\|\bar{\boldsymbol{q}} - \boldsymbol{q}_c\|^2 \geq 0$ and $\|\bar{\boldsymbol{p}} - \boldsymbol{p}_c\|^2 \geq 0$ for all $[\bar{x} \quad \bar{y}]^T, [x_c \quad y_c]^T, [\dot{\bar{x}} \quad \dot{\bar{y}}]^T, [\dot{x}_c \quad \dot{y}_c]^T \in \mathbf{V}$. Firstly, a subspace $\mathbf{V}^* \subset \mathbf{V}$ is defined such that $\bar{\boldsymbol{q}} = \boldsymbol{q}_c$ and $\bar{\boldsymbol{p}} = \boldsymbol{p}_c$ for any $x_c, \dot{x}_c \in \mathbf{V}^*$. This assumption also holds for the case of any $y_c, \dot{y}_c \in \mathbf{V}^*$. Therefore, only the case of $(x_c, \dot{x}_c)$ is needed to be proven here. This implies the sum of attractive and repulsive forces at this point to be equal to zero, but each individual forces are nonzero. Moreover, $\mathbf{C}$ is a positive constant matrix, and $\bar{\beta}'' \geq 0$, $\Omega_c = 0$ at $\bar{\boldsymbol{q}} = \boldsymbol{q}_c, \bar{\boldsymbol{p}} = \boldsymbol{p}_c$ which are already mentioned in the previous section. Hence, $\dot{\bar{V}}_c$ in (5.86) can be rewritten in subspace $\mathbf{V}^*$ by

$$\dot{\bar{V}}_c = -\frac{\mathbf{C}\bar{\beta}_c'}{\bar{\Delta}_c\mathbf{I}_2 + \bar{\boldsymbol{p}}_{Rd}\bar{\boldsymbol{p}}_{Rd}^T}\|\bar{\boldsymbol{q}} - \boldsymbol{q}_c\|^2 + \frac{3\bar{\boldsymbol{p}}_{Rd}^T\big(2\mathbf{K}\bar{\boldsymbol{p}}_{Rd} + \mathbf{C}\sigma(\boldsymbol{\Omega}_c)\big)}{\big(\bar{\Delta}_c\mathbf{I}_2 + \bar{\boldsymbol{p}}_{Rd}\bar{\boldsymbol{p}}_{Rd}^T\big)^2}\|\bar{\boldsymbol{p}} - \boldsymbol{p}_c\|^2. \tag{5.87}$$

Secondly, another subspace $\mathbf{V}^{**} \subset \mathbf{V} \setminus \mathbf{V}^*$ is defined. This means $\|\bar{\boldsymbol{q}} - \boldsymbol{q}_c\|^2 > 0$, and $\|\bar{\boldsymbol{p}} - \boldsymbol{p}_c\|^2 > 0$ for all $[\bar{x} \quad \bar{y}]^T, [x_c \quad y_c]^T, [\dot{\bar{x}} \quad \dot{\bar{y}}]^T, [\dot{x}_c \quad \dot{y}_c]^T \in \mathbf{V}^{**}$. From the definitions of $\bar{\beta}$ in (5.19) and smooth step function $h(\bullet)$ in Chapter 2, it gives

$$\bar{\beta}' = \frac{\partial\bar{\beta}}{\partial h}\frac{\partial h}{\partial\tau}\frac{\partial\tau}{\partial\bar{\chi}}. \tag{5.88}$$

Now using calculation in [125] yields

$$\begin{aligned}\frac{\partial\bar{\beta}}{\partial h} &= -\frac{1}{h^2(\bullet)}, \\ \frac{\partial h}{\partial\tau} &= \big(-h(\bullet) + h^2(\bullet)\big)\big(-\frac{1}{\tau^2} - \frac{1}{(\tau-1)^2}\big), \\ \frac{\partial\tau}{\partial\bar{\chi}} &= \frac{1}{R_{sen}^2/2 - (R_{safe} + R_{obs})^2/2},\end{aligned} \tag{5.89}$$

where functions $h(\bullet)$ and τ have been defined as

$$\begin{aligned} h &= \frac{e^{-\frac{1}{\tau}}}{e^{-\frac{1}{\tau}} + e^{-\frac{1}{1-\tau}}}, \\ \tau &= \frac{\bar{\chi} - (R_{safe} + R_{obs})^2/2}{R_{sen}^2/2 - (R_{safe} + R_{obs})^2/2}. \end{aligned} \tag{5.90}$$

It is shown that $\big(-h(\bullet) + h^2(\bullet)\big) < 0$ for all $\tau \in \big(\frac{(R_{safe}+R_{obs})^2}{2}, \frac{R_{sen}^2}{2}\big)$ [125]. Thus, by substituting (5.89) into (5.88) it gives $\bar{\beta}' < 0$ for all $\tau \in \big(\frac{(R_{safe}+R_{obs})^2}{2}, \frac{R_{sen}^2}{2}\big)$. Since $\bar{\chi}$ is the variable of function $h(\bullet)$, see (5.19), and $\bar{\beta}'$ is inversely proportional to square of absolute value of $h(\bullet)$, see (5.88) and (5.89), the smaller the value of $\bar{\chi}$ is, the larger the value of β' for all $\tau \in \big(\frac{(R_{safe}+R_{obs})^2}{2}, \frac{R_{sen}^2}{2}\big)$. There always exists $(x_c, \dot{x}_c) \in \mathbf{V}^{**}$ such that the part $\bar{\beta}_c'$ is strictly negative, i.e., there exists a strict positive constant b^{**} such that $\bar{\beta}_c' < -b^{**}$. This assumption also holds for the case of any $(y_c, \dot{y}_c) \in \mathbf{V}^{**}$. Therefore, only the case of $(x_c, \dot{x}_c)$ is needed to be proven here. It can be represented $\dot{\bar{V}}_c$ of (5.86) in the subspace $\mathbf{V}^{**}$ as follows

$$\dot{\bar{V}}_c \geq \frac{b^{**}\mathbf{C}}{\bar{\Delta}_c\mathbf{I}_2 + \bar{\boldsymbol{p}}_{Rd}\bar{\boldsymbol{p}}_{Rd}^T}\|\bar{\boldsymbol{q}} - \boldsymbol{q}_c\|^2 + \frac{3\bar{\boldsymbol{p}}_{Rd}^T\big(2\mathbf{K}\bar{\boldsymbol{p}}_{Rd} + \mathbf{C}\sigma(\boldsymbol{\Omega}_c)\big)}{\big(\bar{\Delta}_c\mathbf{I}_2 + \bar{\boldsymbol{p}}_{Rd}\bar{\boldsymbol{p}}_{Rd}^T\big)^2}\|\bar{\boldsymbol{p}} - \boldsymbol{p}_c\|^2 > 0. \tag{5.91}$$

For the special case $\|\bar{\boldsymbol{q}}(t_0) - \boldsymbol{q}_c\| = 0$ and $\|\bar{\boldsymbol{p}}(t_0) - \boldsymbol{p}_c\|^2$, there would be no contradiction in terms of (5.91). This case, however, is never observed in practice since the ever-present physical noise would cause $\|\bar{\boldsymbol{q}}(t^*) - \boldsymbol{q}_c\| \neq 0$ and $\|\bar{\boldsymbol{p}}(t^*) - \boldsymbol{p}_c\| \neq 0$ for some $(x_c, \dot{x}_c) \in \mathbf{V}^{**}$ to be different from 0 at the time $t^* \geq t_0$. The inequality (5.91) can be rewriten as

$$\dot{\bar{V}}_c \geq \frac{b^{**}\mathbf{C}}{\bar{\Delta}_c\mathbf{I}_2 + \bar{\boldsymbol{p}}_{Rd}^*\bar{\boldsymbol{p}}_{Rd}^{*T}}\|\bar{\boldsymbol{q}}^* - \boldsymbol{q}_c\|^2 + \frac{3\bar{\boldsymbol{p}}_{Rd}^{*T}\big(2\mathbf{K}\bar{\boldsymbol{p}}_{Rd}^* + \mathbf{C}\sigma(\boldsymbol{\Omega}_c)\big)}{\big(\bar{\Delta}_c\mathbf{I}_2 + \bar{\Delta}_c\mathbf{I}_2 + \bar{\boldsymbol{p}}_{Rd}^*\bar{\boldsymbol{p}}_{Rd}^{*T}\big)^2}\|\bar{\boldsymbol{p}}^* - \boldsymbol{p}_c\|^2 > 0. \tag{5.92}$$

where, $\boldsymbol{q}^* = \boldsymbol{q}(t^*)$ and $\boldsymbol{p}^* = \boldsymbol{p}(t^*)$, for all time $t \geq t^* \geq t_0 \geq 0$. Since $\|\boldsymbol{q}(t^*) - \boldsymbol{q}_c\| \neq 0$ and $\|\boldsymbol{p}(t^*) - \boldsymbol{p}_c\| \neq 0$, the right-hand side of (5.92) is divergent, and so does the left-hand side. As a result, the critical points $(\boldsymbol{q}_c, \boldsymbol{p}_c)$ are unstable based on the Theorem 4.3 in [57] (see Theorem 2.1.6 in Chapter 2 for the details). The proof of Theorem 6.2.1 is completed.

5.5 Simulation results

This section presents two simulation examples to illustrate the effectiveness of the proposed control laws (5.30). Numerical simulation is carried out by using

the physical parameters of the WMR which is taken from [6]. The parameters are summarized in Table 3.1 in Chapter 3. In the first example, the interaction of the WMR tracking to a tanh-shape reference path is simulated. In this scenario, a stationary obstacle is included on the reference path. The second example simulates the behavior of the WMR tracking a sine-shape reference path while it is capable of avoiding a stationary obstacle on the path. Both results indicate the correctness of the path-tracking and obstacle avoidance control laws.

Tanh-shape and sine-shape paths are chosen as two different reference paths with the following specifications: $x_d = s - 7$, $y_d = -5\tanh(0.2s)$, $s(t) = 0.5t$, $\dot{s} = 0.5$ and $x_d = s$, $y_d = 10\sin(0.15s)$, $s(t) = 0.5t$, $\dot{s} = 0.5$. Hence, these reference paths are regular and satisfies requirements (5.7) mentioned in Assumption 5.1.1. Initial configuration of the WMR is given as $(x(0), y(0), \phi(0))$. The design parameters for control laws (5.24) included $\mathbf{K} = [k_1 \quad 0; 0 \quad k_2]$; $\mathbf{C} = [c_1 \quad 0; 0 \quad c_2]$. To investigate the obstacle avoidance capability of the proposed controllers, specific locations of a stationary obstacle are set up in two different scenarios. Coordinates are detailed as: (x_{obs1}, y_{obs1}), and (x_{obs2}, y_{obs2}). R_{obs} defined in Assumption 5.1.4 is considered to zero in simulation only. This means obstacle is a point in the Cartesian plane. Values are shown in Table 5.1 below. Figures 5.2, 5.3, and 5.4

Table 5.1: Values of design parameters

Parameters	Meaning	Values
$x(0); y(0); \phi(0)$	initial configuration of the actual WMR	$-5; 0; 0.2$
k_1	control gain 1 of the constant matrix $\mathbf{K}$	0.95
k_2	control gain 2 of the constant matrix $\mathbf{K}$	0.95
c_1	constant value 1 of the constant matrix $\mathbf{C}$	1
c_2	constant value 2 of the constant matrix $\mathbf{C}$	1
$x_{obs1}; y_{obs1}$	coordinate of the obstacle in scenario 1	$15; -5$
$x_{obs2}; y_{obs2}$	coordinate of the obstacle in scenario 2	$10; -4$
R_{safe}	radius of physical safety region of the WMR	1
R_{sen}	radius of sensing region of the WMR	2.5
R_{obs}	distance of influence of obstacle	0
h	time step used in Euler method for numerical computation	0.02

illustrate the response of the WMR in scenario 1 in which the obstacle is on the

tanh-shape reference path. In figure 5.2, after departing from its initial location, the WMR starts approaching the reference path. When the obstacle emerges to sensing region, the obstacle avoidance algorithm in motion controllers is active. At this point, the WMR start diverging from the desired path and bypassing the obstacle to avoid a potential collision. Once the obstacle is out of the WMR's sensing range, the obstacle avoidance algorithm is inactive. The WMR returns to its reference path because only the path tracking algorithm is working. Apart from the starting and obstacle avoidance circumstances, errors in position and orientation, i.e., x_e, y_e and ϕ_e and velocities, i.e., v_e and ω_e tend to zero at steady state. Correspondingly, τ_v and τ_ω applied to two wheels tend to constant values, see figures 5.3, and 5.4.

Similarly, figures 5.5, 5.6, and 5.7 illustrate the behavior of the WMR in scenario 2 in which the obstacle is on the sine-shape reference path. Results obtained in this case are also as satisfactory as they should be expected. It is seen from figure 5.5 that the WMR is forced to track smoothly the desired path. No collision between the WMR and the obstacle is guaranteed. Except heading angle tracking error, path tracking errors converge to zero with good performance. Since the orientation variable ϕ is not controlled in this proposed control algorithm, the response of ϕ_e behaves in accordance with the traveling sine-shape path of the WMR, as in figure 5.6.

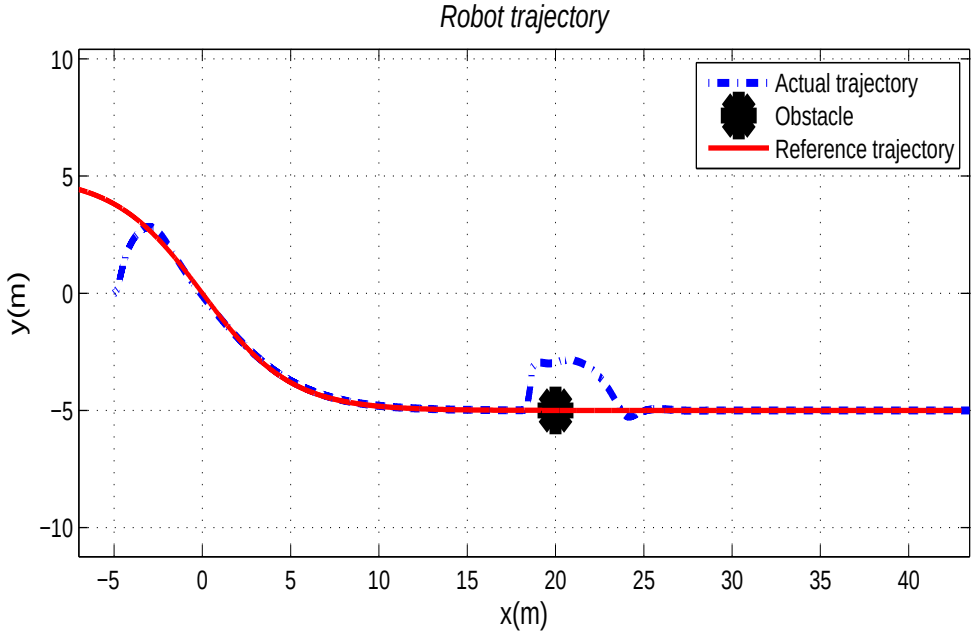

Figure 5.2: Tracking path of the WMR to the tanh-shape reference path - An obstacle is on the reference path.

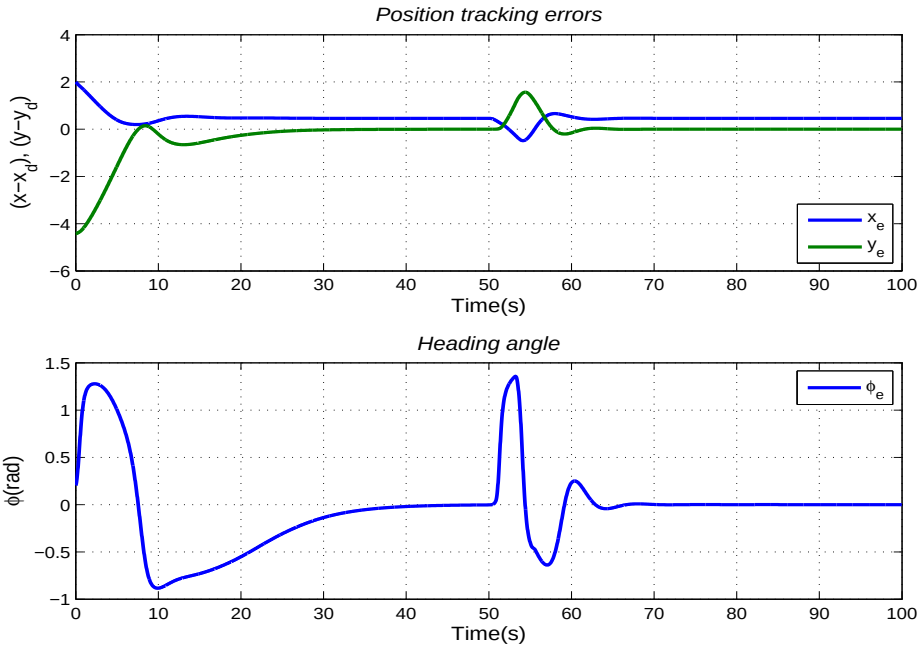

Figure 5.3: Position tracking errors (above); Heading angle tracking error (below).

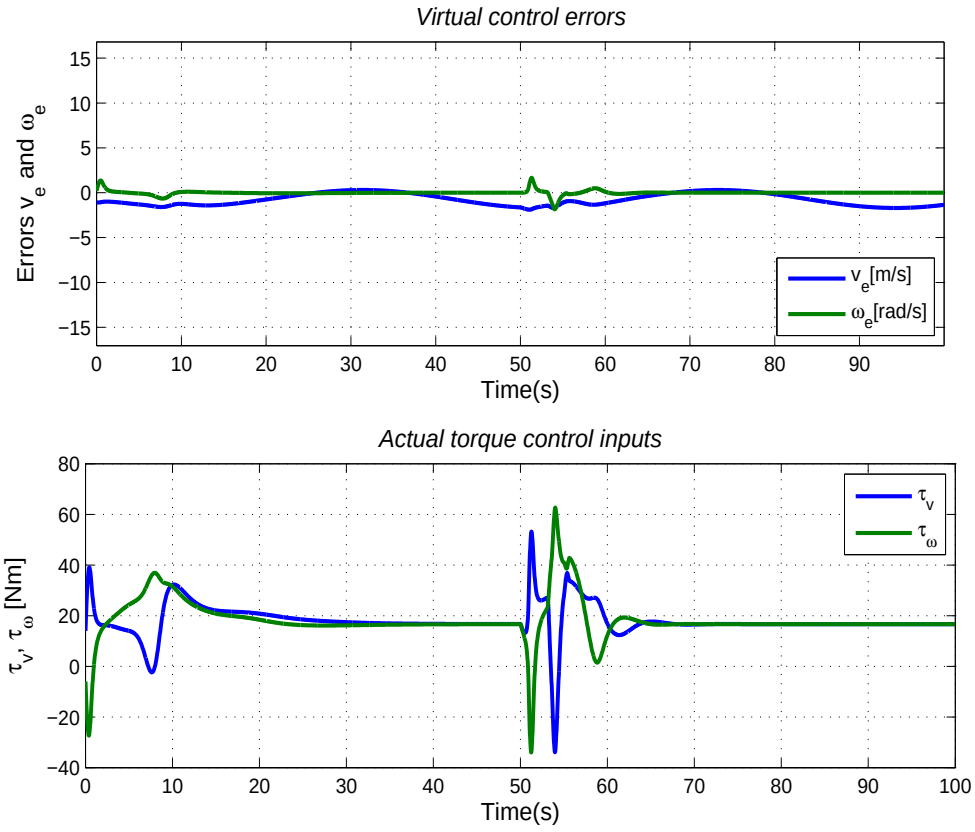

Figure 5.4: Virtual control errors (above) and Actual control inputs (below).

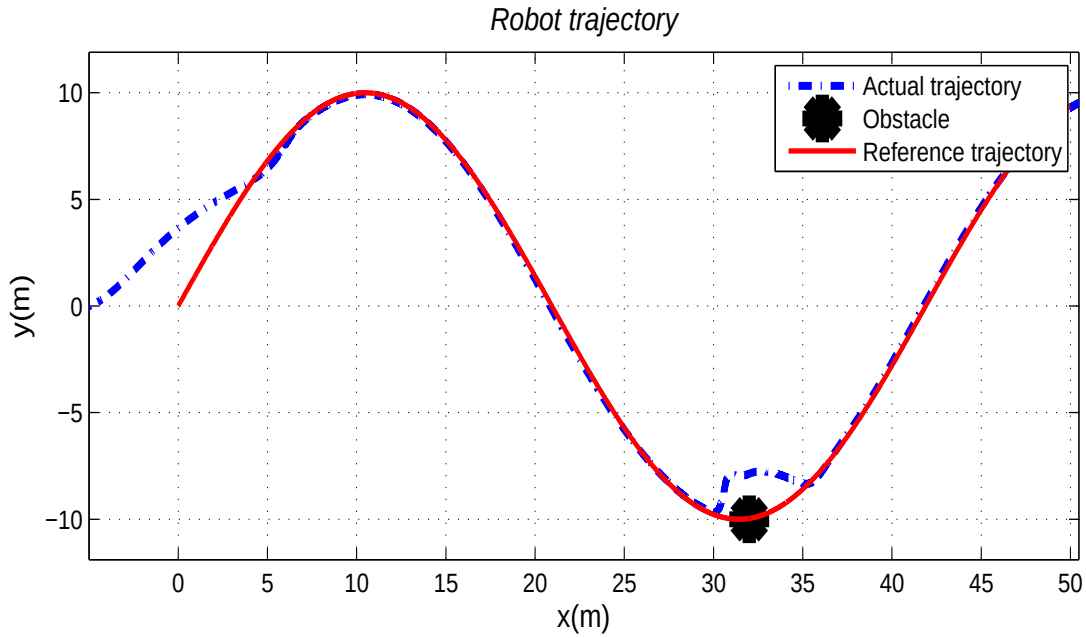

Figure 5.5: Tracking path of the WMR to the sine-shape reference path - An obstacle is on the reference path.

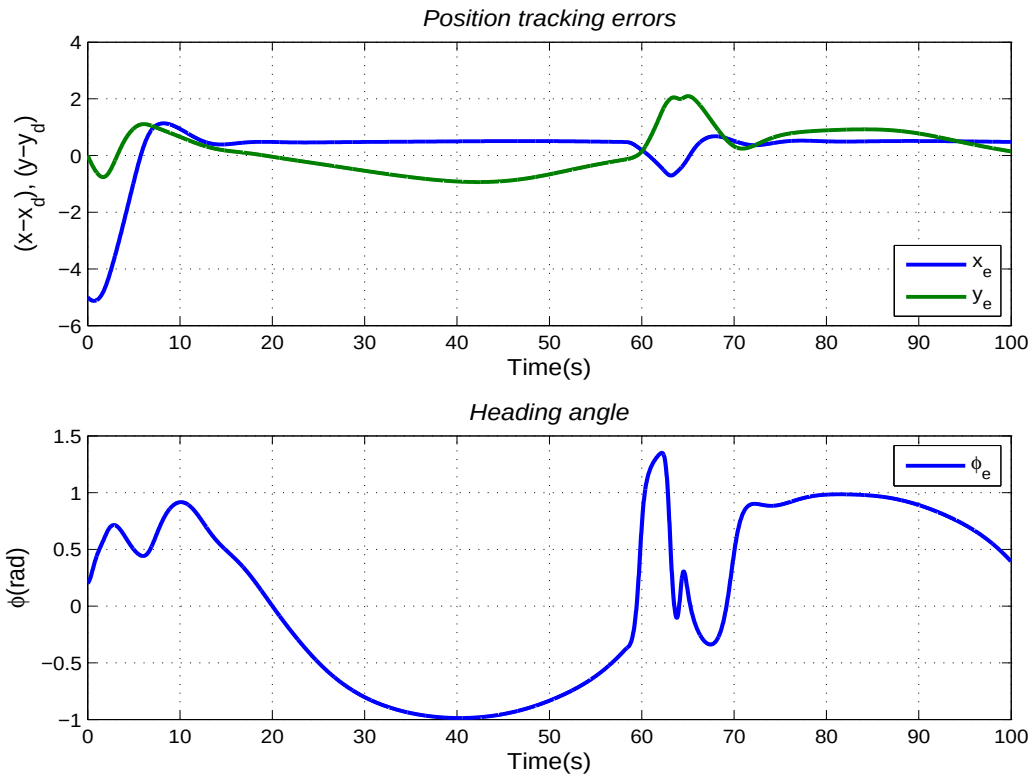

Figure 5.6: Position tracking errors (above); Heading angle tracking error (below).

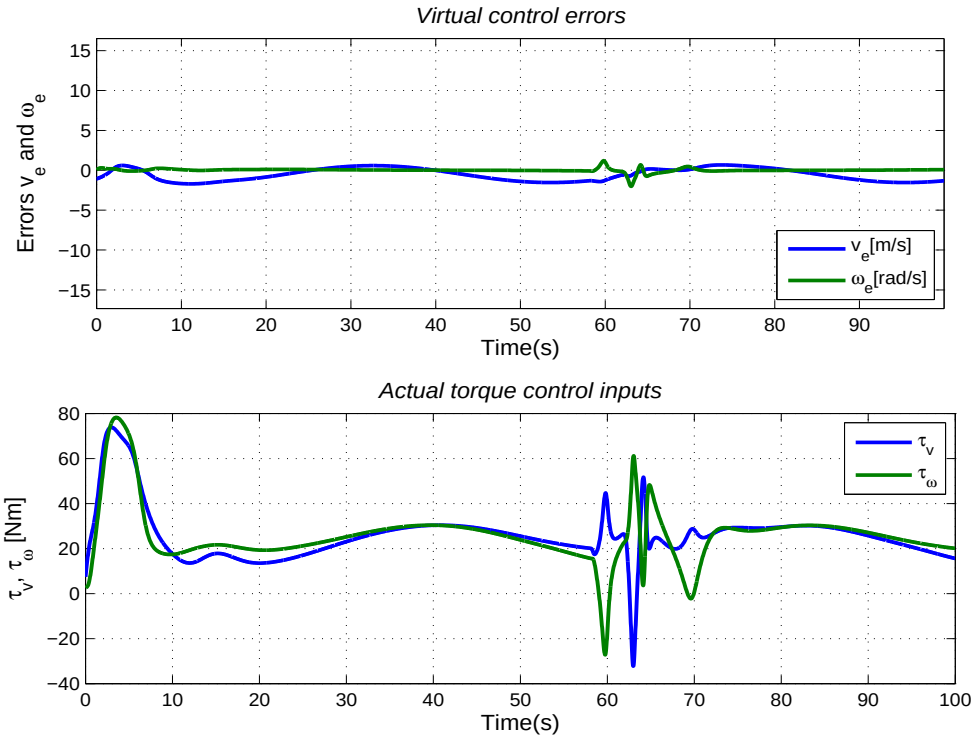

Figure 5.7: Virtual control errors (above) and Actual control inputs (below).

5.6 Conclusions

This chapter has proposed a constructive control scheme to design bounded position controllers for path tracking and collision avoidance of the WMR system. The bounded control design technique is adopted from the work in [4] for second-order systems. The novel pairwise collision avoidance functions developed in [4] is successfully applied to this particular control objective. Through numerical simulation, the proposed controllers have demonstrated that the WMR converges to the reference path from the initial location to the goal while it is capable of avoiding any stationary obstacle along its travelling path. Similar to the navigation function proposed in [119, 122], saddle points emerging in the potential function method is a critical issue. In this chapter, an analytical analysis is provided to prove that only the equilibrium points are locally asymptotically stable while the saddle points are unstable. Thus, the WMR system does not converge to saddle points. Also, it should be emphasized that conventional artificial potential functions [109,113] and navigation functions [119,122,165] built in collision avoidance control methods result in very large control efforts if the relative distance between the WMR and the obstacle is relatively small. Even in worst cases, that value may go up to infinity when a collision occurs. In the proposed control laws,

the designed control vector $\boldsymbol{u}(t)$ is bounded by a strictly positive constant δ, see (5.27). The boundedness of the control $\boldsymbol{u}(t)$ can guarantee control efforts not exceeding a certain value in terms of the relative distance between the WMR and the obstacle, and the relative velocity between the WMR and the virtual reference one, as seen in the construction of $\boldsymbol{u}(t)$ in (5.26). This, in turn, shows the boundedness of the torque control vector $\boldsymbol{\tau}$, due to $\lim_{t\to\infty} \mathbf{A} = 0$ in (5.30). However, in this control algorithm, the orientation of the WMR is not controlled. This issue suggests the author investigate the problem in the next chapter.

Chapter 6

Practical control for path tracking and obstacle avoidance

In the previous chapter, only the position of the WMR has been used in control design while the orientation was not controlled. This chapter takes this particular issue into consideration to develop a practical solution for the WMR about path tracking and obstacle avoidance. The proposed control design is based on a coordinate transformation applying ideas of the transverse function approach in [20, 137, 138, 166]. Basically, an "additional signal input"in terms of the orientation is generated. Regarding practical implementation, this approach gives a stabilization of the WMR's state variables in a small neighbourhood of the desired state variables. Hence, tracking errors can be made arbitrarily small by selecting suitable control parameters instead of being zero as $t \to \infty$. As arbitrary smooth reference paths, including fixed points and non-admissible paths are applied, the proposed feedback controllers guarantee practical stabilization of tracking errors. The advantages of the local potential function represented in [3] are taken to deal with the obstacle avoidance issue. By integrating smooth step functions into the local potential function, there is no need for switching scheme in control design. The resulting controllers are capable of handling both path tracking and obstacle avoidance issues. Simulations are provided in the last section to illustrate the effectiveness of the designed controllers.

6.1 Problem statement

For convenience, the models of the kinematics and dynamics of the nonholonomic WMR which are derived in (2.41) and (2.50) are represented respectively

$$\begin{cases} \dot{x} = v\cos(\phi), \\ \dot{y} = v\sin(\phi), \\ \dot{\phi} = \omega, \end{cases} \tag{6.1}$$
$$\begin{bmatrix} \dot{v} \\ \dot{\omega} \end{bmatrix} = \bar{\mathbf{C}} \begin{bmatrix} \omega^2 \\ -v\omega \end{bmatrix} - \bar{\mathbf{D}} \begin{bmatrix} v \\ \omega \end{bmatrix} + \bar{\mathbf{B}}\boldsymbol{\tau},$$

where the matrices $\bar{\mathbf{C}}$, $\bar{\mathbf{D}}$ and $\bar{\mathbf{B}}$ are defined in (2.51).

6.1.1 Coordinate transformations

In the previous work in Chapter 5, the nonholonomic kinematics of the WMR were converted to double integrator dynamics. Through that transformation, a virtual offset coordinate $\bar{\boldsymbol{q}}(\bar{x}, \bar{y})$ was controlled instead of the inertial coordinate $\boldsymbol{q}(x, y)$ of the center of mass P_C, while the orientation ϕ was not considered. This might result in the undesirable performance of the vehicle's dynamics. Therefore, an approach for the design of practical stabilization is presented here as an alternative and it can extend the applicability of the WMR system in practical manner.

Firstly, some smooth functions $f_x(\alpha), f_y(\alpha), f_\phi(\alpha)$ of an angle variable α are proposed, for all $\alpha \in \mathbb{R}$. These functions and can be chosen such that

$$|f_x(\alpha)| \leq \gamma_1; \quad |f_y(\alpha)| \leq \gamma_2; \quad |f_\phi(\alpha)| \leq \gamma_3. \tag{6.2}$$

where $f_x(\alpha), f_y(\alpha), f_\phi(\alpha)$ are assumed to be bounded differentiable functions and γ_1, γ_2 and γ_3 are positive constants.

By adopting the coordinate transformation in [5, 141], the WMR's dynamics in (6.1) are converted to a new form with an "additional control input". This complement provides an effective way to overcome difficulties because of non-

holonomic constraints. The following variables are introduced

$$\begin{aligned}
\boldsymbol{q} &= \mathbf{R}(-\phi_d)\begin{bmatrix} x \\ y \end{bmatrix} - \mathbf{R}(\phi_e)\begin{bmatrix} f_x(\alpha) \\ f_y(\alpha) \end{bmatrix}, \\
\boldsymbol{q}_d &= \mathbf{R}(-\phi_d)\begin{bmatrix} x_d \\ y_d \end{bmatrix}, \\
\boldsymbol{q}_e &= \boldsymbol{q} - \boldsymbol{q}_d, \\
\phi_e &= \phi - \phi_d - f_\phi(\alpha),
\end{aligned} \tag{6.3}$$

with the rotation matrix $\mathbf{R}(\bullet)$ in Cartesian plane is given by [17]

$$\mathbf{R}(\bullet) = \begin{bmatrix} \cos(\bullet) & -\sin(\bullet) \\ \sin(\bullet) & \cos(\bullet) \end{bmatrix} \tag{6.4}$$

By taking the time derivative both sides of the two last equations in (6.3) and using representations of $\boldsymbol{q}$ and $\boldsymbol{q}_d$, the following expression is obtained

$$\begin{aligned}
\dot{\boldsymbol{q}}_e = \Big(\big(\dot{\mathbf{R}}(-\phi_d)(-\dot{\phi}_d) \begin{bmatrix} x \\ y \end{bmatrix} + \mathbf{R}(-\phi_d) \begin{bmatrix} \dot{x} \\ \dot{y} \end{bmatrix} \big) \\
- \big(\dot{\mathbf{R}}(\phi_e)\dot{\phi}_e \begin{bmatrix} f_x(\alpha) \\ f_y(\alpha) \end{bmatrix} + \mathbf{R}(\phi_e) \begin{bmatrix} f'_x\dot{\alpha} \\ f'_y\dot{\alpha} \end{bmatrix} \big) \Big) - \frac{\partial \boldsymbol{q}_d}{\partial s}\dot{s}, \\
\dot{\phi}_e = \omega - \dot{\phi}_d - f'_\phi\dot{\alpha},
\end{aligned} \tag{6.5}$$

where $f'_x = \frac{\partial f_x}{\partial \alpha}$, $f'_y = \frac{\partial f_y}{\partial \alpha}$, and $f'_\phi = \frac{\partial f_\phi}{\partial \alpha}$. For the convenience of control design later, equations in (6.5) can be represented in vector form as

$$\begin{aligned}
\dot{\boldsymbol{q}}_e &= \mathbf{Q}\begin{bmatrix} v \\ \dot{\alpha} \end{bmatrix} + \boldsymbol{\Delta}_1 + \boldsymbol{\Delta}_2\dot{\phi}_e - \frac{\partial \boldsymbol{q}_d}{\partial s}\dot{s}, \\
\dot{\phi}_e &= \omega - \dot{\phi}_d - f'_\phi\dot{\alpha},
\end{aligned} \tag{6.6}$$

where the terms $\mathbf{Q}$, $\boldsymbol{\Delta}_1$ and $\boldsymbol{\Delta}_2$ have denoted as

$$\begin{aligned}
\mathbf{Q} &= \begin{bmatrix} \mathbf{R}(-\phi_d)\begin{bmatrix} \cos(\phi) \\ \sin(\phi) \end{bmatrix} & -\mathbf{R}(\phi_e)\begin{bmatrix} f'_x \\ f'_y \end{bmatrix} \end{bmatrix}, \\
\boldsymbol{\Delta}_1 &= \begin{bmatrix} -\sin(-\phi_d) & -\cos(-\phi_d) \\ \cos(-\phi_d) & -\sin(-\phi_d) \end{bmatrix} \begin{bmatrix} x \\ y \end{bmatrix}, \\
\boldsymbol{\Delta}_2 &= -\begin{bmatrix} -\sin(\phi_e) & -\cos(\phi_e) \\ \cos(\phi_e) & -\sin(\phi_e) \end{bmatrix} \begin{bmatrix} f_x(\alpha) \\ f_y(\alpha) \end{bmatrix},
\end{aligned} \tag{6.7}$$

It can be seen that the "additional control input" $\dot{\alpha}$ emerges in the representation of the first equation of (6.6). To make this equation solvable for inputs $u, \dot{\alpha}$, the

matrix $\mathbf{Q}$ must be invertible. As such, the first equation of (6.7) described to $\mathbf{Q}$ is expanded to give

$$\mathbf{Q} = \begin{bmatrix} \cos(\phi - \phi_d) & -\cos(\phi_e) f'_x + \sin(\phi_e) f'_y \\ \sin(\phi - \phi_d) & -\sin(\phi_e) f'_x - \cos(\phi_e) f'_y \end{bmatrix}. \tag{6.8}$$

If f'_x and f'_y are carefully selected in (6.8), the matrix $\mathbf{Q}$ will be invertible, i.e., $det(\mathbf{Q})$ is nonzero. Hence, the determinant of the matrix $\mathbf{Q}$ is

$$det(\mathbf{Q}) = \sin(\phi_e) f'_x - \cos(\phi_e) f'_y. \tag{6.9}$$

With the assumptions of boundedness and differentiable of f_x, f_y, and f_ϕ have already made above, we choose those functions following the works in [5, 141]

$$f_x = \gamma_1 \sin(\alpha) \frac{\sin(f_\phi)}{f_\phi}; f_y = \gamma_1 \sin(\alpha) \frac{1 - \cos(f_\phi)}{f_\phi}; f_\phi = \gamma_2 \cos(\alpha), \tag{6.10}$$

where, the constants γ_1 and γ_2 are chosen such that

$$\gamma_1 > 0, \quad 0 < \gamma_2 < \frac{\pi}{2}. \tag{6.11}$$

Based on the proper selections in (6.10) and (6.11), it can be easily calculated that

$$\begin{aligned} &|f_x| \leq \gamma_1; \quad |f_y| \leq \gamma_1; \quad |f_\phi| \leq \gamma_2, \\ &det(\mathbf{Q}) = -\frac{\gamma_1 \gamma_2}{(\gamma_2 \cos(\alpha))^2} \big(\cos(\gamma_2 \cos(\alpha)) - 1 \big) \\ &\Rightarrow |det(\mathbf{Q})| \geq \frac{\gamma_1}{\gamma_2} (1 - \cos(\gamma_2)). \end{aligned} \tag{6.12}$$

The inverse of the matrix $\mathbf{Q}$ is also obtained as follows

$$\mathbf{Q}^{-1} = \frac{1}{det(\mathbf{Q})} \begin{bmatrix} -\sin(\phi_e) f'_x - \cos(\phi_e) f'_y & \cos(\phi_e) f'_x - \sin(\phi_e) f'_y \\ -\sin(\phi - \phi_d) & \cos(\phi - \phi_d) \end{bmatrix}. \tag{6.13}$$

Remark. Through the particular coordinate transformations in (6.3), the "additional control "$\dot{\alpha}$ is created in (6.5). Hence, the nonholonomic constraint problem is overcome, i.e., three control inputs v, ω, and $\dot{\alpha}$ for three state variables x, y, and ϕ. This "additional control"$\dot{\alpha}$ is not available if the coordinate transformations in [39, 41, 53] are employed to describe the tracking errors. In practice, the problem of tracking non-admissible paths which are not solutions to the system's equations is addressed by introducing bounded and smooth functions $f_{(\bullet)}(\alpha)$. With the existence of practical stabilization, the reference paths must not be feasible. Therefore, the applicability in path planning is extended. In other words, it can be described as follows

$$\begin{aligned} \|\boldsymbol{q} - \boldsymbol{q}_d\| &\leq \|\boldsymbol{q}_e\| + |f_x(\alpha), f_y(\alpha)|, \\ |\phi - \phi_d| &\leq |\phi_e| + |f_\phi(\alpha)|, \end{aligned} \tag{6.14}$$

with boundedness of functions $f_x(\alpha), f_y(\alpha)$ and $f_\phi(\alpha)$ have been made in (6.2) for all $\alpha \in \mathbb{R}$. This implies that if the proposed controllers are designed properly to stabilize $\boldsymbol{q}_e$ and ϕ_e at the origin, tracking errors, i.e., $\|\boldsymbol{q} - \boldsymbol{q}_d\|$ and $|\phi - \phi_d|$, are eventually converge to the bounds of $|f_x(\alpha), f_y(\alpha)|$ and $|f_\phi(\alpha)|$, respectively. These bounds can be made arbitrarily small by choosing proper control parameters. This is how practical stabilization is obtained and is re-stated clearly in the control objective later.

6.1.2 Control objective

In regard to the practical control for path tracking and collision avoidance, the following assumptions are made to the reference path, sensing capability and measurements of the WMR's state variables. These assumptions will simplify the control design and associated stability analysis.

Assumption 6.1.1

The reference path $\boldsymbol{q}_d(s(t)) = \begin{bmatrix} x_d(s(t)) & y_d(s(t)) \end{bmatrix}^T$ *is parameterized by a path parameter* s *which is a time-dependent variable and its first derivative. Let* s_d *be the desired value of the path parameter* s*, and the first derivative of* $s_d(t)$ *is bounded by a strictly positive constants* ϵ_0 *and* ϵ_1*,*

$$\epsilon_0 \leq |\dot{s}_d(t)| \leq \epsilon_1, \qquad \forall t \geq 0. \tag{6.15}$$

Moreover, the vector $\boldsymbol{q}_d(s)$ *is regular and differentiable with respect to* s *at least two times and satisfies the bounded conditions*

$$\begin{aligned} &x_d'^2(s) + y_d'^2(s) \geq \epsilon_2, \qquad \forall s \in \mathbb{R}, \\ &\|\dot{\boldsymbol{q}}_d\| \leq \epsilon_3, \quad \|\ddot{\boldsymbol{q}}_d\| \leq \epsilon_4, \end{aligned} \tag{6.16}$$

where $x_d'(s) = \frac{\partial x_d}{\partial s}$ and $y_d'(s) = \frac{\partial y_d}{\partial s}$, and ϵ_2, ϵ_3 and ϵ_4 are strictly positive constants.

Assumption 6.1.2

There exists a strictly positive constant ϵ_5 *such that the desired linear velocity* $v_d(t)$ *is bounded*

$$|v_d(t)| = \sqrt{x_d'^2(s) + y_d'^2(s)}|\dot{s}(t)| \leq \epsilon_5. \tag{6.17}$$

Assumption 6.1.3

The relative position between the WMR and the closest point on an obstacle are accurately measurable for feedback. The WMR has a physical safety ball with a radius R_{safe}, and sensing circular area, R_{sen}, denotes the radius of the region in which the WMR can detect the presence of an obstacle.

Assumption 6.1.4

The obstacle is static and it is considered as a convex polygon whose position, $\boldsymbol{q}_{obs} = \begin{bmatrix} x_{obs} & y_{obs} \end{bmatrix}^T$, and distance of influence, R_{obs} can be accurately measured.

Assumption 6.1.5

There exists a strictly positive constant ϵ_6 such that at the initial time t_0, the WMR initializes at a location $\boldsymbol{q}(t_0) = \begin{bmatrix} x(t_0) & y(t_0) \end{bmatrix}^T$ where it keeps a safe distance from any obstacle with coordinates $\boldsymbol{q}_{obs} = \begin{bmatrix} x_{obs} & y_{obs} \end{bmatrix}^T$ near by

$$\|\boldsymbol{q}(t_0) - \boldsymbol{q}_{obs}\| \geq \epsilon_6,$$

where, $\epsilon_6 \geq \mu_2 + (R_{safe} + R_{obs})$ and μ_2 is a positive constant defined in (6.19).

Remark. 1. The desired linear velocity v_d of the virtual reference vehicle in (6.17) moving on the reference path $\boldsymbol{q}_d$ is specified by the derivative of the path parameter $\dot{s}$ in (6.15). This indicates how fast the WMR should move through $\dot{\boldsymbol{q}}_d$. This chapter aims to obtain the practical stabilization of arbitrary smooth reference paths, including fixed points and non-admissible paths for the position and orientation of the WMR in this chapter. Therefore, the PE condition which normally imposes on the desired linear velocity v_d of the path tracking problem only is not needed.

2. Under the first condition in (6.16), the desired angular velocity described below is well-defined as it is derived from the desired orientation of the virtual reference model.

$$\begin{aligned} \phi_d &= \arctan\Big(\frac{y_d'(s)}{x_d'(s)}\Big), \\ \omega_d(t) = \dot{\phi}_d &= \frac{y_d''(s)x_d'(s) - x_d''(s)y_d'(s)}{x_d'^2(s) + y_d'^2(s)}\dot{s}(t), \end{aligned} \tag{6.18}$$

where the second order partial derivative notations are used: $x_d''(s) = \frac{\partial^2 x_d}{\partial s^2}$ and $y_d''(s) = \frac{\partial^2 y_d}{\partial s^2}$, see Figure (4.1) for visual illustration of ϕ_d.

3. The condition in Assumption 6.1.5 is necessary for the WMR to avoid colliding with any obstacle in the workspace at the initial time t_0.

Control objective

Under the assumptions made above, practical control laws for the path tracking and collision avoidance problems are considered. As such, the controllers practically stabilize the WMR system to arbitrary reference paths with small bounded errors. The WMR asymptotically moves along the reference path at a desired linear velocity $v_d(t)$ while it is capable of avoiding obstacles without any switching control scheme. Fundamentally, for any initial conditions $\boldsymbol{q}(t_0) \in \mathbb{R}^2$ and $\phi(t_0) \in \mathbb{R}$ with $t \geq t_0 \geq 0$, the torque control input vector $\boldsymbol{\tau} = \begin{bmatrix} \tau_v & \tau_\omega \end{bmatrix}^T$ is designed to guarantee

$$\begin{aligned} &\lim_{t\to\infty} \|\boldsymbol{q}(t) - \boldsymbol{q}_d(s(t))\| \leq \mu_0, \\ &\lim_{t\to\infty} |\phi(t) - \phi_d(s(t))| \leq \mu_1, \\ &\|\boldsymbol{q}(t) - \boldsymbol{q}_{obs}\| - (R_{safe} + R_{obs}) \geq \mu_2, \end{aligned} \tag{6.19}$$

where μ_0, μ_1 and μ_2 are strictly positive constants.

6.2 Control design

The control design comprises two steps. In the first step, virtual inputs $v, \dot{\alpha}$ and ω are considered as control signals to stabilize $\boldsymbol{q}_e$ and ω_e at the origin. In the second step, the actual control inputs τ_v and τ_ω are designed to stabilize the linear and angular velocity errors v_e, ω_e and virtual controls at the origin.

6.2.1 Design step 1

As mentioned above, control inputs $v, \dot{\alpha}$ and ω in the kinematic model (6.6) are designed to asymptotically stabilize $\boldsymbol{q}_e$ and ω_e at the origin and to guarantee no collision between the WMR and obstacle within the sensing range. Hence, the following variables are introduced

$$\begin{aligned} v_e &= v - \zeta_v, \\ \omega_e &= \omega - \zeta_\omega, \end{aligned} \tag{6.20}$$

where ζ_v and ζ_ω are virtual controls of v and ω, respectively. To design these virtual controls, the Lyapunov-based potential function is considered:

$$V_1 = \frac{1}{2}\boldsymbol{q}_e^T\boldsymbol{q}_e + \frac{1}{2}\phi_e^2 + \beta. \tag{6.21}$$

It is noted that the collision avoidance function β in equation (6.21) is the same as the function β defined by (4.14) in Chapter 4. Therefore, it is not necessary to duplicate it in this chapter. Readers might refer back to Chapter 4 for the definition and associated properties of the collision avoidance function. Differentiating both sides of (6.21) along the solutions of (6.6) gives

$$\begin{aligned}\dot{V}_1 &= \boldsymbol{q}_e^T\dot{\boldsymbol{q}}_e + \phi_e\dot{\phi}_e + \beta'(\boldsymbol{q}-\boldsymbol{q}_{obs})^T\dot{\boldsymbol{q}} \\ &= \big(\boldsymbol{q}_e + \beta'(\boldsymbol{q}-\boldsymbol{q}_{obs})\big)^T\Big(\mathbf{Q}\begin{bmatrix} v_e+\zeta_v \\ \dot{\alpha}\end{bmatrix} + \boldsymbol{\Delta}_1 + \boldsymbol{\Delta}_2(\omega_e+\zeta_\omega-\dot{\phi}_d-f'_\phi\dot{\alpha}) \\ &\quad - \frac{\partial \boldsymbol{q}_d}{\partial s}\dot{s}\Big) + \phi_e(\omega_e+\zeta_\omega-\dot{\phi}_d-f'_\phi\dot{\alpha}) + \beta'(\boldsymbol{q}-\boldsymbol{q}_{obs})\frac{\partial \boldsymbol{q}_d}{\partial s}\dot{s}, \end{aligned} \tag{6.22}$$

Using denotation $\big(\boldsymbol{q}_e + \beta'(\boldsymbol{q}-\boldsymbol{q}_{obs})\big) = \boldsymbol{\Omega}$ where $\boldsymbol{\Omega}^T = [\Omega_x \quad \Omega_y]$ and $\beta' = \frac{\partial\beta}{\partial(\|\boldsymbol{q}-\boldsymbol{q}_{obs}\|^2/2)}$, virtual controls ζ_v, ζ_ω and $\dot{\alpha}$ can be chosen as:

$$\begin{aligned}\begin{bmatrix}\zeta_v \\ \dot{\alpha}\end{bmatrix} &= \mathbf{Q}^{-1}(-\mathbf{K}\boldsymbol{\Omega} - \boldsymbol{\Delta}_1 + \frac{\partial \boldsymbol{q}_d}{\partial s}\dot{s}), \\ \zeta_\omega &= -k_3\phi_e + \dot{\phi}_d + f'_\phi\dot{\alpha},\end{aligned} \tag{6.23}$$

where $\mathbf{Q}$ has been already proven to be invertible in (6.13), $\mathbf{K} = diag(k_1, k_2)$ is a diagonal positive constant matrix, and k_3 is a positive constant. Substituting chosen virtual control inputs (6.23) into (6.22) yields

$$\begin{aligned}\dot{V}_1 &= -\boldsymbol{\Omega}^T\mathbf{K}\boldsymbol{\Omega} - k_3\phi_e^2 + \boldsymbol{\Omega}^T\Big(\mathbf{Q}\begin{bmatrix} v_e \\ 0\end{bmatrix} - k_3\boldsymbol{\Delta}_2\phi_e\Big) + \omega_e(\phi_e + \boldsymbol{\Omega}^T\boldsymbol{\Delta}_2) \\ &\quad + \beta'(\boldsymbol{q}-\boldsymbol{q}_{obs})\frac{\partial \boldsymbol{q}_d}{\partial s}\dot{s}.\end{aligned} \tag{6.24}$$

Furthermore, the closed-loop system of the kinematic model is obtained as equations (6.20) and (6.23) are substituted into equation (6.7) as follows

$$\begin{aligned}\dot{\boldsymbol{q}}_e &= -\mathbf{K}\boldsymbol{\Omega} + \mathbf{Q}\begin{bmatrix} v_e \\ 0\end{bmatrix} + \boldsymbol{\Delta}_2(-k_3\phi_e + \omega_e), \\ \dot{\phi}_e &= -k_3\phi_e + \omega_e.\end{aligned} \tag{6.25}$$

6.2.2 Design step 2

To facilitate the design of the actual control input vector $\boldsymbol{\tau} = \begin{bmatrix}\tau_v & \tau_\omega\end{bmatrix}^T$, we take the time derivative of both sides of equations (6.20) and substitute into the equation of the dynamic model of the WMR in (6.1) to have

$$\begin{bmatrix}\dot{v}_e \\ \dot{\omega}_e\end{bmatrix} = \bar{\mathbf{C}}\begin{bmatrix}\omega^2 \\ -v\omega\end{bmatrix} - \bar{\mathbf{D}}\begin{bmatrix}v \\ \omega\end{bmatrix} + \bar{\mathbf{B}}\boldsymbol{\tau} - \begin{bmatrix}\dot{\zeta}_v \\ \dot{\zeta}_\omega\end{bmatrix}, \tag{6.26}$$

where the first derivative of ζ_v and ζ_ω with respect to their all components are fully taken as follows

$$\begin{aligned}\dot{\zeta}_v &= \frac{\partial \zeta_v}{\partial \boldsymbol{q}_e}\dot{\boldsymbol{q}}_e + \frac{\partial \zeta_v}{\partial \dot{\boldsymbol{q}}_d}\ddot{\boldsymbol{q}}_d + \frac{\partial \zeta_v}{\partial \phi_d}\dot{\phi}_d + \frac{\partial \zeta_v}{\partial \dot{\phi}_d}\ddot{\phi}_d + \frac{\partial \zeta_v}{\partial x}\dot{x} + \frac{\partial \zeta_v}{\partial y}\dot{y} + \frac{\partial \zeta_v}{\partial \alpha}\dot{\alpha},\\ \dot{\zeta}_\omega &= \frac{\partial \zeta_\omega}{\partial \boldsymbol{q}_e}\dot{\boldsymbol{q}}_e + \frac{\partial \zeta_\omega}{\partial \dot{\boldsymbol{q}}_d}\ddot{\boldsymbol{q}}_d + \frac{\partial \zeta_\omega}{\partial \phi_d}\dot{\phi}_d + \frac{\partial \zeta_\omega}{\partial \dot{\phi}_d}\ddot{\phi}_d + \frac{\partial \zeta_\omega}{\partial x}\dot{x} + \frac{\partial \zeta_\omega}{\partial y}\dot{y} + \frac{\partial \zeta_\omega}{\partial \alpha}\dot{\alpha}.\end{aligned} \tag{6.27}$$

Now considering the Lyapunov function candidate

$$V_2 = V_1 + \frac{1}{2}\begin{bmatrix} v_e & \omega_e \end{bmatrix}\bar{\mathbf{C}}^{-1}\begin{bmatrix} v_e \\ \omega_e \end{bmatrix}. \tag{6.28}$$

Taking the time derivative on both sides of (6.28) along the solutions of (6.24) and (6.26) we obtain the following expression

$$\begin{aligned}\dot{V}_2 = -\boldsymbol{\Omega}^T\mathbf{K}\boldsymbol{\Omega} - k_3\phi_e^2 - k_3\boldsymbol{\Omega}^T\boldsymbol{\Delta}_2\phi_e + \begin{bmatrix} v_e & \omega_e \end{bmatrix}\bar{\mathbf{C}}^{-1}\Big\{\bar{\mathbf{C}}\begin{bmatrix} \omega^2 \\ -v\omega \end{bmatrix} - \bar{\mathbf{D}}\begin{bmatrix} v_e+\zeta_v \\ \omega_e+\zeta_\omega \end{bmatrix}\\ + \bar{\mathbf{B}}\boldsymbol{\tau} - \begin{bmatrix} \dot{\zeta}_v \\ \dot{\zeta}_\omega \end{bmatrix} + \bar{\mathbf{C}}\begin{bmatrix} \boldsymbol{\Omega}^T\mathbf{Q}\begin{bmatrix} 1 & 0 \end{bmatrix}^T \\ (\phi_e + \boldsymbol{\Omega}^T\boldsymbol{\Delta}_2) \end{bmatrix}\Big\} + \beta'(\boldsymbol{q}-\boldsymbol{q}_{obs})\frac{\partial \boldsymbol{q}_d}{\partial s}\dot{s}.\end{aligned} \tag{6.29}$$

For the convenience of calculation, $\dot{V}_2$ can be rearranged as

$$\dot{V}_2 = -\boldsymbol{\Omega}^T\mathbf{K}\boldsymbol{\Omega} - k_3\phi_e^2 - k_3\boldsymbol{\Omega}^T\boldsymbol{\Delta}_2\phi_e + \beta'(\boldsymbol{q}-\boldsymbol{q}_{obs})\frac{\partial \boldsymbol{q}_d}{\partial s}\dot{s} + \Pi_1 + \Pi_2, \tag{6.30}$$

where Π_1 and Π_2 have been denoted as

$$\begin{aligned}\Pi_1 &= v_e\big(\omega^2 - (\bar{\bar{d}}_{11}v_e + \bar{\bar{d}}_{12}\omega_e) - (\bar{\bar{d}}_{11}\zeta_v + \bar{\bar{d}}_{12}\zeta_\omega) - \frac{1}{\bar{c}_1}\dot{\zeta}_v + \boldsymbol{\Omega}^T\mathbf{Q}\begin{bmatrix} 1 \\ 0 \end{bmatrix}\\ &\quad + \bar{\bar{b}}_{11}\tau_v + \bar{\bar{b}}_{12}\tau_\omega\big),\\ \Pi_2 &= \omega_e\big(-v\omega - (\bar{\bar{d}}_{21}v_e + \bar{\bar{d}}_{22}\omega_e) - (\bar{\bar{d}}_{21}\zeta_v + \bar{\bar{d}}_{22}\zeta_\omega) - \frac{1}{\bar{c}_2}\dot{\zeta}_\omega\\ &\quad + (\phi_e + \boldsymbol{\Omega}^T\boldsymbol{\Delta}_2) + \bar{\bar{b}}_{21}\tau_v\omega_e + \bar{\bar{b}}_{22}\tau_\omega\omega_e\big).\end{aligned} \tag{6.31}$$

Coefficients have been denoted in (6.31) as follows: $\bar{\bar{d}}_{11} = \frac{\bar{d}_{11}}{\bar{c}_1}; \bar{\bar{d}}_{12} = \frac{\bar{d}_{12}}{\bar{c}_1}; \bar{\bar{b}}_{11} = \frac{\bar{b}_{11}}{\bar{c}_1}; \bar{\bar{b}}_{12} = \frac{\bar{b}_{12}}{\bar{c}_1}; \bar{\bar{d}}_{21} = \frac{\bar{d}_{21}}{\bar{c}_2}; \bar{\bar{d}}_{22} = \frac{\bar{d}_{22}}{\bar{c}_2}; \bar{\bar{b}}_{21} = \frac{\bar{b}_{21}}{\bar{c}_2}; \bar{\bar{b}}_{22} = \frac{\bar{b}_{22}}{\bar{c}_2}$.

Also, properties of the Young's inequality with the positive constant κ and the Lower bound for the smallest eigenvalue of a symmetric matrix in Chapter 2 are applied to coupling terms in (6.30) and (6.31) to give

$$\begin{aligned}\boldsymbol{\Omega}^T\boldsymbol{\Delta}_2\phi_e &\le \kappa\boldsymbol{\Omega}^T\boldsymbol{\Omega}\|\boldsymbol{\Delta}_2\|^2 + \frac{1}{4\kappa}\phi_e^2,\\ (\bar{\bar{d}}_{12} + \bar{\bar{d}}_{21})v_e w_e &\le (\bar{\bar{d}}_{12} + \bar{\bar{d}}_{21})\big(\kappa v_e^2 + \frac{1}{4\kappa}w_e^2\big),\\ -\boldsymbol{\Omega}^T\mathbf{K}\boldsymbol{\Omega} &\le -\lambda_{min}(\mathbf{K})\boldsymbol{\Omega}^T\boldsymbol{\Omega}.\end{aligned} \tag{6.32}$$

where $\lambda_{min}(\bullet)$ denotes the minimum eigenvalue of the symmetric matrix $\mathbf{K}$. Moreover, from the definition of $\boldsymbol{\Delta}_2$ in (6.12) we have that

$$\boldsymbol{\Delta}_2 = \begin{bmatrix} -(\sin(\phi_e)f_x(\alpha) + \cos(\phi_e)f_y(\alpha)) \\ (\cos(\phi_e)f_x(\alpha) - \sin(\phi_e)f_y(\alpha)) \end{bmatrix}. \tag{6.33}$$

Using the upper bounds of f_x, f_y in (6.12), the norm of $\boldsymbol{\Delta}_2$ can be calculated

$$\begin{aligned} \|\boldsymbol{\Delta}_2\| &= \sqrt{f_x^2(\alpha) + f_y^2(\alpha)} \\ &\leq \sqrt{2}\gamma_1. \end{aligned} \tag{6.34}$$

Substituting (6.34) into the first inequality in (6.32) with $\kappa = 1/2$ and then using these results to substitute back into (6.30) and (6.31) to obtain the following inequality

$$\begin{aligned} \dot{V}_2 \leq & -\big(\lambda_{min}(\mathbf{K}) - k_3\gamma_1^2\big)\boldsymbol{\Omega}^T\boldsymbol{\Omega} - \frac{k_3}{2}\phi_e^2 - (\bar{\bar{d}}_{11} - \frac{\bar{\bar{d}}_{12} + \bar{\bar{d}}_{21}}{2})v_e^2 \\ & - (\bar{\bar{d}}_{22} - \frac{\bar{\bar{d}}_{12} + \bar{\bar{d}}_{21}}{2})\omega_e^2 + \beta'(\boldsymbol{q} - \boldsymbol{q}_{obs})\frac{\partial \boldsymbol{q}_d}{\partial s}\dot{s} \\ & + \Big[v_e\big(\Upsilon_1 + (\bar{\bar{b}}_{11}\tau_v + \bar{\bar{b}}_{12}\tau_\omega)\big) + \omega_e\big(\Upsilon_2 + (\bar{\bar{b}}_{21}\tau_v + \bar{\bar{b}}_{22}\tau_\omega)\big)\Big], \end{aligned} \tag{6.35}$$

where constants Υ_1 and Υ_2 have been denoted as

$$\begin{aligned} \Upsilon_1 &= \omega^2 - (\bar{\bar{d}}_{11}\zeta_v + \bar{\bar{d}}_{12}\zeta_\omega) - \frac{1}{\bar{c}_1}\dot{\zeta}_v + \boldsymbol{\Omega}^T\mathbf{Q}\begin{bmatrix}1\\0\end{bmatrix}, \\ \Upsilon_2 &= -v\omega - (\bar{\bar{d}}_{21}\zeta_v + \bar{\bar{d}}_{22}\zeta_\omega) - \frac{1}{\bar{c}_2}\dot{\zeta}_\omega + (\phi_e + \boldsymbol{\Omega}^T\boldsymbol{\Delta}_2). \end{aligned}$$

This suggests us to choose the actual torque control $\boldsymbol{\tau} = [\tau_v \quad \tau_w]^T$ as follows

$$\begin{aligned} \tau_v &= \frac{-\bar{\bar{b}}_{22}}{\bar{\bar{b}}_{11}\bar{\bar{b}}_{22} - \bar{\bar{b}}_{12}\bar{\bar{b}}_{21}}\big(k_4 v_e + \Upsilon_1\big) + \frac{\bar{\bar{b}}_{12}}{\bar{\bar{b}}_{11}\bar{\bar{b}}_{22} - \bar{\bar{b}}_{12}\bar{\bar{b}}_{21}}\big(k_5\omega_e + \Upsilon_2\big), \\ \tau_w &= \frac{\bar{\bar{b}}_{21}}{\bar{\bar{b}}_{11}\bar{\bar{b}}_{22} - \bar{\bar{b}}_{12}\bar{\bar{b}}_{21}}\big(k_4 v_e + \Upsilon_1\big) - \frac{\bar{\bar{b}}_{11}}{\bar{\bar{b}}_{11}\bar{\bar{b}}_{22} - \bar{\bar{b}}_{12}\bar{\bar{b}}_{21}}\big(k_5\omega_e + \Upsilon_2\big). \end{aligned} \tag{6.36}$$

where k_4 and k_5 are positive constants. It can be easily seen that actual controls τ_v and τ_w are well-defined since:

$$\begin{aligned} \bar{\bar{\mathbf{B}}} &= \begin{bmatrix} \bar{c}_1^{-1} & 0 \\ 0 & \bar{c}_2^{-1} \end{bmatrix}\begin{bmatrix} \bar{b}_{11} & \bar{b}_{12} \\ \bar{b}_{21} & \bar{b}_{22} \end{bmatrix} = \begin{bmatrix} \bar{\bar{b}}_{11} & \bar{\bar{b}}_{12} \\ \bar{\bar{b}}_{21} & \bar{\bar{b}}_{22} \end{bmatrix}, \\ det(\bar{\bar{\mathbf{B}}}) &= \bar{\bar{b}}_{11}\bar{\bar{b}}_{22} - \bar{\bar{b}}_{12}\bar{\bar{b}}_{21} = -\frac{r^2}{2bc^2} \neq 0. \end{aligned}$$

where, all these terms $\bar{c}_1, \bar{c}_2, \bar{b}_{11}, \bar{b}_{12}, \bar{b}_{21}$ and $\bar{b}_{22}$ are defined in (2.51). After substituting the control vector $\boldsymbol{\tau} = [\tau_v \quad \tau_w]^T$ designed in (6.36) into (6.35), the

following result is achieved:

$$\begin{aligned}\dot{V}_2 \leq & -\big(\lambda_{min}(\mathbf{K}) - k_3\gamma_1^2\big)\boldsymbol{\Omega}^T\boldsymbol{\Omega} - \frac{k_3}{2}\phi_e^2 - (k_4 + \bar{\bar{d}}_{11} - \frac{\bar{\bar{d}}_{12} + \bar{\bar{d}}_{21}}{2})v_e^2 \\ & - (k_5 + \bar{\bar{d}}_{22} - \frac{\bar{\bar{d}}_{12} + \bar{\bar{d}}_{21}}{2})\omega_e^2 + \beta'(\boldsymbol{q} - \boldsymbol{q}_{obs})\frac{\partial \boldsymbol{q}_d}{\partial s}\dot{s}.\end{aligned} \tag{6.37}$$

Under proper selection of the constant matrix $\mathbf{K}$ and constant values of $k_3, k_4, k_5, \gamma_1, \gamma_2$ to satisfy the following conditions

$$\begin{aligned}&\lambda_{min}(\mathbf{K}) - k_3\gamma_1^2 \geq \delta_3, \\ &k_4 + \bar{\bar{d}}_{11} - \frac{\bar{\bar{d}}_{12} + \bar{\bar{d}}_{21}}{2} \geq \delta_4, \\ &k_5 + \bar{\bar{d}}_{22} - \frac{\bar{\bar{d}}_{12} + \bar{\bar{d}}_{21}}{2} \geq \delta_5,\end{aligned} \tag{6.38}$$

where δ_3, δ_4, and δ_5 are positive constants, and then (6.37) becomes

$$\dot{V}_2 \leq -W, \tag{6.39}$$

where, $W = \delta_3\boldsymbol{\Omega}^T\boldsymbol{\Omega} + \frac{k_3}{2}\phi_e^2 + \delta_4 v_e^2 + \delta_5\omega_e^2 - \beta'(\boldsymbol{q} - \boldsymbol{q}_{obs})\frac{\partial \boldsymbol{q}_d}{\partial s}\dot{s}$. The closed-loop feedback system for the WMR can be rewritten by substituting (6.36) into (6.26) as follows

$$\begin{aligned}\dot{\boldsymbol{q}}_e &= -\mathbf{K}\boldsymbol{\Omega} + \mathbf{Q}\begin{bmatrix} v_e \\ 0 \end{bmatrix} + \boldsymbol{\Delta}_2(-k_3\phi_e + \omega_e), \\ \dot{\phi}_e &= -k_3\phi_e + \omega_e, \\ \begin{bmatrix} \dot{v}_e \\ \dot{\omega}_e \end{bmatrix} &= -\begin{bmatrix} k_4 + \bar{\bar{d}}_{11} & \bar{\bar{d}}_{12} \\ \bar{\bar{d}}_{21} & k_5 + \bar{\bar{d}}_{22} \end{bmatrix}\begin{bmatrix} v_e \\ \omega_e \end{bmatrix} - \begin{bmatrix} \boldsymbol{\Omega}^T\mathbf{Q}\begin{bmatrix} 1 & 0 \end{bmatrix}^T \\ (\phi_e + \boldsymbol{\Omega}^T\boldsymbol{\Delta}_2) \end{bmatrix}\end{aligned} \tag{6.40}$$

From (6.21), including the definition of function β in Chapter 4, it can be seen that the Lyapunov-based potential function V_2 is positive definite and radially unbounded. These properties will be utilized in the next section for the purpose of stability analysis. The control design has been completed and the results are summarized by the following theorem.

Theorem 6.2.1. *Consider the nonholonomic WMR system described by (6.1) and the reference path is regular. Under the Assumptions 6.1.1, 6.1.2, 6.1.3, 6.1.4, and 6.1.5 and coordinate transformation (6.3), the torque control vector $\boldsymbol{\tau}$ defined by (6.36) solves the control objective (6.19) provided that control gains $\mathbf{K}, k_2, k_3$ and constants γ_1, γ_2 are selected to satisfy conditions (6.12), and (6.38). In particular, the following results hold for all initial conditions $\boldsymbol{q}(x(t_0), y(t_0)) \in \mathbb{R}^2$, $\phi_e(t_0) \in \mathbb{R}$ and $(v_e(t_0), \omega_e(t_0)) \in \mathbb{R}^2$:*

1. *The closed-loop system (6.40) is forward complete.*

2. *The position and orientation of the WMR track their reference path in the sense of practical manner indicated in (6.19), and the WMR asymptotically moves along the path tangentially with a desired linear velocity v_d.*

3. *No collisions between the WMR and obstacles have been guaranteed for all $t \geq t_0 \geq 0$. There are no switchings in the controllers.*

6.3 Stability analysis

Stability analysis in this chapter follows techniques used in [3]. While the original work has represented the proof of forward completeness for a group of mobile robots and no collisions between them, this work shows the proof for the closed-loop system of the single WMR and an obstacle. Properties of equilibrium and saddle points are clarified similarly. Hence, Theorem 6.2.1 is proven in two steps. First, there is no collision between the WMR and any obstacle, and the closed-loop system is forward complete [163]. In the second step, stability properties of equilibrium points are carefully investigated.

6.3.1 Proof of no collisions and forward completeness of closed-loop system

Case 1: ***The obstacle is outside of the WMR's sensing detection range or*** $\|\boldsymbol{q}_e\| > R_{sen}$**.**

Case 1 implies that the collision function β defined in (4.13) is inactive and there is no collision. Property 1 of the function β holds, i.e., $\beta = 0$ and $\beta' = 0$. The inequality (6.39) can be replaced as follows

$$\dot{V}_2 \leq -W_2 \leq 0. \tag{6.41}$$

where, $W_2 = \delta_3 \boldsymbol{\Omega}^T \boldsymbol{\Omega} + \frac{k_3}{2}\phi_e^2 + \delta_4 v_e^2 + \delta_5 \omega_e^2$ is nonnegative-valued, radially unbounded, smooth function for all $\boldsymbol{q}_e(t) \in \mathbb{R}^2$, $\phi_e(t) \in \mathbb{R}$, and $\mathbf{v}_e(t) = [v_e(t) \quad \omega_e(t)]^T \in \mathbb{R}^2$. Integrating both sides of the inequality (6.41) from t_0 to t results in

$$\int_{t_0}^{t} W_2(\tau) d\tau \leq V_2(t_0) - V_2(t) \leq V_2(t_0), \tag{6.42}$$

because V_2 is positive definite and radially unbounded, for all $t \geq t_0 \geq 0$. Using definitions of the function V_2 in (6.28) and its components in (6.21), (6.42) can be expressed in details as follows

$$\begin{aligned}&\frac{1}{2}\boldsymbol{q}_e^T(t)\boldsymbol{q}_e(t) + \frac{1}{2}\phi_e^2(t) + \frac{1}{2}\begin{bmatrix} v_e(t) & \omega_e(t)\end{bmatrix}\bar{\mathbf{C}}^{-1}\begin{bmatrix} v_e(t) \\ \omega_e(t)\end{bmatrix} \leq \\ &\frac{1}{2}\boldsymbol{q}_e^T(t_0)\boldsymbol{q}_e(t_0) + \frac{1}{2}\phi_e^2(t_0) + \frac{1}{2}\begin{bmatrix} v_e(t_0) & \omega_e(t_0)\end{bmatrix}\bar{\mathbf{C}}^{-1}\begin{bmatrix} v_e(t_0) \\ \omega_e(t_0)\end{bmatrix},\end{aligned} \tag{6.43}$$

for all $t \geq t_0 \geq 0$. Particularly, as the Assumption 6.1.5 and definitions of ϕ_e and $\mathbf{v}_e$ are considered, the right-hand side of the inequality (6.46) is obviously bounded by a positive constant depending on the initial conditions. Boundedness of the right-hand side of (6.46) implies that the left-hand side of this inequality must also be bounded. Boundedness of the left-hand side of the inequality (6.46) in turn implies that of $\boldsymbol{q}(x(t), y(t)), \phi_e(t), v_e(t)$, and $\omega_e(t)$ for all $t \geq t_0 \geq 0$. This leads to the implication that $\boldsymbol{q}(x(t), y(t)), \phi_e(t), v_e(t)$, and $\omega_e(t)$ do not escape to infinity in finite time. Therefore, the solutions of the closed-loop system (6.40) exist globally for all $t \geq t_0 \geq 0$ by Theorem 6.2.1. This system is forward complete.

Case 2: ***The obstacle is inside the WMR's sensing detection range or*** $R_{safe} + R_{obs} < \|\boldsymbol{q}_e\| < R_{sen}$**.**

Case 2 addresses the situation when the vehicle approaches closely to an obstacle which is within the detection range of the WMR. As the obstacle avoidance is only considered in this case, the parts related to ϕ_e, v_e, ω_e in the expression of V_2 in (6.28) can be neglected in this analysis. The expression of (6.39) becomes

$$\dot{V}_2 \leq -\delta_3\big(\boldsymbol{q}_e + \beta'(\boldsymbol{q} - \boldsymbol{q}_{obs})\big)^T\big(\boldsymbol{q}_e + \beta'(\boldsymbol{q} - \boldsymbol{q}_{obs})\big) + \beta'(\boldsymbol{q} - \boldsymbol{q}_{obs})\frac{\partial \boldsymbol{q}_d}{\partial s}\dot{s}. \tag{6.44}$$

From the notation of $\boldsymbol{\Omega}$ in (6.23), the relative distances, $\|\boldsymbol{q}_e\|$ and $\|\boldsymbol{q} - \boldsymbol{q}_{obs}\|$ are bounded by upper bounds, i.e., $\|\boldsymbol{q}_e\| \leq \epsilon^*$ and $\|\boldsymbol{q} - \boldsymbol{q}_{obs}\| \leq \bar{\epsilon}^*$, where, ϵ^* and $\bar{\epsilon}^*$ are nonnegative bounded constants. Hence, the inequality (6.44) becomes

$$\dot{V}_2 \leq -\delta_3\big(\epsilon^* + \beta'\|\boldsymbol{q} - \boldsymbol{q}_{obs}\|\big)^2 + |v_d|\beta'\|\boldsymbol{q} - \boldsymbol{q}_{obs}\|, \tag{6.45}$$

Due to the fact that $\beta' = f(\frac{1}{\|\boldsymbol{q} - \boldsymbol{q}_{obs}\|^2})$, see (4.12), as the WMR moves inside the ball $\bar{\mathbf{B}}(R(\epsilon^*, \bar{\epsilon}^*))$, then the part $\|\boldsymbol{q}_e\|$ is dominated by $\beta'\|\boldsymbol{q} - \boldsymbol{q}_{obs}\|$, or $\epsilon^* + \beta'\|\boldsymbol{q} - \boldsymbol{q}_{obs}\| \leq \beta'\|\boldsymbol{q} - \boldsymbol{q}_{obs}\|$. In other words, if the WMR is close to the obstacle,

calculation in terms of obstacle avoidance, $\|\boldsymbol{q}-\boldsymbol{q}_{obs}\|$, significantly outweighs the reference tracking, $\|\boldsymbol{q}_e\|$. Obviously, the collision avoidance task is prioritized during this period of time. Therefore, only the term $\|\boldsymbol{q}-\boldsymbol{q}_{obs}\|$ in the right-hand side of (4.60) is taken into consideration, instead of both $\|\boldsymbol{q}_e\|$, and $\|\boldsymbol{q}-\boldsymbol{q}_{obs}\|$. Moreover, for all $(\boldsymbol{q}-\boldsymbol{q}_{obs}) \in \mathbb{R}^2$ and $\beta' \sim \frac{1}{\|\boldsymbol{q}-\boldsymbol{q}_{obs}\|^2}$, it implies $\beta'\|\boldsymbol{q}-\boldsymbol{q}_{obs}\| \leq \lambda^*\beta^{*'}$, where $\beta^{*'} \sim \frac{1}{\|\boldsymbol{q}-\boldsymbol{q}_{obs}\|}$, and λ^* is a positive constant. Completing squares (6.45) gives

$$\dot{V}_2 \leq -\delta_3(\lambda^*\beta^{*'})^2 + |v_d|\lambda^*\beta^{*'} \leq -(\delta_3-\kappa)(\lambda^*\beta^{*'})^2 + \frac{1}{4\kappa}v_d^2. \tag{6.46}$$

where, κ is a positive constant. Hence, by selecting appropriately the control design constants mentioned in (4.38) such that

$$\delta_3 - \kappa > 0, \tag{6.47}$$

the inequality (6.46) results in

$$\dot{V}_2 \leq -\delta_3^*(\lambda^*\beta^{*'})^2 + \frac{1}{4\kappa}v_d^2 \leq -c_1V_2 + c_2, \tag{6.48}$$

where δ_3^*, c_1 and c_2 are some positive constants. The above inequality (6.48) shows that the closed-loop system (6.40) is forward complete. Properties 2 and 6 of function $\beta(t)$ holds as the condition $(R_{safe}+R_{obs}) < \|\boldsymbol{q}_e\| < R_{sen}$ is satisfied, i.e., $0 < \beta(t) \leq \mu_1$, μ_1 is a positive constant, depending on initial conditions for all $t \geq t_0 \geq 0$. Hence, there are no collisions between the WMR and any obstacle for all $t \geq t_0 \geq 0$.

By combining conclusions of Case 1 and Case 2, the solutions of the closed-loop system (6.40) exist globally for all $t \geq t_0 \geq 0$ by Theorem 6.2.1, and this system is forward complete.

6.3.2 Properties of equilibrium points

When collision avoidance is taken into consideration, it is necessary to predict and evaluate the equilibrium points of the controlled systems. As proven in the previous section that there are no collisions between the WMR and any obstacle within the workspace and all states are bounded for all $t \geq t_0 \geq 0$. In this part, Lemma 2.1.10 (Barbalat-like Lemma) will be used to find the equilibrium points, which the trajectory of the closed-loop system (6.40) converge to. Two conditions of the Barbalat-like Lemma will be investigated for satisfaction by considering the

inequality (6.39).

$$\dot{V}_2 \leq -\delta_3 \boldsymbol{\Omega}^T \boldsymbol{\Omega} - \frac{k_3}{2}\phi_e^2 - \delta_4 v_e^2 - \delta_5 \omega_e^2 + \beta'(\boldsymbol{q} - \boldsymbol{q}_{obs})\frac{\partial \boldsymbol{q}_d}{\partial s}\dot{s} = W_2.$$

Denoting $\boldsymbol{\Omega}^T\boldsymbol{\Omega} = A$ then taking derivative of A with respect to t gives

$$|\dot{A}| = 2\delta_3 |\boldsymbol{\Omega}^T \dot{\boldsymbol{\Omega}}| = 2\delta_3 \big|\boldsymbol{\Omega}^T \big(\frac{\partial \boldsymbol{\Omega}}{\partial \boldsymbol{q}_d}\dot{\boldsymbol{q}}_d + \frac{\partial \boldsymbol{\Omega}}{\partial \boldsymbol{q}}\dot{\boldsymbol{q}}_e\big)\big|. \tag{6.49}$$

Now each part of the right-hand side is calculated as follows

$$\begin{aligned} |\dot{A}_1| = 2\delta_3 \big|\boldsymbol{\Omega}^T \frac{\partial \boldsymbol{\Omega}}{\partial \boldsymbol{q}_d}\dot{\boldsymbol{q}}_d\big| \leq 2\delta_3 \big|\boldsymbol{\Omega}^T \frac{\partial \boldsymbol{\Omega}}{\partial \boldsymbol{q}_d}\frac{\partial \boldsymbol{q}_d}{\partial s}\dot{s}\big| &\leq 2\delta_3 \kappa \boldsymbol{\Omega}^T\boldsymbol{\Omega} + \frac{1}{4\kappa}(\epsilon_1\epsilon_3)^2, \\ &\leq k_1^* A. \end{aligned} \tag{6.50}$$

where, $|\dot{s}| \leq \epsilon_1$ and $\|\frac{\partial \boldsymbol{q}_d}{\partial s}\| \leq \epsilon_3$ in Assumptions 6.1.1 and 6.1.2. $k_1^* = 2\delta_3\kappa$ is a positive constant. Using the expression of $\dot{\boldsymbol{q}}_e$ in (6.40) yields

$$\begin{aligned} |\dot{A}_2| = 2\delta_3 |\boldsymbol{\Omega}^T \dot{\boldsymbol{\Omega}}| = 2\delta_3 \big|\boldsymbol{\Omega}^T \big((1+\beta')\mathbf{I} + \beta''(\boldsymbol{q} - \boldsymbol{q}_{obs})^T(\boldsymbol{q} - \boldsymbol{q}_{obs})\big)\times \\ \big(-\mathbf{K}\boldsymbol{\Omega} + \mathbf{Q}\begin{bmatrix} v_e \\ 0 \end{bmatrix} + \boldsymbol{\Delta}_2(-k_3\phi_e + \omega_e)\big)\big|. \end{aligned} \tag{6.51}$$

Properties of function β in Chapter 4 are applied, i.e., $|\beta'| \leq \mu_2$, and $|\beta''(\boldsymbol{q} - \boldsymbol{q}_{obs})^T(\boldsymbol{q} - \boldsymbol{q}_{obs})| \leq \mu_3$. The right-hand side of (6.51) is expanded to different parts for further calculation as follows

$$|\dot{A}_{21}| \leq 2\delta_3(1 + \mu_2 + \mu_3)\lambda_{min}(\mathbf{K})\boldsymbol{\Omega}^T\boldsymbol{\Omega} = k_{21}^* A, \tag{6.52}$$

where, $\lambda_{min}(\mathbf{K})$ is minimum eigenvalue of the constant matrix $\mathbf{K}$, $k_{21}^* = 2\delta_3\big((1 + \mu_2) + \mu_3\big)\lambda_{min}(\mathbf{K})$ is a positive constant. Completing squares gives

$$\begin{aligned} |\dot{A}_{22}| \leq 2\delta_3 \big|\boldsymbol{\Omega}^T(1 + \mu_2 + \mu_3)\mathbf{Q}\begin{bmatrix} v_e \\ 0 \end{bmatrix}\big| &\leq 2\delta_3(1 + \mu_2 + \mu_3)\big(\kappa\boldsymbol{\Omega}^T\boldsymbol{\Omega} + \frac{1}{\kappa}v_e^2\big) \\ &= k_{221}^* A + k_{222}^* v_e^2, \end{aligned} \tag{6.53}$$

where, $\|\mathbf{Q}\| \leq 2\sqrt{2}$, see (6.7), $k_{221}^* = 2\delta_3(1 + \mu_2 + \mu_3)\kappa$, $k_{222}^* = \sqrt{2}\delta_3(1 + \mu_2 + \mu_3)\frac{1}{\kappa}$ are positive constants. Completing squares yields

$$\begin{aligned} |\dot{A}_{23}| &\leq 2\delta_3 \big|\boldsymbol{\Omega}^T(1 + \mu_2 + \mu_3)\big(-\boldsymbol{\Delta}_2 k_3 \phi_e\big)\big| \\ &\leq 2k_3\delta_3(\gamma_1 + \gamma_2)(1 + \mu_2 + \mu_3)\big(\kappa\boldsymbol{\Omega}^T\boldsymbol{\Omega} + \frac{1}{4\kappa}\phi_e^2\big) = k_{231}^* A + k_{232}^* \phi_e^2, \end{aligned} \tag{6.54}$$

where, $\|\mathbf{\Delta}_2\| \leq \sqrt{2(\gamma_1^2+\gamma_2^2)}$, see (6.2) and (6.7), $k_{231}^* = 2k_3\delta_3\sqrt{2(\gamma_1^2+\gamma_2^2)}(1+\mu_2+\mu_3)\kappa$, $k_{232}^* = k_3\delta_3\sqrt{2(\gamma_1^2+\gamma_2^2)}(1+\mu_2+\mu_3)\frac{1}{4\kappa}$ are positive constants. Completing squares yields

$$\begin{aligned}|\dot{A}_{24}| &\leq 2\delta_3\big|\mathbf{\Omega}^T(1+\mu_2+\mu_3)\mathbf{\Delta}_2\omega_e\big| \\ &\leq 2\delta_3\sqrt{2(\gamma_1^2+\gamma_2^2)}(1+\mu_2+\mu_3)\big(\kappa\mathbf{\Omega}^T\mathbf{\Omega}+\frac{1}{4\kappa}\omega_e^2\big) = k_{241}^*A + k_{242}^*\omega_e^2, \quad (6.55)\end{aligned}$$

where, $k_{241}^* = 2\delta_3\sqrt{2(\gamma_1^2+\gamma_2^2)}(1+\mu_2+\mu_3)\kappa$, $k_{242}^* = \delta_3\sqrt{2(\gamma_1^2+\gamma_2^2)}(1+\mu_2+\mu_3)\frac{1}{2\kappa}$ are positive constants.

Denoting $\phi_e^2 = B$ then taking derivative of B with respect to t and substituting $\dot{\phi}_e$ in (6.40) results in

$$\frac{k_3}{2}|\dot{B}| = \frac{k_3}{2}|2\phi_e\dot{\phi}_e| = k_3|\phi_e(-k_3\phi_e+\omega_e)| \leq k_3^2B + k_3\kappa B + \frac{k_3}{4\kappa}\omega_e^2, \quad (6.56)$$

Denoting $v_e^2 = C$ and $\omega_e^2 = D$ then taking derivative of C and D with respect to t and substituting $\dot{v}_e$ and $\dot{\omega}_e$ in (6.40), respectively, yields

$$\delta_4|\dot{C}| = 2\delta_4|v_e\dot{v}_e| = 2\delta_4|v_e\big((-k_4-\bar{\bar{d}}_{11})v_e - \bar{\bar{d}}_{12}\omega_e - \mathbf{\Omega}^T\mathbf{Q}\begin{bmatrix}1 & 0\end{bmatrix}^T\big)|. \quad (6.57)$$

The right-hand side of (6.57) is expanded to different parts for further calculation as follows

$$|\dot{C}_1| = 2\delta_4|v_e\big((-k_4-\bar{\bar{d}}_{11})v_e| \leq 2\delta_4(k_4+\bar{\bar{d}}_{11})v_e^2 = k_{31}^*C, \quad (6.58)$$

where, $k_{31}^* = 2\delta_4(k_4+\bar{\bar{d}}_{11})$ is positive constant. Next, completing squares gives

$$|\dot{C}_2| \leq 2\delta_4\bar{\bar{d}}_{12}(\kappa v_e^2 + \frac{1}{4\kappa}\omega_e^2) = k_{321}^*C + k_{322}^*D, \quad (6.59)$$

where, $k_{321}^* = 2\delta_4\bar{\bar{d}}_{12}\kappa$, $k_{322}^* = \delta_4\bar{\bar{d}}_{12}\frac{1}{2\kappa}$ are positive constants.

$$|\dot{C}_3| = 2\delta_4| - v_e\mathbf{\Omega}^T\mathbf{Q}\begin{bmatrix}1 & 0\end{bmatrix}^T| \leq 2\delta_4(\kappa v_e^2 + \frac{1}{\sqrt{2}\kappa}\mathbf{\Omega}^T\mathbf{\Omega}) = k_{331}^*C + k_{332}^*A \quad (6.60)$$

where, $\|\mathbf{Q}\| \leq 2\sqrt{2}$, $k_{331}^* = 2\delta_4\kappa$, $k_{332}^* = \sqrt{2}\delta_4\frac{1}{\kappa}$ are positive constants.

$$\delta_5|\dot{D}| = 2\delta_5|\omega_e\dot{\omega}_e| = 2\delta_5|\omega_e\big(-\bar{\bar{d}}_{21}v_e - (k_5+\bar{\bar{d}}_{22})\omega_e - (\phi_e + \mathbf{\Omega}^T\mathbf{\Delta}_2)\big)|. \quad (6.61)$$

The right-hand side of (6.61) is expanded to different parts for further calculation as follows

$$|\dot{D}_1| \leq 2\delta_5\bar{\bar{d}}_{21}|\omega_e v_e| \leq 2\delta_5\bar{\bar{d}}_{21}(\kappa|\omega_e^2 + \frac{1}{4\kappa}v_e^2) = k_{411}^*D + k_{412}^*C, \quad (6.62)$$

where, $k^*_{411} = 2\delta_5\bar{\bar{d}}_{21}\kappa$, $k^*_{412} = \delta_5\bar{\bar{d}}_{21}\frac{1}{2\kappa}$ are positive constants.

$$|\dot{D}_2| \leq 2\delta_5(k_5 + \bar{\bar{d}}_{22})\omega_e^2 = k^*_{42}D, \tag{6.63}$$

where, $k^*_{42} = 2\delta_5(k_5 + \bar{\bar{d}}_{22})$ is positive constant. Next, completing squares gives

$$|\dot{D}_3| \leq 2\delta_5(\kappa\omega_e^2 + \frac{1}{4\kappa}\phi_e^2) = k^*_{431}D + k^*_{432}B, \tag{6.64}$$

where, $k^*_{431} = 2\delta_5\kappa$ and $k^*_{432} = \delta_5\frac{1}{2\kappa}$ are positive constants.

$$|\dot{D}_4| = 2\delta_5|\omega_e\big(-\boldsymbol{\Omega}^T\boldsymbol{\Delta}_2)\big)| \leq 2\delta_5(\kappa\omega_e^2 + \sqrt{2(\gamma_1^2+\gamma_2^2)}\frac{1}{4\kappa}\boldsymbol{\Omega}^T\boldsymbol{\Omega}) = k^*_{441}D + k^*_{442}A, \tag{6.65}$$

where, $\|\boldsymbol{\Delta}_2\| \leq \sqrt{2(\gamma_1^2+\gamma_2^2)}$, see (6.2) and (6.7), $k^*_{441} = 2\delta_5\kappa$, $k^*_{412} = \delta_5\sqrt{2(\gamma_1^2+\gamma_2^2)}\frac{1}{2\kappa}$ are positive constants.

The last section has shown $\|\boldsymbol{q}(t)\|$ to be bounded and greater than a positive constant for all $t \geq t_0 \geq 0$. Properties of function β in (4.11), i.e., $|\beta'| \leq \mu_2$ and $|\beta''(\boldsymbol{q}-\boldsymbol{q}_{obs})^T(\boldsymbol{q}-\boldsymbol{q}_{obs})| \leq \mu_3$, can be used for the last calculation. It has been already mentioned $\beta' = f(\frac{1}{\|\boldsymbol{q}-\boldsymbol{q}_{obs}\|^2})$, see (4.12), as the WMR moves inside the ball $\bar{\mathbf{B}}(R(\epsilon^*,\bar{\epsilon}^*))$, then the part $\|\boldsymbol{q}-\boldsymbol{q}_{obs}\|$ is also dominated by β'. Denoting the last part $\beta'(\boldsymbol{q}-\boldsymbol{q}_{obs})\frac{\partial\boldsymbol{q}_d}{\partial s}\dot{s} = E$ then taking derivative of E with respect to t yields

$$|\dot{E}| = \big|\beta''(\boldsymbol{q}-\boldsymbol{q}_{obs})^T(\boldsymbol{q}-\boldsymbol{q}_{obs})\frac{\partial\boldsymbol{q}_d}{\partial s}\dot{s} + (\beta'\frac{\partial\boldsymbol{q}_d}{\partial s}\dot{s})^T\dot{\boldsymbol{q}}_e + \beta'(\boldsymbol{q}-\boldsymbol{q}_{obs})^T\frac{\partial^2\boldsymbol{q}_d}{\partial s^2}\dot{s}\big|. \tag{6.66}$$

The right-hand side of (6.66) is expanded to different parts for further calculation as follows

$$|\dot{E}_1| = |\beta''(\boldsymbol{q}-\boldsymbol{q}_{obs})^T(\boldsymbol{q}-\boldsymbol{q}_{obs})\frac{\partial\boldsymbol{q}_d}{\partial s}\dot{s}| \leq \mu_3\epsilon_1\epsilon_3 \leq k^*_{51}E. \tag{6.67}$$

Subtituting $\dot{\boldsymbol{q}}_e$ in (6.40) into $\dot{E}_2$ below gives

$$|\dot{E}_2| = \big|(\beta'\frac{\partial\boldsymbol{q}_d}{\partial s}\dot{s})^T\dot{\boldsymbol{q}}_e\big| = \big|(\beta'\frac{\partial\boldsymbol{q}_d}{\partial s}\dot{s})^T\big(-\mathbf{K}\boldsymbol{\Omega} + \mathbf{Q}\begin{bmatrix}v_e\\0\end{bmatrix} + \boldsymbol{\Delta}_2(-k_3\phi_e+\omega_e)\big)\big|. \tag{6.68}$$

The right-hand side of (6.68) is expanded to different parts for further calculation as follows

$$\begin{aligned}|\dot{E}_{21}| = \big|(\beta'\frac{\partial\boldsymbol{q}_d}{\partial s}\dot{s})^T\big(-\mathbf{K}\boldsymbol{\Omega}\big)\big| &\leq \lambda_{min}(\mathbf{K})\big(\kappa\boldsymbol{\Omega}^T\boldsymbol{\Omega} + \frac{1}{4\kappa}(\mu_2\epsilon_1\epsilon_3)^2\big)\\ &\leq k^*_{211}A + \lambda_{min}(\mathbf{K})\frac{1}{4\kappa}(\mu_2\epsilon_1\epsilon_3)^2,\end{aligned} \tag{6.69}$$

where, $k^*_{21} = \lambda_{min}(\mathbf{K})\kappa$ is a positive constant.

$$|\dot{E}_{22}| = \big|(\beta'\frac{\partial\boldsymbol{q}_d}{\partial s}\dot{s})^T\mathbf{Q}\begin{bmatrix}v_e\\0\end{bmatrix}\big| \leq 2\sqrt{2}\big(\kappa v_e^2 + \frac{1}{4\kappa}(\mu_2\epsilon_1\epsilon_3)^2\big)$$

$$\leq k_{22}^{*}C + \frac{\sqrt{2}}{2\kappa}(\mu_2\epsilon_1\epsilon_3)^2, \tag{6.70}$$

where, $\|\mathbf{Q}\| \leq 2\sqrt{2}$, $k_{22}^{*} = 2\sqrt{2}\kappa$ is a positive constant.

$$\begin{aligned}|\dot{E}_{23}| = \big|(\beta'\frac{\partial \boldsymbol{q}_d}{\partial s}\dot{s})^T\boldsymbol{\Delta}_2(-k_3\phi_e)\big| &\leq \sqrt{2(\gamma_1^2+\gamma_2^2)}k_3\big(\kappa\phi_e^2 + \frac{1}{4\kappa}(\mu_2\epsilon_1\epsilon_3)^2\big) \\ &\leq k_{23}^{*}B + \sqrt{2(\gamma_1^2+\gamma_2^2)}k_3\frac{1}{4\kappa}(\mu_2\epsilon_1\epsilon_3)^2, \end{aligned} \tag{6.71}$$

where, $\|\boldsymbol{\Delta}_2\| \leq \sqrt{2(\gamma_1^2+\gamma_2^2)}$, $k_{23}^{*} = \sqrt{2(\gamma_1^2+\gamma_2^2)}k_3\kappa$ is a positive constant.

$$\begin{aligned}|\dot{E}_{24}| = \big|(\beta'\frac{\partial \boldsymbol{q}_d}{\partial s}\dot{s})^T\boldsymbol{\Delta}_2\omega_e\big| &\leq \sqrt{2(\gamma_1^2+\gamma_2^2)}\big(\kappa\omega_e^2 + \frac{1}{4\kappa}(\mu_2\epsilon_1\epsilon_3)^2\big) \\ &\leq k_{22}^{*}D + \sqrt{2(\gamma_1^2+\gamma_2^2)}\frac{1}{4\kappa}(\mu_2\epsilon_1\epsilon_3)^2, \end{aligned} \tag{6.72}$$

where, $k_{24}^{*} = \sqrt{2(\gamma_1^2+\gamma_2^2)}\kappa$ is a positive constant.

$$|\dot{E}_3| = \big|\beta'(\boldsymbol{q}-\boldsymbol{q}_{obs})^T\frac{\partial^2 \boldsymbol{q}_d}{\partial s^2}\dot{s}\big| \leq \epsilon_1\epsilon_4 E = k_{53}^{*}E, \tag{6.73}$$

where, $\dot{s} \leq \epsilon_1$, $\frac{\partial^2 \boldsymbol{q}_d}{\partial s^2} \leq \epsilon_4$, see, (6.15) and (6.16). Finally, the upper bounds of $|\dot{A}|$, $|\dot{B}|$, $|\dot{C}|$, $|\dot{D}|$, and $|\dot{E}|$ are grouped and added together to give

$$\begin{aligned} |\dot{A}| &\leq k_A A, \\ |\dot{B}| &\leq k_B B, \\ |\dot{C}| &\leq k_C C, \\ |\dot{D}| &\leq k_D D, \\ |\dot{E}| &\leq k_E E, \end{aligned} \tag{6.74}$$

where, constant $k_{(\bullet)}$ is summary of corresponding constants with respect to function $(\bullet)$. (6.74) can be written in the short form as follows

$$|\frac{dW_2}{dt}| \leq k_\Sigma W, \tag{6.75}$$

where, $|\frac{dW_2}{dt}| \leq |\dot{A}| + |\dot{B}| + |\dot{C}| + |\dot{D}| + |\dot{E}|$. k_Σ is a positive constant, and W is denoted in (6.39). This concludes that the first condition of the Lemma 2.1.10 (Babarlat-like Lemma) holds.

Now the second condition of the Lemma 2.1.10 is examined by integrating both sides of (6.39) to result in

$$\int_0^\infty W_2(t)dt \leq -\int_0^\infty \dot{V}_2(t)dt = V_2(t_0) - V_2(\infty) \leq V_2(t_0) \tag{6.76}$$

Due to the positive definite and radially unbounded function V_2 in (6.28), the right-hand side of the inequality above, i.e., $V_2(t_0)$, is obviously bounded by a

positive constant depending on the initial conditions. Therefore, two conditions of Barbalat-like Lemma hold.

Applying Theorem 8.4 in [57] (see Theorem 2.1.8 in Chapter 2), the convergence of $W(t)$ in (6.39) exists and is finite by

$$\lim_{t\to\infty}\left[\delta_3\boldsymbol{\Omega}^T(t)\boldsymbol{\Omega}(t)+\frac{k_3}{2}\phi_e^2(t)+\delta_4 v_e^2(t)+\delta_5\omega_e^2(t)-\beta'(t)\big(\boldsymbol{q}(t)-\boldsymbol{q}_{obs}\big)\frac{\partial \boldsymbol{q}_d}{\partial s}\dot{s}\right]=0. \tag{6.77}$$

The limit equation (6.77) implies that

$$\begin{aligned}
&\lim_{t\to\infty}\big(\frac{k_3}{2}\phi_e^2(t)+\delta_4 v_e^2(t)+\delta_5\omega_e^2(t)\big)=0,\\
&\lim_{t\to\infty}\Big(\beta'(t)(\boldsymbol{q}(t)-\boldsymbol{q}_{obs})^T\frac{\partial \boldsymbol{q}_d}{\partial s}\dot{s}_d\Big)=0,\\
&\lim_{t\to\infty}\boldsymbol{\Omega}(t)=0.
\end{aligned} \tag{6.78}$$

Because of the positive definite and radially unbounded function V_2, and the proven boundedness of $\phi_e(t), v_e(t)$, and $\omega_e(t)$ for all $t\geq t_0\geq 0$. Moreover, no collision which has already been proven means $\beta'(t)=0$ as $t\to\infty$. Therefore, the first two limits of (6.78) mean those terms globally asymptotically converge to zero. Lastly, from the denotation of $\boldsymbol{\Omega}$ after (6.22), $\lim_{t\to\infty}\boldsymbol{\Omega}(t)=0$ means

$$\lim_{t\to\infty}\Big(\begin{bmatrix}\Omega_x(t)\\ \Omega_y(t)\end{bmatrix}\Big)=\lim_{t\to\infty}\Big(\begin{bmatrix}x(t)-x_d(s(t))\\ y(t)-y_d(s(t))\end{bmatrix}+\beta'(t)\begin{bmatrix}x(t)-x_{obs}\\ y(t)-y_{obs}\end{bmatrix}\Big)=0. \tag{6.79}$$

The equation (6.79) implies that $\boldsymbol{q}=\begin{bmatrix}x(t) & y(t)\end{bmatrix}^T$ approaches either to $\boldsymbol{q}_d=\begin{bmatrix}x_d & y_d\end{bmatrix}^T$ or a vector denoted by $\boldsymbol{q}_c=\begin{bmatrix}x_c & y_c\end{bmatrix}^T$ as $t\to\infty$. This means that the equilibrium points can be $\boldsymbol{q}_d$ or $\boldsymbol{q}_c$. Therefore, it is necessary to investigate the stability properties of these equilibrium points by considering the behavior of the first equation of the closed-loop system (6.40)

$$\dot{\boldsymbol{q}}_e=-\mathbf{K}\boldsymbol{\Omega}+\mathbf{Q}\begin{bmatrix}v_e\\ 0\end{bmatrix}+\boldsymbol{\Delta}_2(-k_3\phi_e+\omega_e). \tag{6.80}$$

Near the equilibrium point $\boldsymbol{q}_{eq}=\begin{bmatrix}x_{eq} & y_{eq}\end{bmatrix}^T$, which can be either $\boldsymbol{q}_d=\begin{bmatrix}x_d & y_d\end{bmatrix}^T$ or $\boldsymbol{q}_c=\begin{bmatrix}x_c & y_c\end{bmatrix}^T$, it can be represented by

$$\dot{\boldsymbol{q}}_e=-\mathbf{K}\frac{\partial\boldsymbol{\Omega}}{\partial\boldsymbol{q}}(\boldsymbol{q}-\boldsymbol{q}_{eq})+\mathbf{Q}\begin{bmatrix}v_e\\ 0\end{bmatrix}+\boldsymbol{\Delta}_2(-k_3\phi_e+\omega_e), \tag{6.81}$$

where the general gradient of $\boldsymbol{\Omega}(t)$ with respect to vector $\boldsymbol{q}$ is given by

$$\frac{\partial \boldsymbol{\Omega}}{\partial \boldsymbol{q}} = \begin{bmatrix} \frac{\partial \boldsymbol{\Omega}}{\partial \Omega_x}\frac{\partial \Omega_x}{\partial x} & \frac{\partial \boldsymbol{\Omega}}{\partial \Omega_x}\frac{\partial \Omega_x}{\partial y} \\ \frac{\partial \boldsymbol{\Omega}}{\partial \Omega_y}\frac{\partial \Omega_y}{\partial x} & \frac{\partial \boldsymbol{\Omega}}{\partial \Omega_y}\frac{\partial \Omega_y}{\partial y} \end{bmatrix} \tag{6.82}$$

In the previous section, the forward completeness of the closed-loop system (6.40), and $\lim_{t\to\infty}\phi_e(t) = 0$, $\lim_{t\to\infty}(v_e(t), \omega_e(t)) = 0$ has already been proven, see (6.78). This implies $\lim_{t\to\infty}\big(\mathbf{Q}\begin{bmatrix} v_e & 0 \end{bmatrix}^T + \boldsymbol{\Delta}_2(-k_2\phi_e + \omega_e)\big) = 0$, see (6.81). Therefore, it is necessary to prove that the desired equilibrium point $\boldsymbol{q}_d$ is locally asymptotically stable and that the saddle point $\boldsymbol{q}_c$ is locally unstable. Consequently, the actual trajectory of the WMR, $\boldsymbol{q}(t)$, must approach the reference path $\boldsymbol{q}_d$ from almost everywhere except from the set described by the assumption 6.1.1 and the set denoted by $\boldsymbol{q}_c$, which is unstable.

Proof of asymptotic stability of an equilibrium point

In order to show that the equilibrium point $\boldsymbol{q}_d(x_d, y_d)$ is locally asymptotically stable, we linearize around a desired equilibrium point by calculating elements of the Jacobian matrix $\frac{\partial \boldsymbol{\Omega}}{\partial \boldsymbol{q}}|_{\boldsymbol{q}=\boldsymbol{q}_d}$ in (6.82). Results can be achieved by applying associated properties of function β and its first and second derivatives, i.e., β' and β'', described in Chapter 4.

$$\begin{aligned} &\beta'_d = \beta'|_{\boldsymbol{q}=\boldsymbol{q}_d} = 0; \beta''_d = \beta''|_{\boldsymbol{q}=\boldsymbol{q}_d}, \\ &\frac{\partial \boldsymbol{\Omega}}{\partial \boldsymbol{q}}|_{\boldsymbol{q}=\boldsymbol{q}_d} = \mathbf{I}_2 + \beta''_d(\boldsymbol{q} - \boldsymbol{q}_{obs})(\boldsymbol{q} - \boldsymbol{q}_{obs})^T. \end{aligned} \tag{6.83}$$

To investigate the stability behavior of the point $\boldsymbol{q} = \boldsymbol{q}_d$, the following Lyapunov function candidate is considered

$$V_d = \sqrt{1 + \|(\boldsymbol{q} - \boldsymbol{q}_d)\|^2} - 1 \tag{6.84}$$

Taking the time derivative both sides of (6.84) along the solution of (6.80), in which $\boldsymbol{q}_{eq}$ is replaced by $\boldsymbol{q}_d$, results in

$$\begin{aligned} \dot{V}_d = &-\frac{\mathbf{K}\|(\boldsymbol{q} - \boldsymbol{q}_d)\|^2}{\sqrt{1 + \|(\boldsymbol{q} - \boldsymbol{q}_d)\|^2}} - \frac{\mathbf{K}\beta''_d}{\sqrt{1 + \|(\boldsymbol{q} - \boldsymbol{q}_d)\|^2}}\big((\boldsymbol{q} - \boldsymbol{q}_{obs})^T(\boldsymbol{q} - \boldsymbol{q}_d)\big)^2 \\ &+ \frac{(\boldsymbol{q} - \boldsymbol{q}_d)^T}{\sqrt{1 + \|(\boldsymbol{q} - \boldsymbol{q}_d)\|^2}}\big(\mathbf{Q}\begin{bmatrix} v_e & 0 \end{bmatrix}^T + \boldsymbol{\Delta}_2(-k_2\phi_e + \omega_e)\big). \end{aligned} \tag{6.85}$$

It is realized that $\mathbf{K}$ is a positive constant matrix, and $\beta''|_{\boldsymbol{q}=\boldsymbol{q}_d} \geq 0$, see property 4 of function β. Also, It has already been proven that $\lim\limits_{t\to\infty}\big(\mathbf{Q}\begin{bmatrix} v_e & 0 \end{bmatrix}^T + \boldsymbol{\Delta}_2(-k_2\phi_e + \omega_e)\big) = 0$ in the previous subsection. Therefore, the equilibrium point $\boldsymbol{q}_d(x_d, y_d)$ is locally asymptotically stable.

Proof of instability of a critical point

Similarly, elements of the Jacobian matrix $\frac{\partial \boldsymbol{\Omega}}{\partial \boldsymbol{q}}$ in (6.82) are calculated by substituting $\boldsymbol{q} = \boldsymbol{q}_c$. Properties β described in Chapter 4 are utilized to yield

$$\begin{aligned} \beta_c' &= \beta'|_{\boldsymbol{q}=\boldsymbol{q}_c}; \quad \beta_c'' = \beta''|_{\boldsymbol{q}=\boldsymbol{q}_c}, \\ \frac{\partial \boldsymbol{\Omega}}{\partial \boldsymbol{q}}|_{\boldsymbol{q}=\boldsymbol{q}_c} &= (1+\beta_c')\mathbf{I}_2 + \beta_c''(\boldsymbol{q}-\boldsymbol{q}_{obs})(\boldsymbol{q}-\boldsymbol{q}_{obs})^T. \end{aligned} \tag{6.86}$$

To evaluate the stability of the linearized system (6.81) at the critical point $\boldsymbol{q}_c(x_c, y_c)$, the following Lyapunov function candidate is considered

$$V_c = \sqrt{1+\|\boldsymbol{q}-\boldsymbol{q}_c\|^2} - 1. \tag{6.87}$$

Taking the time derivative of (6.87) along the solution of (6.81) with $\boldsymbol{q}_{eq} = \boldsymbol{q}_c$ yields

$$\begin{aligned} \dot{V}_c = &\frac{-\mathbf{K}(1+\bar{\beta'}_c)}{\sqrt{1+\|\boldsymbol{q}-\boldsymbol{q}_c\|^2}}\|\boldsymbol{q}-\boldsymbol{q}_c\|^2 - \frac{\mathbf{K}\beta_c''}{\sqrt{1+\|\boldsymbol{q}-\boldsymbol{q}_c\|^2}}\big((\boldsymbol{q}-\boldsymbol{q}_{obs})^T(\boldsymbol{q}-\boldsymbol{q}_c)\big)^2 \\ &+ \frac{(\boldsymbol{q}-\boldsymbol{q}_c)^T}{\sqrt{1+\|\boldsymbol{q}-\boldsymbol{q}_c\|^2}}\big(\mathbf{Q}\begin{bmatrix} v_e & 0 \end{bmatrix}^T + \boldsymbol{\Delta}_2(-k_2\phi_e + \omega_e)\big). \end{aligned} \tag{6.88}$$

It is observed from the fact that a saddle point emerges only if three points $\boldsymbol{q}_c$, $\boldsymbol{q}_{obs}$ and $\boldsymbol{q}_d$ are collinear and the point $\boldsymbol{q}_{obs}$ must be in the middle of the two points $\boldsymbol{q}_c$ and $\boldsymbol{q}_d$. Otherwise, the coordinates of the actual mobile robot, $\boldsymbol{q}$, will converge to the reference trajectory, $\boldsymbol{q}_d$, by all means. This refers back to the previous situation of the desired equilibrium point. To investigate stability properties of the critical point $\boldsymbol{q}_c(x_c, y_c)$, each part of (6.88) will be evaluated carefully. Let $\mathbf{V}$ be a vector space over the field $\mathbb{R}^2$, in which $\|\boldsymbol{q}-\boldsymbol{q}_c\|^2 \geq 0$ for all $[x \quad y]^T, [x_c \quad y_c]^T \in \mathbf{V}$. Firstly, a subspace $\mathbf{V}^* \subset \mathbf{V}$ is defined such that $\boldsymbol{q} = \boldsymbol{q}_c$ for any $x_c \in \mathbf{V}^*$. This assumption also holds for the case of any $y_c \in \mathbf{V}^*$. Therefore, only the case of x_c is proven here. This implies the sum of attractive and repulsive forces at this point to be equal to zero, but each individual forces are nonzero. Moreover, $\mathbf{K}$ is a positive constant matrix, and $\beta'' \geq 0$ which are already mentioned in the previous section. Hence, $\dot{V}_c$ in (6.88) can be rewritten in subspace $\mathbf{V}^*$ by

$$\begin{aligned} \dot{V}_c = &-\frac{\mathbf{K}(1+\bar{\beta'}_c)}{\sqrt{1+\|\boldsymbol{q}-\boldsymbol{q}_c\|^2}}\|\boldsymbol{q}-\boldsymbol{q}_c\|^2 \\ &+ \frac{(\boldsymbol{q}-\boldsymbol{q}_c)^T}{\sqrt{1+\|\boldsymbol{q}-\boldsymbol{q}_c\|^2}}\big(\mathbf{Q}\begin{bmatrix} v_e & 0 \end{bmatrix}^T + \boldsymbol{\Delta}_2(-k_2\phi_e + \omega_e)\big). \end{aligned} \tag{6.89}$$

Secondly, another subspace $\mathbf{V}^{**} \subset \mathbf{V} \setminus \mathbf{V}^{*}$ is defined. This means $\|\boldsymbol{q} - \boldsymbol{q}_c\|^2 > 0$ for all $[x \quad y]^T, [x_c \quad y_c]^T \in \mathbf{V}^{**}$. According to the definitions of β in Chapter 4 and smooth step function $h(\bullet)$ in Chapter 2, it gives

$$\beta' = \frac{\partial \beta}{\partial h}\frac{\partial h}{\partial \tau}\frac{\partial \tau}{\partial \|\boldsymbol{q}_e - \boldsymbol{q}_{obs}\|^2/2}. \tag{6.90}$$

Using results calculated in [125] has

$$\begin{aligned}
&\frac{\partial \beta}{\partial h} = -\frac{1}{h^2(\bullet)},\\
&\frac{\partial h}{\partial \tau} = \big(-h(\bullet) + h^2(\bullet)\big)\big(-\frac{1}{\tau^2} - \frac{1}{(\tau-1)^2}\big),\\
&\frac{\partial \tau}{\partial \|\boldsymbol{q} - \boldsymbol{q}_{obs}\|^2/2} = \frac{1}{R_{sen}^2/2 - (R_{safe} + R_{obs})^2/2}
\end{aligned} \tag{6.91}$$

where functions $h(\bullet)$ and τ have been defined as

$$\begin{aligned}
h &= \frac{e^{-\frac{1}{\tau}}}{e^{-\frac{1}{\tau}} + e^{-\frac{1}{1-\tau}}},\\
\tau &= \frac{\|\boldsymbol{q} - \boldsymbol{q}_{obs}\|^2/2 - (R_{safe} + R_{obs})^2/2}{R_{sen}^2/2 - (R_{safe} + R_{obs})^2/2}.
\end{aligned} \tag{6.92}$$

It is revealed that $\big(-h(\bullet)+h^2(\bullet)\big) < 0$ for all $\tau \in \big(\frac{(R_{safe}+R_{obs})^2}{2}, \frac{R_{sen}^2}{2}\big)$ [125]. Thus, by substituting (6.91) into (6.90) it gives $\beta' < 0$ for all $\tau \in \big(\frac{(R_{safe}+R_{obs})^2}{2}, \frac{R_{sen}^2}{2}\big)$. Since $\frac{\|\boldsymbol{q}-\boldsymbol{q}_{obs}\|^2}{2}$ is the variable of function $h(\bullet)$, see (6.91), and β' is inversely proportional to the square of absolute value of $h(\bullet)$, see (6.90) and (6.91), the smaller the relative distance between the WMR and a potential obstacle is, i.e., $\frac{\|\boldsymbol{q}-\boldsymbol{q}_{obs}\|^2}{2}$, the larger the value of β' for all $\tau \in \big(\frac{(R_{safe}+R_{obs})^2}{2}, \frac{R_{sen}^2}{2}\big)$. There always exists $x_c \in \mathbf{V}^{**}$ such that the part $(1+\beta_c')$ is strictly negative, i.e., there exists a strict positive constant b^{**} such that $(1+\beta_c') < -b^{**}$. This assumption also holds for the case of any $y_c \in \mathbf{V}^{**}$. Hence, only the case of x_c is necessary to prove. It can be represented $\dot{V}_c$ of (6.89) in the subspace $\mathbf{V}^{**}$ as follows

$$\begin{aligned}
\dot{V}_c = &-\frac{\mathbf{K}(1+\beta_c')}{\sqrt{1+\|\boldsymbol{q}-\boldsymbol{q}_c\|^2}}\|\boldsymbol{q}-\boldsymbol{q}_c\|^2\\
&+\frac{(\boldsymbol{q}-\boldsymbol{q}_c)^T}{\sqrt{1+\|\boldsymbol{q}-\boldsymbol{q}_c\|^2}}\big(\mathbf{Q}\begin{bmatrix} v_e & 0\end{bmatrix}^T + \boldsymbol{\Delta}_2(-k_2\phi_e + \omega_e)\big)
\end{aligned} \tag{6.93}$$

Using $(1+\beta_c') < -b^{**}$ for any $[x_c \quad y_c]^T \in \mathbf{V}^{**}$ we can express (6.93) as

$$\begin{aligned}
\dot{V}_c &\geq \frac{(b^{**}\mathbf{K} - \kappa)}{\sqrt{1+\|\boldsymbol{q}-\boldsymbol{q}_c\|^2}}\|\boldsymbol{q}-\boldsymbol{q}_c\|^2 - \frac{\|\mathbf{Q}\begin{bmatrix} v_e & 0\end{bmatrix}^T + \boldsymbol{\Delta}_2(-k_2\phi_e + \omega_e)\|^2}{4\kappa\sqrt{1+\|\boldsymbol{q}-\boldsymbol{q}_c\|^2}}\\
&\geq b^{**}\lambda_{max}(\mathbf{K})V_c - \frac{\|\mathbf{Q}\begin{bmatrix} v_e & 0\end{bmatrix}^T + \boldsymbol{\Delta}_2(-k_2\phi_e + \omega_e)\|^2}{4\kappa\sqrt{1+\|\boldsymbol{q}-\boldsymbol{q}_c\|^2}},
\end{aligned} \tag{6.94}$$

where $\kappa > 0$ is a strictly positive constant, $\lambda_{max}(\mathbf{K})$ is maximum eigenvalue of constant matrix $\mathbf{K}$. In the last section, system (6.40) is forward complete and $\lim_{t\to\infty}\left(\mathbf{Q}\begin{bmatrix} v_e & 0\end{bmatrix}^T + \mathbf{\Delta}_2(-k_2\phi_e + \omega_e)\right) = 0$.
For the special case $\|\boldsymbol{q}(t_0) - \boldsymbol{q}_c\| = 0$, there would be no contradiction in terms of (6.94). This case, however, is never observed in practice since the ever-present physical noise would cause $\|\boldsymbol{q}(t^*) - \boldsymbol{q}_c\| \neq 0$ for some $x_c \in \mathbf{V}^{**}$ to be different from 0 at the time $t^* \geq t_0$. The inequality (6.94) can be rewriten as

$$\begin{aligned}\dot{V}_c &\geq \frac{(b^{**}\mathbf{K} - \kappa)}{\sqrt{1 + \|\boldsymbol{q}^* - \boldsymbol{q}_c\|^2}}\|\boldsymbol{q}^* - \boldsymbol{q}_c\|^2 - \frac{\|\mathbf{Q}\begin{bmatrix} v_e & 0\end{bmatrix}^T + \mathbf{\Delta}_2(-k_2\phi_e + \omega_e)\|^2}{4\kappa\sqrt{1 + \|\boldsymbol{q}^* - \boldsymbol{q}_c\|^2}} \\ &\geq b^{**}\lambda_{max}(\mathbf{K})V_c, \end{aligned} \tag{6.95}$$

where, $\boldsymbol{q}^* = \boldsymbol{q}(t^*)$, for all time $t \geq t^* \geq t_0 \geq 0$. The last part of (6.94) is ignored here due to the explanation above. Since $\|\boldsymbol{q}(t^*) - \boldsymbol{q}_c\| \neq 0$, the right-hand side of (6.95) is divergent, and so does the left-hand side. As a result, the critical point $\boldsymbol{q}_c$ is unstable based on the Theorem 4.3 in [57] (see Theorem 2.1.6 in Chapter 2 for the details). The proof of Theorem 6.2.1 is completed.

6.4 Simulation results

To verify the correctness of the proposed control laws (6.37), numerical simulation is carried out by using the physical parameters of the WMR which is taken from [6]. The physical parameters are summarized in Table 3.1 in Chapter 3. In this section, we simulate the behavior of the WMR tracking a tanh-shape reference path while avoiding stationary obstacle along its path.
Specifications for the reference path are as follows: $x_d = s - 10$, $y_d = -5\tanh(0.2s)$, $s(t) = 0.5t$, $\dot{s} = 0.5$. Hence, the reference path is regular and satisfies requirements (6.20) mentioned in Assumption 6.1.1. To investigate the obstacle avoidance capability of the proposed controllers, we set up the location of a stationary obstacle as: (x_{obs}, y_{obs}). R_{obs} defined in Assumption 6.1.4 is considered to zero in simulation only. This means the obstacle is a point in the Cartesian plane. The values of design parameters for control laws (6.38) are shown in Table 6.1 below. With a simple calculation, it is seen that selection of such values satisfy conditions in (6.16) and (6.40).

The trajectory of the WMR tracks to the desired path is shown in figure 6.1. The WMR starts approaching the reference after leaving its initial location. When the obstacle emerges to the sensing region, the obstacle avoidance algorithm in

Table 6.1: Values of design parameters

Parameters	Meaning	Values
$x(0); y(0); \phi(0)$	initial configuration of the actual WMR	$-5; 0; 0.2$
k_1	control gain 1 of the constant matrix $\mathbf{K}$	0.95
k_2	control gain 2 of the constant matrix $\mathbf{K}$	0.95
k_3	control gain of controllers	0.5
k_4	control gain of controllers	1
k_5	control gain of controllers	1
γ_1	constant value 1 defined in (6.16)	1
γ_2	constant value 2 defined in (6.16)	1
$x_{obs}; y_{obs}$	coordinates of the obstacle	$20; -5$
R_{safe}	radius of physical safety region of the WMR	1
R_{sen}	radius of sensing region of the WMR	2.5
R_{obs}	distance of influence of obstacle	0
h	time step used in Euler method for numerical computational	0.02

robot's motion controllers is active. At this point, the WMR start diverging from the desired path and bypassing the obstacle to avoid a potential collision. Once the obstacle is out of the robot's sensing range, the obstacle avoidance algorithm is inactive. The WMR returns to its reference path because only the path tracking algorithm is working. Errors in position and orientation, i.e., x_e, y_e and ϕ_e are plotted in figure 6.2. These errors tend to an acceptable small value at steady state provided to practical control. Hence, explanation in remark (6.19) is consolidated and control objective in (6.23) is verified. Meanwhile, errors in velocities, i.e., v_e and ω_e plotted in 6.3 tend to zero asymptotically because actual velocities track smoothly to that reference. Correspondingly, τ_v and τ_ω applied to two wheels tend to constant values at steady state, see figure 6.3.

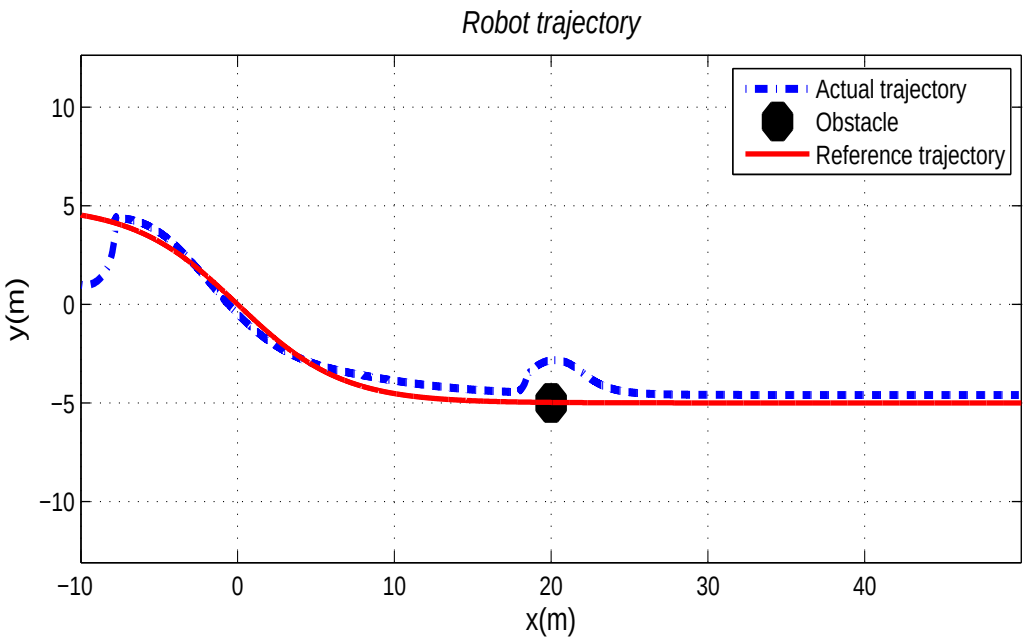

Figure 6.1: Tracking path of actual robot to the tanh-shape reference path - An obstacle is on the reference path.

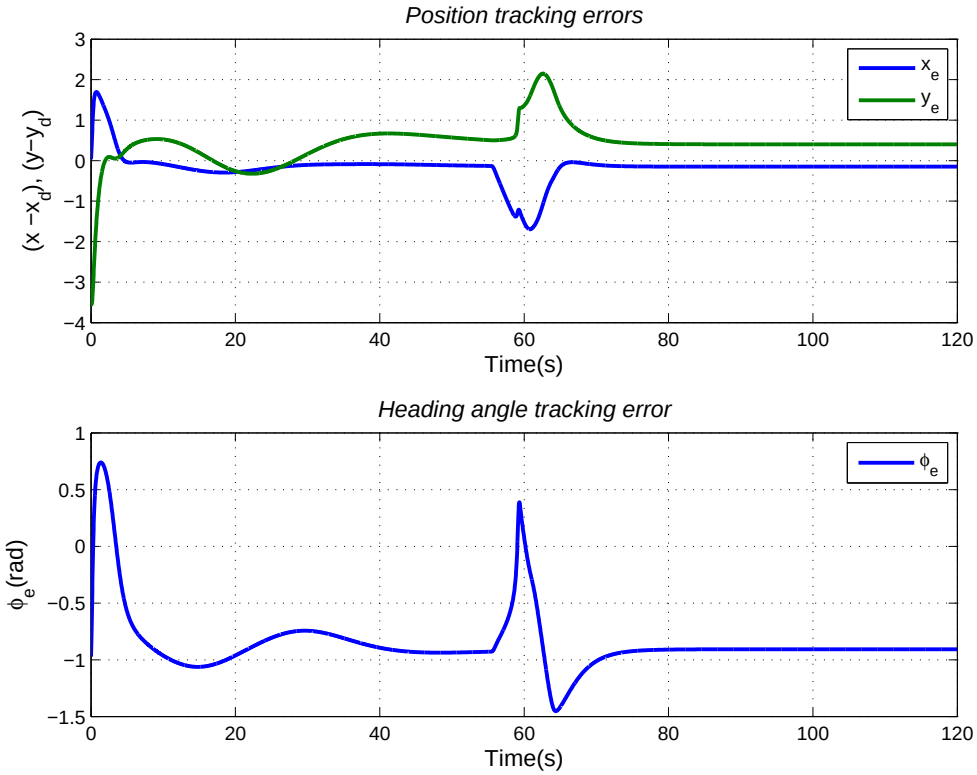

Figure 6.2: Position tracking errors (above); Orientation error (below).

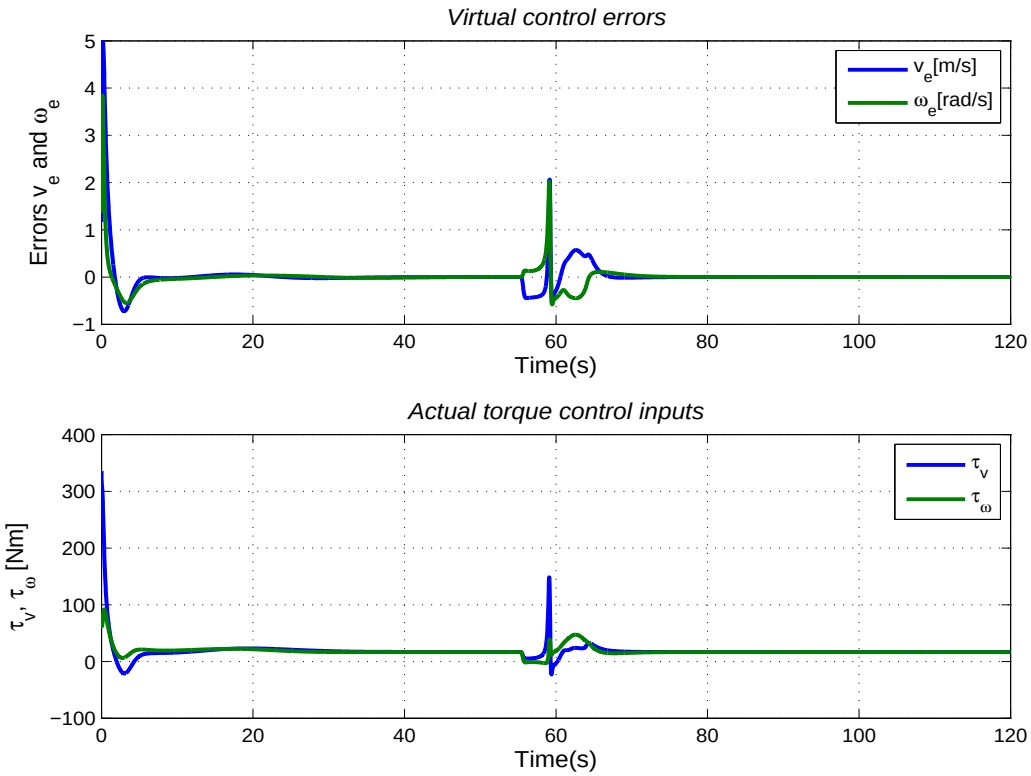

Figure 6.3: Virtual control errors (above) and Actual control inputs (below).

6.5 Conclusions

In this chapter, a practical control method for path tracking and collision avoidance of the WMR system was successfully presented. This designing scheme used the Lyapunov's direct method and the standard backstepping technique. By relying on the works in [5], the issue of uncontrolled orientation in chapter 5 was fully solved by this approach. The control objective has been obtained in the sense of practical manner mentioned in (6.23), i.e., tracking errors could not converge to zero. With the use of the smooth step function embedded into the potential function, switching control is not needed between two modes of obstacle-free and obstacle avoidance. Numerical simulation has demonstrated the practical convergence of actual trajectory to the reference path from the initial location to the goal. Moreover, obstacle avoidance task is executed smoothly if any stationary obstacle is on the traveling path of the WMR. Since saddle points emerging in potential function method is a critical issue, this work provided an analytical analysis to prove that the WMR system does not converge to saddle points.

Chapter 7

Conclusions and future works

In conclusion, this chapter summarizes the main contributions of the author's research. Also, some possible future research directions that might be of particular interests are outlined.

7.1 Contributions revisited

This dissertation has mainly concentrated on the problems of motion control and obstacle avoidance of the nonholonomic WMR system. Therefore, the contributions involved two matters: Path-following in the obstacle-free workspace and path tracking with obstacle existence. Here is a brief summary of the main results of the dissertation.

1. Under the assumption of the obstacle-free workspace, a global stability of the solutions for the path-following problem was achieved in Chapter 3. Based on the recent level curve approach, the author successfully designed the global state-feedback controllers for the WMR at dynamic level using Lyapunov's direct and standard backstepping methods. Compared to the origin method reported in [88], this approach has offered a boundedness of immediate controls and torque control inputs.

2. Chapter 4 has dealt with path tracking and obstacle avoidance problems in a combined framework. While many other studies proposed switching control solutions for this problem, a smooth step function is integrated into the designed control algorithm to surpass switching control. Results showed that the closed system is globally asymptotically stable. By applying the novel local potential functions [3] to deal with obstacle avoidance, the local

minimum problem, which is a critical issue in the classical potential function approach, has been solved. Moreover, as concerns the saddle point appearing in the potential function method, this work provided an analytical analysis to prove that the WMR system has not converged to that saddle point.

3. In chapter 5, a new bounded position control algorithm for the problem of path tracking and obstacle avoidance has been obtained. The control scheme adopted the works of pairwise collision avoidance functions introduced in [4] and coordinate transformation in [62]. The boundedness of designed control signals ensured control efforts not to exceed a certain value in terms of relative distance and speed, see the construction of $\boldsymbol{u}(t)$ in (5.24). This in turn shows the boundedness of the torque control vector $\boldsymbol{\tau}$, due to $\lim_{t\to\infty} \mathbf{A} = 0$ in (5.28). The inherent saddle point problem has been carefully analyzed in this chapter. Hence, only the equilibrium point set has been locally asymptotically stable while the saddle point set has been unstable. This meant that the WMR system did not converge to saddle points.

4. In chapter 6, a new algorithm for the practical control of path tracking and obstacle avoidance is presented. Based on the main ideas of transverse function approach, a new coordinate transformation was deployed to handle the orientation of the vehicle. This solved the problem of nonholonomic constraints. Moreover, a smooth step function was integrated into the potential function so that there was no need of switching control scheme. Stability analysis showed that obstacle avoidance has been guaranteed for all $t \geq t_0 \geq 0$ under suitable initial conditions, i.e., Assumption 6.1.5. In terms of practical manner, tracking errors could not converge to zero, they converged to a ball with a center being at the origin and adjustable small radius. The advantage is that feedback controllers could stabilize the WMR system of arbitrary reference paths, including fixed points and non-feasible paths.

7.2 Future work

In spite of the endeavour spent on problems of motion control and obstacle avoidance of WMRs in this dissertation, the results are limited. The author believes that there are still many directions to be investigated for future work. Below are

several research directions that are of particular interest in future.

1. In this research, it is assumed that all state variables are fully measured. In fact, the issues of inaccuracy and expensive cost of measurement devices are real challenges. Therefore, designing output feedback controllers using observer control methods should be considered to overcome these challenges, e.g., [106, 167].

2. Another fundamental matter in feedback control design is to cope with problems of system uncertainties, external disturbance or neglected dynamics in the design model [168]. These impacts normally affect the system's performance. To this end, a deployment of adaptive and robust control should be taken into account, i.e., [103, 169].

3. Regarding a clustered environment, most of researches assume obstacles to be in stationary status. This is still far from various applications in practice. WMRs can work in a dynamic clustered environment with moving obstacles or targets, i.e., sharing workspace with human being or other autonomous vehicles. Hence, problems of multi-obstacles and moving obstacles/targets should be interesting for further investigation. Given that obstacle moves under a certain velocity, i.e., $\dot{\boldsymbol{q}}_{obs} \leq \epsilon$, and ϵ is a positive constant. Hence, the term $\beta'(\boldsymbol{q} - \boldsymbol{q}_{obs})^T \dot{\boldsymbol{q}}_{obs}$ exists and must be added to (4.15) or (6.22) for control design, in case of Chapter 4 or Chapter 6, respectively. Controllers would be designed successfully if a proper approach were given for control design and stability analysis. Proposed methods in this thesis can be applied to a certain extent to solve the problem.

4. Tracking problem of WMRs can be investigated in terms of optimality. From this viewpoint, the minimum of a meaningful cost functional that incorporates integral penalty on tracking error state and the control must be considered. Some solid foundations in the literature, e.g., [69,71,170,171] can facilitate this particular research direction.

5. Apart from control designs for a single vehicle, another direction for future work is an extension of cooperation and coordination of multi-vehicle systems. Particularly, formation control, which has been an important matter in coordinated control for a group of autonomous vehicles, draws great attention of researchers because of various potential applications but truly challenging [172, 173].

Bibliography

[1] K. D. Do, "Global output-feedback path-following control of unicycle-type mobile robots: A level curve approach," *Robotics and Autonomous Systems*, vol. 74, pp. 229–242, 2015.

[2] ——, "Bounded controllers for formation stabilization of mobile agents with limited sensing ranges," *IEEE Transactions on Automatic Control*, vol. 52, no. 3, pp. 569–576, 2007.

[3] ——, "Formation tracking control of unicycle-type mobile robots with limited sensing ranges," *IEEE Transactions on Control Systems Technology*, vol. 16, no. 3, pp. 527–538, 2008.

[4] ——, "Bounded assignment formation control of second-order dynamic agents," *IEEE/ASME Transactions on Mechatronics*, vol. 19, no. 2, pp. 477–489, 2014.

[5] K. D. Do and M. W. Lau, "Practical formation control of multiple unicycle-type mobile robots with limited sensing ranges," *Journal of Intelligent & Robotic Systems*, vol. 64, no. 2, pp. 245–275, 2011.

[6] K. D. Do and J. Pan, "Global output-feedback path tracking of unicycle-type mobile robots," *Robotics and Computer-Integrated Manufacturing*, vol. 22, no. 2, pp. 166–179, 2006.

[7] F. Lambercy and J. Tharin. (2013, Fer) Khepera iii user manual version 3.5. [Online]. Available: http://ftp.k-team.com/KheperaIII/UserManual/Kh3.Robot.UserManual.pdf

[8] S. G. Tzafestas, *Introduction to mobile robot control*. Elsevier, 2013.

[9] R. M. Murray, "Recent research in cooperative control of multivehicle systems," *Journal of Dynamic Systems, Measurement, and Control*, vol. 129, no. 5, pp. 571–583, 2007.

[10] T. Arai, E. Pagello, and L. E. Parker, "Advances in multi-robot systems," *IEEE Transactions on Robotics and Automation*, vol. 18, no. 5, pp. 655–661, 2002.

[11] I. Kolmanovsky and N. H. McClamroch, "Developments in nonholonomic control problems," *IEEE Transactions on Control Systems*, vol. 15, no. 6, pp. 20–36, 1995.

[12] R. W. Brockett, "Asymptotic stability and feedback stabilization," in *Differential Geometric Control Theory*. Birkhauser, 1983, pp. 181–191.

[13] G. Oriolo, A. De Luca, and M. Vendittelli, "Wmr control via dynamic feedback linearization: design, implementation, and experimental validation," *IEEE Transactions on Control Systems Technology*, vol. 10, no. 6, pp. 835–852, 2002.

[14] C. Samson, "Control of chained systems application to path following and time-varying point-stabilization of mobile robots," *IEEE Transactions on Automatic Control*, vol. 40, no. 1, pp. 64–77, 1995.

[15] B. d'Andrea Novel, G. Bastin, and G. Campion, "Modelling and control of non-holonomic wheeled mobile robots," in *Proceedings of 1991 IEEE International Conference on Robotics and Automation, 1991.* IEEE, 1991, pp. 1130–1135.

[16] Z. Qu, *Cooperative control of dynamical systems: applications to autonomous vehicles*. Springer Science & Business Media, 2009.

[17] R. M. Murray, Z. Li, and S. S. Sastry, *A mathematical introduction to robotic manipulation*. CRC Press, 1994.

[18] A. M. Bloch, J. C. Baillieul, C. Marsden, Jerrold E, and C. Crouch, P. E, *Nonholonomic mechanics and control*, ser. Interdisciplinary Applied Mathematics. New York: Springer, 2003.

[19] C. C. de Wit, B. Siciliano, and G. Bastin, *Theory of robot control*. Springer Science & Business Media, 2012.

[20] P. Morin and C. Samson, "Motion control of wheeled mobile robots," in *Springer Handbook of Robotics*. Springer Berlin Heidelberg, 2008, pp. 799–826.

[21] ——, "Trajectory tracking for non-holonomic vehicles: overview and case study," in *Proceedings of the Fourth International Workshop on Robot Motion and Control, 2004.* IEEE, 2004, pp. 139–153.

[22] Z.-P. Jiang and H. Nijmeijer, "Tracking control of mobile robots: a case study in backstepping," *Automatica*, vol. 33, no. 7, pp. 1393–1399, 1997.

[23] T.-C. Lee, K.-T. Song, C.-H. Lee, and C.-C. Teng, "Tracking control of unicycle-modeled mobile robots using a saturation feedback controller," *IEEE Transactions on Control Systems Technology*, vol. 9, no. 2, pp. 305–318, 2001.

[24] A. M. Bloch, M. Reyhanoglu, and N. H. McClamroch, "Control and stabilization of nonholonomic dynamic systems," *IEEE Transactions on Automatic Control*, vol. 37, no. 11, pp. 1746–1757, 1992.

[25] A. Astolfi, "Discontinuous control of nonholonomic systems," *Systems & Control Letters*, vol. 27, no. 1, pp. 37–45, 1996.

[26] ——, "Exponential stabilization of a wheeled mobile robot via discontinuous control," *Journal of Dynamic Systems, Measurement, and Control*, vol. 121, no. 1, pp. 121–126, 1999.

[27] C. C. De Wit and O. Sordalen, "Exponential stabilization of mobile robots with nonholonomic constraints," *IEEE Transactions on Automatic Control*, vol. 37, no. 11, pp. 1791–1797, 1992.

[28] T. Floquet, J.-P. Barbot, and W. Perruquetti, "Higher-order sliding mode stabilization for a class of nonholonomic perturbed systems," *Automatica*, vol. 39, no. 6, pp. 1077–1083, 2003.

[29] S. S. Ge, Z. Wang, and T. H. Lee, "Adaptive stabilization of uncertain nonholonomic systems by state and output feedback," *Automatica*, vol. 39, no. 8, pp. 1451–1460, 2003.

[30] P. Tsiotras and J. Luo, "Control of underactuated spacecraft with bounded inputs," *Automatica*, vol. 36, no. 8, pp. 1153–1169, 2000.

[31] A. Bloch and S. Drakunov, "Stabilization and tracking in the nonholonomic integrator via sliding modes," *Systems & Control Letters*, vol. 29, no. 2, pp. 91–99, 1996.

[32] C. Samson, "Time-varying feedback stabilization of car-like wheeled mobile robots," *The International journal of Robotics Research*, vol. 12, no. 1, pp. 55–64, 1993.

[33] J.-B. Pomet, "Explicit design of time-varying stabilizing control laws for a class of controllable systems without drift," *Systems & Control Letters*, vol. 18, no. 2, pp. 147–158, 1992.

[34] R. T. M'Closkey and R. M. Murray, "Convergence rates for nonholonomic systems in power form," in *Proceedings of the American Control Conference, 1993*. IEEE, 1993, pp. 2967–2972.

[35] K. D. Do and J. Pan, "Adaptive global stabilization of nonholonomic systems with strong nonlinear drifts," *Systems & Control Letters*, vol. 46, no. 3, pp. 195–205, 2002.

[36] W. E. Dixon, Z.-P. Jiang, and D. M. Dawson, "Global exponential setpoint control of wheeled mobile robots: a lyapunov approach," *Automatica*, vol. 36, no. 11, pp. 1741–1746, 2000.

[37] Z.-P. Jiang, "Iterative design of time-varying stabilizers for multi-input systems in chained form," *Systems & Control Letters*, vol. 28, no. 5, pp. 255–262, 1996.

[38] E. Panteley and A. Loria, "On global uniform asymptotic stability of nonlinear time-varying systems in cascade," *Systems & Control Letters*, vol. 33, no. 2, pp. 131–138, 1998.

[39] R. Fierro and F. L. Lewis, "Control of a nonholomic mobile robot: Backstepping kinematics into dynamics," *Journal of Robotic Systems*, vol. 14, no. 3, pp. 149–163, 1997.

[40] E. Lefeber and H. Nijmeijer, "Adaptive tracking control of nonholonomic systems: an example," in *Proceedings of the 38th IEEE Conference on Decision and Control, 1999*, vol. 3. IEEE, 1999, pp. 2094–2099.

[41] T. Fukao, H. Nakagawa, and N. Adachi, "Adaptive tracking control of a nonholonomic mobile robot," *IEEE Transactions on Robotics and Automation*, vol. 16, no. 5, pp. 609–615, 2000.

[42] O. Sordalen and O. Egeland, "Exponential stabilization of nonholonomic chained systems," *IEEE Transactions on Automatic Control*, vol. 40, no. 1, pp. 35–49, 1995.

[43] R. T. M'closkey and R. M. Murray, "Exponential stabilization of driftless nonlinear control systems using homogeneous feedback," *IEEE Transactions on Automatic Aontrol*, vol. 42, no. 5, pp. 614–628, 1997.

[44] Y. Hu, S. S. Ge, and C.-Y. Su, "Stabilization of uncertain nonholonomic systems via time-varying sliding mode control," *IEEE Transactions on Automatic Control*, vol. 49, no. 5, pp. 757–763, 2004.

[45] P. Kokotović and M. Arcak, "Constructive nonlinear control: a historical perspective," *Automatica*, vol. 37, no. 5, pp. 637–662, 2001.

[46] M. W. Spong, S. Hutchinson, and M. Vidyasagar, *Robot modeling and control*. Hoboken (N.J.): John Wiley & Sons, 2006.

[47] C. C. De Wit, H. Khennouf, C. Samson, and O. J. Sordalen, "Nonlinear control design for mobile robots," *Recent trends in mobile robots*, vol. 11, pp. 121–156, 1993.

[48] A. De Luca, G. Oriolo, and C. Samson, "Feedback control of a nonholonomic car-like robot," *Robot motion planning and control*, pp. 171–253, 1998.

[49] K. D. Do and J. Pan, *Control of ships and underwater vehicles: design for underactuated and nonlinear marine systems*. Springer Science & Business Media, 2009.

[50] T. I. Fossen, *Guidance and control of ocean vehicles*. John Wiley & Sons, Ltd, 1994.

[51] Renwei and R. W. Beard, *Distributed Consensus in Multi-vehicle Cooperative Control: Theory and Applications*. Springer, 2008.

[52] G. Antonelli, T. I. Fossen, and D. R. Yoerger, "Underwater robotics," in *Springer handbook of robotics*. Springer, 2008, pp. 987–1008.

[53] K. D. Do, Z.-P. Jiang, and J. Pan, "Simultaneous tracking and stabilization of mobile robots: an adaptive approach," *IEEE Transactions on Automatic Control*, vol. 49, no. 7, pp. 1147–1152, 2004.

[54] J. Huang, C. Wen, W. Wang, and Z.-P. Jiang, "Adaptive stabilization and tracking control of a nonholonomic mobile robot with input saturation and disturbance," *Systems & Control Letters*, vol. 62, no. 3, pp. 234–241, 2013.

[55] A. P. Aguiar, J. P. Hespanha *et al.*, "Trajectory-tracking and path-following of underactuated autonomous vehicles with parametric modeling uncertainty," *IEEE Transactions on Automatic Control*, vol. 52, no. 8, pp. 1362–1379, 2007.

[56] E. Panteley, E. Lefeber, A. Loria, and H. Nijmeijer, "Exponential tracking control of a mobile car using a cascaded approach," in *Proceedings of the IFAC workshop on motion control*. Pergamon Grenoble, France, 1998, pp. 221–226.

[57] H. K. Khalil, *Nonlinear systems*, 3rd ed. New Jewsey, Prentice Hall, 2002.

[58] M. Krstic, P. V. Kokotovic, and I. Kanellakopoulos, *Nonlinear and Adaptive Control Design*, 1st ed. New York, NY, USA: John Wiley & Sons, Inc., 1995.

[59] J. Huang, C. Wen, W. Wang, and Z.-P. Jiang, "Adaptive output feedback tracking control of a nonholonomic mobile robot," *Automatica*, vol. 50, no. 3, pp. 821–831, 2014.

[60] D. Chwa, "Tracking control of differential-drive wheeled mobile robots using a backstepping-like feedback linearization," *IEEE Transactions on Systems, Man, and Cybernetics-Part A: Systems and Humans*, vol. 40, no. 6, pp. 1285–1295, 2010.

[61] Y. Yamamoto and X. Yun, "Effect of the dynamic interaction on coordinated control of mobile manipulators," *IEEE Transactions on Robotics and Automation*, vol. 12, no. 5, pp. 816–824, 1996.

[62] J. R. Lawton, R. W. Beard, and B. J. Young, "A decentralized approach to formation maneuvers," *IEEE Transactions on Robotics and Automation*, vol. 19, no. 6, pp. 933–941, 2003.

[63] M. Defoort, T. Floquet, A. Kokosy, and W. Perruquetti, "A novel higher order sliding mode control scheme," *Systems & Control Letters*, vol. 58, no. 2, pp. 102–108, 2009.

[64] J.-M. Yang and J.-H. Kim, "Sliding mode control for trajectory tracking of nonholonomic wheeled mobile robots," *IEEE Transactions on Robotics and Automation*, vol. 15, no. 3, pp. 578–587, 1999.

[65] D. Chwa, "Sliding-mode tracking control of nonholonomic wheeled mobile robots in polar coordinates," *IEEE Transactions on Control Systems Technology*, vol. 12, no. 4, pp. 637–644, 2004.

[66] D. Gu and H. Hu, "Receding horizon tracking control of wheeled mobile robots," *IEEE Transactions on Control Systems Technology*, vol. 14, no. 4, pp. 743–749, 2006.

[67] H. Li, W. Yan, and Y. Shi, "A receding horizon stabilization approach to constrained nonholonomic systems in power form," *Systems & Control Letters*, vol. 99, pp. 47–56, 2017.

[68] M. Krstić and Z.-H. Li, "Inverse optimal design of input-to-state stabilizing nonlinear controllers," *IEEE Transactions on Automatic Control*, vol. 43, no. 3, pp. 336–350, 1998.

[69] M. Krstić and P. Tsiotras, "Inverse optimal stabilization of a rigid spacecraft," *IEEE Transactions on Automatic Control*, vol. 44, no. 5, pp. 1042–1049, 1999.

[70] K. D. Do, "Global inverse optimal tracking control of underactuated omnidirectional intelligent navigators (odins)," *Journal of Marine Science and Application*, vol. 14, no. 1, pp. 1–13, 2015.

[71] W. Luo, Y.-C. Chu, and K.-V. Ling, "Inverse optimal adaptive control for attitude tracking of spacecraft," *IEEE Transactions on Automatic Control*, vol. 50, no. 11, pp. 1639–1654, 2005.

[72] T. Das and I. N. Kar, "Design and implementation of an adaptive fuzzy logic-based controller for wheeled mobile robots," *IEEE Transactions on Control Systems Technology*, vol. 14, no. 3, pp. 501–510, 2006.

[73] Z.-G. Hou, A.-M. Zou, L. Cheng, and M. Tan, "Adaptive control of an electrically driven nonholonomic mobile robot via backstepping and fuzzy approach," *IEEE Transactions on Control Systems Technology*, vol. 17, no. 4, pp. 803–815, 2009.

[74] D. Chwa, "Fuzzy adaptive tracking control of wheeled mobile robots with state-dependent kinematic and dynamic disturbances," *IEEE Transactions on Fuzzy Systems*, vol. 20, no. 3, pp. 587–593, 2012.

[75] R. Fierro and F. L. Lewis, "Control of a nonholonomic mobile robot using neural networks," *IEEE Transactions on Neural Networks*, vol. 9, no. 4, pp. 589–600, 1998.

[76] Y. Kanayama, Y. Kimura, F. Miyazaki, and T. Noguchi, "A stable tracking control method for an autonomous mobile robot," in *Proceedings of 1990 IEEE International Conference on Robotics and Automation, 1990.* IEEE, 1990, pp. 384–389.

[77] M. Amoozgar and Y. Zhang, "Trajectory tracking of wheeled mobile robots: A kinematical approach," in *Proceedings of the IEEE/ASME International Conference on Mechatronics and Embedded Systems and Applications (MESA), 2012.* IEEE, 2012, pp. 275–280.

[78] S. Blažič, "A novel trajectory-tracking control law for wheeled mobile robots," *Robotics and Autonomous Systems*, vol. 59, no. 11, pp. 1001–1007, 2011.

[79] E. Lefeber, J. Jakubiak, K. Tchon, and H. Nijmeijer, "Observer based kinematic tracking controllers for a unicycle-type mobile robot," in *Proceedings of 2001 ICRA. IEEE International Conference on Robotics and Automation, 2001*, vol. 2. IEEE, 2001, pp. 2084–2089.

[80] J. Koo, S. Choi, and S. Won, "Observer-based trajectory tracking control for a wheeled mobile robot," in *Proceedings of the 7th Asian Control Conference, 2009.* IEEE, 2009, pp. 1644–1649.

[81] K. D. Do, Z.-P. Jiang, and J. Pan, "Underactuated ship global tracking under relaxed conditions," *IEEE Transactions on Automatic Control*, vol. 47, no. 9, pp. 1529–1536, 2002.

[82] M. I. El-Hawwary and M. Maggiore, "Global path following for the unicycle and other results," in *Proceedings of the American Control Conference, 2008.* IEEE, 2008, pp. 3500–3505.

[83] K. D. Do and J. Pan, "State-and output-feedback robust path-following controllers for underactuated ships using serret–frenet frame," *Ocean Engineering*, vol. 31, no. 5, pp. 587–613, 2004.

[84] D. Soetanto, L. Lapierre, and A. Pascoal, "Adaptive, non-singular path-following control of dynamic wheeled robots," in *Proceedings of 42nd IEEE Conference on Decision and Control, 2003*, vol. 2. IEEE, 2003, pp. 1765–1770.

[85] S. Sun and P. Cui, "Path tracking and a practical point stabilization of mobile robot," *Robotics and Computer-Integrated Manufacturing*, vol. 20, no. 1, pp. 29 – 34, 2004.

[86] C. Nielsen and M. Maggiore, "Maneuver regulation via transverse feedback linearization: Theory and examples," in *Proceedings of the IFAC symposium on nonlinear control systems (NOLCOS), Stuttgart, Germany*, 2004, pp. 59–66.

[87] L. Consolini, M. Maggiore, C. Nielsen, and M. Tosques, "Path following for the pvtol aircraft," *Automatica*, vol. 46, no. 8, pp. 1284–1296, 2010.

[88] A. Morro, A. Sgorbissa, and R. Zaccaria, "Path following for unicycle robots with an arbitrary path curvature," *IEEE Transactions on Robotics*, vol. 27, no. 5, pp. 1016–1023, 2011.

[89] L. Lapierre and D. Soetanto, "Nonlinear path-following control of an auv," *Ocean Engineering*, vol. 34, no. 11, pp. 1734–1744, 2007.

[90] R. Skjetne, T. I. Fossen, and P. Kokotovic, "Output maneuvering for a class of nonlinear systems," in *Proceedings of 15th IFAC World Congress on Automatic Control, IFAC, Barcelona, Spain.* IFAC, 2002.

[91] R. Skjetne, T. I. Fossen, and P. V. Kokotović, "Robust output maneuvering for a class of nonlinear systems," *Automatica*, vol. 40, no. 3, pp. 373–383, 2004.

[92] R. Skjetne, U. Jørgensen, and A. R. Teel, "Line-of-sight path-following along regularly parametrized curves solved as a generic maneuvering problem," in *Proceedings of 50th IEEE Conference on Decision and Control and European Control Conference, 2011.* IEEE, 2011, pp. 2467–2474.

[93] A. P. Aguiar, J. P. Hespanha, and P. V. Kokotović, "Performance limitations in reference tracking and path following for nonlinear systems," *Automatica*, vol. 44, no. 3, pp. 598–610, 2008.

[94] A. P. Aguiar, J. P. Hespanha, and P. V. Kokotovic, "Path-following for non-minimum phase systems removes performance limitations," *IEEE Transactions on Automatic Control*, vol. 50, no. 2, pp. 234–239, 2005.

[95] K. D. Do, "Bounded controllers for global path tracking control of unicycle-type mobile robots," *Robotics and Autonomous Systems*, vol. 61, no. 8, pp. 775–784, 2013.

[96] K. Sakurama and K. Nakano, "Path tracking control of lagrange systems with obstacle avoidance," *International Journal of Control, Automation and Systems*, vol. 10, no. 1, pp. 50–60, 2012.

[97] R. Skjetne, T. I. Fossen, and P. V. Kokotović, "Adaptive maneuvering, with experiments, for a model ship in a marine control laboratory," *Automatica*, vol. 41, no. 2, pp. 289–298, 2005.

[98] K. D. Do, "Global robust adaptive path-tracking control of underactuated ships under stochastic disturbances," *Ocean Engineering*, vol. 111, pp. 267–278, 2016.

[99] W. Ren, J.-S. Sun, R. W. Beard, and T. W. McLain, "Nonlinear tracking control for nonholonomic mobile robots with input constraints: An experimental study," in *Proceedings of the American Control Conference, 2005.* IEEE, 2005, pp. 4923–4928.

[100] S. Sun and P. Cui, "Path tracking and a practical point stabilization of mobile robot," *Robotics and Computer-Integrated Manufacturing*, vol. 20, no. 1, pp. 29–34, 2004.

[101] B. Park, S. Yoo, J. Park, and Y. Choi, "Adaptive output-feedback control for trajectory tracking of electrically driven non-holonomic mobile robots," *IET Control Theory & Applications*, vol. 5, no. 6, pp. 830–838, 2011.

[102] K. Shojaei, A. M. Shahri, and A. Tarakameh, "Adaptive feedback linearizing control of nonholonomic wheeled mobile robots in presence of parametric and nonparametric uncertainties," *Robotics and Computer-Integrated Manufacturing*, vol. 27, no. 1, pp. 194–204, 2011.

[103] M.-S. Kim, J.-H. Shin, S.-G. Hong, and J.-J. Lee, "Designing a robust adaptive dynamic controller for nonholonomic mobile robots under modeling uncertainty and disturbances," *Mechatronics*, vol. 13, no. 5, pp. 507–519, 2003.

[104] G. BesançOn, "Global output feedback tracking control for a class of lagrangian systems," *Automatica*, vol. 36, no. 12, pp. 1915–1921, 2000.

[105] S. J. Yoo, J. B. Park, and Y. H. Choi, "Adaptive output feedback control of flexible-joint robots using neural networks: dynamic surface design approach," *IEEE Transactions on Neural Networks*, vol. 19, no. 10, pp. 1712–1726, 2008.

[106] H. K. Khalil and L. Praly, "High-gain observers in nonlinear feedback control," *International Journal of Robust and Nonlinear Control*, vol. 24, no. 6, pp. 993–1015, 2014.

[107] D. Swaroop, J. K. Hedrick, P. P. Yip, and J. C. Gerdes, "Dynamic surface control for a class of nonlinear systems," *IEEE Transactions on Automatic Control*, vol. 45, no. 10, pp. 1893–1899, 2000.

[108] O. Khatib, "Real-time obstacle avoidance for manipulators and mobile robots," *The International journal of Robotics Research*, vol. 5, no. 1, pp. 90–98, 1986.

[109] J. Latombe, *Robot Motion Planning*, ser. The Springer International Series in Engineering and Computer Science. Springer US, 1991.

[110] F. Fahimi, C. Nataraj, and H. Ashrafiuon, "Real-time obstacle avoidance for multiple mobile robots," *Robotica*, vol. 27, no. 2, pp. 189–198, 2009.

[111] L. Huang, "Velocity planning for a mobile robot to track a moving targeta potential field approach," *Robotics and Autonomous Systems*, vol. 57, no. 1, pp. 55–63, 2009.

[112] D. H. Kim, H. Wang, and S. Shin, "Decentralized control of autonomous swarm systems using artificial potential functions: Analytical design guidelines," *Journal of Intelligent and Robotic Systems*, vol. 45, no. 4, pp. 369–394, 2006.

[113] S. S. Ge and Y. J. Cui, "New potential functions for mobile robot path planning," *IEEE Transactions on Robotics and Automation*, vol. 16, no. 5, pp. 615–620, 2000.

[114] Y. Koren and J. Borenstein, "Potential field methods and their inherent limitations for mobile robot navigation," in *Proceedings of 1991 IEEE International Conference on Robotics and Automation, 1991.* IEEE, 1991, pp. 1398–1404.

[115] E. Rimon and D. E. Koditschek, "Exact robot navigation using artificial potential functions," *IEEE Transactions on Robotics and Automation*, vol. 8, no. 5, pp. 501–518, 1992.

[116] R. Olfati-Saber, "Flocking for multi-agent dynamic systems: Algorithms and theory," *IEEE Transactions on Automatic Control*, vol. 51, no. 3, pp. 401–420, 2006.

[117] M. Hoy, A. S. Matveev, and A. V. Savkin, "Algorithms for collision-free navigation of mobile robots in complex cluttered environments: a survey," *Robotica*, vol. 33, no. 3, pp. 463–497, 2015.

[118] L. Zeng and G. M. Bone, "Mobile robot collision avoidance in human environments," *International Journal of Advanced Robotic Systems*, vol. 10, no. 1, p. 41, 2013.

[119] H. G. Tanner and A. Kumar, "Towards decentralization of multi-robot navigation functions," in *Proceedings of the IEEE International Conference on Robotics and Automation, 2005.* IEEE, 2005, pp. 4132–4137.

[120] H. G. Tanner and A. Boddu, "Multiagent navigation functions revisited," *IEEE Transactions on Robotics*, vol. 28, no. 6, pp. 1346–1359, 2012.

[121] D. E. Koditschek and E. Rimon, "Robot navigation functions on manifolds with boundary," *Advances in Applied Mathematics*, vol. 11, no. 4, pp. 412–442, 1990.

[122] S. G. Loizou and K. J. Kyriakopoulos, "Navigation of multiple kinematically constrained robots," *IEEE Transactions on Robotics*, vol. 24, no. 1, pp. 221–231, 2008.

[123] T. Urakubo, "Stability analysis and control of nonholonomic systems with potential fields," *Journal of Intelligent & Robotic Systems*, pp. 1–17, 2017.

[124] H. G. Tanner, S. G. Loizou, and K. J. Kyriakopoulos, "Nonholonomic navigation and control of cooperating mobile manipulators," *IEEE Transactions on Robotics and Automation*, vol. 19, no. 1, pp. 53–64, 2003.

[125] K. D. Do, "Relative formation control of mobile agents for gradient climbing and target capturing," *International Journal of Control*, vol. 84, no. 6, pp. 1098–1114, 2011.

[126] L. García-Delgado, J. Noriega, D. Berman-Mendoza, A. Leal-Cruz, A. Vera-Marquina, R. Gómez-Fuentes, A. García-Juárez, A. Rojas-Hernández, and I. E. Zaldívar-Huerta, "Repulsive function in potential field based control with algorithm for safer avoidance," *Journal of Intelligent & Robotic Systems*, vol. 80, no. 1, p. 59, 2015.

[127] L. Lapierre, R. Zapata, and P. Lepinay, "Combined path-following and obstacle avoidance control of a wheeled robot," *The International Journal of Robotics Research*, vol. 26, no. 4, pp. 361–375, 2007.

[128] L. A. V. Reyes and H. G. Tanner, "Flocking, formation control, and path following for a group of mobile robots," *IEEE Transactions on Control Systems Technology*, vol. 23, no. 4, pp. 1268–1282, 2015.

[129] D. M. Stipanović, P. F. Hokayem, M. W. Spong, and D. D. Šiljak, "Cooperative avoidance control for multiagent systems," *Journal of Dynamic Systems, Measurement, and Control*, vol. 129, no. 5, pp. 699–707, 2007.

[130] S. Mastellone, D. M. Stipanović, C. R. Graunke, K. A. Intlekofer, and M. W. Spong, "Formation control and collision avoidance for multi-agent nonholonomic systems: Theory and experiments," *The International Journal of Robotics Research*, vol. 27, no. 1, pp. 107–126, 2008.

[131] E. J. Rodríguez-Seda, C. Tang, M. W. Spong, and D. M. Stipanović, "Trajectory tracking with collision avoidance for nonholonomic vehicles with acceleration constraints and limited sensing," *The International Journal of Robotics Research*, vol. 33, no. 12, pp. 1569–1592, 2014.

[132] A. Sgorbissa and R. Zaccaria, "Integrated obstacle avoidance and path following through a feedback control law," *Journal of Intelligent & Robotic Systems*, vol. 72, no. 3-4, p. 409, 2013.

[133] K. D. Do, "Global path-following control of stochastic underactuated ships: A level curve approach," *Journal of Dynamic Systems, Measurement, and Control*, vol. 137, no. 7, p. 071010, 2015.

[134] ——, "Coordination control of underactuated odins in three-dimensional space," *Robotics and Autonomous Systems*, vol. 61, no. 8, pp. 853–867, 2013.

[135] ——, "Synchronization motion tracking control of multiple underactuated ships with collision avoidance," *IEEE Transactions on Industrial Electronics*, vol. 63, no. 5, pp. 2976–2989, 2016.

[136] Y. Yamamoto and X. Yun, "Coordinating locomotion and manipulation of a mobile manipulator," *IEEE Transactions on Automatic Control*, vol. 39, no. 6, pp. 1326–1332, 1994.

[137] P. Morin and C. Samson, "Control of nonholonomic mobile robots based on the transverse function approach," *IEEE Transactions on Robotics*, vol. 25, no. 5, pp. 1058–1073, 2009.

[138] ——, "Practical stabilization of driftless systems on lie groups: the transverse function approach," *IEEE Transactions on Automatic Control*, vol. 48, no. 9, pp. 1496–1508, 2003.

[139] M. Fruchard, P. Morin, and C. Samson, "A framework for the control of nonholonomic mobile manipulators," *The International Journal of Robotics Research*, vol. 25, no. 8, pp. 745–780, 2006.

[140] D. Pazderski, D. K. Waśkowicz, and K. Kozłowski, "Motion control of vehicles with trailers using transverse function approach," *Journal of Intelligent & Robotic Systems*, vol. 77, no. 3-4, pp. 457–479, 2015.

[141] K. D. Do, "Practical control of underactuated ships," *Ocean Engineering*, vol. 37, no. 13, pp. 1111–1119, 2010.

[142] S. Sastry, *Nonlinear systems: analysis, stability, and control*. Springer Science & Business Media, 2013, vol. 10.

[143] Y. Lin, E. D. Sontag, and Y. Wang, "A smooth converse lyapunov theorem for robust stability," *SIAM Journal on Control and Optimization*, vol. 34, no. 1, pp. 124–160, 1996.

[144] J.-J. E. Slotine and W. Li, *Applied nonlinear control*. Prentice hall Englewood Cliffs, NJ, 1991, vol. 199, no. 1.

[145] H. Nijmeijer and A. Van der Schaft, *Nonlinear dynamical control systems*. Springer, 1990, vol. 175.

[146] A. Isidori, *Nonlinear control systems*. Springer Science & Business Media, 2013.

[147] W. Lohmiller and J.-J. E. Slotine, "On contraction analysis for non-linear systems," *Automatica*, vol. 34, no. 6, pp. 683–696, 1998.

[148] M. Malisoff and F. Mazenc, *Constructions of strict Lyapunov functions*. Springer Science & Business Media, 2009.

[149] Z. Chen and J. Huang, *Stabilization and regulation of nonlinear systems*. Springer, 2015.

[150] D. M. Dawson, J. Hu, and T. C. Burg, *Nonlinear control of electric machinery*. Marcel Dekker, Inc., 1998.

[151] N. Sarkar, X. Yun, and V. Kumar, "Control of mechanical systems with rolling constraints application to dynamic control of mobile robots," *The International Journal of Robotics Research*, vol. 13, no. 1, pp. 55–69, 1994.

[152] B. d'Andrea Novel, G. Bastin, and G. Campion, "Dynamic feedback linearization of nonholonomic wheeled mobile robots," in *Proceedings of 1992 IEEE International Conference on Robotics and Automation, 1992*. IEEE, 1992, pp. 2527–2532.

[153] N. Sarkar, X. Yun, and V. Kumar, "Control of mechanical systems with rolling constraints application to dynamic control of mobile robots," *The International Journal of Robotics Research*, vol. 13, no. 1, pp. 55–69, 1994.

[154] H. Choset, K. M. Lynch, S. Hutchinson, G. A. Kantor, W. Burgard, L. E. Kavraki, and S. Thrun, *Principles of Robot Motion: Theory, Algorithms, and Implementations*. Cambridge, MA: MIT Press, June 2005.

[155] F. L. Lewis, D. M. Dawson, and C. T. Abdallah, *Robot manipulator control: theory and practice*. CRC Press, 2003.

[156] Y. F. Zheng, *Recent trends in mobile robots*. World Scientific Publishing Co., Inc., 1994, vol. 11.

[157] S. Garrido, L. Moreno, D. Blanco, and P. Jurewicz, "Path planning for mobile robot navigation using voronoi diagram and fast marching," *International Journal of Robotics and Automation*, vol. 2, no. 1, pp. 42–64, 2011.

[158] L. Garcia-Delgado, A. Dzul, V. Santibáñez, and M. Llama, "Quad-rotors formation based on potential functions with obstacle avoidance," *IET Control Theory & Applications*, vol. 6, no. 12, pp. 1787–1802, 2012.

[159] S. G. Tzafestas, *Introduction to Mobile Robot Control*. Reading, Massachusetts: Elsevier, 2014.

[160] J. Borenstein and Y. Koren, "The vector field histogram-fast obstacle avoidance for mobile robots," *IEEE Transactions on Robotics and Automation*, vol. 7, no. 3, pp. 278–288, 1991.

[161] S. S. Ge and Y. J. Cui, "Dynamic motion planning for mobile robots using potential field method," *Autonomous Robots*, vol. 13, no. 3, pp. 207–222, 2002.

[162] B. Siciliano, L. Sciavicco, L. Villani, and G. Oriolo, *Robotics: Modelling, Planning and Control*. Springer Science & Business Media, 2008.

[163] D. Angeli and E. D. Sontag, "Forward completeness, unboundedness observability, and their lyapunov characterizations," *Systems & Control Letters*, vol. 38, no. 4, pp. 209–217, 1999.

[164] D. V. Dimarogonas, S. G. Loizou, K. J. Kyriakopoulos, and M. M. Zavlanos, "A feedback stabilization and collision avoidance scheme for multiple independent non-point agents," *Automatica*, vol. 42, no. 2, pp. 229–243, 2006.

[165] L. Valbuena and H. G. Tanner, "Hybrid potential field based control of differential drive mobile robots," *Journal of Intelligent & Robotic Systems*, vol. 68, no. 3-4, pp. 307–322, 2012.

[166] P. Morin and C. Samson, "Transverse function control of a class of non-invariant driftless systems. application to vehicles with trailers," in *Proceedings of 47th IEEE Conference on Decision and Control, 2008.* IEEE, 2008, pp. 4312–4319.

[167] H. Nijmeijer and T. I. Fossen, *New directions in nonlinear observer design.* London ; New York : Springer, 1999, vol. 244.

[168] Z.-P. Jiang and L. Praly, "Design of robust adaptive controllers for nonlinear systems with dynamic uncertainties," *Automatica*, vol. 34, no. 7, pp. 825–840, 1998.

[169] Z. Li, S. S. Ge, M. Adams, and W. S. Wijesoma, "Adaptive robust output-feedback motion/force control of electrically driven nonholonomic mobile manipulators," *IEEE Transactions on Control Systems Technology*, vol. 16, no. 6, pp. 1308–1315, 2008.

[170] R. A. Freeman and P. Kokotovic, "Inverse optimality in robust stabilization," *SIAM journal on Control and Optimization*, vol. 34, no. 4, pp. 1365–1391, 1996.

[171] Z.-H. Li and M. Krstić, "Optimal design of adaptive tracking controllers for nonlinear systems," in *Proceedings of the American Control Conference, 1997*, vol. 2. IEEE, 1997, pp. 1191–1197.

[172] S.-J. Chung and J.-J. E. Slotine, "Cooperative robot control and concurrent synchronization of lagrangian systems," *IEEE Transactions on Robotics*, vol. 25, no. 3, pp. 686–700, 2009.

[173] Y. Cao, W. Yu, W. Ren, and G. Chen, "An overview of recent progress in the study of distributed multi-agent coordination," *IEEE Transactions on Industrial Informatics*, vol. 9, no. 1, pp. 427–438, 2013.